Microwave Techniques for the Preparation of Polymer Foams

A thesis submitted to The University of Manchester for the degree of

Doctor of Philosophy

in the Faculty of Engineering and Physical Sciences

2005

Alexander Edward Stockley Clarke

School of Materials

(EKQF2)

Th26070

Contents

List of Figures

List of Tables

List of Symbols and Abbreviations

Symbols

ω	Angular frequency
α	Degree of cure / conversion
β	Beta
c	Speed of light
ρ	Density
γ	Interfacial tension
γ_{ab}	Interfacial energy between an additive and a gas bubble
γ_{ap}	Interfacial energy between an additive and a polymer
γ_{bp}	Interfacial energy between a gas bubble and a polymer
ε	Strain
λ	Wavelength
σ	Stress
σ_c^{I}	Compressive strength perpendicular to direction of foaming
σ_c^{II}	Compressive strength parallel to direction of foaming
σ_{pl}	Plastic yield point
Γ^*	Reflection coefficient
ε^*	Complex dielectric permittivity
ε'	Dielectric constant
ε''	Dielectric loss factor
ε_0	Permittivity of free space
δ	Dielectric loss tangent
ρ	Density
ρ_f	Foam density
ρ_s	Base polymer density
ρ_g	Cell gas density
$S(\theta)$	Wetting angle geometric factor
$\tau_{1/2}$	Half life time
A	Area
A_{ab}	Interfacial area between an additive particle and a gas bubble

A_{ap}	Interfacial area between an additive particle and polymer
A_{bp}	Interfacial area between a gas bubble and polymer
C_v	Specific heat capacity
C^*	Concentration of gas clusters that have reached critical size
C_0	Concentration of gas molecules in solution
E	Electric field strength
E	Young's modulus
E^*	Foam elastic modulus
E_s	Polymer elastic modulus
F	Force
f	Frequency
f_0	Frequency factor for homogeneous nucleation
f_{cav}	Resonant frequency of empty cavity
f_{sam}	Resonant frequency of cavity containing sample
G	Ratio of material volume to cell volume
ΔG_{hom}	Gibbs free energy change for homogeneous nucleation
ΔH_m	Melting enthalpy
ΔH_c	Melting enthalpy of a perfectly crystalline sample
h_0	Original sample height
h	Sample height at given strain
k	Reaction rate constant
k	Boltzmann constant
M	Mass
ΔP	Differential gas pressure
P	Power
Q	Quality factor
Q_{cav}	Quality factor of empty cavity
Q_{sam}	Quality factor of cavity containing sample
R	Universal gas constant
r	Radius
r^*	Critical radius
T	Temperature
t	Time
$tan\ \delta$	Loss tangent

T_m	Melting temperature
T_d	Decomposition temperature
V	Volume
V_b	Bubble volume
W_1	Weight of steel mesh cage
W_2	Weight of steel mesh cage containing sample
W_3	Weight of steel mesh cage containing sample and stapled ends
W_4	Weight of steel mesh cage containing sample after extraction
W_1	Mass of empty pycnometer
W_2	Mass of sample and empty pycnometer
W_3	Mass of full pycnometer
W_4	Mass of sample and full pycnometer
Z_0	Characteristic impedance
Z_s	Probe impedance

Abbreviations

AC	Alternating current
ADC(E)	Azodicarbonamide
ADC	Analog-digital converter
AM	Amplitude modulation
ASTM	American society of testing and materials
AT	Attenuator
BA	Blowing agent
CBA	Chemical blowing agent
CCD	Charge coupled device
CFC	Chlorofluorocarbon
DC	Direct current
DCP	Dicumyl peroxide
DSC	Differential scanning calorimetry
EM	Electromagnetic
EMA	Ethylene methyl acrylate
EVA	Ethylene vinyl acetate
Eqn.	Equation
FM	Frequency modulation
FVM	Frequency varying method
GPIB	General purpose interface bus
HFSS	High frequency structure simulator
IR	Infrared
ISM	Industrial, scientific and medical
LDPE	Low density polyethylene
MA	Microwave amplifier
MUT	Material under test
PBA	Physical blowing agent
PC	Personal computer
PE	Polyethylene
PID	Proportional integral derivative
PS	Power sensor
PTFE	Polytetrafluoroethylene
RF	Radio frequency

SEM	Scanning electron microscopy
TBPB	Tertiary butyl perbenzoate
TE	Transverse electric
TEM	Transverse electromagnetic
TGA	Thermogravimetric analysis
TM	Transverse magnetic
TV	Television
TWT	Travelling wave tube
UHF	Ultra high frequency
UV	Ultra violet
VFM	Variable frequency microwave
VNA	Vector Network analyser

Abstract

A novel microwave processing technique for the heating and foaming of ethylene vinyl acetate (EVA) copolymers with different percentages by weight vinyl acetate content (6, 18 and 28 %) was investigated as an alternative to conventional production techniques. The foam formulations comprised ethylene vinyl acetate copolymer, an organic peroxide crosslinking agent and a blowing agent based on azodicarbonamide.

Thermal characterisation was performed on the formulation components to determine the likely foam processing conditions. Dielectric characterisation was also performed in order to determine the dielectric response of materials as a function of both frequency (1 - 10 GHz) and temperature (25 – 250 °C). The results showed that each of the formulation components had sufficiently high loss at 2.45 GHz to allow heating; it was also shown that dielectric loss increased with increasing frequency. The loss factor of the EVA base polymers increased with increasing vinyl acetate content which was attributed to the increase in polymer polarity. As temperature was increased, the loss of the EVA polymers increased. This was a result of increased molecular freedom due to polymer viscosity reduction and melting of the crystalline regions of the polymers.

Initial microwave foaming was performed on EVA 206 (6 % vinyl acetate) using a section of rectangular waveguide as the microwave applicator. A 30 W microwave amplifier was used as the power source. It was found that foaming took place predominantly in the centre of the samples and the foamed portions appeared to be encapsulated in a thick unfoamed skin which was confirmed by analysis of detailed images obtained using a scanning electron microscope. This was attributed to heat loss from the sample surface.

The main thrust of this work concentrated on using a newly developed combination microwave / hot air oven for the batch processing of EVA foams using variable frequency (200 W) microwave heating. Supplemental hot air heating (170 °C) was used to reduce the thickness of the foam skin encountered earlier. Crosslinking of the base polymers was investigated using conventional and microwave heating. It was found that the microwave heated samples had lower gel content than those heated conventionally. It was found that microwave heated foams could be produced that were comparable with conventionally heated samples. Six microwave heating frequencies were used to evenly distribute the microwave field throughout the samples. The densities of the EVA 328 (28 % vinyl acetate) microwave heated foams were found to be comparable with the conventionally heated EVA 328 foams. The foams based on EVA 218 (18 % vinyl acetate) had slightly higher densities than the conventional foams which was attributed to their lower polarity and hence lower microwave heating efficiency. Foams based on EVA 328 had lower densities than conventional samples (at the upper expansion temperature range) and showed less degradation. Compression testing revealed that, generally, the microwave heated foams had slightly higher Young's modulus than the conventional foams which was attributed to their higher density. Scanning electron microscopy was used to examine the cellular structure of the conventionally and microwave heated foams. Cell sizes for the microwave foams were marginally larger than the conventional foams suggesting that localised overheating of the samples due to non uniform microwave field distribution was occurring.

Declaration

No portion of the work referred to in this thesis has been submitted in support of an application for another degree or qualification of this or any other university or other institution of learning.

Alexander Edward Stockley Clarke.

Copyright Statement

Acknowledgements

Firstly I would like to thank my supervisors Dr. Richard Day and Dr. Geoff Sims for their guidance, support and encouragement throughout this work. I would also like to thank Dr. Zhipeng Wu for his valuable assistance with equipment design. Furthermore, I would like to thank the Engineering and Physical Sciences Research Council (EPSRC) for providing the funding for this project.

I would like to convey my appreciation to the staff of Manchester Materials Science Centre. In particular I would like to thank Andy Zadoroshnyj and Gerard Healey for their help with many of technical aspects of this work, Polly Crook for her help and advice with thermal characterisation, Peter Kenway and Mike Faulkner for their assistance with electron microscopy, Robin Hadley and Margaret Banton in photography, the administrative staff particularly Olwen Richert, Gary Ingham in computing and the workshop technicians for their help with equipment manufacture.

I would like to express my appreciation to the members of the Microwave Processing Group past and present especially Dr. Grace Atkinson, Dr. Rozita Yusoff, Dr. Sawitree Petchuay and Dr. Parnia Navabpour, for their help, friendship and support during the course of this project. Thanks also to Dr. Coswald Stephen Sipaut for his help in the early stages of this work.

I am deeply indebted to Dr. Alan Nesbitt whose wealth of knowledge, expertise and assistance with numerous aspects of this project has been invaluable.

I am incredibly grateful to my mum, Jane, my dad, Keith, my sister, Emily, Tony and Caroline, for the seemingly infinite ways in which they have supported and helped over the last few years. I would also like to extend my thanks to my future in-laws, David, Sheila and Andrea for everything that they have done.

Finally, I would like to thank my fiancée Katherine for her unwavering support and encouragement throughout the entirety of this PhD.

CHAPTER 1: INTRODUCTION

1.1: Background of Polymer Foams

Cellular materials such as polymer foams have a vast range of current and potential applications. Although natural cellular materials such as cork have been used for hundreds of years, modern synthetic materials such as polyethylene foam have been the subject of notable industrial attention since the mid 1970's (Khunniteecool, Sims and, White, 1994). Polyolefin foams display a range of advantageous properties which include good ageing properties, low water absorption, stability against weathering and UV degradation when physically crosslinked. (Rodriguez-Perez *et al.*, 1997). Uses include packaging, flotation devices, soft furnishings, sports and footwear applications particularly shoe inserts and insoles (Sims and Khunniteekool, 1996 **(a)**), insulation and structural components. Other desirable attributes include the ability to absorb mechanical shock and sound and therefore foams find other uses in areas such as machine housings and supports. Plastic foams exist as two-phase materials in which gas cells (generated by a blowing agent) are enclosed within a solid macromolecular phase (Almanza, Rodriguez-Perez and Saja, 2001) (Cardoso *et al.*, 1998).

1.2: Foam Characterisation

On a structural level, foams may generally be divided into two separate classes, open and closed cell. In closed cell foams such as polyolefin foams, the gas cells are discrete non-interconnecting regions trapped within a macromolecular phase. In contrast open cell foams, such as polyurethane foams, may be accurately described as a continuous phase of ambient air in which the highly dispersed polymer phase exists as an interpenetrating solid phase network (Klempner and Frisch, 1991) i.e. the cells do not possess any walls and are, therefore, interconnected. All that remains of the cell structure are the ribs and struts, which formed the interstices of the cells. In reality most foams are neither, 100 % open or 100 % closed cell but exist as a combination of the two (with one type in the vast majority). It is possible to adjust the ratio of open and closed cells within a foam by careful selection of additives and by various methods of introducing the gaseous phase.

The density of a polymer foam greatly influences its end usage i.e. high density rigid foams may be used for structural applications whereas low density flexible foams are more suited to packaging and cushioning uses. Typically plastic foams may be produced with densities ranging from ~1.6 - 960 kg / m^3. As the majority of foam characteristics are directly related to density it is important that it may be accurately determined. Density is commonly determined using equation 1.1,

$$\rho = \rho_p(1-G) + \rho_g$$

(Eqn. 1.1)

where ρ is the foam density, ρ_p is the true density of the base polymer (ratio of total mass to difference between total material volume and cell volume), G is the ratio of total material volume to cell volume and ρ_g is the cell gas density. In practice, however, foam density may be calculated from equation 1.2,

$$\rho = \frac{M}{V}$$

(Eqn. 1.2)

where M is sample mass and V is sample volume (Klempner and Frisch, 1990).

Foams are comprised of at least two parts, a solid polymeric phase and a second gaseous phase which is dispersed within it. Other phases, which may be present, include fillers such as glass, ceramics and metals as well as pigments and polymer based fillers.

1.3: Principles of the Foaming Process

In the polymer foaming process there are three key steps, nucleation, bubble growth and bubble stabilisation (Shafi, Joshi and Flumerfelt, 1997). The most common foaming processes may be simply described as the distribution of a gas through a polymer matrix (whilst fluid) and the stabilisation of the foam produced. A number of methods are available for the distribution of gas. These include; the mixing of a chemical blowing agent with a base polymer and gas generation by subsequent thermal decomposition of the blowing agent, incorporation of a low boiling point liquid such as pentane which is then volatilised by heating, the saturation of a polymer with gas whilst under pressure and expansion by heating and pressure reduction.

Other methods include the mechanical frothing of latexes and the inclusion of hollow glass spheres within a polymer system (Klempner and Frisch, 1991).

1.3.1: Cell Nucleation

The initial step in foam cell formation is nucleation. There are a number of ways in which nucleation may be achieved, bubbles may spontaneously form within a truly homogenous super saturated polymer phase (Frisch and Saunders, 1972), this is known as self-nucleation. If, however, a nucleating agent is present (normally a very fine powder) this provides an energetically favourable point (liquid solid interface) from which bubbles may form at lower gas concentrations. If bubble formation proceeds via this mechanism the cells are said to form by a nucleation process. It is often the case that the polymer liquid phase will contain very small air bubbles. These do not act as nucleation sites, as the formation of a bubble is no longer necessary, however, they do provide sites for bubble growth as gas may diffuse from the surrounding saturated polymer melt into the existing air bubble. In continuous production and extrusion processes, high nucleation rates may be achieved by the gas saturation of a polymer under high pressure. The solubility of the gas is then reduced (promoting nucleation) by a rapid reduction of pressure (Park, Baldwin and Suh, 1995). As nucleation is a rate process, bubbles nucleated at different times have different radii. The greatest nucleation rate is at t_0 and decreases as the gas concentration in the surrounding melt decreases with time (Shafi, Joshi and Flumerfelt, 1997).

The main concept in the bubble nucleation theory can be understood by the consideration of a volatile liquid which is not in contact with the gaseous phase and wets (i.e. has zero contact angle with) all surfaces it contacts. Simple thermodynamics demonstrates that nucleation within this liquid will generate bubbles entirely within the liquid and is described as homogenous nucleation. This may be contrasted with heterogeneous nucleation where nucleation takes place at the interface between the volatile liquid and another phase it contacts (Blander and Katz, 1975; Cole, 1974).

Nucleation rate and the interfacial properties of a volatile liquid are related by classic nucleation theory. The better the wetting of a substrate by the fluid, the greater the probability that homogeneous nucleation will take place within the fluid interior rather

than heterogeneous nucleation at the interface. Classical nucleation theory has been modified to account for changes in free volume and interfacial energy terms when applied to microcellular foam nucleation (Colton and Suh, 1987 **(a)**, **(b)** and **(c)**). When a bubble of gas is generated during homogeneous nucleation, through a reversible thermodynamic process, there is an associated excess energy which is outlined by equation 1.3,

$$\Delta G_{\text{hom}} = -V_b \Delta P + A_{bp} \gamma_{bp}$$

(Eqn. 1.3)

where ΔG_{hom} is the Gibbs free energy change for homogenous nucleation, V_b is the volume of the bubble nucleus, ΔP is the differential pressure of the gas bubble (saturation pressure), A_{bp} is the bubble surface area and γ_{bp} is the surface energy of the polymer – bubble interface. If expansion is isotropic then the bubble is considered spherical with radius r. Equation 1.3 then becomes,

$$\Delta G_{\text{hom}} = -\left(\frac{3}{4}\right)\pi\, r^3 \Delta P + 4\pi\, r^2 \gamma_{bp}$$

(Eqn. 1.4)

and is illustrated graphically by figure 1.1.

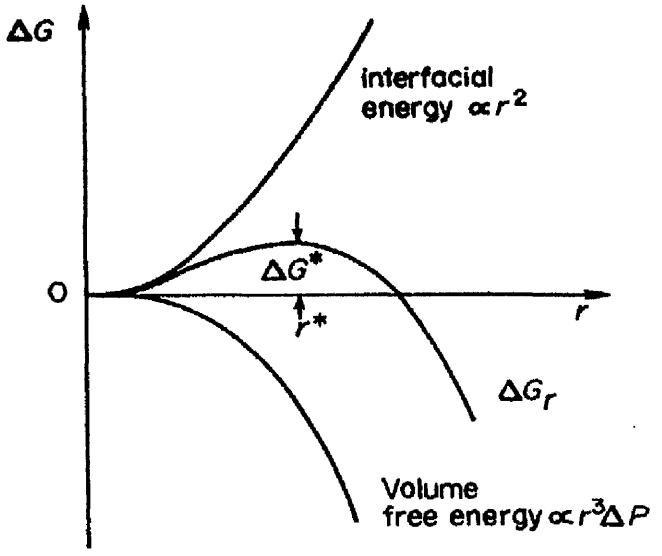

Figure 1.1: Free energy change associated with homogeneous nucleation of a spherical cell of radius r (Colton and Suh, 1987 **(a)**)

Thus, the production of fine cells requires a greater increase in system free energy. Furthermore, the coalescence of cells, and ultimately, foam collapse is energetically favoured unless prevented by processes such as crosslinking or cooling. Figure 1.1 also demonstrates that there is a critical radius r^* which is given by equation 1.5. The Gibbs free energy for homogeneous nucleation of a critical nucleus is given by equation 1.6 (Colton and Suh, 1987 **(a)**).

$$r^* = \frac{2\gamma_{bp}}{\Delta P} \qquad \textit{(Eqn. 1.5)}$$

$$\Delta G^*_{\text{hom}} = \frac{16\pi}{3\Delta P^2}\gamma^3_{bp} \qquad \textit{(Eqn. 1.6)}$$

The critical radius is associated with a maximum free energy. At r^*, $(dG/dr) = 0$ and $(d^2G/dr^2) < 0$, therefore the bubble nucleus is in an unstable equilibrium with its environment. When r is less than r^* system free energy can only be decreased by r decreasing to 0 meaning that the gas would go into solution in the polymer. If however r is greater than r^*, then bubble growth causes a reduction in the free energy and growth of the bubble is favoured energetically.

Equation 1.6 also shows that a decrease in the energy of the bubble interface or an increase in the saturation pressure will cause a decrease in the Gibbs free energy. This will be shown to increase nucleation rate and cell density. The nucleation rate of gas bubbles may be calculated using equation 1.7,

$$C^* = C_{0\exp}\left(\frac{-\Delta G^*_{\text{hom}}}{kT}\right) \qquad \textit{(Eqn. 1.7)}$$

where C^* is the number of gas clusters that reach a critical size to form stable nuclei (assuming a Boltzmann distribution), C_0 is gas molecule concentration within the polymer, ΔG^*_{hom} is given by equation 1.6, k is the Boltzmann constant and T is the absolute temperature in Kelvin. A critical nucleus may be converted to a stable nucleus by the addition of one more gas molecule. If this takes place with a frequency f_0, the homogenous nucleation rate may be given by equation 1.8,

$$N_{\text{hom}} = f_0 C_0 \exp\left(\frac{-\Delta G^*_{\text{hom}}}{kT}\right)$$

(Eqn. 1.8)

where N_{hom} is the homogeneous nucleation rate.

Heterogeneous nucleation takes place when a third phase is present. A bubble may be formed at the interface of the two other phases (a liquid and a solid) and can be described by classical nucleation theory. Consideration of the nucleus of a gas bubble at the interface of a polymer and a solid additive particle is shown in figure 1.2.

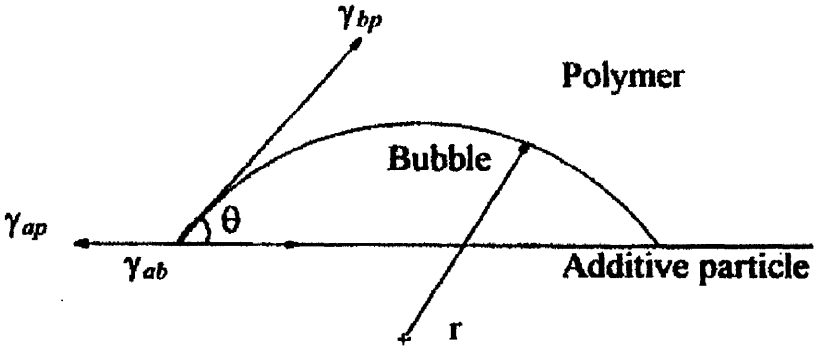

Figure 1.2: Heterogeneous nucleation characteristics (Colton and Suh, 1987 **(a)**)

A balance of interfacial surface tension gives:

$$\gamma_{ap} = \gamma_{ab} + \gamma_{bp}\cos\theta$$

(Eqn. 1.9)

where γ_{ap}, γ_{ab}, γ_{bp}, are the interfacial tensions of the solid particle – polymer, solid particle bubble and bubble – polymer, respectively, and θ is the wetting angle of the interface. Thus the excess free energy is given by equation 1.10,

$$\Delta G_{het} = -V_b \Delta P + A_{bp}\gamma_{bp} + A_{ab}\gamma_{ab} - A_{ap}\gamma_{ap}$$

(Eqn. 1.10)

where V_b is the bubble volume and A_{bp}, A_{ab} and A_{ap} are the areas of the bubble – polymer, additive particle – bubble and additive particle – polymer interfaces respectively. Rearranging equation 1.10 gives equation 1.11,

$$\Delta G_{het} = \left[-\left(\frac{4}{3}\right)\pi r^3 \Delta P + 4\pi r^2 \gamma_{bp}\right] S(\theta)$$

(Eqn. 1.11)

where $S(\theta)$ is defined by equation 1.12.

$$S(\theta) = \left(\frac{1}{4}\right)(2+\cos\theta)(1-\cos\theta)^2$$

(Eqn. 1.12)

According to Colton and Suh (Colton and Suh, 1987 **(a)**) for a typical wetting angle of 20°, $S(\theta)$ is in the order of 10^{-3}. The energy barrier for heterogeneous nucleation can, therefore, be largely reduced by the presence of an interface. This type of nucleation will be favoured over homogeneous nucleation due to its lower energy barrier.

The conclusions reached by Colton and Suh (Colton and Suh, 1987 **(a)**, **(b)** and **(c)**) show that when producing microcellular foam (cell size 10 microns or less) (a saturation process), there are three types of nucleation process. Below the solubility limit of additives in the polymer, additives in solution act to increase the polymer free volume which results in homogeneous nucleation within the free volume. Well above the solubility limit, heterogeneous nucleation is dominant because it lowers the nucleation activation energy to below that of homogeneous nucleation. In the vicinity of the solubility limit, both heterogeneous and homogeneous nucleation occurs. On consideration of chemical blowing agent processes, different factors (from those of the saturation process) may also be involved. It has been proposed (Simonik and Svoboda, 1990) that during the atmospheric expansion of a polymeric material and gas generation by chemical reaction, the gas is nucleated on blowing agent residues and not significantly dissolved in the polymer melt. According to others (Benning, 1969), in the chemical blowing agent method, particles of the blowing agent are completely dissolved in the polymer and, therefore, cell size is partially dependant upon the particle size and dispersion of the blowing agent in the polymer.

1.3.2: Cell Growth

After cell nucleation has relived the super-saturation in the dissolved gas process, no new bubbles are formed and the cells begin to grow as gas from the surrounding polymer matrix diffuses in. During this process mass, momentum and energy are transferred between the growing cell and its surrounding fluid (Arefmanesh and Advani, 1995). As gas diffuses into the nucleated cells, a gas concentration gradient is established which propagates radially from each cell (Shafi *et al.*, 1996; Shafi *et al.*, 1997). The initial bubble is ideally a sphere which grows due to the interaction of the differential pressure, ΔP, between the interior and exterior of the cell and the

interfacial tension γ. The equilibrium bubble radius, r, is related to these factors as shown by equation 1.13 (Klempner and Frisch, 1991).

$$\Delta P = \frac{2\gamma}{r} \qquad \textit{(Eqn.1.13)}$$

The differential pressure is larger for a small bubble at a fixed surface tension. Smaller bubbles tend to equalise these pressures by either growing faster, rupturing the intercellular walls, or by diffusion of gas from the small to the large cells as shown by equation 1.14 (Klempner and Frisch, 1991),

$$\Delta P_{1,2} = 2\gamma\left(\frac{1}{r_1} - \frac{1}{r_2}\right) \qquad \textit{(Eqn.1.14)}$$

where $\Delta p_{1,2}$ is the pressure difference between the two different cells having radii r_1 and r_2. As a consequence the average bubble size in a polydisperse system increases with time. The lower the value of γ the lower the difference in pressure different sized cells, which leads to greater cellular system stability and smaller average cell size.

Initially, bubbles are spherical in shape, however as bubble size increases it is not possible for this shape to be maintained. As the cells grow a number of system properties begin to change. As cell size increases there is a corresponding reduction in density. If the volume fraction of the gas is sufficiently high the cells begin to impinge on one another, a polyhedral structure develops and the polymer matrix forms thin walls and struts between the cells. The type of cellular structure and final cell size distribution is affected by both nucleation rate and cell growth dynamics. An increase in nucleation rate or a decrease in cell growth rate will favour a large number of smaller cells being formed (Shafi *et al.*, 1997).

1.3.3: Cell Stabilisation

The cells in a polymer foam continue to grow as gas rapidly diffuses in until bubble stabilisation is achieved or pressure equilibrium is reached. The cell walls are, however, stretched very thin, unstable and are liable to rupture to form open cells if not sufficiently stabilised. Stabilisation of polymer foams may be achieved by a

number of routes, by chemical means resulting in complete gelation (crosslinking) or by physical processes such as cooling below the polymer melting point which prevents polymer flow (Klempner and Frisch, 1991). Two dimensional representations of idealised cellular structures at different stages of bubble growth are shown in figure 1.3 and explained below.

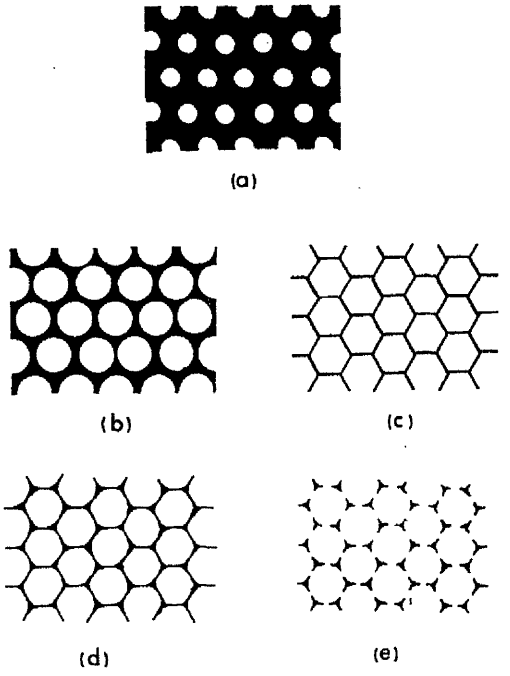

Figure 1.3: Two-dimensional projections of some idealised foam structures at various stages of bubble expansion (Harding, 1965)

1. Initially, small spherical bubbles are uniformly dispersed throughout the polymer melt as shown in figure 1.3a. If foam stabilisation took place at this stage, a high density foam would be formed.
2. The lowest density achievable with spherical bubbles of uniform size is when they are closely packed together displacing surrounding polymer as shown by figure 1.3b. Harding (Harding, 1965) suggested, however, that this configuration is unstable and is not typically adopted by polymer foam structures.
3. Further expansion is accompanied by a reduction in density, consequentially the large bubbles distort such that the cells are bounded by polyhedra with plane surfaces of uniform thickness as depicted in figure 1.3c. These surfaces are termed cell walls, windows or membranes.

4. The stability of a low density cellular structure in a liquid foam may be influenced by gravitational and capillary forces which encourage flow towards the lines along which the cell walls intersect. This movement of liquid polymer results in the thinning of the cell walls and formation of ribs (struts) at the lines of intersection between the cells as represented by figure 1.3d.
5. Further drainage will cause cell membranes to rupture and if the structure is stabilised at this stage, the resultant foam will be open-cell and consist of a three-dimensional array of interconnecting polymer struts as represented by figure 1.3e.

The excessive drainage of polymer will sometimes result in the collapse of the cellular structure during manufacture. Drainage may be limited by increasing the viscosity of the polymer. Methods of increasing viscosity include chemical reaction and molecular weight increase through polymerisation, crosslinking or temperature reduction in thermoplastics (Suh and Webb, 1985).

1.4: Cellular Structure

Liquid foams are at their most stable when the constituent gas bubbles are spherical as the capillary pressure and the interfacial area are both minimised (Bikerman, 1973). The closest possible packing arrangement for a monodisperse structure consisting of spherical cells is obtained when each cell is in contact with 12 others and the volume of the gas phase is 74 %. If the gas volume is increased beyond this point, the spheres will tend to become polygons and will ideally form dodecahedrons which have pentagonal faces. The geometrical characteristics of a regular 14 – hedron (surface comprising six squares and eight hexagons) are better suited to the formation of an ideal foam structure as they are closer to the geometry of a sphere than a regular 12 - hedron (surface comprising regular pentagons only) (Harding, 1965).

In reality, the cellular structure that tends to be adopted by real foams is based upon the shape of a 12 – hedron with regular pentagonal faces as shown by figure 1.4.

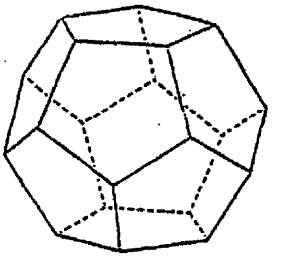

Figure 1.4: Pentagonal – dodecahedral cell (Hilyard and Cunningham, 1994)

This type of cell structure is found in many types of foam (rigid and flexible) and foams based on different polymers. Furthermore this type of cell is favoured in foams based on crosslinked low density polyethylene and crosslinked ethylene vinyl acetate polymer foams (Sims and Khunniteekool, 1995) with density ranges comparable to the foams in this work. As well as formulation and processing conditions, the mechanical properties of foams are also dependant on cellular structure. One extremely important aspect which has been the subject of significant work (Gibson and Ashby, 1997; Khunniteekool and Sims, 1994) is the influence of foam density on its mechanical properties.

1.5: Foam Structure / Property Relationships

The cells present within foamed polymers may be closed with membranes / faces spanning the cell struts resulting in discrete enclosed cells, or open / interconnecting cells where no membranes are present and the gaseous phase is continuous throughout the foam. Examples of the two cell types are depicted in figure 1.5.

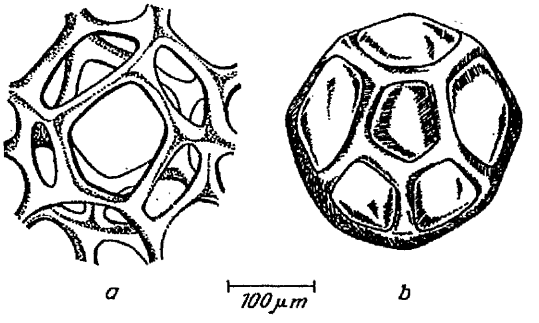

Figure 1.5: Examples of (a) open and (b) closed cellular structures (Klempner and Frisch, 1991)

Open cell structures are only obtained if two conditions are satisfied. Firstly, each spherical polygonal cell must have at least two pores or two broken faces. Secondly, the vast majority of cell ribs must belong to at least three gas structural elements (Blair, 1967; Klempner and Frisch, 1991). The differences between the two cell types

are responsible for the varying properties of foamed polymers which contain varying proportions of each cell structure. When compared to closed cell polymers, open cell foamed plastics have a higher moisture and gas permeability, less effective in terms of heat and electrical insulation and have superior sound damping properties. The cells in open cell foam are continuous, open to the atmosphere and, therefore, contain air. The cells in closed cell foam are discrete and enclosed. The gas contained within closed cells depends on the blowing agent used and may contain additional hydrogen, carbon dioxide, nitrogen or volatile liquids. These additional gasses may have some effect on the mechanical performance of the foam, however as the foam ages, the cell gas is replaced by air as a result of diffusion. Increasing the proportion of open cells within a foamed plastic has been shown to reduce foam compressive and tensile properties (Frisch and Saunders, 1972).

1.5.1: Cell Size

On consideration of polymeric foams with the same density, the same base polymer and the same proportions of open to closed cells, a general trend of increasing flexural modulus with increasing cell size is observed. This has been illustrated for a variety of foams including polyethylene foams (Benning, 1967; Skochdopole and Rubens, 1965) and polyurethane foams (Hilyard, 1982). Deanin (Deanin, 1985) reports that increasing cell size may often be correlated with an increase in modulus and stiffness (attributed to thicker cell walls), good shock absorption, higher thermal conductivity by convection and radiation and increased permeability. By way of contrast, smaller cell size often results in higher strength as more cells must be ruptured before failure, higher ultimate elongation (again due to the increased number of cells which must be ruptured) and increased thermal insulation as small cells reduce conduction and convection (more cell walls for the heat to travel through).

1.5.2: Cell Shape

Anisotropy (due to cell elongation) is the main reason why, in reality, the morphology of foams deviates from theoretical predictions. Cells tend to align themselves in the direction of foam rise as the stresses that occur during foaming are not uniformly distributed throughout the foam. As a result, the cells expand along the direction of minimum local stress (Klempner and Frisch, 1991). In the production of polyurethane foams it is common for the cells to align themselves in the direction of foam rise

(Hilyard, 1982), however, for thermoplastic foams this is not always the case. Polystyrene, when produced by bead expansion moulding, is found to have cells which are isotropic, furthermore, crosslinked polyethylene foam when moulded under high pressure throughout the process, produces isotropic cells (Benning, 1969). The stretching of dodecahedral cells is represented schematically in figure 1.6.

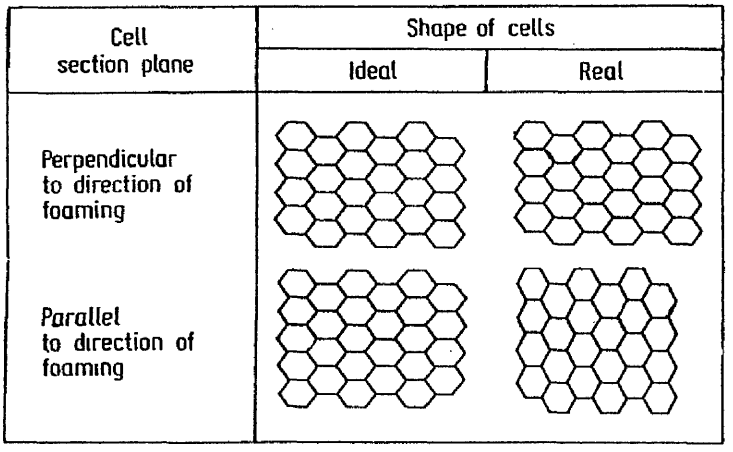

Figure 1.6: Schematic views of cell elongation during foaming (Harding, 1967)

As a consequence of anisotropy, the mechanical properties of a foam are often different in the direction of foam rise. For example, the compressive strength of an isotropic foam in the parallel to the direction of rise is always better than perpendicular to the direction of rise. Figure 1.7 demonstrates the effect of cell shape (height to width ratio) and test orientation on the compressive properties of some low density rigid foams (listed subsequently).

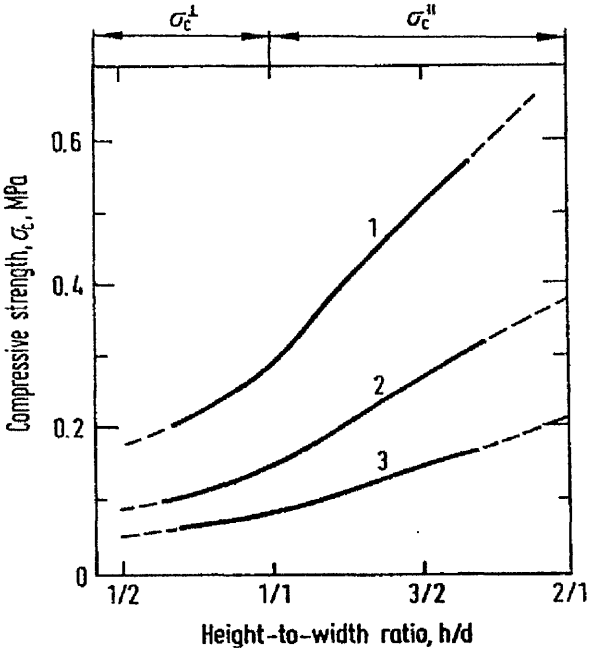

Figure 1.7: Effect of height to width ratio on compressive strength (Harding, 1967)

The curves shown in figure 1.7 represent the following foamed polymers;

1. Polyurethane (ρ = 48 kg m^{-3}) also polystyrene (ρ = 32 kg m^{-3}).
2. Polyurethane (ρ = 32 kg m^{-3}).
3. Polyurethane (ρ = 24 kg m^{-3}) also phenolic resin (ρ = 32 kg m^{-3}).

where σ_c^{I} and σ_c^{II} are the compressive strengths perpendicular and parallel to the direction of foaming, respectively.

1.6: Deformation of Closed Cell Polymer Foams

1.6.1: Compression Behaviour

Polymer foams are commonly used as mechanical energy absorbers because of their ability to absorb impact energy of force without generating high stress (Iannace *et al.*, 2001). This section focuses purely on closed cell foams as these types are used in this work. During compressive deformation, the behaviour of closed cell, elastic – plastic polymer foams show a number of mechanical responses. These are shown schematically in figure 1.8.

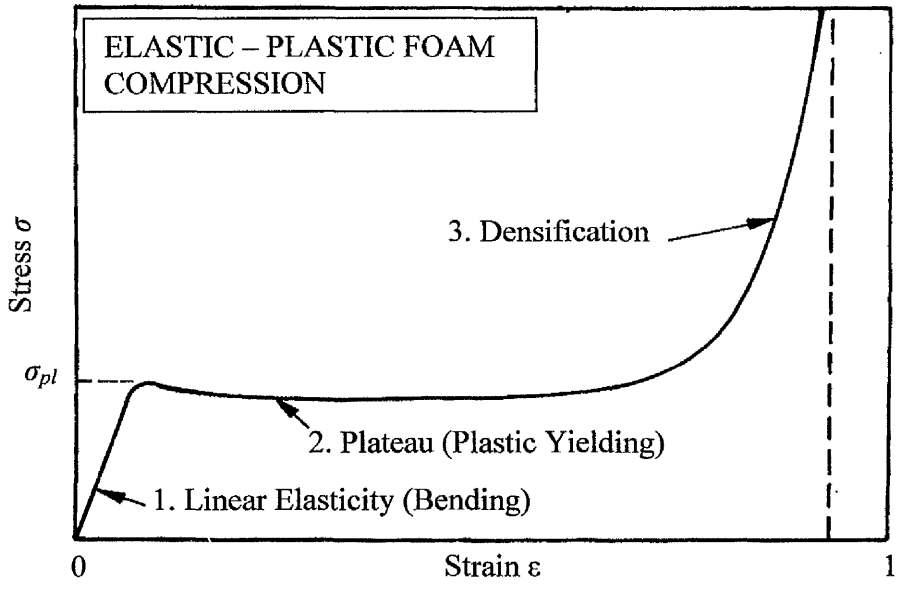

Figure 1.8: Schematic compression stress – strain curve for an elastic – plastic foam showing; 1. Linear elasticity, 2. Plastic collapse and 3. Densification (Gibson and Ashby, 1997)

1. Linear Elasticity

At low strain values (usually 5% or less), the relationship between stress and strain is linear. In this region, elastic recoverable deformation takes place. For closed cell foams, cell edge bending, stretching of the membranes (cell

faces) between the edges axially to the direction of stress, and compression of cell gas are the main contributory mechanisms to foam stiffness (modulus). Since the cell walls are so thin, their resistance to compression in the direction of applied stress may be ignored. This is represented graphically by figure 1.9.

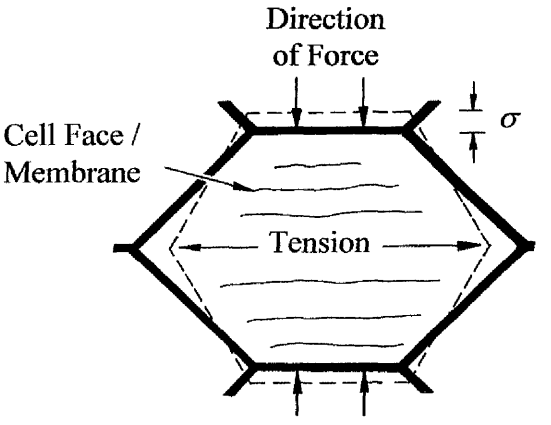

Figure 1.9: Stretching of cell faces during compression (Gibson and Ashby, 1997)

If the cell faces do not rupture during the elastic region, compression of the gas within the cells may also increase stiffness and contribute to the mechanical properties (Mills and Zhu, 1999). If the gas pressure is close to atmospheric pressure (common with man made foams), then the contribution at this stage is negligible and may be ignored. The compressive Young's modulus is the slope of this initial linear section (Gent and Thomas, 1959; Gibson and Ashby, 1997).

2. Plateau (Plastic Bending)

Upon reaching the plastic yield point, σ_{pl}, stress is no longer proportional to strain. If the gas pressure in the cells is significantly greater than atmospheric pressure then the cell membranes will be in tension and will, therefore, contribute towards the plastic yield stress. However, the cell pressure in man made foams is usually very close to atmospheric pressure and will, therefore, have negligible contribution initial foam collapse (Zhang *et al.*, 2003). The stress strain curve then levels out to form a plateau region where, as strain increases, there is little corresponding increase in stress. The plateau region shown in figure 1.8 is a result of the non recoverable plastic deformation of the cellular structure. Plastic deformation takes place in the cell struts and the

cell membranes. The cell struts form plastic hinges which rotate and permanently deform. The plastic collapse of the cells also causes deformation of the cell membranes which span the cell faces. As they are very thin, the cell membranes easily crumple in the direction of load and in this way have negligible contribution to the overall foam stiffness. However, at right angles to the load direction, the cell membranes undergo stretching as shown in figure 1.10. The work required to do this contributes significantly to the yield strength of the foam (Gibson and Ashby, 1997).

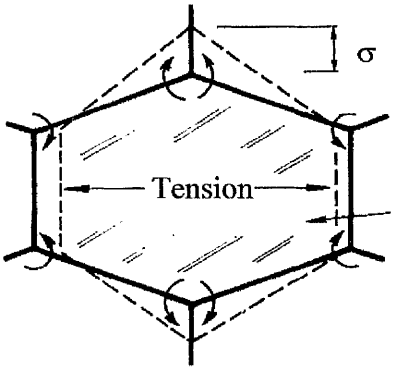

Figure 1.10: Formation of plastic hinges during plastic yielding and collapse

During collapse, the contribution of the gas within the cells must also be considered. If the gas is at atmospheric pressure then its contribution is usually very small. However if the pressure is greater than atmospheric then its contribution becomes significant.

3. Densification

At high strain values, the compressive stress rapidly increases and is a result of foam densification. At this point, the compression of the foam becomes so great that the cell struts and membranes come into contact. At this point, the volume within the cells has been reduced to such an extent that the foam begins to behave more like a solid which produces the steep rise in stress.

1.6.2: Foam Density / Property Relationships

The effect of foam density upon mechanical properties is perhaps the most widely investigated physical relationship regarding polymer foams. It has been shown that foam properties are heavily reliant upon density (O'Connor, 1999; Khunniteekool and

Sims, 1995). Generally speaking, a reduction in foam density will cause a reduction in mechanical properties. The relationship between modulus and density is described by the classic equation shown in equation 1.15 (Gibson and Ashby, 1997),

$$E^* = K(\rho^*)^n \qquad \textit{(Eqn. 1.15)}$$

where E^* is the elastic (Young's) modulus of the foam, K is an empirically determined[15)]

where E^* is the elastic (Young's) modulus of the foam, K is an empirically determined constant, $\rho*$ is the density of the foam and n is also an empirically determined constant, normally in the range of 1 to 2 and may vary with the specific property. K is related to temperature and the properties of the polymer matrix. Alternatively, foam properties may be predicted using the assumption that the gas phase of the foam makes no contribution to the mechanical properties. In this case the relationship can be expressed using equation 1.16 (Klempner and Frisch, 1991),

$$E^* = E_s\left(\frac{\rho^*}{\rho_s}\right)^n \qquad \textit{(Eqn. 1.16)}$$

where E_s is the elastic modulus of the base polymer matrix and ρ_s is its density. The expression $\rho* /\rho_s$ may also be defined as the relative density and is an extremely important foam characteristic (Gibson and Ashby, 1997). Equations 1.15 and 1.16 have limited validity in terms of elastic properties in tension and compression but do not account for differences in cellular structure (Hilyard, 1982).

In the case of closed cell polymer foams, a variety of deformation mechanisms contribute to the compressive response. These are accounted for and described further in sections 1.6.2.1 to 1.6.2.3 using the simplified model of a closed cell shown in figure 1.11.

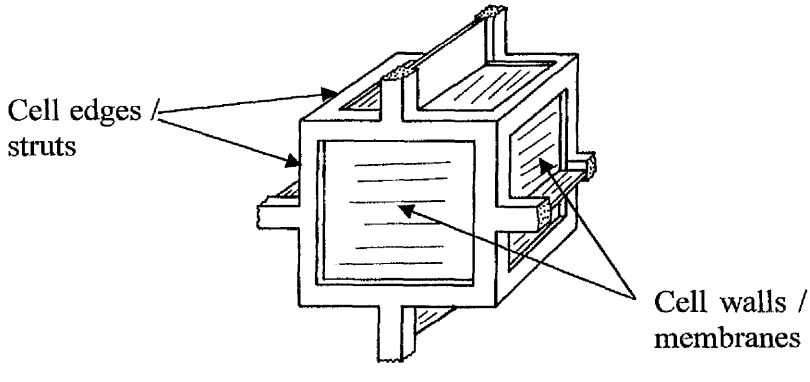

Figure 1.11: Simplified model of a closed cell foam

1.6.2.1: Initial Elastic Compression (Young's Modulus)

The initial linear response of a plastic – elastic foam to compression is a linear region where stress is proportional to strain and the deformation is recoverable. The Young's modulus may be predicted using equation 1.17,

$$\frac{E^*}{E_s} \approx \phi^2\left(\frac{\rho^*}{\rho_s}\right)^2 + (1-\phi)\frac{\rho^*}{\rho_s} + \frac{p_0(1-2v^*)}{E_s(1-\rho^*/\rho_s)}$$

Edge bending Face stretching Gas pressure

(Eqn. 1.17)

where E^* is the Young's modulus of foam, E_s is the Young's modulus of the solid polymer, ϕ is the fraction of the polymer within the cell struts, ρ^* is the foam density, ρ_s is solid polymer density, p_0 is the cell internal gas pressure and v is Poisson's ratio (the negative ratio of the lateral to the axial strain). Equation 1.17 is comprised of three terms which account for the possible mechanical contributions to the modulus i.e. strut bending, face stretching and internal cell gas pressure. Usually when foams are left after manufacture, the cell gas pressure equilibrates with atmospheric pressure. Since the internal gas pressure is much less than the Young's modulus of the base polymer, the third term in the equation becomes negligible (Zhang *et al.*, 2003). Equation 1.17 can, therefore, be reduced to equation 1.18.

$$\frac{E^*}{E_s} \approx \phi^2\left(\frac{\rho^*}{\rho_s}\right)^2 + (1-\phi)\frac{\rho^*}{\rho_s}$$

(Eqn. 1.18)

It may be noticed from equation 1.18 that E^*/E_s is proportional to ρ^*/ρ_s and that plotting the two terms against one another will result in a straight line. An estimation of the value of ϕ may be determined from the slope of the plot.

1.6.2.2: Plastic Yield Stress

The plastic yield region (point of curve inflection) represents the point at which stress and strain cease to be proportional and non-recoverable plastic deformation of the cell struts and membranes begins. An estimation of stress at a given strain in this region may be obtained using equation 1.19,

$$\frac{\sigma_{el}{}^{*}}{E_s} = 0.05\left(\frac{\rho^*}{\rho_s}\right)^2 + \frac{p_0 - p_{at}}{E_s}$$

(Eqn. 1.19)

where $\sigma_{el}{}^{*}$ is the elastic collapse stress and p_{at} is atmospheric pressure. If it is assumed that the gas pressure inside the cells equals atmospheric pressure then $p_0 - p_{at}$ becomes zero so the above equation may be reduced to equation 1.20.

$$\frac{\sigma_{el}{}^{*}}{E_s} \approx 0.05\left(\frac{\rho^*}{\rho_s}\right)^2$$

(Eqn. 1.20)

1.6.2.3: Post Collapse Behaviour

After the elastic yield point, the stress strain curve forms a flat plateau region where cell collapse takes place. Here allowances are made for the contribution of the internal cell pressure to the mechanical response. Theoretical stress values at given strain values may be calculated using equation 1.21,

$$\underset{\text{Wall Buckling}}{\frac{\sigma_{el}{}^{*}}{E_s} = 0.05\left(\frac{\rho^*}{\rho_s}\right)^2} + \underset{\text{Gas Compression}}{\frac{p_0\varepsilon}{E_s\left(1-\varepsilon-\rho^*/\rho_s\right)}}$$

(Eqn. 1.21)

where ε is strain. In addition to the term which accounts for the cell wall buckling contribution, a second term is added to allow for the stress contribution made by compression of the gas present within the closed foam cells.

1.7: Thermoplastic Crosslinking

Crosslinking bestows a range of new and enhanced properties on a thermoplastic polymer such as improved mechanical properties and resistance to organic solvents (Miroslav and Sebenik, 1993). Polymer melt strength and cell stability are increased during the foaming process thus reducing the danger of thermal collapse. Thermoformability is also improved which is required for many automotive applications. Many polyolefin foaming processes (particularly those involving a chemical blowing agent) require a certain level of base polymer crosslinking. All of these methods with the exception of the multi functional azide depend upon free radical generation for crosslinking.

1.7.1: The Crosslinking Requirement

Below their melting point, polyolefins demonstrate very high viscoelasticity. As temperatures are increased beyond this point, this property rapidly diminishes. This would result in thermal foam collapse (accompanied by blowing agent gas loss) due to the base polymer melt strength being insufficient to withstand the internal gas pressure generated by the blowing agent. As a consequence, foaming would only be possible within a very small window thus severely restricting the versatility and general viability of the whole process. To provide the necessary melt strength enhancement such that blowing agent gas retention is possible, polyolefins are crosslinked. This helps prevent thermal collapse, excessive drainage of material (and inevitable thinning) from the cell walls, and greatly expands the temperature range over which foaming is feasible. These benefits are outlined in figure 1.12 (Shiina, Tsuchiya and Nakae, 1972).

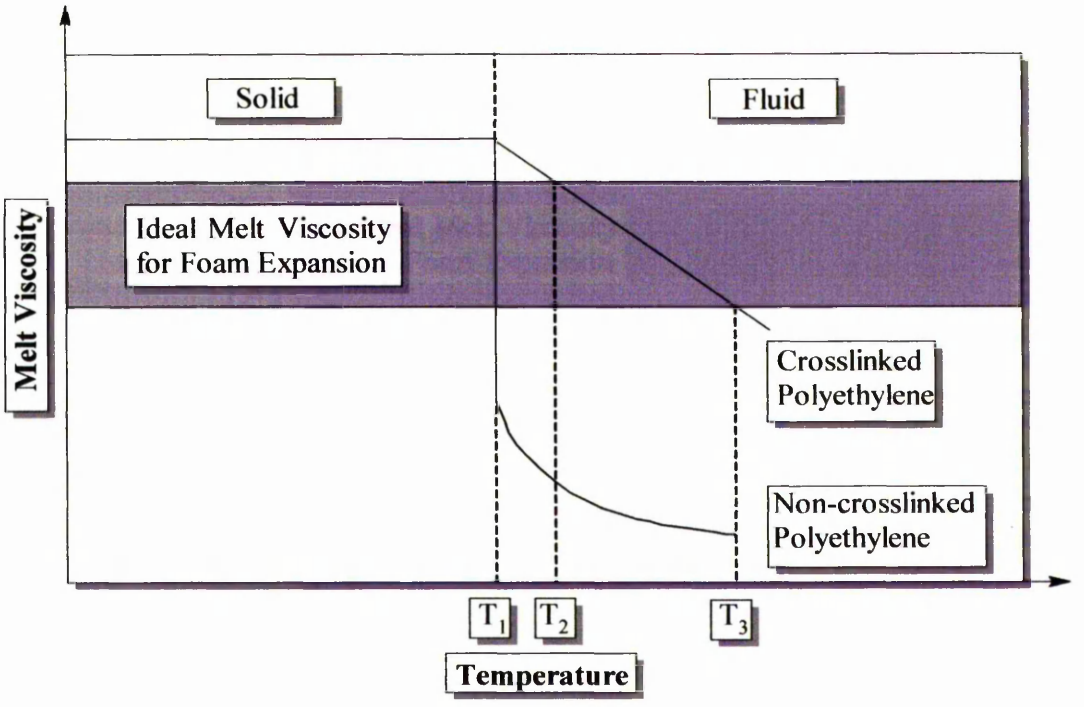

Figure 1.12: Effect of crosslinking on polyethylene

As figure 1.12 shows, the rubbery plateau of the polyethylene melt is extended resulting in an extended temperature range over which foaming may be accomplished. Mixing of the base polymer with the blowing and crosslinking agent is carried out between the polymer melting temperature, T_1, and T_2 where melt viscosity is low.

Dissociation of the crosslinking agent and subsequent polymer crosslinking then takes place between T_2 and T_3. After crosslinking, the compound is then heated further in order to effect blowing agent decomposition to generate the gas required for foaming. It is critical that crosslinking takes place at temperatures above the mixing temperature, to avoid premature crosslinking, but below the blowing agent decomposition temperature.

1.7.2: Crosslinking Techniques

There are four main industrial techniques for the crosslinking of polyolefins (Klempner and Frisch, 1991; Jer Tai, 1999).

1.7.2.1: Organo-silane (Silane Moisture Curing)

The initial step in organo-silane crosslinking is the grafting of a polyfunctional silane onto the main chain of a polyolefin polymer as shown schematically by equation 1.22.

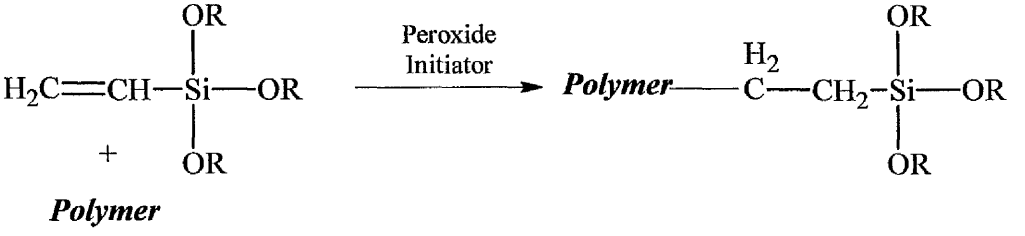

(Eqn. 1.22)

The silane group contains an unsaturated vinyl group as well as a number of alkoxy groups, which may then be hydrolysed as illustrated by equation 1.23.

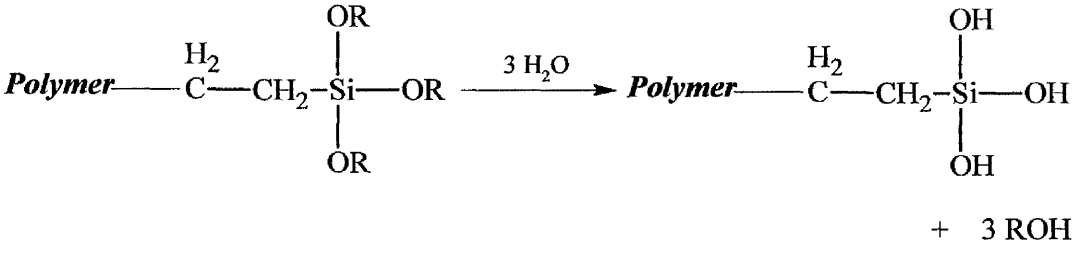

(Eqn. 1.23)

After hydrolysation, of the alkoxy groups, condensation takes place in the presence of a suitable catalyst (usually dibutyltin dilaurate) resulting in the formation of a siloxane bond, outlined in equation 1.24.

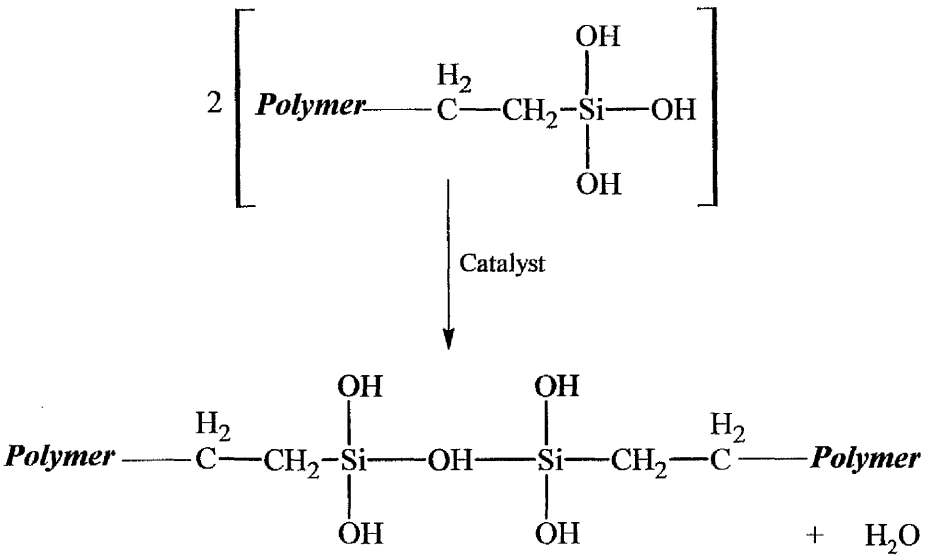

(Eqn. 1.24)

Although expensive and, therefore, infrequently used for polyolefin foam manufacture, silane crosslinking may be used with polyethylene and polypropylene polymers.

1.7.2.2: High-energy Radiation

There are various types of high-energy radiation that are exploited commercially in the crosslinking of thermoplastics. These include, x-, γ-ray, neutron and electron beam radiation of which the latter is the most common. Electron beam processing has been used in a variety of applications such as rubber vulcanisation, crosslinking of polyethylene sheet prior to foaming and improving the heat resistance of electrical flex insulation (Hoshi *et al.*, 1995). Many investigations concerning the crosslinking of polyethylene use electron beam energies of ~ 5 MeV although work has been undertaken using 10 MeV beams to improve penetration of thick components (Gheysari and Behjat, 2001). Crosslinking with electron beams proceeds by the generation of free radicals although it may to a certain extent take place by ionic reactions (Ghazali, Johnson and Dahlan, 1999). The energy from the electron has the effect of severing carbon-hydrogen bonds in the polymer chain thus generating free radicals as may be seen from equation 1.25.

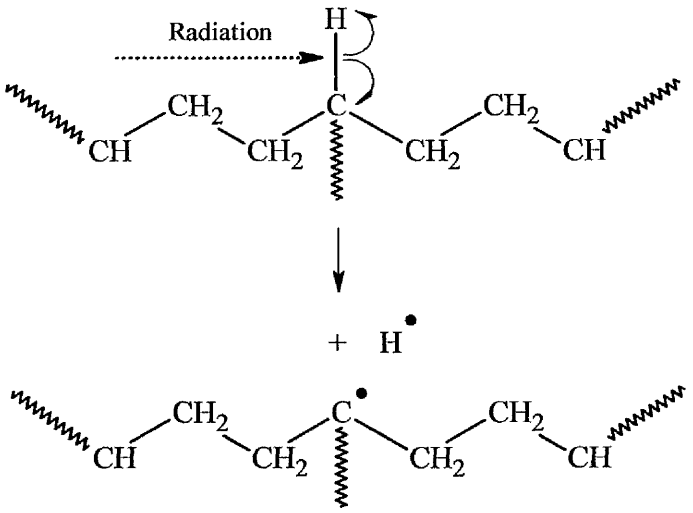

(Eqn. 1.25)

The hydrogen atoms extracted are preferentially tertiary hydrogens (found at the polymer chain branch points) as these bonds are the weakest (Kircher, 1987). The polymer chain radicals may then combine to form crosslinks as shown by equation 1.26 or chain scission may occur as illustrated by equations 1.26 and 1.27.

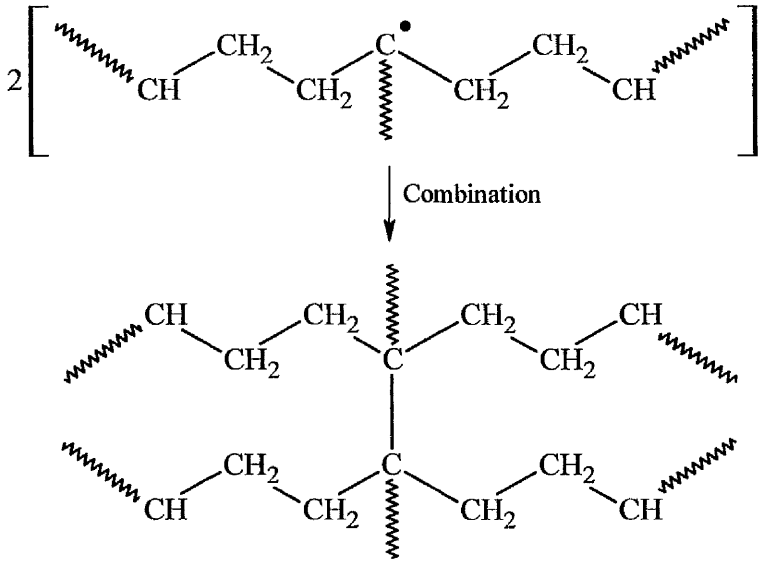

(Eqn. 1.26)

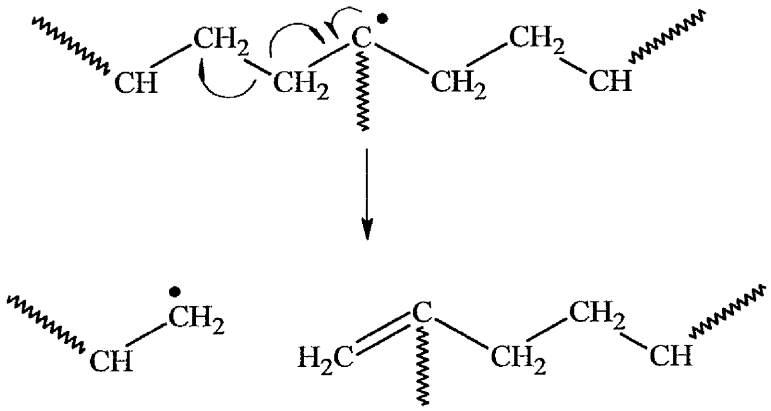

(Eqn. 1.27)

1.7.2.3: Functional Azide

Multi functional azides are often used in the crosslinking of polypropylene. Other crosslinking techniques involving free radicals present problems due to the occurrence of chain scission (β cleavage) within the polymer. Polypropylene contains a relatively high proportion of tertiary hydrogen atoms (compared with PE and EVA), which have lower bond energy than primary hydrogens. The lower bond energy corresponds to an increase in radical stability resulting in a decreased probability of dimerisation (Kircher, 1987). The chance of side reactions such as chain cleavage or combination with a primary radical is, therefore, increased. Multi functional azides alleviate this problem by crosslinking through a nitrene insertion reaction in which free radicals are not generated. Although free radical generation causes chain scission within other polymers, the important factor is that the rate of crosslinking far outweighs the rate of chain scission. This is not the case with polypropylene hence the requirement for a non free radical approach to crosslinking.

1.7.2.4: Peroxide Crosslinking

Peroxide crosslinking is a chemical method that proceeds via the thermal decomposition / cleavage of the peroxide to produce two oxy radicals as outlined in equation 1.28.

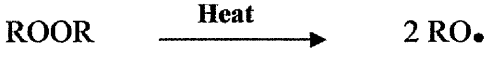

(Eqn. 1.28)

The oxy radicals generated may then abstract tertiary hydrogens (preferentially for reasons previously mentioned) resulting in polymer chain radicals, although other side reactions may take place. For crosslinking to take place two polymer radicals on adjacent chains must combine as previously shown by equation 1.26. Consideration of the peroxide decomposition temperature and the base polymer melting temperature must be taken into account when selecting a suitable peroxide crosslinking agent. Dissociation should take place above the polymer processing temperature to prevent premature crosslinking. There are numerous organic peroxides used industrially some of which are shown in figure 1.13 with their associated half life times ($\tau_{1/2}$).

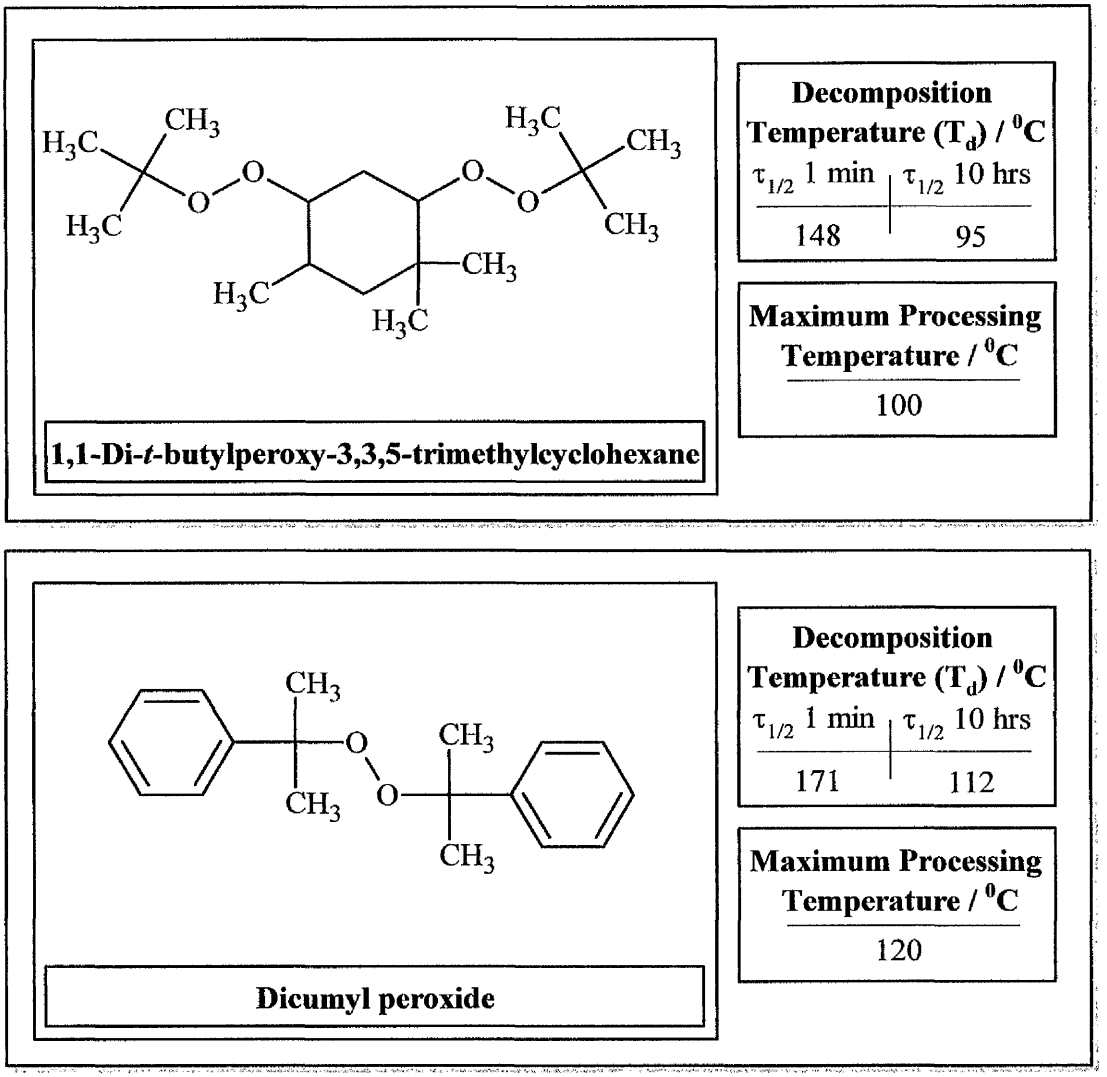

Figure 1.13: Common organic peroxide crosslinking agents (Klempner and Frisch, 1991) (continued overleaf)

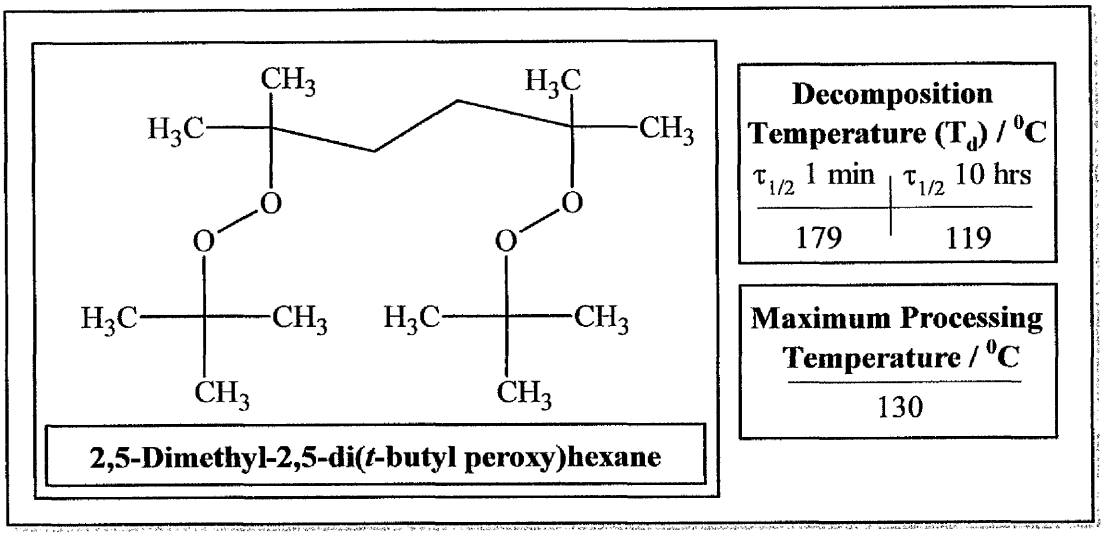

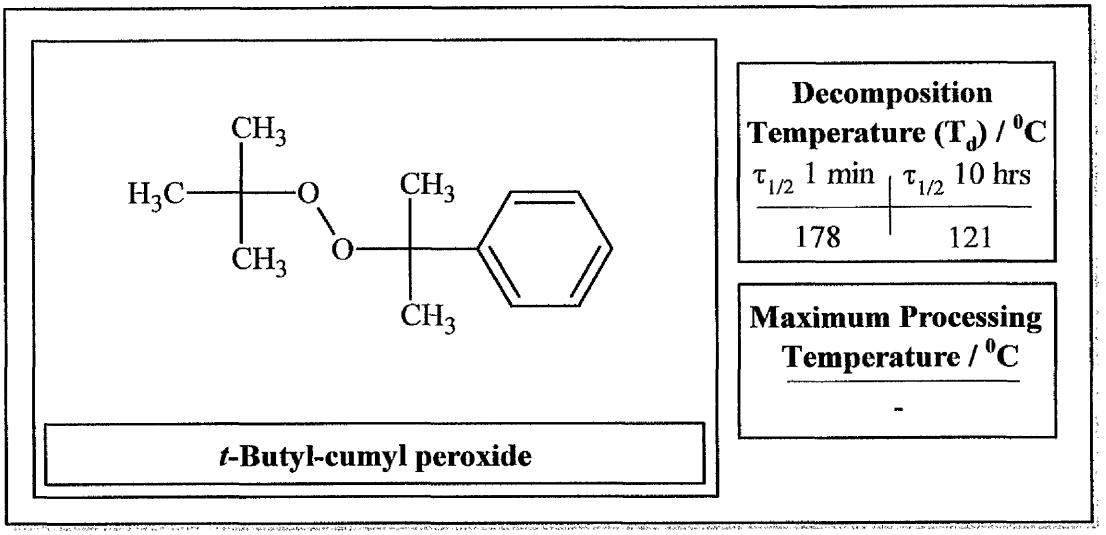

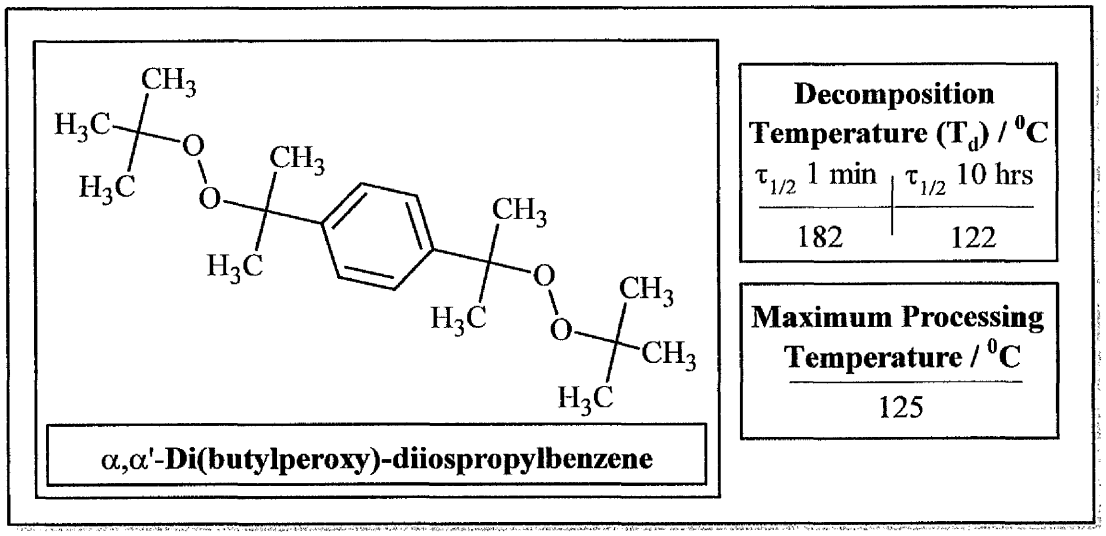

Figure 1.13: Common organic peroxide crosslinking agents (Klempner and Frisch, 1991) (continued)

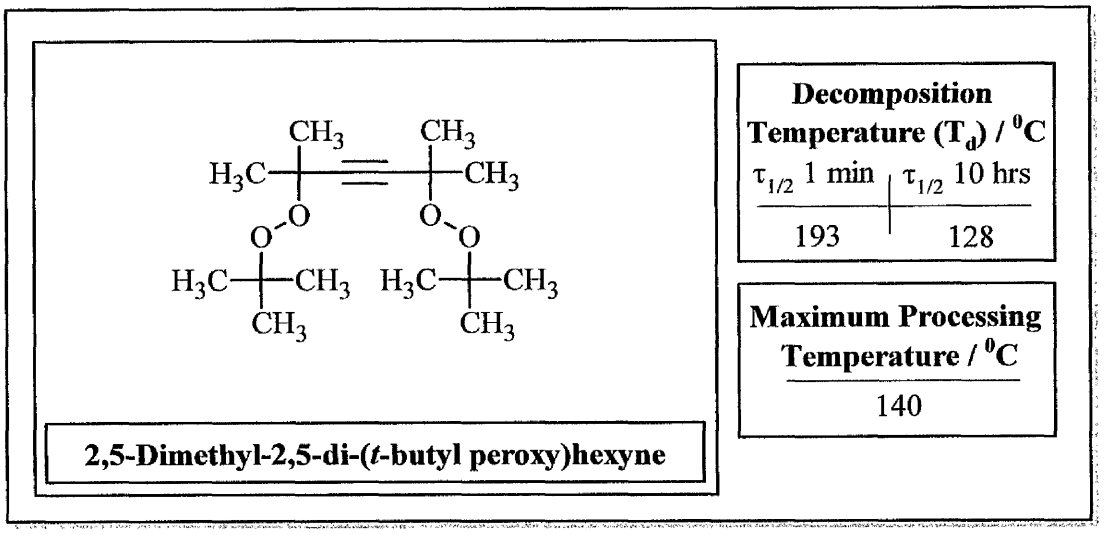

Figure 1.13: Common organic peroxide crosslinking agents (Klempner and Frisch, 1991) (continued)

1.7.3: Dicumyl Peroxide

Of the above mentioned crosslinking agents, the most suitable for polyolefin foam manufacture is dicumyl peroxide (DCP). The reason for its popularity is that its decomposition temperature is high enough to prevent premature crosslinking during compounding (particularly relevant for polymers with melting points of 100-120 ^{0}C such as polyethylene and ethylene vinyl acetate) but low enough to allow sufficient crosslinking rates during processing. As with other peroxide crosslinking agents crosslinking involves the generation of free radical species, which are produced by the thermal cleavage of the peroxide bond. This is outlined in equation 1.29 (Kmiec and Kamath, 1980).

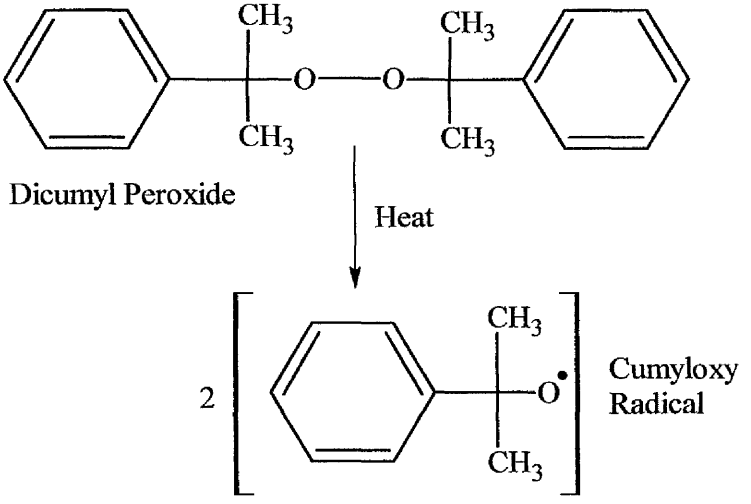

(Eqn. 1.29)

There are two main pathways the reaction may then follow. Hydrogen abstraction from a polymer chain by the cumyloxy radical may occur generating a polymer chain radical and 2-phenyl propan-2-ol. Alternatively β scission may take place producing acetophenone and a methyl radical as outlined in equation 1.30.

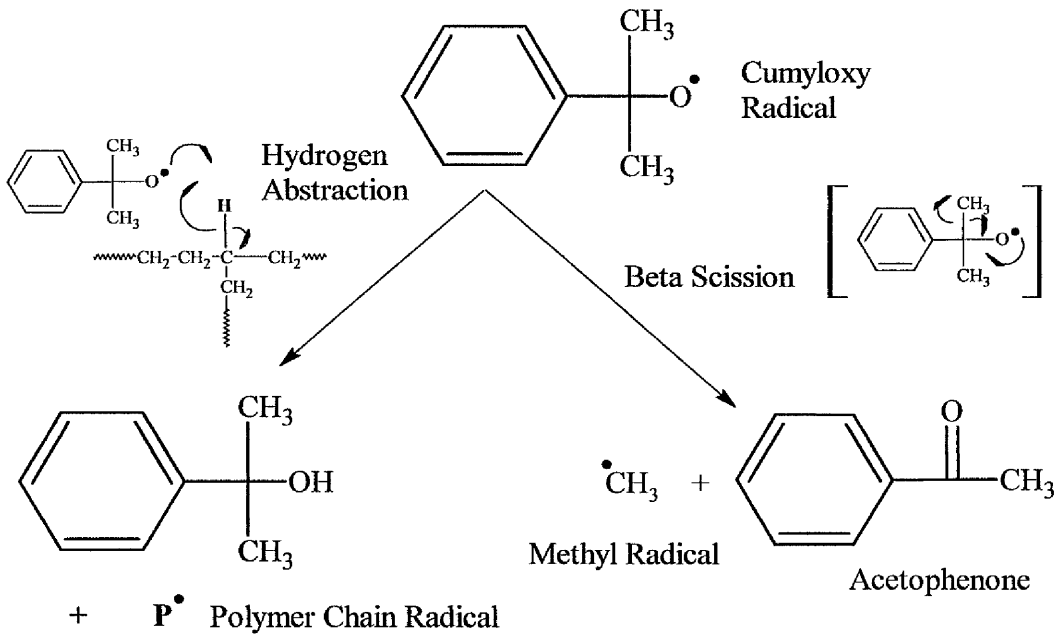

(Eqn. 1.30)

Equation 1.30 shows that methyl radicals may be generated by beta scission of the cumyloxy radical. The methyl radicals may also abstract hydrogen from a polymer chain to form a polymer radical. Crosslink formation requires the mutual termination of two adjacent polymer chain radicals as outlined in equation 1.31.

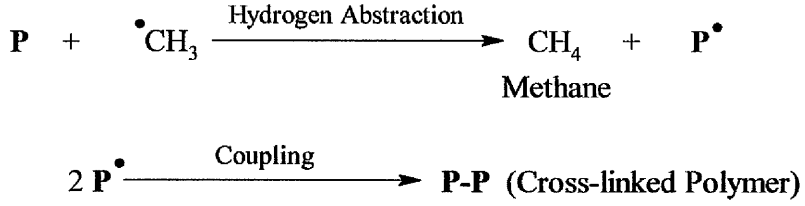

(Eqn. 1.31)

Methane has been known to form microcavities and accounts for 98 % gas production during the reaction of DCP (Kircher, 1987). The production of acetophenone is responsible for the intense and characteristic smell associated with the thermal decomposition of DCP.

1.8: Blowing Agents

A fundamental requirement in the formation of a polymeric foam is the introduction of a gaseous phase into a polymer matrix. The gas is then allowed to expand to produce cells, which are then stabilised by additional crosslinking and / or melt cooling. Gas introduction is often achieved by the use of a blowing agent, which, are classed as polymer additives and are designed and selected to decompose during the processing stage. During decomposition a large volume of gas is liberated and distributed within the polymer melt in small discrete cells thus forming a foamed structure (Quinn, 2001).

Blowing agents may be broadly divided into two classes, chemical and physical blowing agents. The class to which a blowing agent belongs is entirely dependant upon the method by which gas is introduced to the polymer.

1.8.1: Physical Blowing Agents

A point worthy of emphasis is that physical blowing agents (PBA's) do not undergo any chemical changes during gas liberation and that gas evolution takes place purely by a physical process. There are three main mechanisms of PBA gas liberation. These include evaporation of a low boiling point liquid, the desorption of an adsorbed component (on an inert substrate commonly diatomaceous earth, activated carbon, silicates or calcium carbonate) and direct gas saturation of a base polymer under elevated temperature and pressure. Physical blowing agents are often volatile liquids such as pentane (used in the expansion of polystyrene) and also encompass gasses introduced directly into molten polymer under high pressure, often nitrogen or carbon dioxide (Sims and O' Connor, 1998). Foaming with PBA's is achieved by the rapid reduction of pressure (as in gas saturation techniques) or by an increase in temperature. An advantage associated with the use of volatile liquids is that the process of evaporation reduces latent heat in the system thus enhancing melt strength and increasing foam stabilisation. However the pumping and storage facilities required for these liquids as well as the additional risk from explosion and flammability represent a significant drawback (Klempner and Frisch, 1991).

The use of halogenated hydrocarbons such as chlorofluorocarbons (CFC's) was once widespread in foam manufacture. Since the discovery of their adverse effect on

stratospheric ozone and the subsequent restrictions placed on their usage, demand for these materials has understandably fallen (Sims and O' Connor, 1998). As a consequence of these problems, much research attention is now being focussed on the development of chemical blowing agents.

1.8.2: Chemical Blowing Agents

Chemical blowing agents (CBA's) are a group of materials that are designed to decompose and evolve a large quantity of gas during foam processing. Gas production involves the chemical reaction of the blowing agent or the interaction with other additives. Some of the most widely used CBA's are depicted with relevant data in figure 1.14 (Methven, 1990; Klempner and Frisch, 1991).

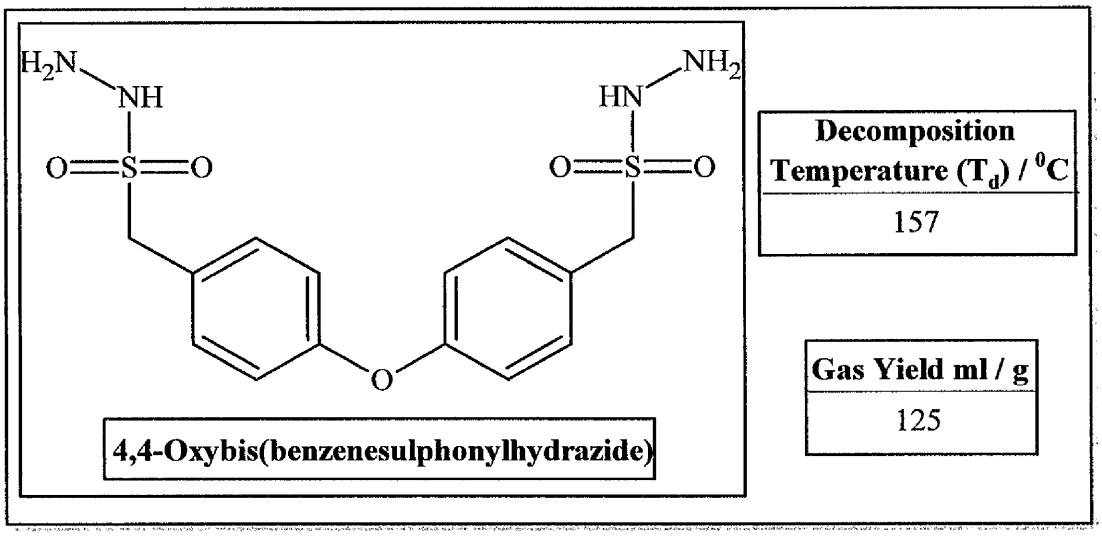

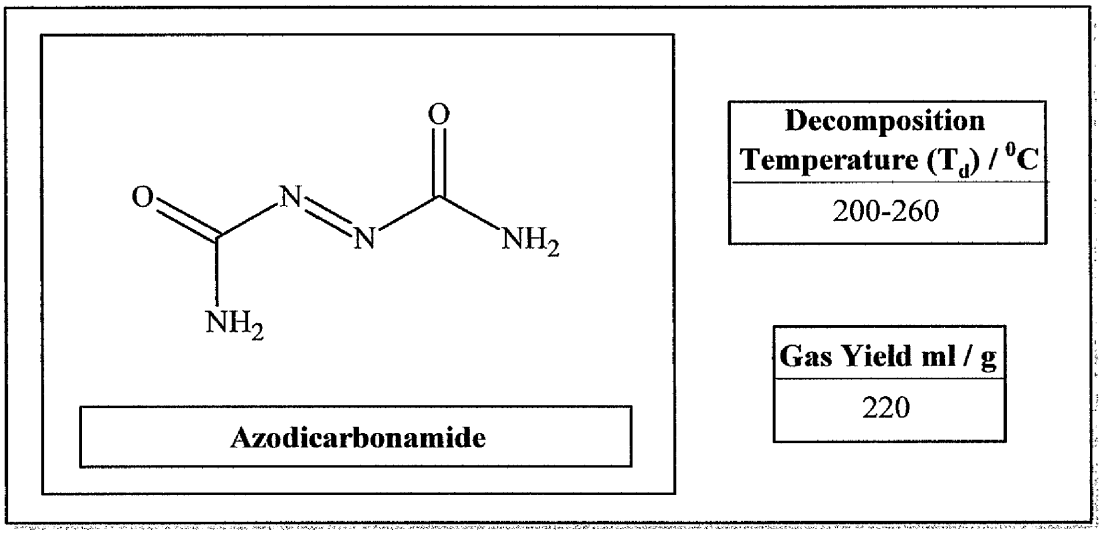

Figure 1.14: Common chemical blowing agents (continued overleaf)

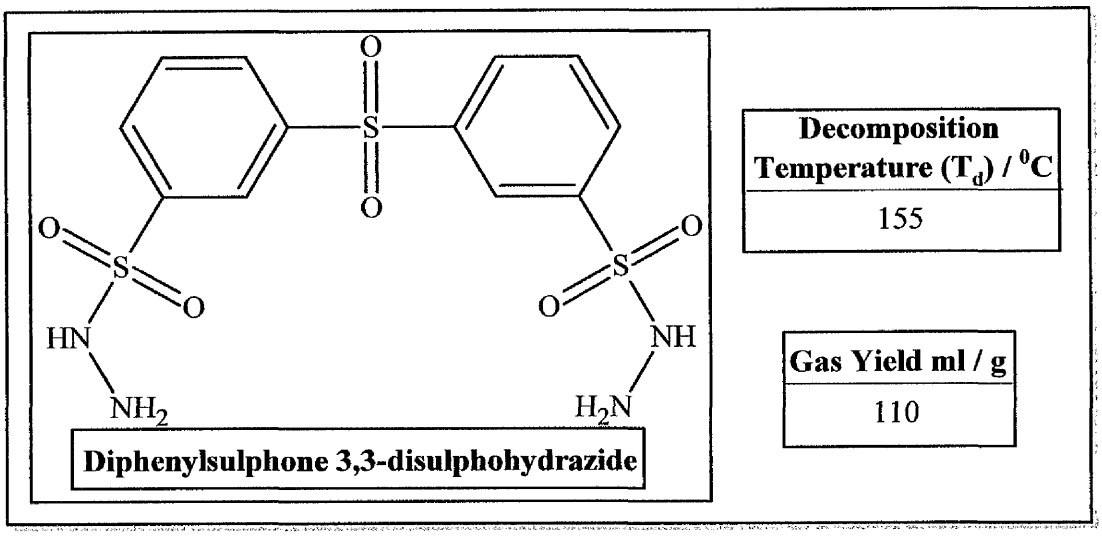

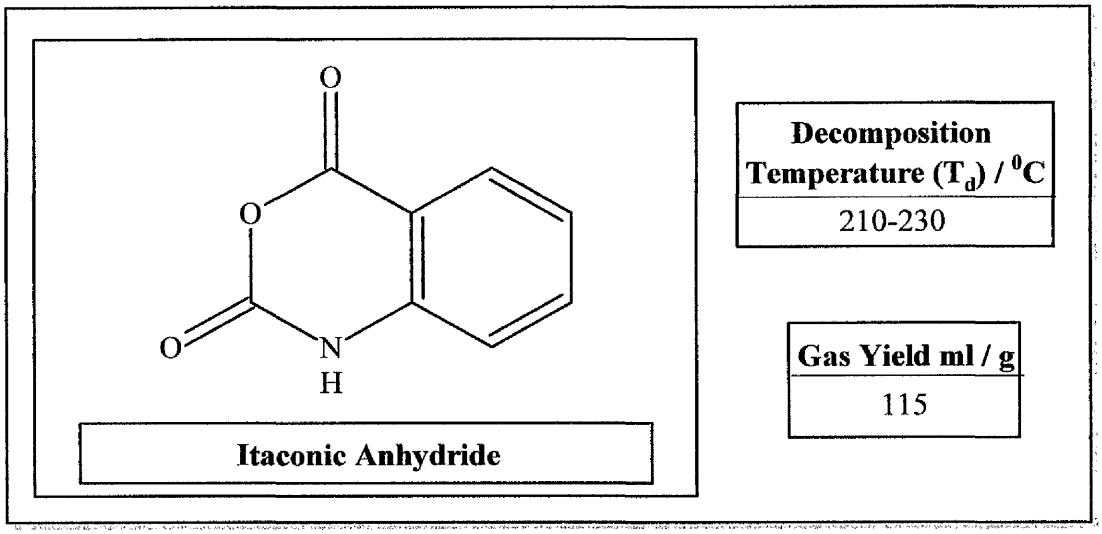

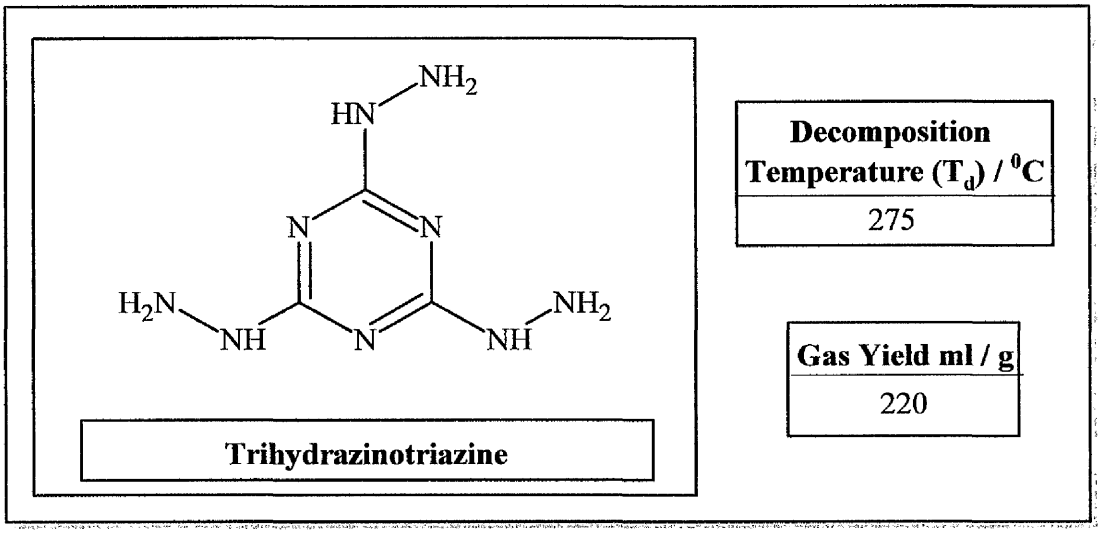

Figure 1.14: Common chemical blowing agents (continued)

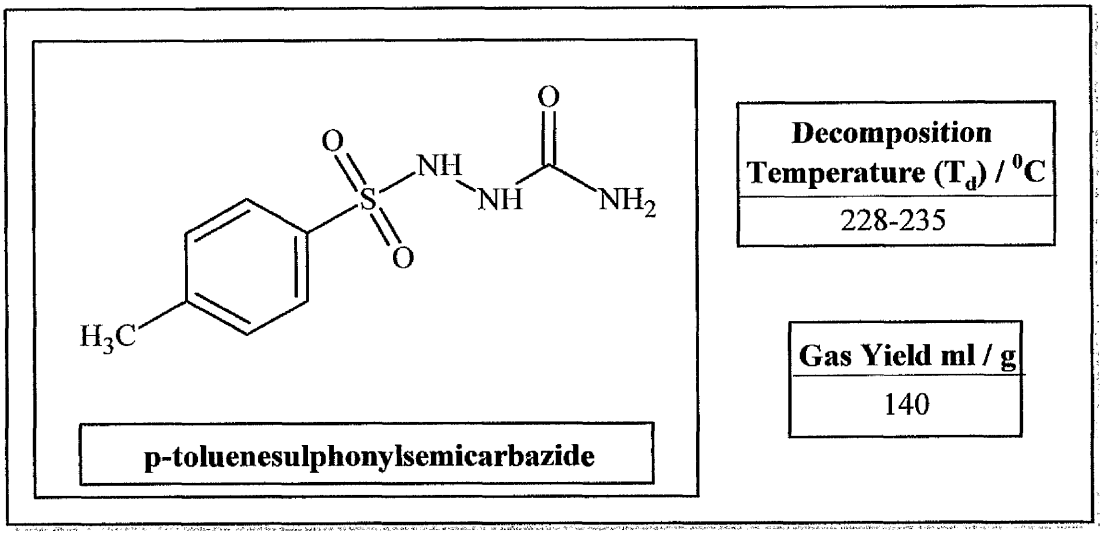

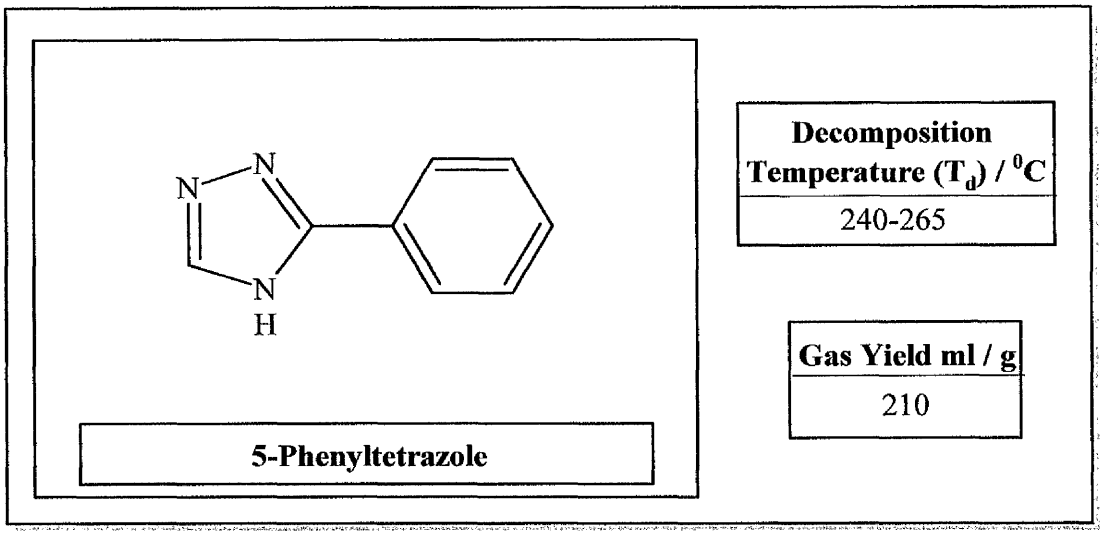

Figure 1.14: Common chemical blowing agents (continued)

CBA's that liberate gas as a result of thermal decomposition are known as porofors. Often the main gasses evolved are nitrogen and carbon dioxide as well as other gasses in smaller quantities.

1.8.3: Azodicarbonamide

The most industrially important blowing agent, particularly for the production of crosslinked polyethylene and PVC foams (Sims and Jaafar, 1994), is azodicarbonamide (ADC), which accounts for the vast majority of CBA consumption (~ 90%) in Western Europe (Methven, 1990). The reason for this popularity stems from the ability to dictate to a large extent the decomposition temperature. The range of achievable decomposition temperatures is compatible with processing temperatures of a broad range of thermoplastics. Decomposition temperatures generally range from

155 ^{0}C for highly activated grades to 220 ^{0}C for pure ADC. Reduction in decomposition temperature is achieved with the use of suitable activators (also known as kickers); commonly used activators include zinc salts (often ZnO). Additives may also be used to modify the gas yield and release rate of ADC (Jaafar and Sims, 1993). A summary of the benefits associated with ADC is presented below (Sims and O'Connor, 1998; Klempner and Frisch, 1991).

i. Large gas volume evolved per unit weight.
ii. High rate of gas yield.
iii. Decomposition characteristics may be modified to accommodate a range of thermoplastics.
iv. Decomposition products and residues are of low toxicity.
v. Loss of cell gas through diffusion to atmosphere is negligible as the primary decomposition product is nitrogen which constitutes the main fraction of the atmosphere.

Although the main reaction product of ADC is nitrogen the overall process is highly complex involving numerous side reactions and the production of sublimate and a residue. Many of the important pathways are shown below in equations 1.32-1.39 (Jaafar and Sims, 1993; Methven 1990).

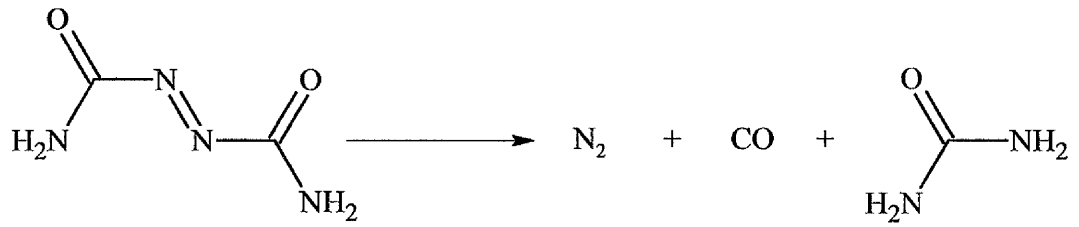

Azodicarbonamide Urea

(Eqn. 1.32)

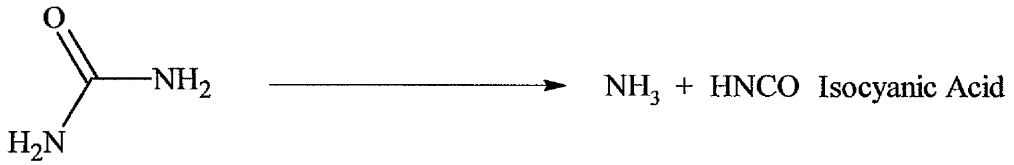

(Eqn.1.33)

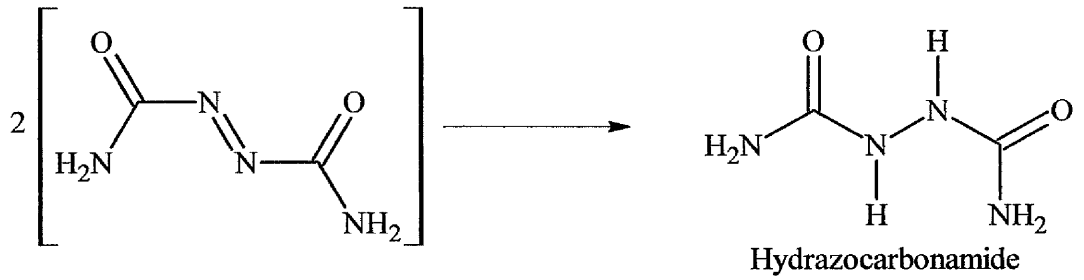

Hydrazocarbonamide

+ N_2 + 2HNCO

(Eqn. 1.34)

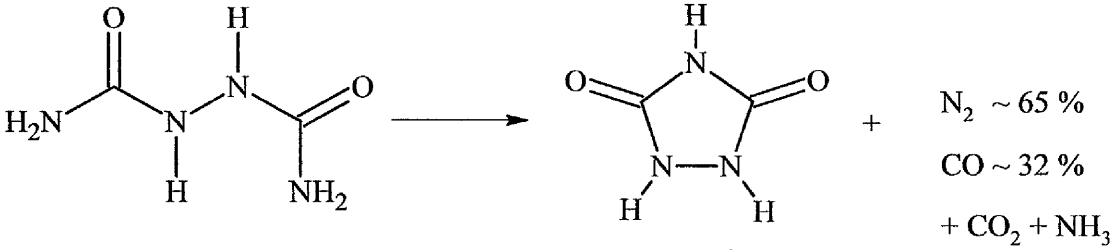

Urazole

+ N_2 ~ 65 %
CO ~ 32 %
+ CO_2 + NH_3
+ Sublimate

(Eqn. 1.35)

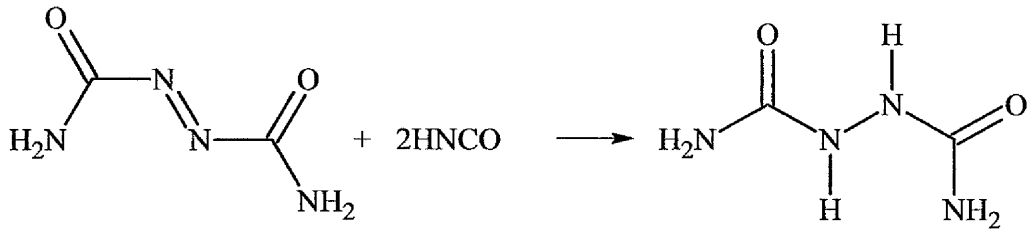

Hydrazocarbonamide

+ N_2 + 2CO

(Eqn. 1.36)

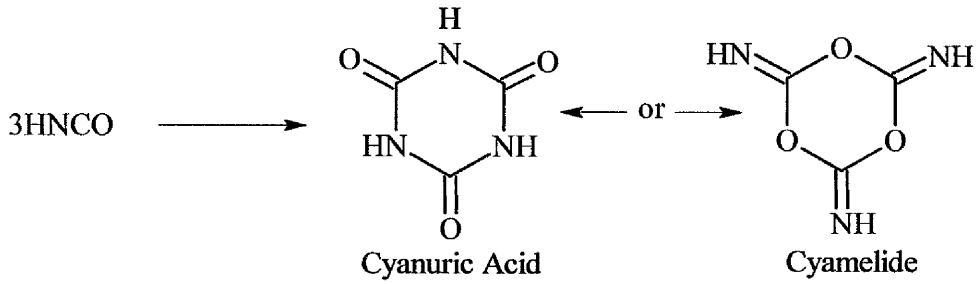

Cyanuric Acid Cyamelide

(Eqn. 1.37)

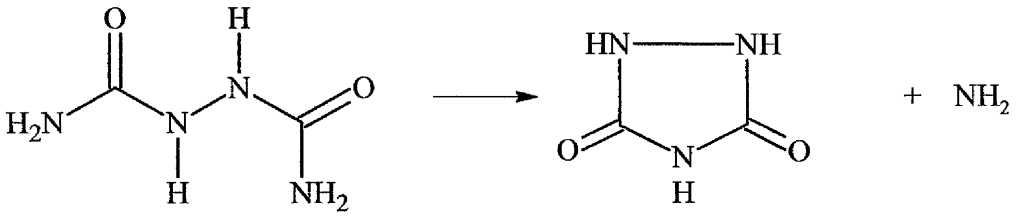

(Eqn. 1.38)

$$HNCO + H_2O \longrightarrow CO_2 + NH_3$$

(Eqn. 1.39)

1.9: Foam Expansion and Control

The easiest way of describing the process of foam expansion and control is when crosslinking, blowing agent decomposition and volumetric expansion occur relative to one another. When crosslinking at ambient pressure using a peroxide, it is important that sufficient crosslinking has taken place to provide the increase in melt strength necessary to retain the gas generated by the blowing agent. Figure 1.15 depicts the events occurring during simultaneous chemical crosslinking and foaming.

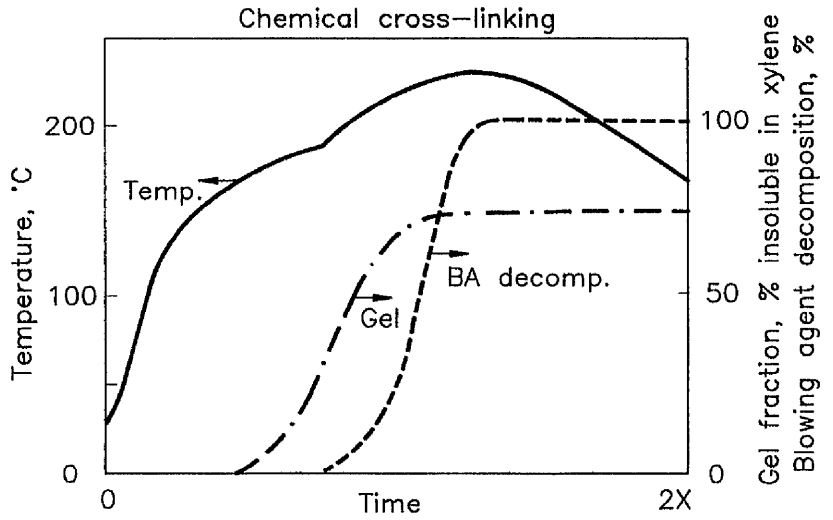

Figure 1.15: Thermal history of the chemically crosslinked foaming process

As figure 1.15 shows, at the beginning of blowing agent decomposition, the gel fraction is around 30 % and the temperature is in the region of 170 °C. Heating to this point must proceed gradually in order to allow the peroxide time to decompose and produce sufficient crosslinking before blowing agent decomposition begins. Both the blowing and crosslinking agents react to heat. It is important, therefore, that they

have sufficiently different half-life times. As a result careful selection of raw materials and precise control of process conditions are necessary (Klempner and Frisch, 1991; Trageser, 1977).

When crosslinking is achieved using radiation, all crosslinking is completed before blowing agent decomposition and expansion take place, as outlined in figure 1.16.

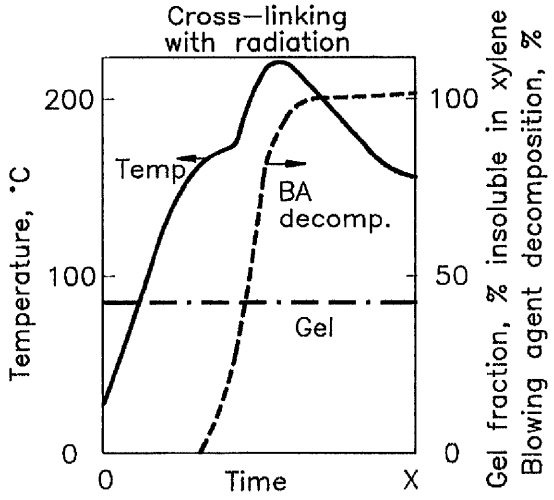

Figure 1.16: Thermal history of the radiation crosslinked foaming process (Trageser, 1977)

This process does not suffer the heating rate restrictions imposed by the crosslinking rate and can take place twice as fast. This is also applicable to batch processes where crosslinking and full or partial blowing agent decomposition take place under pressure and precede volumetric expansion. As such, selection of blowing agents in these systems is made much simpler as the timing of crosslinking relative to expansion is controlled by means other than heat (Klempner and Frisch, 1991; Trageser, 1977).

1.10: Methods of Crosslinked Polyolefin Foam Production

The production of crosslinked, cellular polyolefins has been of significant commercial interest in Europe and Northern America since the mid 1970's (Puri and Collington, 1988 **(a)**). The literature reports many processes including batch and continuous methods.

1.10.1: Crosslinked Polyethylene Foam Production

Globally there are four main processes that account for the majority of crosslinked polyethylene foam production. These were developed and are operated by The Hitachi Chemical Co. (Asaaka *et al.,* 1968), Toray Industries Inc (Shinohara *et al.,*

1971), Furukawa Electric Co. (Hosoda and Shina, 1972) and Sekisui Chemical Co. (Sagane *et al.*, 1973). These polyethylene foam production methods are all based on either semi-continuous or continuous extrusion methods. The Toray and Sekisui processes use electron beam radiation for crosslinking whilst Hitachi and Furukawa processes use chemical crosslinking methods. A fifth process of commercial importance is the nitrogen impregnation process developed and operated by Zotefoams (Cooper, 1961; Cooper, 1972).

1.10.1.1: Chemically Crosslinked Techniques

The chemical crosslinking process operated by Furukawa and Hitachi is represented below by figure 1.17.

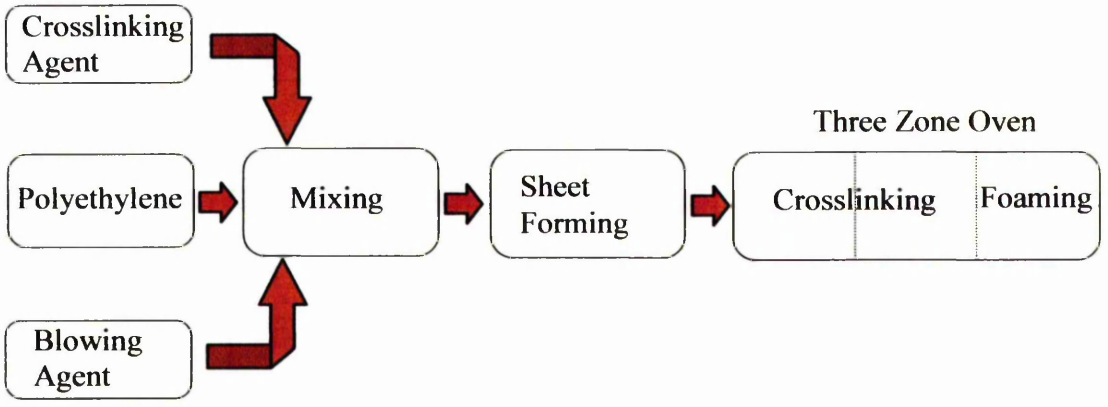

Figure 1.17: Flow diagram outlining the chemically crosslinked, continuous polyolefin foam production process (Klempner and Frisch, 1991)

The first step involves the mixing of the polymer with crosslinking and blowing agents in a twin-screw extruder or internal mixer and is performed at temperatures above the base polymer melting point but below temperatures where crosslinking occurs. After mixing, the masterbatch is pelletized before being extruded as a polymer sheet. Compounding with crosslinking and blowing agent takes place at temperatures above the melting point of the polymer but low enough to prevent dissociation of the thermally unstable crosslinking agent. The extruded sheet dimensions are pre-calculated such that the foamed sheet has the desired density, thickness and width. Great care must be taken with regards to temperature control during the mixing and sheet formation phases of the process. As the peroxide is thermally unstable, there is a risk of premature crosslinking. The sheet is then passed

through and heated in a multi zone hot air convection oven to allow crosslinking and expansion. The type of oven used in the Furukawa process is shown schematically in figure 1.18.

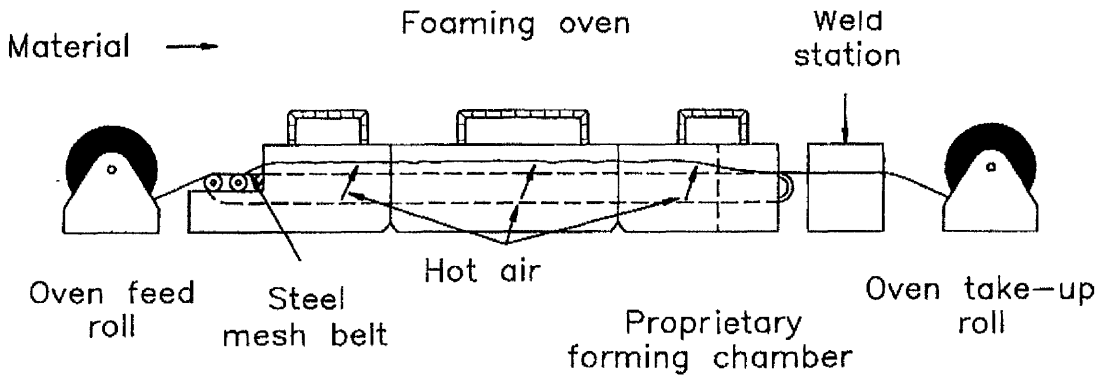

Figure 1.18: Furukawa horizontal foaming oven (Klempner and Frisch, 1991)

The Furukawa method uses a continuous steel mesh belt to carry the uncrosslinked, unexpanded compounded sheet through a three zone foaming oven. In the first zone of the oven, temperatures are set at around 140 °C, which is high enough to perform some crosslinking and permit stress relaxation of the polymer sheet. Higher temperatures are then used in the second zone of the oven, typically between 170 °C and 210 °C, to perform rapid crosslinking of the polymer sheet. In the third oven zone, temperatures are raised to 220 – 250 °C in order to decompose the blowing agent and generate the gas necessary for expansion. Directly impinging hot air flow from a series of slots in plenum chambers that are positioned directly above and below the conveyor are used to maximise heat transfer into the unexpanded sheet. The air jets also release the polymer sheet from the wire conveyor after crosslinking and support it during the expansion phase of the process. It is important that the sheet is released from the conveyor otherwise tearing of the foam and poor density reduction will result (Puri and Collington, 1988 **(a)**).

Although the Hitachi and Furukawa processes are, in many respects, very similar, the Hitachi process differs by the inclusion of an infrared preheating crosslinking oven and the replacement of the wire mesh belt in the expansion zone of the oven with freely rotating steel rolls. Although the process requires more critical control over the crosslinking rate and the balance between crosslinking and expansion, it has a number of advantages. The separate crosslinking section results in a higher level of surface crosslinking, which gives lower foam densities than the Furukawa process. Expansion of the crosslinked sheet is totally unrestricted on leaving the crosslinking section

resulting in a smoother surface and fine cell structure. The increased strength allows free expansion to take place in the air stream resulting in smooth skin and low pinhole formation (Klempner and Frisch, 1991; Puri and Collington, 1988 **(a)**).

1.10.1.2: Radiation Crosslinked Techniques

The radiation crosslinking methods of polyolefin foam production, operated by Toray Industries and the Sekisui Chemical Co., are based on four main steps, mixing, extrusion, crosslinking and expansion. The steps are outlined in figure 1.19.

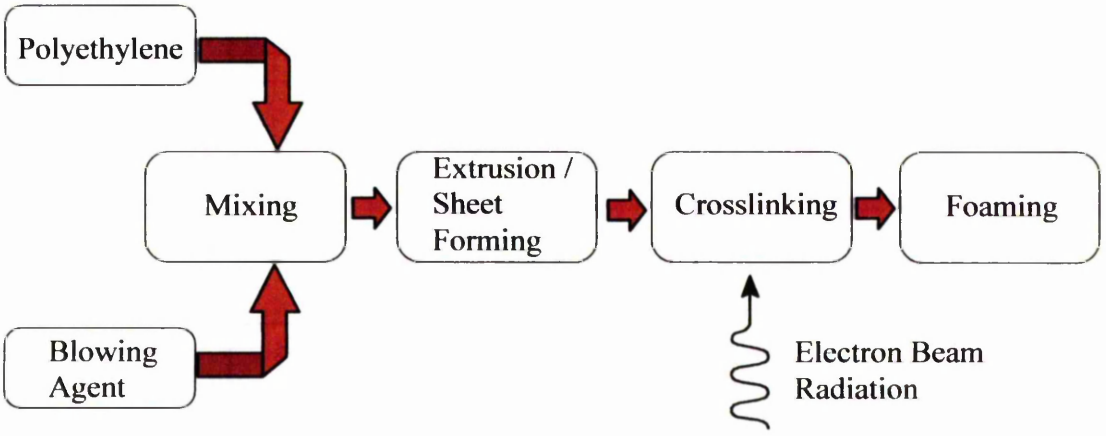

Figure 1.19: Flow chart outlining the radiation crosslinked polyolefin foam process (Klempner and Frisch, 1991)

The advantage of using radiation crosslinking is the complete separation of the crosslinking and expansion phases of the process. The temperatures used for chemical crosslinking and expansion overlap (Trageser, 1977). This results in a degree of blowing agent decomposition and foam expansion taking place before the sheet in completely crosslinked through its thickness. As a result, the elasticity of the melt will vary through the sheet thickness during the expansion process, leading to variations in cell size, cell agglomeration and density variations.

The initial step involves the blending of a large amount of blowing agent (10-20 phr) with the base polymer. Conventional single screw extruders are unable to provide the required level of mix homogeneity. Thus, intensive mixing devices such as ribbon blenders, Banbury mixers or two-roll mixers are used before the polymer and blowing agent are fed into an extruder. Powdered resin grades are also used to facilitate the mixing process. After mixing and forming by extrusion, the unexpanded sheet is exposed to a suitable radiation source (electron beam or cobalt 60 gamma ray source).

The crosslinking mechanism is essentially the same as chemical crosslinking, and is a free radical reaction. The energy from the electron beam removes a hydrogen atom from a polymer chain generating polymer chain radicals, which then react together to form crosslinks (Ghazali *et al.*, 1999). Expansion is then carried out as a separate operation and it is the oven design in this part of the process that distinguishes the two main production methods. The Sekisui and Toray foaming ovens are shown in figures 1.20 and 1.21.

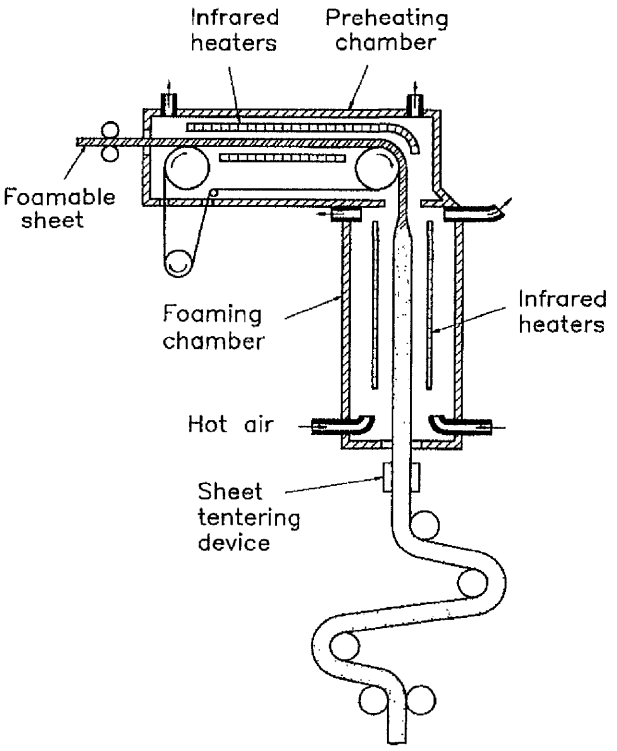

Figure 1.20: Sekisui vertical foaming oven (Sagane *et al.*, 1973).

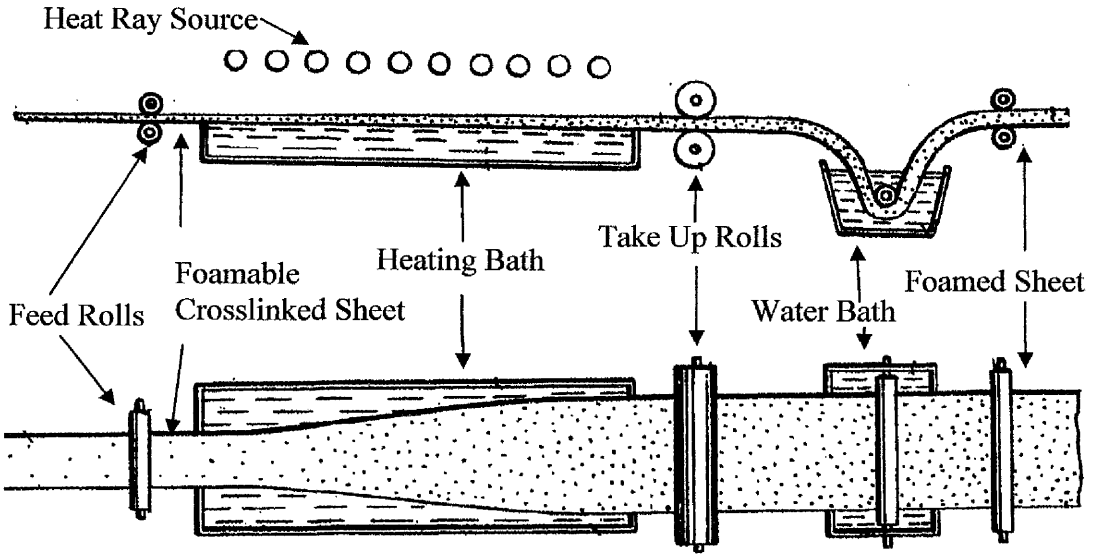

Figure 1.21: Toray foaming oven (Shinohara *et al.*, 1971)

The Sekisui method utilises a vertical foaming oven arrangement. The crosslinked foamable sheet is first carried on an endless steel mesh belt through an infrared preheating chamber where it is heated to around 150 °C. The mesh belt is coated with a fluorocarbon resin or a mould release compound to prevent the sheet from sticking to the mesh. Temperatures of 200 °C and above are used in the main foaming chamber, which uses a combination of re-circulating hot air and infrared heater banks. The sheet begins expanding as soon as it passes from the preheating section in to the foaming chamber. A sheet tentering device is used to keep the sheet spread out as it exits the oven.

In the Toray process, the polymer sheet is continuously introduced into the oven and expanded whilst afloat in a bath of molten salts allowing expansion to freely take place in all directions. The top of the foam sheet is heated using banks of infrared heaters, whilst heat is supplied to the bottom side by conduction from molten salts. As oxygen is excluded from the bottom of the sheet during expansion, this side is smooth and free from the effects of oxidative degradation.

1.10.1.3: Injection Moulding Batch Techniques

Injection moulding permits the manufacture of relatively complex articles with the advantages of minimised post moulding fabrication and a reduction in scrap material compared with compression moulding and extrusion techniques. The process is based on the simultaneous crosslinking and foaming of LDPE or EVA copolymers in a heated mould cavity.

The equipment is similar to that used in conventional injection moulding, however, the use of shut off nozzles and high injection rates are unnecessary as neither the crosslinking agent or the blowing agent are decomposed prior to injection. Screw design and accurate melt temperature control (100-115 °C) are important to maximise mixing efficiency whilst avoiding predecomposition of crosslinking or blowing agents. One of the major difficulties associated with this method is mould design. Heat transfer within the cavity can be problematic as can heat transfer uniformity over the total internal mould surface (Puri and Collington, 1988 **(b)**; Lee, 1997). Other design considerations include:

i. It is essential that the tool be insulated to maintain a surface temperature of 160-200 °C, dependant upon part wall thickness. Small variations in surface temperature, particularly around the parting line, may result in variations in crosslink density which would lead to surface splitting during expansion / ejection.

ii. The mould draw angles must allow for the considerable instantaneous part expansion upon mould opening and ejection. Again problems may be encountered with surface splitting.

iii. Insulated sprue bushes are required in order to reduce nozzle heat build up.

iv. Large mould clamping forces are required to withstand the large internal mould pressures generated by decomposition of the blowing agent and foam expansion.

1.10.1.4: The Nitrogen Autoclave Process

The nitrogen autoclave process (also known as the BXL process) is not widely used, although production has increased significantly in the last few years (Smith, 2000), and it has been operated successfully for ~50 years by Zotefoams plc. The technique is used for the foaming of high and medium density polyethylene as well as other metallocene polymers including EVA. The three fundamental phases of the nitrogen autoclave process are represented in figure 1.22.

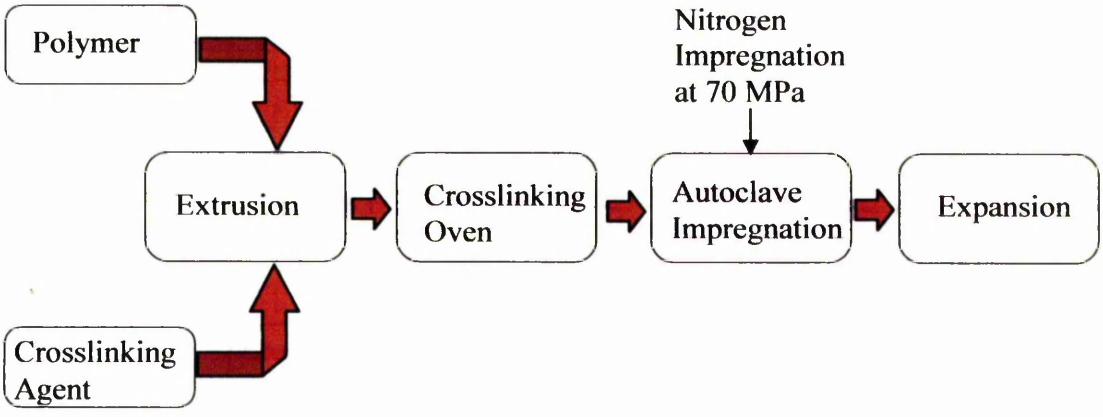

Figure 1.22: Outline of the nitrogen autoclave process (Eaves, 1988)

Phase 1. Extrusion and Crosslinking

An extruder is fed with granulated polymer accompanied by the relevant quantities of peroxide crosslinking agent and other required additives (no blowing agent is added at this point). The extruder is equipped with mixing elements such that the uniform distribution of additives within the polymer matrix is ensured. The extrudate is then passed through a die to produce a continuous polymer sheet, which is then cut to size. Decomposition of the peroxide crosslinking agent is then performed, by heating the sheet in a convection oven. Alternatives to peroxide crosslinking include electron beam and gamma radiation, these are particularly useful where the required extrusion temperature is high enough to preclude the use of peroxides.

Phase 2. Gassing

Having been cut to shape, the crosslinked polymer sheets are transferred into autoclaves. The temperature is then raised to above the softening point of the polymer and pure nitrogen is introduced to the autoclave. Henry's law may be used to relate the solubility of nitrogen in polyethylene to gas pressure at a known temperature, this law is, therefore, employed to control the quantity of gas dissolved in the polymer, which will in turn, dictate the final foam density. Crosslinking must also be considered as this stabilises the polymer and prevents flow during the gas uptake process. Crosslinking also improves the surface finish of the final product. After several hours, saturation is complete, and the pressure within the autoclave is rapidly reduced. This has the effect of decreasing the solubility of the gas within the polymer and hence promotes cell nucleation. Precise control is required during this section of the process, as the rate of gas release will determine the final foam cell size. After cooling the sheets, which exhibit around 10- 30 % expansion, are removed from the autoclave, at this stage they may be classified as foams (albeit very high density ~720 kg m^{-3}) with cell sizes of between 80 and 100 microns.

Phase 3. Expansion

The sheets are then transferred to a second autoclave. Here they are heated under low air pressure (to prevent premature expansion) to above the softening point of the polymer. The pressure is then reduced and the sheet expands to its final size. Although the capital outlay for the processing equipment is high and the internal dimensions of the autoclaves restrict the size of the product, the technique benefits

from some significant advantages. These include high uniformity of cell structure, no blowing agent residue, control over foam density by process parameters instead of formulation variables and environmentally safe blowing agent (ERP, 1961; ERP, 1972; Eaves and Witten, 1998; Eaves, 1993). Furthermore, the odour generated by the decomposition products of ADC is avoided. As the nitrogen used for expansion is abundant in the atmosphere, the foams show good ageing properties and excellent dimensional stability as exchange of cellular gas with the atmosphere (~80 % N_2) has a negligible effect. It is also possible to modify the density and cell size by variation of the process conditions instead of formulation variations (Eaves and Witten, 1998).

1.10.2: Press Moulding

Press moulding techniques (compression moulding) are purely batch process techniques and were originally beset by problems concerning poor platen area utilisation and inevitable economical implications. Many of these issues have been addressed by developments which have resulted from the demand for complex, thick section, non-laminated components (Puri and Collington **(b)**, 1988). The technique may be split into two subgroups: one step and two step processes as outlined by figure 1.23.

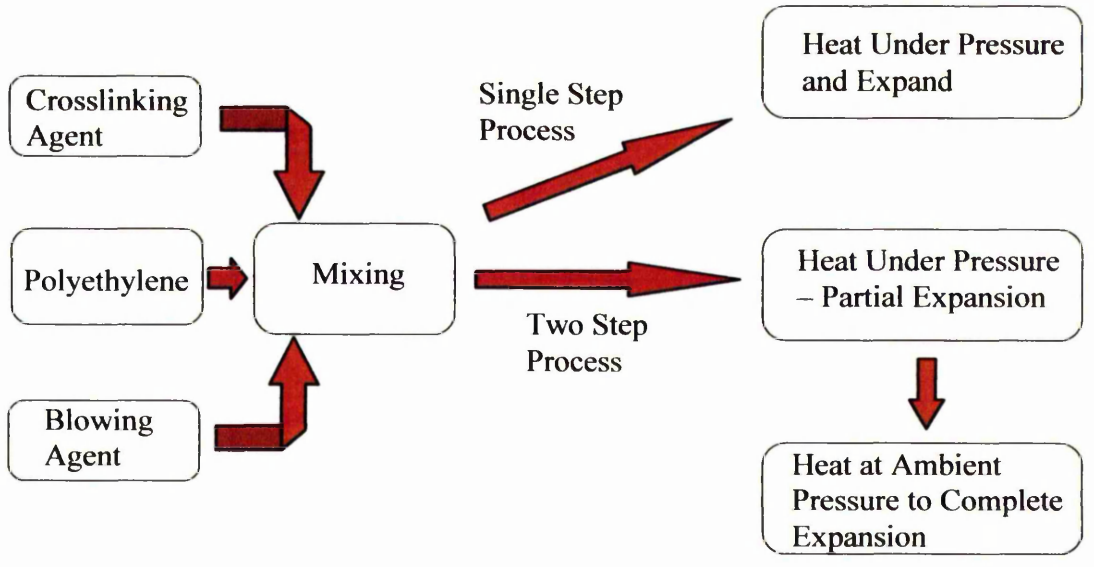

Figure 1.23: Crosslinked polyethylene foam compression moulding process

1.10.2.1: Single Stage Moulding

Essentially the single stage compression moulding technique involves the filling of a mould with polymer mixed with crosslinking and blowing agent. The mould is then closed and heated under pressure to effect crosslinking agent dissociation and blowing agent decomposition. The mould is then opened resulting in simultaneous, instant expansion and ejection of the component. The drawbacks inherent to this method (listed below) have hindered its development.

i. Mould designs must allow for the high internal pressures generated by the production of gas by the blowing agent. High clamping pressures are also required.

ii. To reduce the risk of splitting and moulding deformation, high mould opening speeds, in the order of 10 cm per second and greater, are required. This necessitates the use of bottom opening presses or modifications to the hydraulic system to facilitate increased opening speeds.

iii. Low-density materials limit the platen area usage to around 30 %. Areas in excess of this may result in splitting of the moulding or contact being made with the mould guide pillars and / or platen surface on expansion again resulting in surface imperfections or splitting.

1.10.2.2: The Heat Transfer Process

This process follows the same method as the single stage process, however, lower temperatures are used such that crosslinking takes place but only partial blowing agent decomposition is achieved. After opening the mould, the component exhibiting a small degree of expansion is quickly transferred to a circulating hot air oven to complete blowing agent decomposition and component expansion. In this way the expansion at the press may be limited so that increased use of the platen area may be achieved and the economics of the process are improved. Greater control of the expansion process also results in less surface splitting and improved cell size control.

1.10.2.3: The Heat and Chill Process

The primary stage in this process (developed by Schering Industrial Chemicals) is

again similar to that used in the single stage process. The times and temperatures used, however, ensure the complete reaction of crosslinking and blowing agent. The platens and mould are then water cooled under pressure to below the softening point of the polymer. The mould is then opened and the blank showing a small degree of suppressed expansion is transferred to a circulating hot air oven (set at above the softening point of the polymer) to allow expansion to take place. This allows maximum platen area usage as very little expansion takes place at the mould. A high degree of control promotes fine cell structure and allows the production of low-density materials (typically 25-250 kg m^3).

1.11: Microwave Heating

The use of microwaves for heating applications dates back to the 1940's and is, therefore, a recently developed process for energy transfer. The first successful polymer industry application was achieved in the 1960's in the rubber tyre industry whilst other applications were found in textiles and food (Wei, Shidaker and Hawley, 1996). The advantages of this technique include rapid volumetric heating, reduced cycle times, the ability to selectively heat target components within a compound and more accurate temperature control. It is also not necessary to for the heated component to be in contact with a heating surface.

1.11.1: Nature of Microwaves

Microwaves are oscillating electromagnetic waves and occupy the region of the electromagnetic spectrum corresponding to waves of wavelength 1mm to 1m, and frequencies (v) of 300 GHz to 300 MHz, respectively (Jacob *et al.*, 1995) as illustrated by figure 1.24.

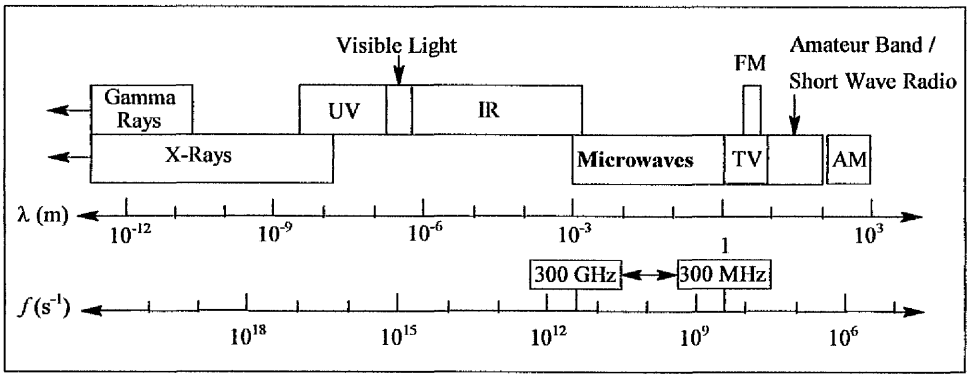

Figure 1.24: Microwave heating frequency locations in the electromagnetic spectrum (Wei, Shidaker and Hawley, 1996)

Microwaves are commonly used for communication applications such as mobile telephones but the main non-communication use is heating. Frequencies are designated by the International Telecommunication Union for industrial, scientific and medicinal (ISM) purposes. Most of these non-communication frequencies are used for heating purposes. Common ISM frequencies include 915 GHz and 2.45 GHz although other frequencies may be used provided sufficient leakage prevention measures are implemented (Wei, Shidaker and Hawley, 1996).

1.11.2: Microwave-Material Interactions

Many materials may be heated by the application of microwaves. The electric field component of the microwaves interacts with any polar (charged) groups within the material. Non-conducting materials are transparent to microwave energy whilst highly conductive materials are opaque, this results in total microwave reflection. Between these two extremes lie dielectric materials, which exhibit various degrees of absorption (Prasad *et al.*, 1998). The different electrical characteristics of these materials are shown in figure 1.25.

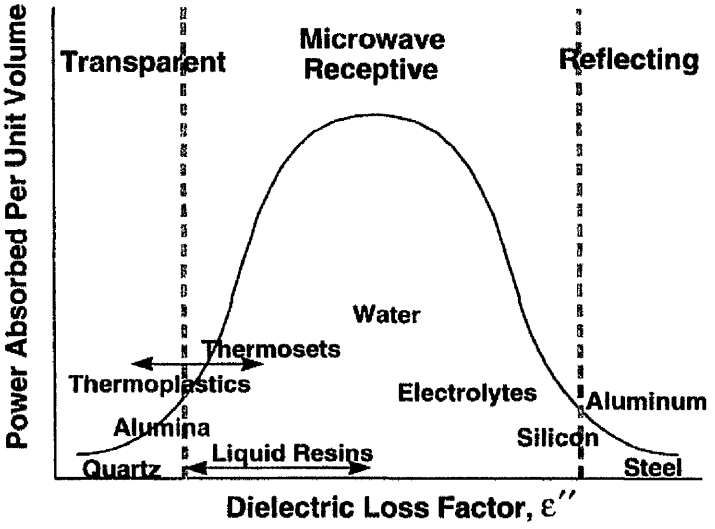

Figure 1.25: Relationship between power absorption and dielectric loss factor for a variety of common materials (Thostenson and Chou, 1999)

If the charged groups are freely mobile a current is induced i.e. the material is a conductor. If the polar groups are bound and their movement is restricted, however, the groups align themselves with the electric field, this is termed dielectric polarisation and the material is a dielectric (e.g. polymers). Under ambient conditions

these polar groups undergo thermal Brownian motion. The application of incident microwave radiation causes the normally random orientation of the groups to become ordered. Dipole relaxation then takes place and the dipoles return to the random state. Holding the alignment of the dipoles requires the input of energy, therefore as relaxation takes place this energy is released as heat (Jow *et al.*, 1987).

1.11.3: Dielectric Properties

There are a number of distinct mechanisms by which electromagnetic energy may interact with materials and contribute towards their total dielectric response. The mechanisms include electronic polarisation, atomic polarisation, dipole (orientation) polarisation and polarisation of interfacial charges, also known as Maxwell Wagner polarisation. The contribution provided by each of these mechanisms to the overall dielectric properties of a material is strongly dependent upon the frequency of the applied electromagnetic field. The frequency dependence is shown by figure 1.26.

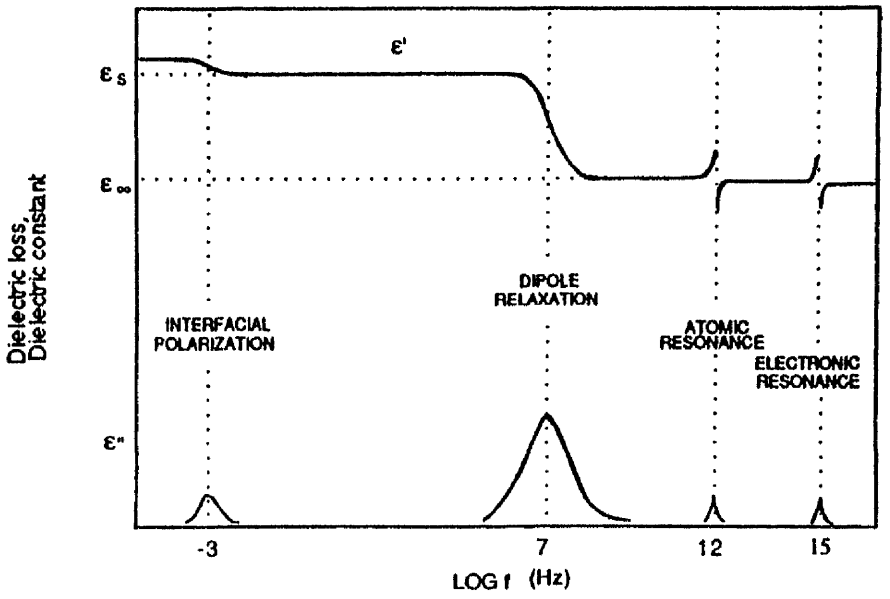

Figure 1.26: Schematic representation of the dielectric spectrum for a polar molecule (Chen *et al.*, 1993)

At the higher end of the frequency scale, electronic polarisation is observed and arises as a result of the displacement of the electrons relative to the positive atomic nuclei. This type of polarisation takes place in all materials.

Lower down the scale atomic polarisation is encountered and is a result of the displacement of atoms relative to one another in a molecule. Although still extremely rapid, this type of resonance occurs at lower frequencies than electronic polarisation as the relatively massive and, therefore, heavy nuclei are unable to resonate as rapidly as the much smaller, lighter electrons (Chen *et al.,* 1993). Atomic polarisation takes place in the infrared region of the electromagnetic spectrum. The penetration depth in this range is very small ($<< 10^{-4}$ m) in most solids. Heating takes place primarily at the surface as energy is deposited there in a thin layer. Heating of the solid bulk is then reliant upon conduction from the heated surface of the solid to the cool interior (Bykov *et al.,* 2001).

In between interfacial polarisation and atomic polarisation regions dipole relaxation takes place. In this region the polarisability effects of atomic and electronic polarization are unchanged as the extremely rapid resonance of the electrons and atomic nuclei are easily able to remain in equilibrium with the field. Dipole relaxation is a result of the tendency of molecules with permanent dipoles to align themselves with the applied field. Since the microwave field oscillates with time, the dipoles are constantly realigning themselves with it and are, therefore, in a constant state of mechanical oscillation. It is the motion of these dipoles with the applied field and the friction that the movement causes which converts the electric energy of the microwave field into thermal energy. Dipole relaxation is fundamentally related to frequency, as the energy dissipation is constant per field cycle. Thus the amount of energy dissipated increases as the frequency is increased, assuming dipole displacement remains constant. Power absorption peaks are observed in the frequency spectrum as molecules have mechanical resonances, the frequency of which varies between molecules (Meredith, 1998).

The interaction of a dielectric is controlled by its complex permittivity ε* which is defined by equation 1.40,

$$\varepsilon^* = \varepsilon' - j\varepsilon''$$

(Eqn. 1.40)

where ε' is a measure of the polarisability (real permittivity) of the material and describes the capacitive properties of the system, j is the imaginary number $\sqrt{-1}$ and

ε'' is the loss factor which is related to the conductive component of the system. The dielectric loss tangent may also be used to describe the dielectric response as shown in equation 1.41.

$$\tan\delta = \frac{\varepsilon''}{\varepsilon'}$$

(Eqn. 1.41)

The extent to which polarisation takes place and the amount of energy required to accomplish it dictates the loss factor of a material (ε''). The loss factor itself is made primarily from two separate routes of absorption as described by equation 1.42,

$$\varepsilon'' = \varepsilon_D'' + \frac{\sigma}{\omega\varepsilon_0}$$

(Eqn. 1.42)

where ε_D'' is the contribution made from dipolar reorientation polarisation and $\sigma/\omega\varepsilon_0$ outlines the loss from resistive heating, where σ is the electrical conductivity, ω is the angular frequency of the microwaves (and is derived from $\omega = 2\pi f$ where f is microwave frequency) and ε_0 is the permittivity of free space (Wei, Shidaker and Hawley, 1996).

Materials that are easily polarised by small electric fields are relatively easy to heat. Molecular agitation may be achieved by the rapid alternation of the polarising field. The energy transferred to the material in this way manifests itself as heat.

If a material is to be heated with the use of microwave energy the microwaves must be able to enter the material and convey energy. The rate at which electrical energy is converted to heat is strongly dependent upon the loss factor. The heating of materials by microwave methods depends upon the dielectric power absorption. This is described by equation 1.43,

$$P = KfE^2\varepsilon' \tan\delta$$

(Eqn. 1.43)

where P is the power dissipation in W / cm^3, K is a constant which is equal to 55.61 × 10^{-14}, f is the frequency applied in hertz (Hz), E is the field strength in V / cm^3, ε' is

the dielectric constant (permittivity) and tan δ is the dielectric loss tangent (Chen *et al.*, 1993).

ε' and tan δ are both dependant upon the temperature of the sample and the frequency. The electromagnetic field energy dissipated as heat per unit volume of material is proportional to the dielectric loss factor ε'', the square of the field strength (E^2) and the frequency of the applied field (f). The rate of conversion of microwave energy into thermal energy is dictated by the dielectric loss factor, ε'' (DeMeuse *et al.*, 1991), and the electric field strength.

1.12: Microwave Components

Microwave radiation is a product of the acceleration of charge. Most microwave sources use vacuum tubes to obtain the high power levels and frequencies required for microwave heating. Vacuum tubes that are used for heating include magnetrons, klystrons, cross-field amplifiers and travelling wave tubes (TWT). These types of microwave generator were advanced by development in the 1980's. Devices such as magnetrons, however, can trace their origins back to World War II (Laverghetta, 1988).

1.12.1: Magnetrons

Magnetrons underwent considerable development during the Second World War when there was a need for high power microwave generators for high precision radar applications. They are the cheapest and most readily available microwave sources as they are mass produced. Their efficiency, reliability and low cost has resulted in them being used in all domestic microwave ovens (Thostenson and Chou, 1999; Laverghetta, 1998; Wheeler, 1963). The basic layout of a typical magnetron is depicted in figure 1.27.

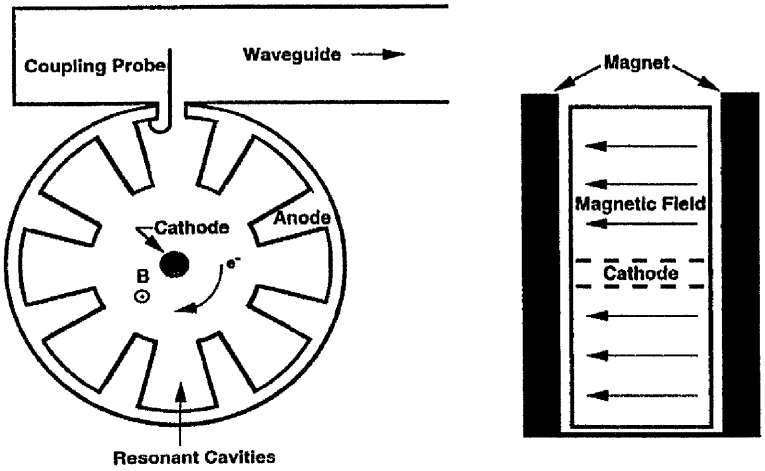

Figure 1.27: Schematic diagram of magnetron top (left) and side (right) views (Thostenson and Chou, 1999)

The main components of a magnetron are enclosed under high vacuum and comprise a cylindrical heated cathode, a circular anode arrangement containing a number of equally spaced resonant cavities tuned to the desired operating frequency and a high strength magnet al.igned axially to the anode / cathode assembly. In vacuum tube devices the anode is set to a considerably higher potential than the cathode. Loosely bound valence electrons are displaced from the cathode by heating. They are then accelerated towards the anode by the strong electric field set up by the potential difference. Magnetrons use an external magnet to create a magnetic field orthogonal to the electric field, which exerts a circumferential force on the electrons as they travel towards the anode. This causes the electrons to travel in a spiral pattern resulting in a swirling cloud of electrons. As the electrons pass the resonant structures, oscillations are set up in the cloud, the frequencies of which depend on the size of the cavities. Magnetrons are, therefore, only capable of generating microwaves of a fixed frequency. The microwave energy is coupled from one of the resonant cavities to a transmission line through a coaxial line or waveguide launcher. Power output may by controlled by intermittent use of the magnetron (thus controlling average power) or by variation of the cathode current amplitude where continuous microwave power is required.

1.12.2: Klystrons

Klystrons are often used in heating processes where there is a requirement for a high power heating system, as they are capable of outputs of up to 50 kW. The main components of a klystron are represented in figure 1.28.

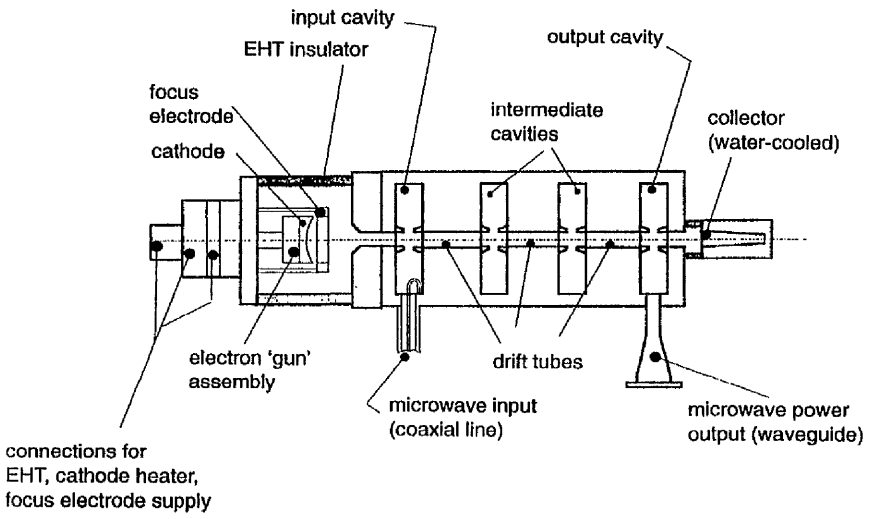

Figure 1.28: Schematic of a high power klystron (Maloney and Faillon, 1974)

An electron gun generates an intense electron beam which is accelerated towards the resonator assembly by an extra high DC voltage applied between the gun and resonator assembly. A solenoid is used to apply an external magnetic field in order to collimate the electron beam (essential to prevent high energy electrons hitting and melting the cavity structure thus destroying the klystron). The electrons pass through the first cavity and interact with the microwave electric field. The interaction results in the acceleration and deceleration of electrons within the beam. Therefore as the electrons leave the first cavity some are travelling faster than the average velocity and some slower. As the electrons continue through the drift tubes, the faster electrons catch up with the slower ones which forms bunches at intervals along the electron beam causing high electron cloud density. Intermediate cavities are located at these bunch positions and microwave energy is induced within them. The electric fields further intensify the electron bunching. The pattern of further cavities is repeated until the final cavity where the bunching is most intense. Here the power coupled to it is transferred to the output waveguide (Meredith, 1998).

1.12.3: Travelling Wave Tubes

Travelling wave tubes (TWT's) are essentially electronic amplifying devices capable of variable frequency microwave output, which accept weak RF input signals and amplify them thousands of times. A characteristic of TWT's is that they are capable of very wide bandwidth (Laverghetta, 1988). The main components of a TWT are the electron gun assembly, the RF interaction circuitry, the focussing magnets and the

collector (Thostenson and Chou, 1999; Laverghetta, 1988). These are outlined in figure 1.29.

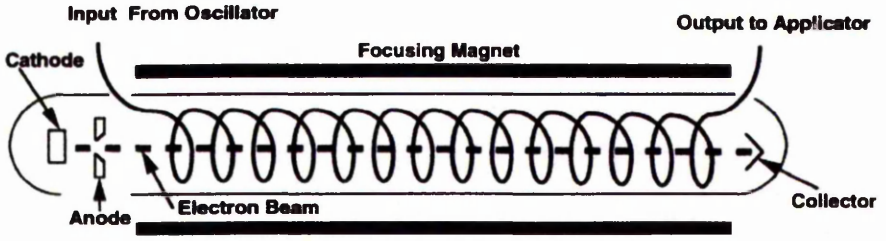

Figure 1.29: Cross section of a TWT (Thostenson and Chou, 1999)

As with a magnetron the cathode is heated to remove loosely bound electrons and emit them as a continuous stream, which is accelerated towards and through the anode. However unlike magnetrons, the TWT does not create the frequency of the oscillations but only serves to amplify the signal. The signal is generally produced by a voltage controlled oscillator that then sends the signal to the TWT for amplification. Rapid switching of the output frequency is, therefore, possible by variation of the oscillator input voltage. The absence of resonant structures within the TWT allows the amplification of a wide range of frequencies (bandwidth) in the same tube. After passing through the anode the electron beam is focused by the external magnet and forced into a slow wave structure, in this case a helix. The purpose of the wire helix is to slow down the phase velocity (axial to the direction of the helix) of the microwave energy. Thus the pitch of the helix dictates the microwave phase velocity. As the microwave signal travels along the helix, the axial component of the electromagnetic field interacts with the electron beam which causes the acceleration and deceleration of electrons within the beam as shown schematically by figure 1.30.

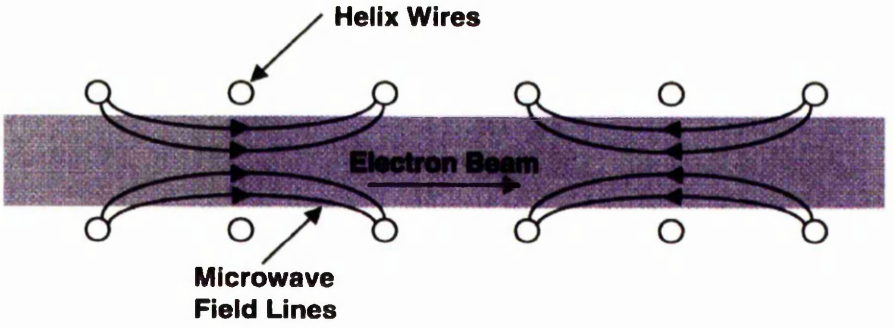

Figure 1.30: The interaction of the electron beam with the axial component of the electromagnetic wave (Thostenson and Chou, 1999)

Electrons are accelerated and decelerated by the interaction with the electromagnetic field. Amplification occurs when the electron beam is slightly faster than the phase velocity of the helix. In this instance more electrons are decelerated and therefore surrender energy to the microwave field resulting in amplification. The electron beam is eventually dissipated in the collector in the form of heat.

1.12.4: Transmission Lines

A transmission line may be defined as a device that transfers energy from one point to another. The activity of the energy en route must, however, be taken into consideration. Lines for coupling microwave energy from the source to the applicator may take many forms including coaxial cable, stripline, microstrip and waveguide. Coaxial cables are basically two concentric conductors, which are divided by an insulating material. They are convenient for low power and frequency applications, however, losses within the cable become significant at higher power and frequency levels thus necessitating the use of waveguides. Waveguides are hollow (often rectangular) tubes through which electromagnetic waves may propagate. There are two modes of microwave propagation possible within a waveguide, these are transverse electric and transverse magnetic (TE and TM, respectively). TE modes have zero electric field in the direction of propagation and TM modes have zero magnetic field in the direction of propagation. The most common waveguide mode is TE_{10} with the subscripts referring to the number of maxima and minima in each direction of the cross section of waveguide.

1.12.5: Microwave Applicators

Numerous microwave applicators are available including single and multimode cavities, waveguides and travelling wave applicators. The design of the applicator is crucial as it is here that the microwave energy is transferred to the material to be heated. For industrial processing, resonant applicators such as single and multimode devices are often used due to their high field strength although the type of applicator used may depend on the material to be heated.

1.12.5.1: Single Mode Microwave Cavities

Single mode cavities are designed around a solution to Maxwell equations to support a single mode. The cavities are, therefore, often the size of a single wavelength.

Although single modes result in non uniform field distribution within a cavity, a single predictable maxima or 'hot spot' is generated. If the location of the high field intensity is known it can offer some advantages. The generation of localised heating can be used in the joining of ceramics (Thostenson and Chou, 1999) and other materials, as heat may be focussed at the joint interface rather than the bulk of the material. Single mode cavities are also widely used for laboratory scale analysis where small sample volumes are often used. It is possible to place samples directly into the area of maximum field intensity for the most efficient coupling. Both curing reactions and studies of microwave-material interactions (e.g. dielectric measurements) may be studied in this way.

1.12.5.2: Multimode Microwave Cavities

Multimode resonant applicators are comprised of a metallic enclosure, which exhibits multiple reflections when a microwave signal is coupled into it. Superposition of incident and reflected waves gives rise to standing wave patterns or modes (Metaxas, 1991). Unlike single mode cavities, multimode applicators are not designed around the solutions to electromagnetic field equations and they may support numerous high order modes simultaneously. They are instead mainly developed by trial and error. They are also often much larger than single mode cavities as the greater the size of a multimode cavity, the more resonant modes may exist within it. For a rectangular cavity the mode equation for the resonant frequencies is described by equation 1.45 (Thostenson and Chou, 1999),

$$f_{nml} = c\left[\left(\frac{l}{2d}\right)^2 + \left(\frac{m}{2b}\right)^2 + \left(\frac{n}{2a}\right)^2\right]^{\frac{1}{2}}$$

(Eqn. 1.44)

where f_{nml} is the TE_{nml} or TM_{nml} modes resonant frequency, c is the speed of light, n, m, l, are the number of half sinusoidal variations in the standing wave pattern along the x, y, and z axis, a, b, d are the cavity dimensions.

A drawback to multi mode cavities is the presence of numerous localised field intensities. This results in localised heating effects in large components. As the previous equation shows a solution to this may be to increase the longest dimension of the cavity to increase the number of modes. As the number of modes increases they begin to overlap and even out the field distribution. Unfortunately this is not always

practical, the common microwave frequency of 2.45 GHz would require a 40 ft long applicator. Increasing frequency shortens the wavelength and therefore reduces the size of applicator needed for enhanced uniformity but at the expense of penetration depth. A common example of a multimode cavity is the domestic microwave oven, which uses a frequency of 2.45 GHz. These ovens often use rotating turntables so that the food passes through areas of high and low field intensity thus increasing uniformity. Wave stirrers create the same type of field distribution by reflecting the field off irregularly shaped metal blades and, therefore, continuously redistributing the modes.

1.13: Hybrid Heating

The heating efficiency of a polymer using microwave energy is primarily dependent upon its dielectric loss factor which in turn is reliant upon temperature and the microwave frequency. As most processing methods are carried out at a fixed ISM frequency, variation of the temperature can be used to raise the loss factor.

Low dielectric loss materials such as insulators and glassy thermoplastics are extremely difficult to heat from ambient temperatures as very little of the microwave energy is absorbed. In order to heat such materials using microwaves, hybrid heating may be used. Hybrid heating may be applied actively by the use of additional conventional heat sources. By conventional heating, the dielectric relaxation loss maxima may be shifted to the microwave region thus increasing the coupling efficiency of the microwave energy. Hybrid heating may also be provided passively by the inclusion of higher loss microwave susceptible materials that are able to absorb the microwave energy, convert it to heat and transfer it to the bulk of the material (Chen *et al.,* 1995). This method is used in the microwave sintering of ceramics where materials such as zirconia and alumina must be raised to higher critical coupling temperatures at which microwaves are then readily absorbed. Silicon carbide, which has a high loss factor, may be used as a stimulus to facilitate the processing of otherwise microwave transparent ceramics (Amri and Saidane, 2003, Zhao *et al.,* 2000).

1.14: Microwave Processing of Polymer Foams

The literature reports few references to the production of polymer foams using microwave heating techniques. Pip (Pip, 1988) reports a method for the foaming of

synthetic resin, which in this case is polymethacrylimide (a copolymer comprising a 3:2 ratio of methacrylic acid and methacrylonitrile). The invention details the simultaneous use of hot air convection and microwave heating. A foamable slab of polymer containing 8 % polymer weight of formamide / tertiary butanol blowing agent was heated to the polymer softening point of 160 ^{0}C for half an hour. The slab was then treated to pulsed microwave radiation over 10-second time intervals with 50-second pauses in between. The 650 W microwave oven had been modified such that hot air and microwave heating could be performed simultaneously. The product was a foamed slab with a density of ~38 kg m^3.

Initial attempts at foaming using microwave heating alone produced a material that although showing a degree of expansion, was severely cracked at the surface. This was a consequence of the way in which microwaves heat materials. Heating takes place from within the material and hence it is here that foaming is initiated. Since the external surfaces of the material are relatively cool compared with the bulk of the material they are unable to expand with the rest of the material and hence to relieve the internal expansive forces so that cracking and splitting takes place. To overcome these problems it was necessary to employ hot air heating to soften the material surfaces to their softening point such that they may expand with the bulk of the material on foaming.

The suitability of acrylonitrile and methacrylonitrile copolymers for microwave heating is mainly due to the presence of polar structures, which respond efficiently to microwave heating. It was recommended by Pip (Pip, 1988) that for effective foaming to take place the polymer should be comprised of at least 80 % by weight of acrylic acid or methacrylic acid and of acrylonitrile or methacrylonitrile units.

Other examples in the invention using similar heating methods, describe the foaming of a weakly crosslinked copolymer of methacrylonitrile and methacrylic acid. The heating of a monomer mixture containing blowing agent is also described. Curing of pre-foamed polymethacrylamide components using microwave radiation is described by Porter *et al.* (Porter *et al.*, 1973). The technique involves the heating of a pre-foamed sample enclosed in a mould and containing a delayed action crosslinking system. Upon heating, the crosslinking system is activated and network formation takes place.

A method for the production of foams formed by the microwave curing of an epoxy pre-polymer incorporating hollow glass microspheres has been reported by Palumbo and Tempesti (Palumbo and Tempesti, 1998). The prepolymer used was diglycidyl ether of bisphenol A (DER 332 produced by Dow Chemical) which was hardened using 4,4'-diamino diphenyl methane (DDM). A stoichiometric mixture of the two compounds was mixed with 3M Scotchlite type K37 microspheres with a density of 0.37g / cm^3. Microwave heating was performed using radiation with a frequency of 2.45 GHz and a three step heating cycle of 2 hours at 20 W, 1 hour at 25 W and 1 hour at 30 W. For comparison samples were also cured using conventional thermal techniques, curing was performed over a 24 hour period at 60 ^{0}C. The cured samples were 75 × 100 mm square although no mention of sample thickness could be found. It was found that the two different methods resulted in different foam morphologies, higher crosslink density at the interface (for microwave cured samples) and evidence of different mechanical testing failure mechanisms at the particle matrix interface.

1.14.1: Microwave Crosslinking of Polyethylene and Ethylene Vinyl Acetate

Crosslinking of polyethylene using microwave heating has been carried out by Menges (Menges *et al.*, 1979; Menges *et al.*, 1980). Crosslinking of Polyethylene in a microwave field was attempted, using microwave active additives to improve the microwave activity of polyethylene (Menges *et al.*, 1979). The authors point out that although heating pure polyethylene in a microwave field is not feasible due to its lack of polarity, it is rarely crosslinked in the pure form. It is often blended with additives and auxiliary components, which are polar and capable of absorbing microwave energy and producing a temperature rise within the material as a whole. It was postulated that in principle, the crosslinking of polyethylene may take place in accordance with the following three processes:

1. Through the use of an additive that is highly active in the microwave field, a PE-peroxide-additive mixture is uniformly heated in the microwave field to temperatures at which thermal decomposition of the peroxide commences.

2. When highly active additives such as carbon black and slightly polar peroxides are used, both components are present in the non-polar PE in the form of a complex compound, i.e. the highly active component and the peroxide molecule are always to be found in direct proximity. The energy

absorbed by the highly active auxiliary from the microwave field is thus primarily transferred to the adjacent peroxide molecule. In such a case, it is not necessary for the temperature of the total material to rise to a level at which the peroxide molecules undergo thermal decomposition, i.e. decomposition of the peroxide molecule is possible at lower mean overall temperatures.

3. When peroxides that are highly active in the microwave field are used, the additional use of active auxiliaries is unnecessary. In this instance, the peroxide molecule in the UHF field itself comprises the energy source and peroxide decomposition is also possible at low, measurable material temperatures.

The research used five peroxide crosslinking agents and three highly microwave active components such as carbon black, triallyloxy-s-triazine and halogen containing hydrocarbons to permit heating of polyethylene using microwave radiation. The additives used are shown in table 1.1.

Table 1.1: Microwave active additives

Name	Chemical Structure
Triallyloxy -s-triazine	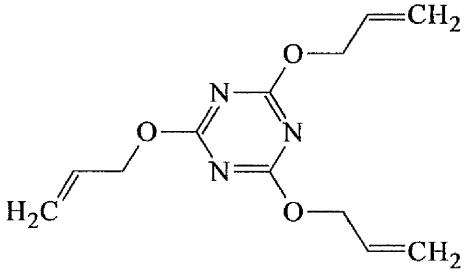
Chlorinated Polyethylene	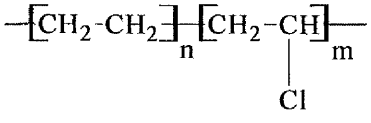
Carbon Black	C

The peroxide Crosslinking agents used were dicumyl peroxide, cumene hydroperoxide, di-t-butyl peroxide, t-butylcumyl-peroxide and di-(t-butyl-

peroxiisopropyl)-benzene. The polymer-auxiliary-blends were produced by mixing in an extruder. The compounds, having been preheated to various levels in a conventional oven, were then subjected to microwave radiation in a microwave oven operating at a frequency of 2.45 GHz and an output power of 2.1 kW. The sample temperature was monitored by periodic interruption of the heating cycle and measurement with a thermocouple. After heating the gel content of the samples was measured by xylene extraction.

The results showed that chlorinated PE only exhibited slight microwave activity whereas the addition of 5 % by weight carbon black or triallyloxy-s-triazine allowed heating of the PE-additive mixture from 100 °C to 180 °C after several minutes exposure to microwave radiation. In general, increasing levels of triallyloxy-s-triazine resulted in a decrease in the microwave exposure time required to obtain high degrees of crosslinking with all the crosslinking agents with the exception of cumene hydroperoxide. Addition of 10 % by weight of chlorinated PE resulted in very low levels of crosslinking when cumene hydroperoxide and di-t-butyl peroxide were used. Higher levels of crosslinking were observed when dicumyl peroxide and t-butylcumyl-peroxide were used (~ 80 % gel after 1 Minute exposure time). The use of carbon black also resulted in significant crosslinking levels after short exposure times with the exception of cumene hydroperoxide.

Since the polar additive groups are unchanged during the crosslinking process, the crosslinked polymer retains its microwave activity and can, therefore, undergo heating in a UHF field. As such its use in cable insulation applications may be limited. Further work by Menges (Menges *et al.*, 1980) describes a technique by which polyethylene may be crosslinked using tertiary butyl perbenzoate (TBPB) as the radical former and microwave energy absorber. The chemical structure of TBPB is shown in figure 1.31.

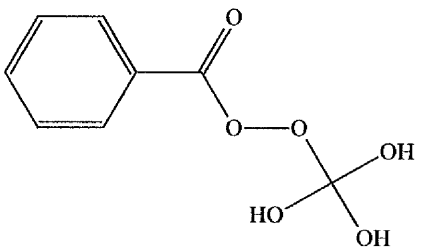

Figure 1.31: Tertiary butyl perbenzoate

The authors state that TBPB is capable of absorbing the microwave energy that is necessary to thermally decompose and form crosslinks and that the resulting decomposition products do not permit reheating of the crosslinked compound by a microwave field.

After preparing PE compounds with 5 % by weight TBPB, 300 g flat section samples were heated using a 2.1 kW microwave oven operating at 2.45 GHz. The samples were subjected to various levels of preheating in a conventional oven before exposure to microwave heating. In all cases, regardless of the level of preheating, the maximum temperature reached by the samples was 190 °C after which no further increase in temperature occurred, even after periods of prolonged irradiation. The time taken by the samples to reach 190 °C was dependent upon initial preheat temperature and varied from four minutes at an initial sample temperature of 0 °C, to one minute at an initial temperature of 120 °C.

The results indicated that peroxide decomposition and crosslink formation were taking place at lower than expected temperatures and at increased rates. This was attributed to localised heating effects in the vicinity of the peroxide molecules. It was suggested, that as the peroxide molecules were responsible for converting the microwave energy to heat and supplying it to the material in the immediate vicinity, the temperature close to the peroxide molecules may be much higher than the mean temperature of the bulk of the material. At sufficiently high local temperatures, there exists the possibility of peroxide decomposition and crosslink formation, regardless of the average sample temperature.

Menges *et al.* (Menges *et al.,* 1980) postulate that heating the PE / TBPB compound beyond 190 °C using microwave radiation was not possible, as the microwave absorbing peroxide had been completely converted to decomposition products that had little or no microwave activity. There is no report in the work of any observed decrease in the sample temperature after this point during continued microwave exposure, which would be expected on the decomposition of the sole microwave active component in the system. There was also attempted reheating of the samples from cold using the microwave system mentioned earlier. Since this was not possible it would strongly indicate that the TPBP was the primary microwave energy absorbing component in the system.

A method for the production of crosslinked ethylene vinyl acetate / ethylene methyl acrylate blends using microwave heating has been reported by Cassagnau and Michel (Cassagnau and Michel, 1994). A technique was developed whereby a resonant cavity operating in the TE_{01} mode was used to crosslink EVA and EMA, each with ~28 % by weight acetate and acrylate groups respectively, by an exchange reaction between the ester groups of the two miscible polymers in the presence of a dibutyltin oxide catalyst. The equipment used in the work is outlined in figure 1.32.

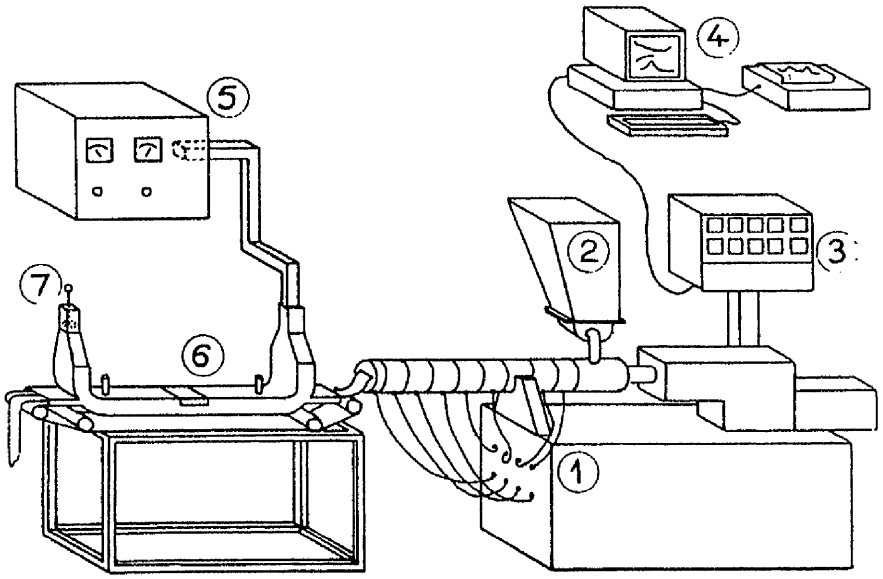

Figure 1.32: Online extrusion and microwave processing. 1: Twin screw extruder; 2: Hopper; 3: Temperature control; 4: Data acquisition; 5: Generator power; 6: Microwave applicator; 7: Microwave reflector.

The microwave heating apparatus included a magnetron operating at a frequency of 2.45 GHz with a power output of 1.2 kW. The microwaves were directed into the applicator, which also acted as the process chamber and incorporated microwave traps to prevent leakage of microwave radiation. The EVA/EMA/catalyst blend (50/50/5 by weight) was mixed using a twin screw extruder which was placed in line with the microwave applicator. The blended polymers and catalyst were extruded in flat sheet and cylindrical forms to study the effect of the sample shape on the curing process. The extruded sample was fed into the microwave applicator on a PTFE conveyor belt, which allowed continuous processing of the polymer sheet. A maximum extruder temperature of 165 °C and residence time of 200 s was used to ensure that no crosslinking took place before the material entered the microwave applicator. Sample temperatures at the inlet and outlet of the microwave applicator were measured using

an infrared pyrometer. Two inlet temperatures were used, 25 °C and 140 °C, and the residence time within the microwave applicator was varied to achieve various levels of crosslinking.

It was found that the flat sheet strip samples achieved a higher gel content and outlet temperature than the cylindrical samples at any given applicator residence time (same inlet temperature), although it is unclear whether the sample volumes were the same. This was attributed to the effect of the samples geometry on the microwave field, thus the research was concentrated on the strip samples. Cross sections of the strip samples were divided into five sections and the gel content of each zone measured to determine the microwave curing uniformity. It was found that the gel content was similar in the four inner sections but was significantly lower in the outer region. It was concluded that the lower gel fraction was due to a lower degree of microwave absorption in the boundary regions of the sample. Although the variation in the gel content throughout the sample may be a result of non uniform field distribution, a possibility not considered was the effect of surface heat loss. The sample heating was by microwave radiation only and heat losses from the sample surface would result in a lower temperature in the sample extremities compared with the bulk of the material. This would explain the lower degree of crosslinking in these regions.

1.14.2: Microwave Foaming of Polyethylene and Ethylene Vinyl Acetate

Menges and co workers (Menges *et al.,* 1983) have developed a technique for the foaming of crosslinked polyethylene. Traditionally polyethylene has proved problematic to heat using microwave radiation. This is due to the lack of polar structures within the polyethylene polymer chain and subsequent low loss factor. Polymers such as polyethylene are, however, seldom used in the pure state and often incorporate additives that are extremely polar (Kircher, 1987). Menges describes a technique whereby microwave active blowing and crosslinking agents are blended with molten polymer in an extruder. The homogenised compound is then extruded as a strand and heated with microwaves, with a frequency of 2.45 GHz and a power output of 2 kW, until foaming occurred. No cooling was allowed to take place between the extrusion and microwave heating processes for the sake of economy and presumably to take advantage of the increase in loss factor that usually accompanies elevated temperatures.

Open cell polyolefin foams have also been produced using microwave radiation heating methods and mechanical deformation techniques (Katsuya *et al.*, 1993). A technique is described whereby a foamable polyolefin sheet is prepared by compounding the polymer with a crosslinking and blowing agent on a two-roll mill. The polymer was then shaped under pressure in a heated mould although no crosslinking or foaming takes place at this stage. The temperature used was 120 ^{0}C. Partial dissociation of the crosslinking agent and decomposition of the blowing agent is then effected by exposure of the component to microwave radiation. Heating under atmospheric conditions was then performed to complete the crosslinking and foaming reactions and to facilitate foam expansion.

Subsequent intercommunication (rupturing of cell walls) between the cells was achieved by passing the foamed components through even spaced rolls a number of times. The mechanical deformation resulted in the rupture of the cell walls producing foam with close to 100 % open cell content.

The crosslinking and blowing agents used are frequently used in polyolefin foam manufacture, many of which are outlined in figures 1.2 and 1.3. It is recommended in the invention that when the base polymer is EVA, that the vinyl acetate content is between 0.1 and 50 % in order to allow microwave heating to take place in the absence of plasticiser.

Foaming of both EVA and PE polymers, using domestic microwave ovens was attempted by Curran (Curran, 1998). Compounds were based on traditional foamable formulations, namely a polyolefin base polymer blended with DCP crosslinking and ADC blowing agents. Microwave susceptible compounds such as silica and barium titanate were also added to the PE formulations in an effort to increase the loss factor. The temperature increases generated in PE formulations using microwave heating were, however, found to be insufficient to cause crosslinking and blowing agent decomposition. It was surmised that despite the addition of microwave susceptible compounds, the loss factor was still too low to allow effective heating rates and temperatures to be reached.

EVA was successfully foamed using conventional heating, microwave heating alone and microwave heating in conjunction with hot air convection heating (hybrid

heating). It was found that foams produced using conventional and hybrid methods showed variability in density and cell size whilst those produced using microwave heating alone were of low density and exhibited reduced cell size. The successful microwave heating of EVA in comparison with polyethylene was attributed to the presence of polar groups along the EVA polymer chain.

1.15: Objectives

Reports in the literature on the production of polymer foams using microwave heating methods are comparatively rare. Fewer still are concerned directly with polyolefin foam production. The reports that do exist, however, indicate that crosslinking and subsequent foaming of polyethylene and ethylene vinyl acetate copolymers is possible provided that steps are taken such that the loss factor of the material is sufficiently high to allow efficient microwave – material interaction. This is particularly pertinent to polyethylene due to its inherently non polar nature.

The main objectives of this work are:

- To characterise the dielectric and thermal properties of the materials used and to investigate their dielectric response to changes in microwave frequency and temperature in order to define the best processing conditions.

- Design, construct and develop a combined microwave / hot air heating applicator and control system for the batch production of EVA foam samples. The system will be capable of heating samples using microwave radiation alone or in conjunction with hot air.

- Investigate the effect of processing conditions on the properties of the foam samples produced.

- To contrast the properties of the microwave foams with a range of comparable conventionally produced samples, in terms of density, mechanical properties and cellular structure.

The work aims to combat some of the problems associated with traditional foaming methods by the use of microwave heating, both alone and in conjunction with convection heating. It is anticipated that this may help to overcome some of the

problems associated with poor thermal conductivity, such as uneven foaming due to thermal gradients, by using microwave energy to heat the polymer more uniformly throughout its thickness.

CHAPTER 2: EXPERIMENTAL

2.1: Raw Materials

The materials used in this work are commonplace in traditional polyolefin foam formulations. The materials comprised ethylene vinyl acetate base polymers, a peroxide crosslinking agent and an azodicarbonamide blowing agent.

2.1.1: Base Polymers

Various grades of EVA (Ethylene Vinyl Acetate) copolymer, manufactured by Exxon Chemicals, were used in this work. EVA was used instead of pure polyethylene because of its higher polar group content and increased microwave activity (with respect to pure polyethylene). The specifications are shown in table 2.1 (Exxon, 2004).

Table 2.1: Specifications for EVA base polymers

Exxon Product Code	Mean Vinyl Acetate Content / % wt	Melt Flow Index / g/10 min	Density / kg m^{-3}
UL00206	6.5	2.5	923
UL00218	18.4	1.7	939
UL00328	27.6	3	952

For convenience EVA UL00206, UL00218 and UL00328 will subsequently be referred to as EVA 206, 218 and 328 respectively.

2.1.2: Crosslinking Agent

When selecting a crosslinking agent it is important that it is compatible with the melting and processing temperatures of the base polymer. Dicumyl peroxide (DCP) was chosen, as its dissociation temperature range was compatible with both the polymer melting, and foam processing temperatures. A useful method for determining the compatibility of a crosslinking agent is by examination of its half-life data. DCP has a half life ($\tau_{1/2}$) of 10 hours at 115 °C (which allows blending with a

low risk of gelation), and a $\tau_{1/2}$ of 1 minute at 171 °C (which is ideal for processing) (Akzo Nobel, 2001).

The crosslinking agent used was Perkadox BC-40K-pd produced by Akzo Nobel Chemicals Ltd. The peroxide is supplied as a fine grey powder consisting of 40 % DCP on an inert clay substrate. It was, therefore, necessary to adjust the quantities used to give DCP content equivalent to 100 %.

2.1.3: Blowing Agent

An azodicarbonamide (ADC) blowing agent was used in all foam formulations. This is a widely used blowing agent as it has a high gas yield and the facility to adjust its decomposition temperature with the use of suitable activators (Sims and Jaafar, 1994). Standard unactivated ADC blowing agents have a decomposition temperature of around 205-220 °C; this range may be expanded to around 155-220 °C by the addition of activators. The decomposition of ADC may, therefore, be tailored to suit the melting point of a particular polymer. The blowing agent used was unactivated ADC-E-C2 Porofor (subsequently referred to as ADCE) which has a decomposition range of 180-220 °C and is manufactured by Bayer AG. The unactivated grade was chosen, as its decomposition range is much higher than that of the crosslinking agent. This facilitated separation of the crosslinking and expansion phases of the foaming process.

2.2: Sample Preparation

Sample formulations were based on 200 g samples of EVA base polymer. Crosslinking and blowing agents were, therefore, added as parts per hundred resin (phr). Formulations contained 8 phr blowing agent and 0.5 phr crosslinking agent.

2.2.1: Milling and Blending of the Base Polymer

Blending of the EVA base polymer with the blowing and crosslinking agents was performed with the use of the thermostatically controlled, electrically heated two-roll mill depicted in figure 2.1.

Figure 2.1: Two-roll mill

The temperatures of the rolls were initially set slightly higher than the melting range of the base polymer. Small additions of the polymer were then loaded onto the rolls with melting allowed to take place between additions and the nip gap adjustment fully closed (approx. 3 mm gap). The mill rolls and nip gap are outlined by figure 2.2.

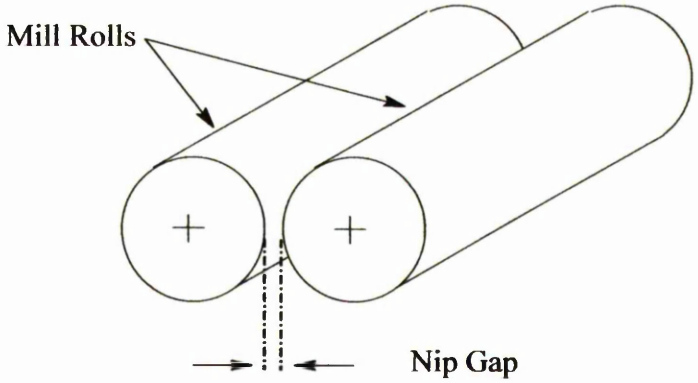

Figure 2.2: Mill roll nip gap

During the addition of the polymer the nip gap was gradually increased so that a rolling bank of polymer with a width of ~15-20 mm was maintained. When the addition of the polymer was complete, the rolls were stopped and the thermostat temperature was reduced by approximately 10 °C. This was done to allow the polymer to cool to a point where it became rubbery and easily processable. After cooling the rolls were restarted and the addition of blowing agent (in the case of

foamable samples) was performed over a period of 10 minutes. Having completed blowing agent addition, the crosslinking agent was then added. Addition of the crosslinking agent was carried out last and over a shorter period in order to reduce the possibility of premature gelation. During addition of the blowing and crosslinking agents, the polymer was repeatedly cut, folded and fed back into the rolls to ensure consistency of the mix.

The same method was used for the blending of non-foamable samples but with the omission of the blowing agent. During the milling process great care was taken to ensure that any polymer granules and additives that escaped from the nip rolls were collected and processed back into the sample. Having completed the milling process, the compounded polymer was allowed to cool before being stripped from the rolls and cut into conveniently sized strips.

2.2.2: Compression Moulding Techniques

The next stage in the production of foamable material was compression moulding. This technique is commonly used as a standard industrial batch technique (Puri and Collington, 1988) for producing foams and is particularly relevant for EVA foam production. This technique was designed to allow the controlled decomposition of crosslinking and blowing agents within the polymer matrix. The process that this work was concerned with involved foam expansion at atmospheric pressure. This technique was, therefore, modified such that it performed two main functions. These were to press the compounded polymer into a conveniently uniform shape from which foamable samples could be obtained and to allow various degrees of crosslinking to be carried out for gel content determinations and foaming studies. As the microwave curing process took place at atmospheric pressure the mould temperature was set high enough to mould the compounded polymer and in some cases perform various degrees of crosslinking, but low enough as to prevent blowing agent decomposition.

2.2.2.1: Non-foamable Crosslinked Polyolefin Matrix

For the purpose of initial gel content determination, samples of crosslinked polymer were compression moulded using a three part mild steel mould comprising of two flat plates (10 mm thick) with a square, 5 mm thick steel spacing gasket. Crosslinking was then performed at different temperatures over various time periods to show the effect of these variables on the crosslinking reaction.

2.2.2.2: Foamable Polyolefin Formulations

Foamable samples were prepared by compression moulding polymer blended with both crosslinking and blowing agents. For initial studies involving EVA 206, flat sheets were produced using the method described in section 2.2.2.1. The temperature used was high enough to allow melting and moulding of the polymer but low enough such that no crosslinking or expansion took place. Later studies involved the use of larger circular foamable samples. The mould used is shown in figure 2.3.

Figure 2.3 Circular foam blank mould

The mould was made from mild steel and had a 60 ° tapered cavity wall to facilitate ejection of the moulded sample (O'Connor, 1999). The mould depth was 10 mm and the diameter was 110 mm decreasing to 100 mm at the bottom. A steel plate was used to seal the top of the mould.

2.3: Foaming Techniques

2.3.1: Conventional Oven Foaming

Foams were produced using conventional methods for comparison with foams produced using microwave heating. The samples were pre-crosslinked in the mould. It was not possible to crosslink samples in the oven as the polymer began to flow before crosslinking took place (some industrial methods avoid this problem by floating the foamable sheet on a cushion of hot air). The crosslinked, foamable sample was then transferred to circulating hot air convection oven to allow decomposition of the blowing agent and foam expansion to take place.

2.3.2: Microwave Foaming

Two microwave heating methods were used in this work for the production of EVA foams. Initially, small foam samples were produced using a section of waveguide as the microwave applicator. These small samples were produced using microwave heating only. Larger foam samples were then produced in a multimode combination oven (described in greater detail in chapter 6) using a narrowband (2.3-2.5 GHz) 200 W solid-state amplifier.

2.3.2.1: Waveguide Microwave Foaming

Initial microwave foaming investigations involved EVA 206 polymer samples containing crosslinking and blowing agent. These were prepared for microwave foaming studies from the compounded, compression moulded sheets as described in section 2.2.2.2. Rectangular samples were cut from the moulded sheets (25 × 15 × 5 mm). A 3 mm diameter hole was then drilled into each of the samples, the purpose of which was to accommodate a fluoroptic thermometer contained within a quartz glass tube. The glass tube was necessary to prevent hot polymer from adhering to the delicate (and expensive) thermometer probe. The equipment used for heating is represented pictorially and schematically below in figures 2.4 and 2.5.

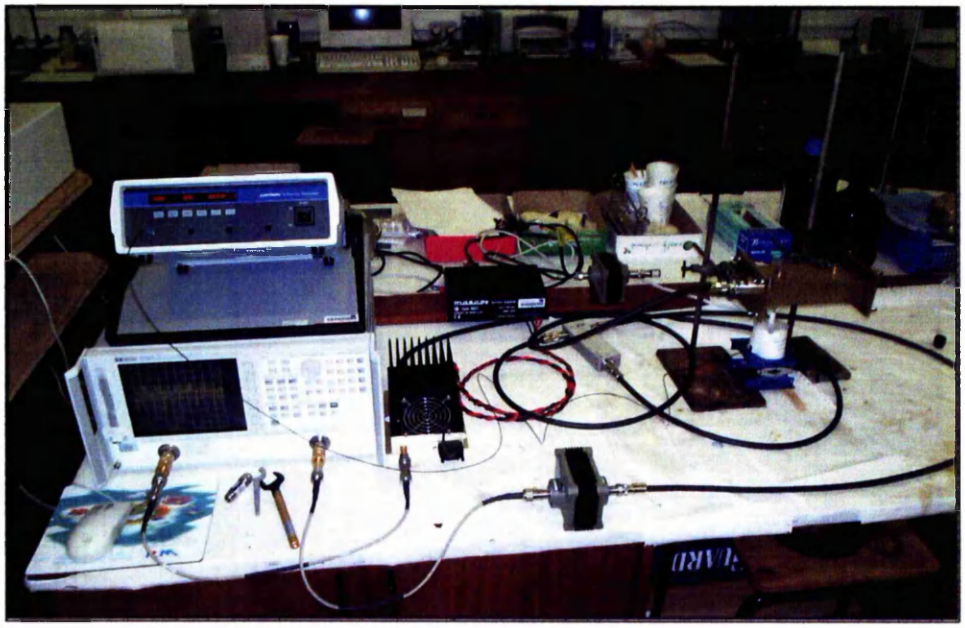

Figure 2.4: Microwave waveguide heating equipment

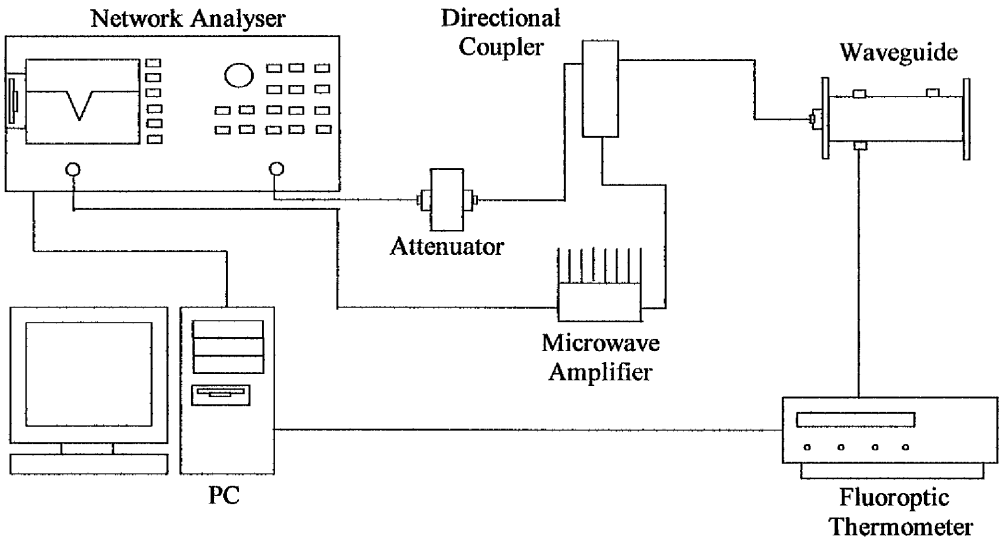

Figure 2.5: Microwave waveguide heating equipment (schematic diagram)

The microwave signal was generated by a vector network analyser (VNA). The output port of the VNA was connected to a 30 W microwave amplifier which in turn was connected to the waveguide, via a directional coupler, by microwave coaxial cable. Having placed the sample in the waveguide, the resonant frequency was measured and selected as the single heating frequency. Temperature measurement was performed by a Luxtron fluoroptic thermometry system as described in section 2.6.1.

2.3.2.2: Narrowband Variable Frequency Microwave Foaming

The oven was pre-heated to the required temperature by setting the temperature on the PID controller and switching the air circulation fan on. The oven was then allowed to reach the required temperature. A 3 mm hole was drilled into the side of the foam blank to a depth of 30 mm. This was to allow insertion of a glass capillary tube (3 mm outside diameter), which was sealed at one end. The oven microwave and hot air control system is schematically represented in chapter 6. The heaters and fan were then switched off and the lid frame removed from the oven and the lid opened. A PTFE sheet was placed in the oven on top of the foam support and sprayed with mould release agent to prevent the foam sticking during heating. The sample was then placed on top of the PTFE sheet and the temperature probes were fed through 1.6 mm holes in the oven wall. The air temperature probe was placed directly in the air stream from the circulation fan, 150 mm from the outlet. The sample probe (which controlled the microwave heating temperature) was inserted directly into the sample using the capillary tube as a protective conduit.

The oven lid was then closed and the lid frame re-fitted. A coaxial microwave cable was connected between the output / reflection port of the network analyser and the N-type connector (soldered to the end of the antenna) on the lid of the oven. The frequency range of the network analyser was then set to 2.3 – 2.5 GHz, and the reflected power as a function of frequency measured. In an effort to distribute the microwave field as evenly as possible during heating, six different frequencies between 2.3 and 2.5 GHz were used. These were selected from the frequency values that displayed the lowest values of reflected power and the least variation between samples.

Having selected the heating frequencies, the microwave cable was disconnected from the output port of the network analyser and connected to the output port of the 200W solid-state microwave amplifier. Another microwave cable was connected between the output port of the network analyser and the input port of the amplifier. The heating frequencies were then entered into the computer control program (as described in chapter 6) along with the heating power (network analyser output power), set point temperature, low temperature limit and minimum power. The program was then started and the heaters and circulation fan restarted.

When the required foaming time had elapsed the heaters and fan were turned off. To prevent exposure to microwave radiation the power to the microwave amplifier was disconnected and the microwave cable removed before opening the oven lid and removing the foamed specimen

2.4: Characterisation Methods

Unless there were obvious visual differences between foams produced by different methods, such as dramatically different cell size or evidence of foam collapse, it would not be feasible to rely upon visual analysis of the specimens to determine any differences. Thus the techniques outlined in this section were used to provide clear information, which could then be interpreted to show any differences arising from changing processing conditions.

2.4.1: Dielectric Property Measurements

The dielectric properties of the separate formulation components were determined in order to ascertain their heating efficiency in a microwave field. The dielectric

measurements were made as functions of frequency and temperature. Measurements were achieved using a number of techniques.

2.4.1.1: The Cavity Perturbation Technique

The cavity perturbation was used to determine the dielectric properties of the materials used at frequencies close to 2.45 GHz. Dielectric measurements may be made, by recording the changes in the resonant frequency and Q factor when a sample is introduced into a resonant cavity. Q factor is a measure of the cavity efficiency with regards to storing electric energy and is defined by equation 2.1 (Meredith, 1998),

$$Q = \frac{f_{res}}{\Delta f_{3db}}$$

(Eqn. 2.1)

where f_{res} is the resonant frequency of the cavity and Δf_{3db} is the width of the resonant peak measured 3db from the maximum.

A requirement of the technique is that the frequency shift due to the introduction of a sample into the cavity is much smaller than the resonant frequency of the cavity. It is for this reason that it is preferable to use small samples, which will cause a small frequency shift. The resonant shift of the cavity increases with increasing permittivity of the sample, conversely the Q factor decreases as the material loss factor increases and the microwave field within the cavity becomes more perturbed (Jow *et al.*, 1987; Jow *et al.*, 1988).

2.4.1.2: Dielectric Probe Measurements

The use of resonant cavities for determining the dielectric properties of materials has a number of limitations. The quality factor of the cavity (used in the calculation of the dielectric properties) depends on the reflective qualities of the cavity internal surfaces but also on there being continuous conduction between all the mating surfaces of the cavity, good contact in localised areas is not sufficient. Error can be introduced when the samples are removed and replaced (for the purpose of obtaining average data) as it is unlikely the samples will be relocated in exactly the same position within the cavity, thus affecting the results. Furthermore, the cavity resonant frequency was fixed at 2.45 GHz and could, therefore, only provide dielectric data with regards to that frequency. Should the dielectric properties need to be measured over a range of

frequencies, this would require the construction of numerous cavities to cover the desired frequency range, which would be undesirable financially.

Open-ended coaxial dielectric probes represent a convenient method of measuring dielectric properties of materials over a wide frequency and temperature range (Bringhurst *et al.*, 1997; Gershon *et al.*, 1999). The probe is an open ended coaxial waveguide and consists of a central core, insulated from the outer conductor by a hermetic glass to metal seal. The probe is depicted in figure 2.6.

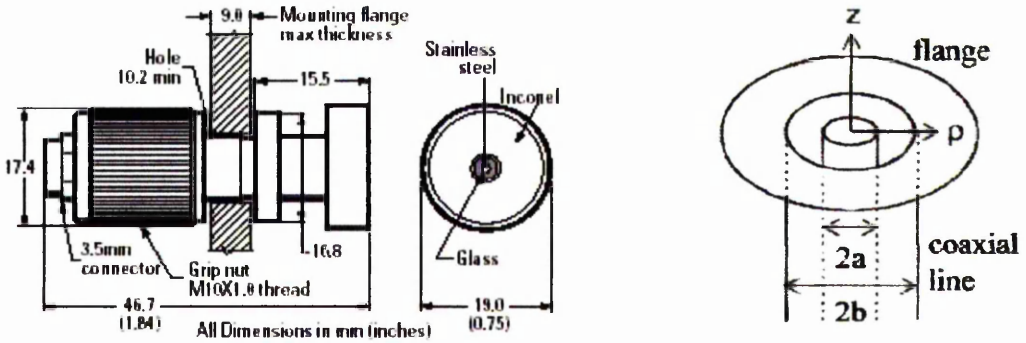

(a) (b)

Figure 2.6: The dielectric probe, (a) schematic (Hewlett Packard, 1999) and (b) critical dimensions (Wang, Niu and Xu, 1998)

The technique is reliant on the reflection of a signal from the end of a transmission line. The magnitude and phase of the reflected signal is dependant upon the electrical properties of the impedance, which terminates the line i.e. the sample. Usually a number of measurements are made at certain frequencies within the desired frequency range (Sheen and Woodhead, 1999).

The probe was held in contact with the material under test (MUT) and a Hewlett Packard network analyser with a frequency range of 20 MHz – 20 GHz was used to measure the reflection coefficient. The reflection coefficient was then used to determine the electromagnetic parameters of the MUT. The complex permittivity of a material is related to reflection coefficient by equation 2.2,

$$\Gamma^*(\omega,\varepsilon^*) = \frac{Z_s - Z_0}{Z_s + Z_0}$$

(Eqn. 2.2)

where Z_S is the probe impedance and Z_0 is the characteristic impedance (Garcia-Ruiz and Aviles-Castro, 2000). To determine the complex permittivity and permeability simultaneously, at least two independent reflections are necessary. The reflection coefficient Γ^* *(a, b, f,ε (f), μ (f), d)* is a complicated function of the coaxial dimensions a and b (as shown in figure 2.6 (b)), frequency *f*, EM parameters ε and μ, and the sample thickness *d*. The frequency varying method (FVM) obtains the required independent reflection coefficients by varying the frequency. Only one swept frequency measurement across the desired range is needed, all that remains then is to extract the parameters from the measured data. The FVM is based on two points. Firstly, frequency is an independent variable for the reflection coefficient, as can be seen from Γ *(a, b, f,ε (f), μ (f), d)*, hence, the reflection coefficient changes with frequency. Secondly, since the EM properties of materials ε *(f)* and μ *(f)* are themselves functions of frequency, the interpolation techniques are introduced into the process of extracting ε and μ from the frequency swept reflection data.

When using the FVM method, the broadband frequency swept reflection coefficients are measured and the complex permittivity and permeability are then reconstructed from the multiple reflection coefficients according to the adopted interpolation technique. The extracted parameters represent an average of the actual values over these frequency points; this process continues over the entire frequency range (Wang, Niu and Xu, 1998).

When connected to a network analyser, the probe is capable of measuring dielectric properties over the range of 50 MHz to 20 GHz. Although the probe was primarily designed for the measurement of liquids, the measurement of solids is also possible if a good contact is made between the sample and the probe face. In practice, with solid samples, a small amount of air will be present between the probe face and the sample, which will cause some degree of error.

To make a measurement, the probe must be connected to a suitable network analyser with a cable capable of handling the desired frequency range. A signal is then generated by the network analyser and transmitted into the sample by the probe. The signal is emitted through the central core of the probe. It travels through the sample and returns to ground via the probes outer conductor. It is necessary that the sample

dimensions are larger than those of the electric field. This is represented schematically in figure 2.7.

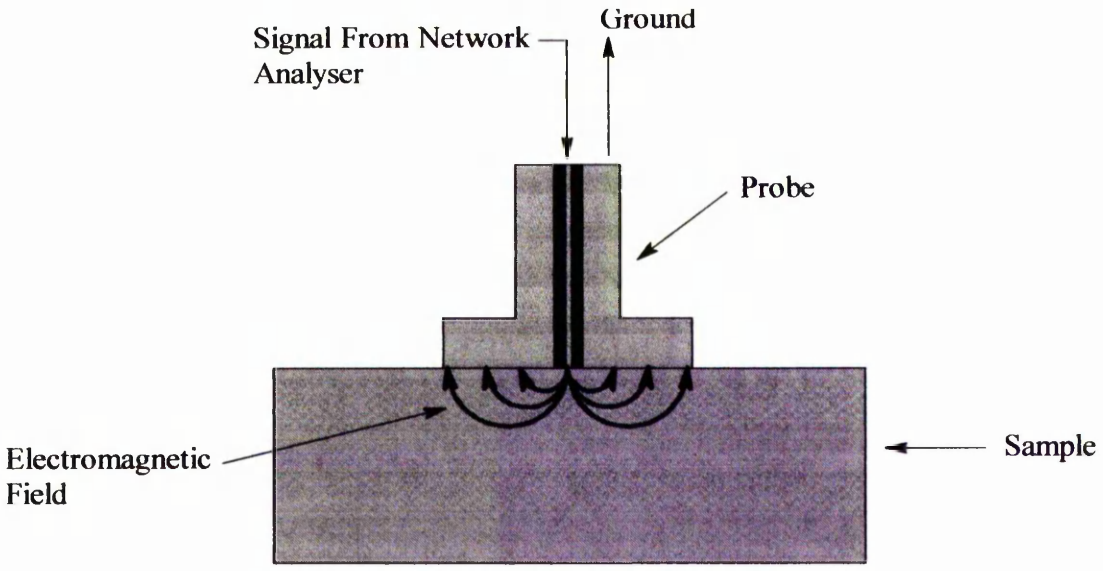

Figure 2.7: Dielectric probe measurement

The probe was mounted over a scissor jack platform and connected to an 8720ET Transmission / Reflection HP Network analyser (frequency range 50 MHz – 20 GHz) as shown below by figure 2.8.

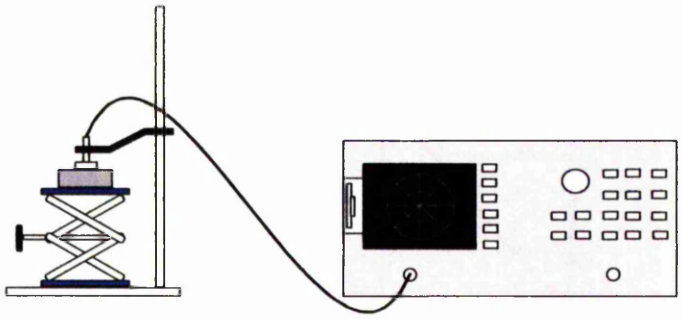

Figure 2.8: Dielectric probe set up

Before use, the frequency range was set to 50 MHz-20 GHz and the probe calibrated. Calibration was achieved by taking measurements of air and water at 25 °C. A measurement was also taken with a shorting block connecting the central and outer conductors. The probe was then pressed against the sample (ensuring that the faces of the probe and the sample were parallel to minimize any air gap between them) and a measurement taken.

2.4.2: Gel Content Measurement

The gel contents of crosslinked non-foamable polymer samples were determined in accordance with standard commonly used techniques (ASTM D 2765-90, 1990). Small samples of the crosslinked polymer matrix (between 0.3 and 0.5 g, all weights were recorded on an analytical balance to an accuracy of 0.0001 g) were cut and placed into a pre-weighed (W_1) stainless steel mesh cage. The cage containing the sample was then re-weighed (W_2), sealed by stapling shut both ends and weighed again (W_3). After weighing the cages were placed in a spherical reaction vessel and completely submerged in xylene. A soaking period of twenty-four hours at ambient temperature was then allowed. After soaking, a condenser was attached to the reaction vessel and the completed assemble placed on a thermostatically controlled isomantle (accurate to ± 1 ^{0}C) as shown by figure 2.9.

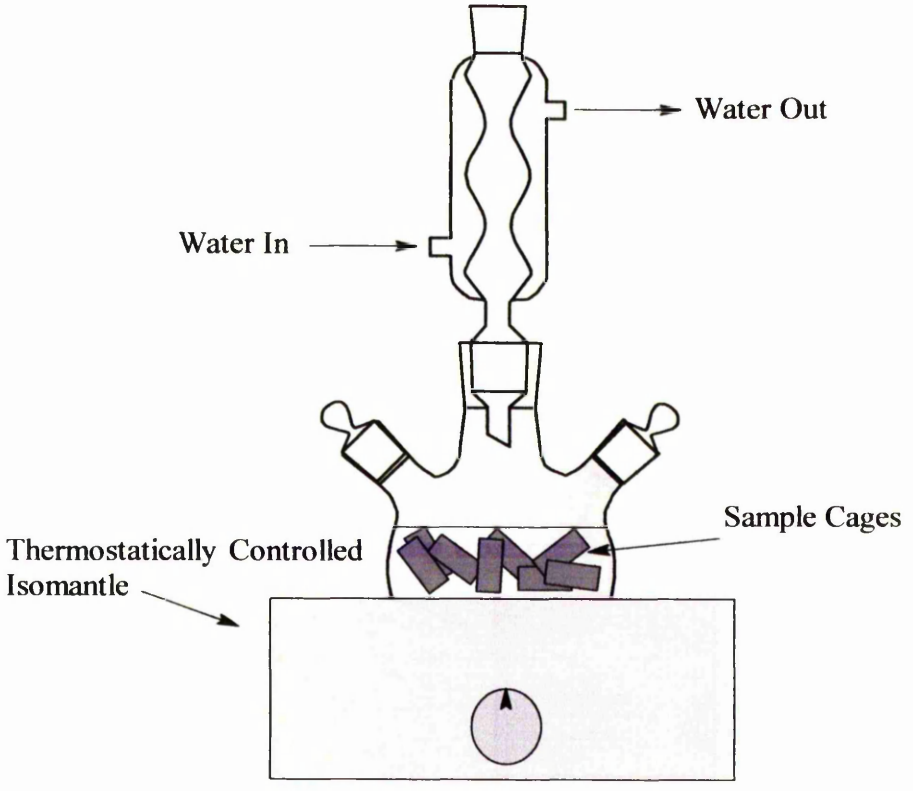

Figure 2.9: Gel content reflux apparatus

The temperature was then increased until the boiling point of xylene was reached (140 ^{0}C). Refluxing was then allowed to take place for twenty-four hours. On completion the services were disconnected and the sample cages were removed from the solvent. Care was taken such that the sample cages were removed before the temperature of the solvent had time to fall significantly. This was carried out in order to prevent any

of the dissolved polymer fraction from precipitating from the solution and forming a layer on the surface of the solvent cages. The increase in cage weight this would have caused would have lead to an artificially high gel content value. The cages were then allowed to cool on absorbent paper in a fume cupboard for one hour to allow the evaporation of a large degree of solvent. After cooling the cages were placed in a pre-heated vacuum oven to facilitate the extraction of the remaining solvent from the samples. The samples were heated at 130 ^{0}C under vacuum (< 0.01 bar) for six hours. To prevent damage to the vacuum pump seals from the solvent, a solvent trap was installed in the vacuum line. When solvent extraction was complete, the cages were allowed to cool to ambient temperature before being weighed for the final time (W_4). Equation 2.3 was then used to determine the gel content of each sample.

$$Gel\ Content(\%) = \frac{W_3 - W_4}{W_2 - W_1} \times 100$$

(Eqn. 2.3)

2.4.3: Thermal Characterisation

2.4.3.1: Thermogravimetric Analysis

Thermogravimetric analysis (TGA) was used to measure the weight changes of samples as a function of temperature under a controlled atmosphere. The results can provide information on the decomposition temperatures of materials. It is also possible to observe the stages of the decomposition.

Thermogravimetric analysis may be used to monitor the degree and rate of change of a material as a function of time or temperature. This may be carried out in a controlled atmosphere such as nitrogen. The technique is a useful way of following sample weight changes due to decomposition, oxidation or dehydration.

A Thermal Analysis (TA) Instruments High Resolution Thermogravimetric Analyser, model number TGA 2950 (equipped with an auto sampler) was used to determine the effects of increasing temperature (ramp) profiles and isothermal temperatures on the crosslinking and blowing agents.

The TGA 2950 operates on the null-balance principle. The main components of the instrument are outlined in figure 2.10.

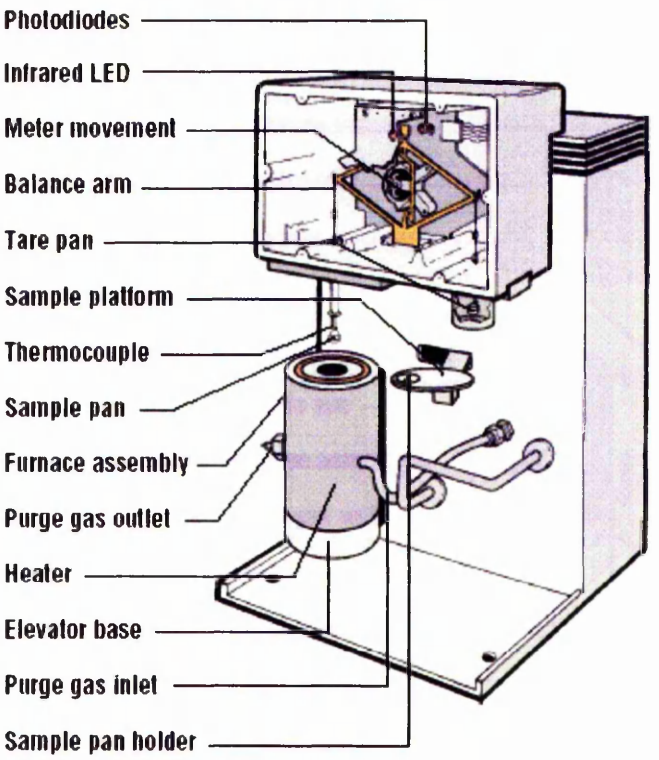

Figure 2.10: TGA 2950 outline (T.A. Instruments, 2005)

The system uses a highly sensitive transducer attached to a taut-band suspension system in order to detect the very small weight changes in the sample during heating. The balance arm is maintained in the horizontal (null) position by an optically activated servo loop, which regulates the amount of current flowing through the transducer coil. Any change in the sample weight causes the beam to move which is detected by an arrangement of photosensitive diodes, an infrared light source and a flag positioned at the tip of the balance arm. The flag controls the amount of light reaching each photodiode. As the beam and flag become unbalanced and move, the light received by each photodiode becomes unequal. A signal is then relayed to control programme where it is nulled. This causes a change in the amount of current supplied to the transducer, which rotates the balance arm back to the null position. The amount of current required is directly proportional to the sample weight.

Samples were load onto platinum sample pans, which were then lowered into the TGA furnace. The samples were then subjected to the desired heating profile and the change in their weight was recorded.

2.4.3.2: Differential Scanning Calorimetry

Differential scanning calorimetry (DSC) is a commonly used thermal analysis method that is used to determine first and second order transitions in materials by detecting relative heat changes compared to a reference sample (Young and Lovell, 1991). Two types of DSC, heat flux and power compensated, are recognised (Haines, 1995), both of which were used in this work. The heating cells used in both methods are shown in outline by figure 2.11.

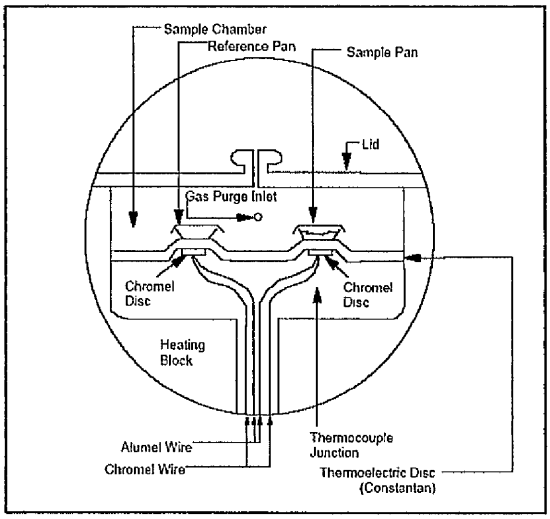

(a)

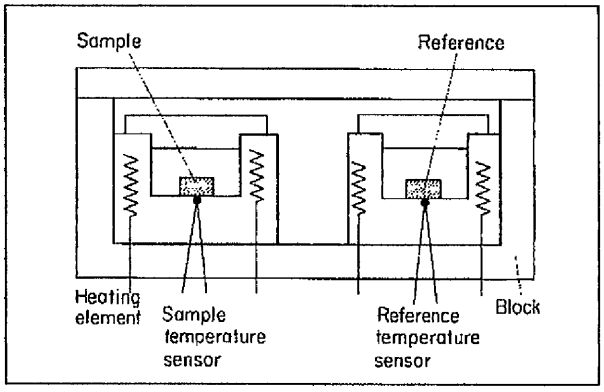

(b)

Figure 2.11: Schematic diagrams of, (a) heat flux (T.A. Instruments, 2005) and (b) power compensated (Rabek, 1980) DSC cells

In heat flux DSC, the sample and reference are heated from the same power source and the temperature difference between them is measured. This is then converted to a power difference. For power compensated DSC, the sample and reference are heated

using separate heat sources. The power difference required to keep the two at the same temperature is recorded.

The technique was used to characterise the behaviour, during heating, of the base polymers and additives required for foam production. A TA instruments Q100 heat flux compensated DSC was used to analyse the thermal transitions of the base polymers and the crosslinking agent. A Perkin Elmer Pyris 1 differential scanning calorimeter (power compensated) was used to obtain information regarding the physical changes of the blowing agent

Before each test was run, any aluminium pans were removed and the DSC cell was cleaned to remove any residue that may have been left from previous runs. This involved heating the cell up to 600 °C for 5 minutes before cooling back to ambient temperature. After cooling, the internal surfaces were then swabbed with a cotton bud dipped in acetone to complete the cleaning process. It was also necessary to calibrate the DSC before use. Calibration was performed using a 15 mg indium sample sealed in an aluminium sample pan. Indium was chosen as it has a very well defined melting peak and a melting temperature of 157 °C. The indium sample was heated between 120 °C and 200 °C.

DSC was used to confirm the dissociation ranges of the DCP and ADCE that are given in the literature. Generally heating rates of 15 K per minute were used as this was comparable with the heating rates of the conventional and microwave ovens. DSC was also used for a small scale kinetics study on the dissociation of DCP. Heating rates of 5, 10, 12 and 15 K per minute were used in this case. For the EVA samples, DSC was used to determine the melting range of the polymer. Polymer crystallinity values were determined using equation 2.4, (Dutta *et al.,* 1996; Sims and Khunniteekool, 1996 **(b)**) which compares the melting enthalpy of a sample to that of a perfectly crystalline sample,

$$Percent\ Crystallinity = \frac{\Delta H_m}{\Delta H_c} \times 100$$

(Eqn. 2.4)

where ΔH_m is the melting enthalpy of the sample and ΔH_c is the melting enthalpy of a perfectly crystalline polyethylene sample, 286.6 J / g (Kamp, 1980; Brandrup *et al.,* 1999).

2.4.4: Microwave Calorimeter

2.4.4.1: Calorimetric Analysis

Thermal analysis using a microwave heated calorimeter was carried out on the various formulation components. This was done in order to compare with conventional DSC measurements and, therefore, determine any differences caused by the different heating methods. The equipment was designed to emulate the operation of a conventional power compensated differential scanning calorimeter. A schematic representation of the microwave calorimeter is shown below by figure 2.12.

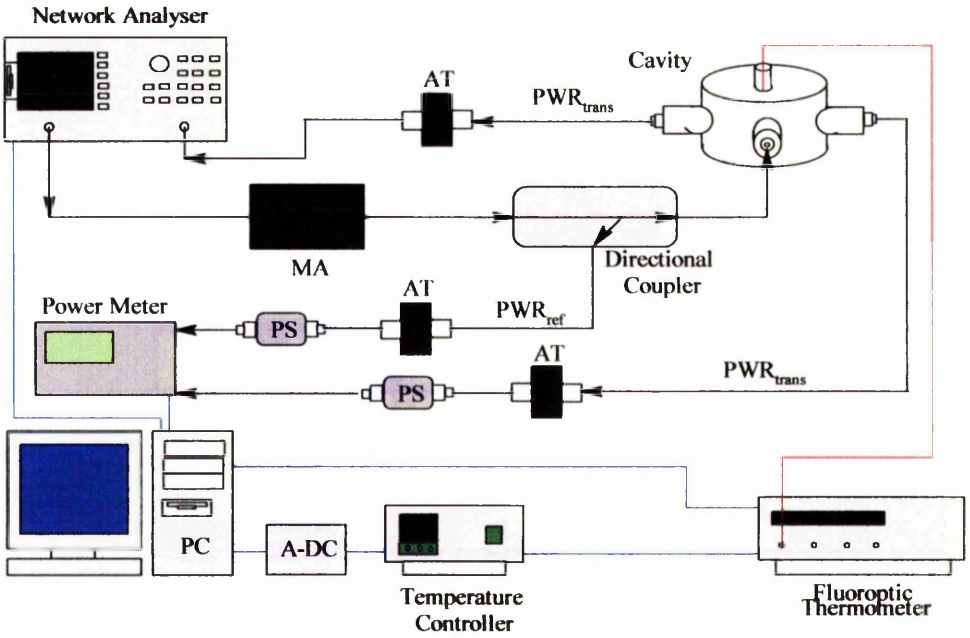

Figure 2.12: Microwave heated calorimeter outline

A Hewlett Packard HP 8714 ET network analyser was used as the primary signal generator and was capable of a maximum power output of 1 mW. The signal from the output port of the network analyser was fed via a flexible coaxial cable to a narrowband microwave amplifier (MA) (manufactured by Microwave Amplifiers Ltd) with a frequency range of 2.3-2.7 GHz and a specified gain of 44.5 dB. From equation 2.5, it can be seen that for a gain of 44.5 dB, the maximum output of the amplifier is ~ 30 W (approximately as gain will vary with frequency),

$$Power\ (dB) = 10 \times \log_{10} (Signal / Reference) \qquad (Eqn.\ 2.5)$$

where Signal is the power of the signal e.g. 30 W and Reference is the reference power e.g. 1mW.

The software performed a control loop which maintained controlled heating and recorded data. The control loop is outlined by the flow diagram shown by figure 2.13.

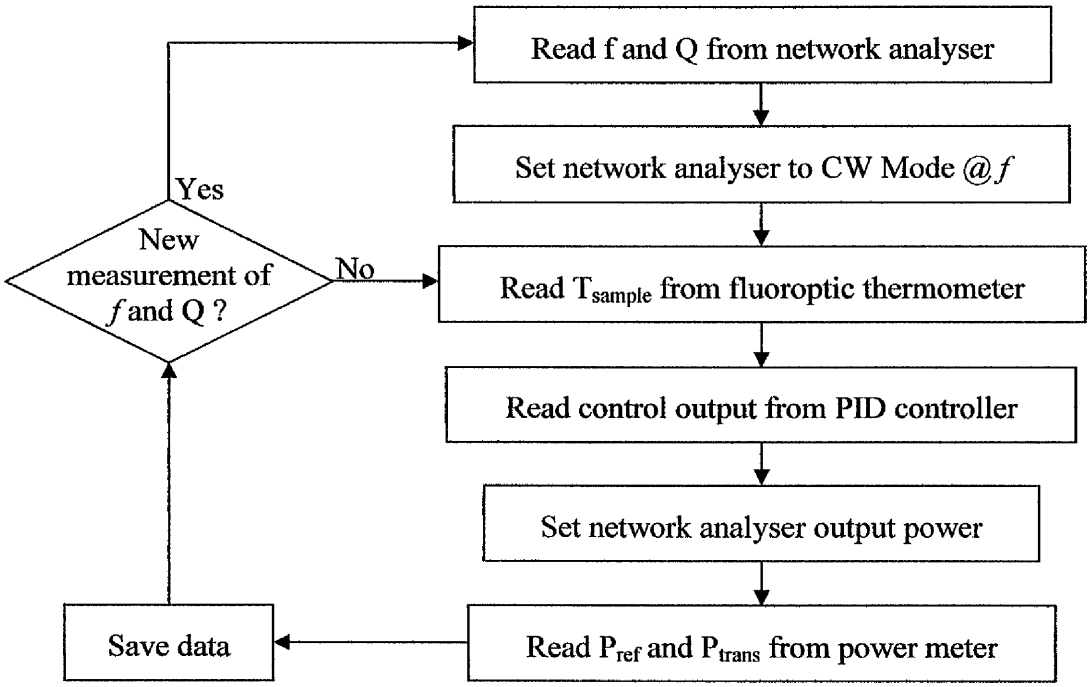

Figure 2.13: Control and data acquisition loop performed by the process control software (Nesbitt *et al.*, 2004).

During heating, the network analyser measured the transmitted signal peak position and bandwidth at operator defined intervals. The cavity quality factor (Q factor) and resonant frequency of the cavity were then determined from these measurements. The computer then set the network analyser to CW (single frequency) mode at the previously determined cavity resonant frequency. Sample temperature measurement was performed using a fluoroptic thermometer (described in further detail in section 2.6.1). The sample temperature was sent as an analog signal from the fluoroptic thermometer to the PID controller. A control output from the PID controller (0-5V), proportional to the source power needed to maintain the desired heating rate or isothermal temperature was then set. The control output signal was then sent through a 12-bit analog-digital converter to the computer. The computer then set the required network analyser output power. The reflected and transmitted power was recorded using Anritsu power sensors (PS) (MA2472B) and an Anritsu power meter (ML2438A), which was connected to a PC by a GPIB (general purpose interface bus). Transmitted power was also recorded directly by the network analyser. It was necessary to use a 30 dB attenuator (AT) to reduce the amplified power to avoid

damage to the network analyser RF input port. The power required for heating was then calculated by subtracting the transmitted and reflected power from the power supplied. The recorded data was then saved and the control loop repeated until the end of the program

After the signal had been amplified it was routed through a coaxial cable and directional coupler to the cavity. To calculate the power which had been dissipated and absorbed by the sample, both transmitted and reflected power values were required. Direct measurement of the reflected power was not possible as it could not be recorded back through the microwave amplifier. Thus, a directional coupler which allowed the reflected signal to bypass the amplifier was used (Nesbitt *et al.*, 2004).

The signal was launched into the cavity using a loop constructed from semi rigid coaxial cable. The field generated inside the cavity was in the TE_{111} mode, which was perpendicular to the cavity axis with the maximum field intensity located at the centre of the cavity. The apparatus heating cell was a cylindrical brass resonant cavity with dimensions of, radius 58 mm and height 77 mm. At a frequency of 2.45 GHz the cavity resonated in the TE_{111} mode with maximum field intensity concentrated in the centre of the cavity as shown by figure 2.14 (red on the scale bar represents maximum field intensity).

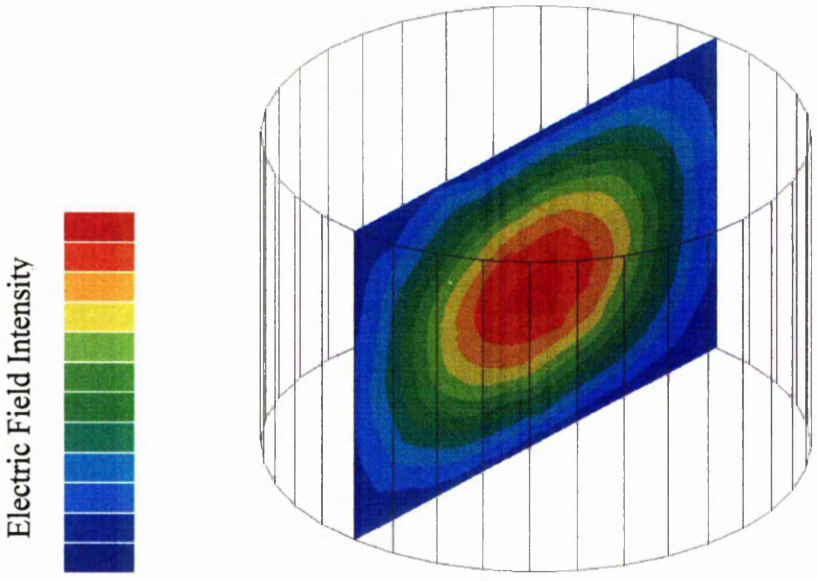

Figure 2.14: Calorimeter electric field distribution generated by Ansoft high frequency structure simulation software (HFSS) v.8.5 (Nesbitt *et al.*, 2004)

Three loops were used inside the cavity, one with a circumference of approximately half a wavelength at 2.45 GHz (~61 mm), which was used to launch the microwaves into the cavity and another two smaller loops each with diameters of approximately 5 mm which were used to detect the transmitted signal (Nesbitt *et al.*, 2004). Figure 2.15 shows the location of the sample in the heating cell.

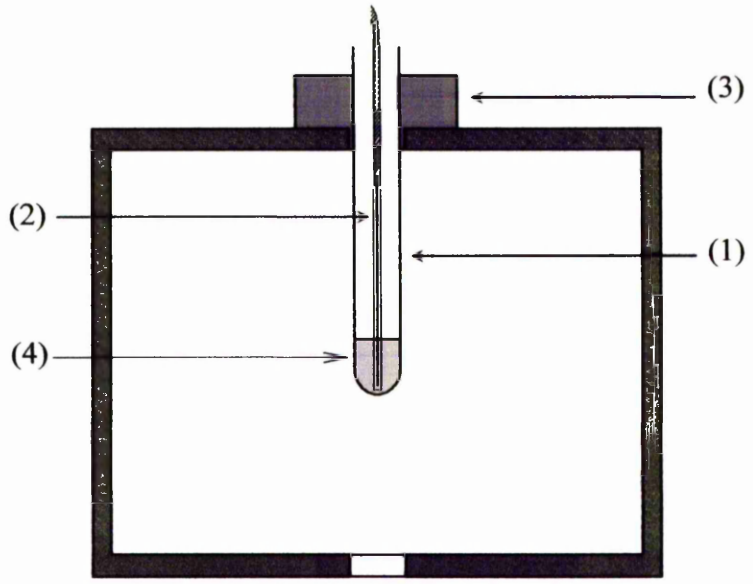

Figure 2.15: Microwave calorimeter heating cell. (1) sample tube, (2) temperature probe, (3) PTFE tube clamp, (4) sample (Nesbitt *et al.*, 2004)

2.4.4.2: Microwave Calorimeter Data Refinement

The data produced by the microwave calorimeter showed the variation in power required to maintain a specified heating rate and thus emulated conventional DSC. It was not possible to draw definite conclusions from the raw data generated by the microwave calorimeter due to the oscillation of the power and temperature readings. Before the data could be analysed, it was necessary to remove the oscillation.

The microwave calorimeter shares a similarity with conventional power compensated DSC data in so much as temperature is plotted against input power. An example of the raw data (generated by heating a sample of DCP BC 40 K pd at 15 K per minute) is shown in figure 2.16.

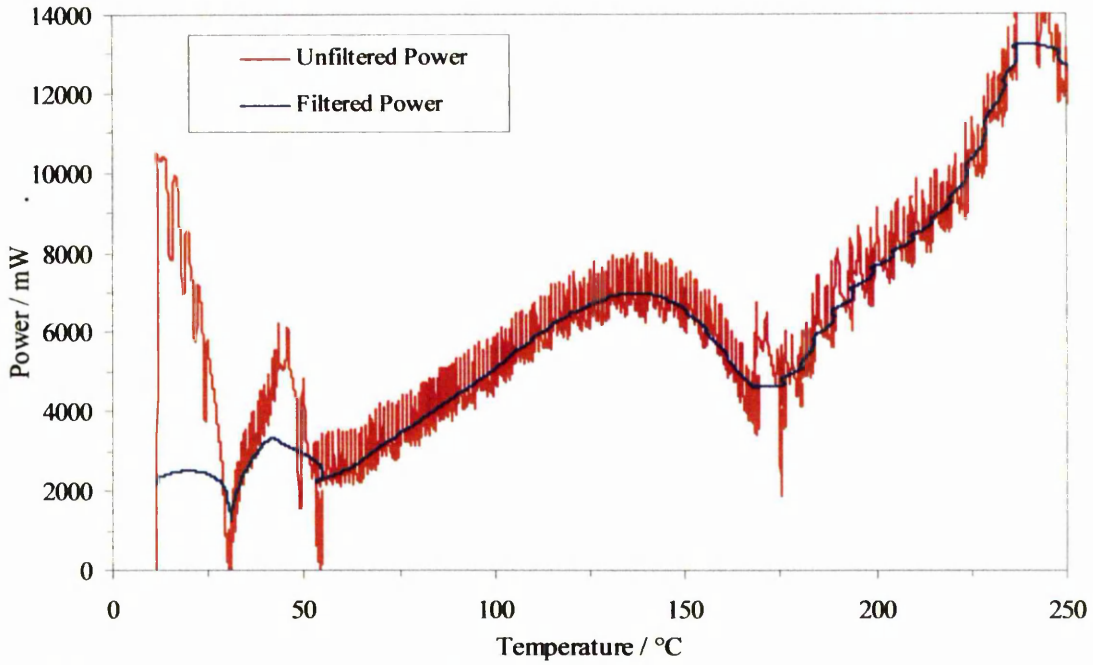

Figure 2.16: Superimposed unfiltered and filtered microwave calorimeter data (heating trace for DCP shown as example)

As figure 2.16 shows, considerable oscillation was present in the power reading. This was a result of the delays due to cycle time of the control program and time taken for the analogue–digital converter to operate. Thus, the data file generated by the microwave calorimeter had a characteristic frequency which was found and processed using a fast Fourier transform filter as shown by the blue line in figure 2.16. It may also be seen that the temperature profile was not perfectly linear and a degree of oscillation was present, as shown by 2.17.

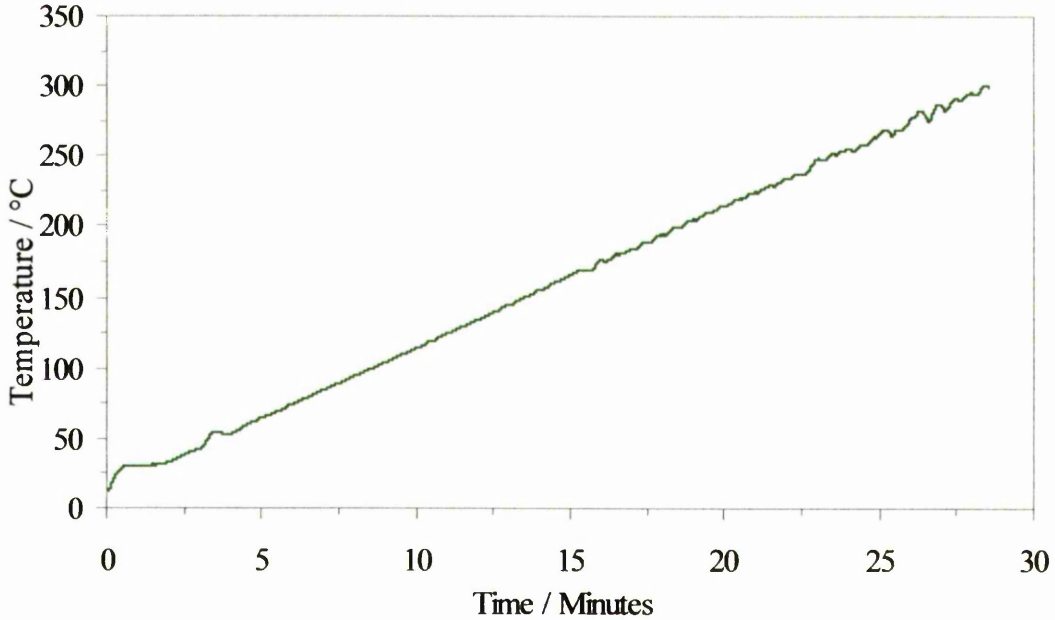

Figure 2.17: DCP oscillating heating rate

The oscillation was due to limitations of the heating algorithm and response time of the system. A linear trend line was then made to fit the data and used to calculate the theoretical linear heating rate and remove the oscillation. The fully processed data is displayed by figure 2.18.

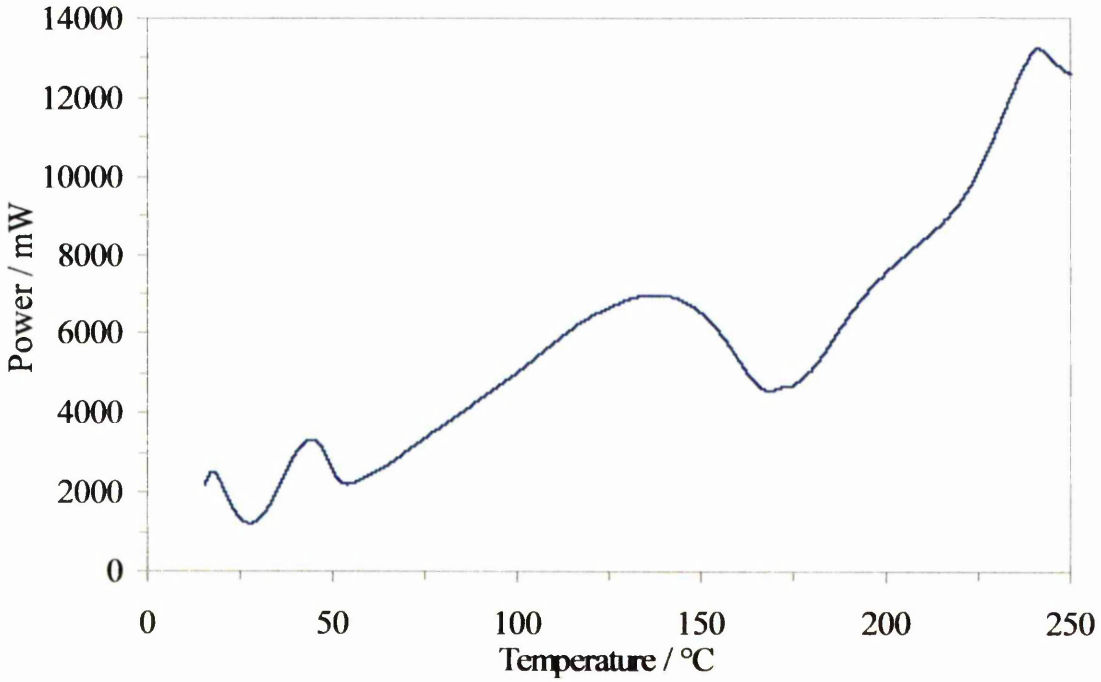

Figure 2.18: Refined microwave calorimeter DCP data

2.4.4.3: Dielectric Measurements

The microwave calorimeter had the facility to make *in situ* dielectric measurements during the heating cycle to provide information on how the dielectric properties changed as the samples were heated. Dielectric property measurement was based on the cavity perturbation technique as described in section 2.4.1.1. During the heating cycle, periodic measurements (10 second intervals) of the resonant frequency and the cavity Q factor were made. The samples were heated at a rate of 15 K min^{-1} and the values of loss factor, ε'' and dielectric constant, ε' were calculated using equations 2.6 and 2.7 (Chen *et al.*, 1996),

$$\varepsilon'' = \frac{1}{B}\left(\frac{1}{Q_s} - \frac{1}{Q_c}\right)\frac{V_c}{V_s}$$

(Eqn. 2.6)

$$\varepsilon' = 1 + \frac{(f_c - f_s)}{f_c}\frac{V_c}{V_s}\frac{1}{A}$$

(Eqn. 2.7)

where f_0 is the resonant frequency for the empty cavity, f_s the resonant frequency for the perturbed cavity, V_{cav} the cavity volume, V_{sam} the sample volume, Q_0 the empty cavity quality factor and Q_s is the perturbed cavity quality factor. A and B are independent parameters which are dependant upon the cavity and sample geometries and the cavity resonant mode. The values of A and B were determined experimentally by calibration using cavity perturbation and dielectric probe sample measurements at room temperature. A and B were then calculated using equations 2.8 and 2.9,

$$A = \frac{(\varepsilon'_{ca} - 1)}{(\varepsilon'_p - 1)}$$

(Eqn. 2.8)

$$B = \frac{\varepsilon''_{ca}}{\varepsilon''_p}$$

(Eqn. 2.9)

where ε'_{ca} and ε''_{ca} were determined using cavity perturbation and equations 2.6 and 2.7. Values of ε'_p and ε''_p were determined at 2.45 GHz using the dielectric probe as described in section 2.4.1.2.

2.5: Foam Characterisation

2.5.1: Density Measurements

The density of foamed samples was determined in order to provide information on parameters such as degree of foam expansion and the efficiency of blowing agent gas usage.

2.5.1.1: Cutting and Weighing

Where the size of the foamed samples was sufficient, the simplest method of measuring density was as follows (ASTM D 3575-93, 1993). Samples produced by compression moulding and by microwave methods had a skin that was first removed, as its density was considerably different from that of the bulk of the sample. Care was taken such that samples were free from defects such as large voids and areas of unfoamed material that would create misleading results. It was also necessary to ensure that the sides of the cut samples were parallel to allow accurate measurement. Cutting of the foam was done using a tool steel hacksaw blade with a freshly ground knife edge in place of the usual serrations. Samples with dimensions 20 × 50 × 50

mm were produced and their dimensions determined to an accuracy of ± 0.01 mm with digital callipers. Sample weights were then accurately determined to 0.0001 g on an analytical balance. The foam density was then calculated according to equation 2.10,

$$\rho_f = \frac{M}{V}$$

(Eqn. 2.10)

where ρ_f is the density of the sample (kg m^{-3}), M is the sample mass (kg) and V is the volume of the sample (m^3). The results quoted are the mean of five separate determinations in order to provide an indication of the experimental variability.

2.5.1.2: Pycnometry

The method outlined in the previous section is convenient for large regularly shaped samples. The size of the samples produced by microwave heating was limited however, as they had to fit through the waveguide entrance allowing for the expansion that took place during foaming. It was not feasible, therefore, to cut and measure these very small samples. Pycnometry was employed to determine the volume of these foam samples. Pycnometry employs the principle of water displacement to calculate the volume (and density) of a sample of known mass. Having previously determined (with an analytical balance to an accuracy of 0.0001g) the mass of the dry bottle and lid, the bottle filled with water and lid and the sample, the bottle was filled with water and the sample inserted. The pycnometer bottle lid (which had a capillary running through it to allow expulsion of displaced water) was then replaced and the excess water was dried from the bottle with an absorbent towel. The bottle was then re-weighed and the specific gravity (SG) of the sample derived from equation 2.11,

$$SG = \frac{W_1}{W_2 - (W_3 - W_1)}$$

(Eqn. 2.11)

where SG is the specific gravity, W_1 is the weight of the foam sample, W_2 is the mass of the pycnometer bottle (filled with water) and lid and W_3 is the mass of the pycnometer bottle, lid water and immersed foam sample. The absolute density (kg m^{-3}) of the sample was obtained by the multiplication of the specific gravity by the density of water at the testing temperature.

2.5.2: Scanning Electron Microscopy

The first stage in the operation of an SEM is the generation of a fine beam of electrons. This is often achieved by using a filament (commonly tungsten) held at a large negative potential (typically between 1 and 50 kV). The anode and specimen are held at earth potential. The beam is focussed onto the specimen using a system of lenses.

When the electrons impinge upon the specimen, a number of different interactions may take place as described below.

1. Backscattering of primary electrons may occur by the interaction with the positively charged nucleus of an atom within the specimen.
2. Secondary electrons may be generated by the collision of a primary electron with and subsequent ejection of an electron a specimen atom.
3. Following the ejection of an electron from a specimen atom, an electron from a less tightly bound state falls into the inner shell. This is accompanied by the emission of a photon, which is often in the X-ray region of the electromagnetic spectrum.

The electron beam, under the control of the scan coils, is scanned across the surface of the specimen in a television like raster or series of parallel lines. When the electron beam strikes the sample, the interactions described above take place. The critical feature of the SEM is the emission of secondary electrons with energies of a few tens of eV and the reflection of much higher energy primary beam electrons as backscattered electrons. The energies of both the backscattered and secondary electrons are highly sensitive to the angle at which the primary electron beam strikes the sample surface. Numerous detectors are located within the specimen chamber to measure the signals that are generated. These are received by a collector and used to modulate the intensity of the electron beam in a cathode ray tube, which is scanning in synchronisation with the microscope beam.

As previously mentioned, the angle at which the primary beam impinges upon the sample and hence the specimen topography, has a great effect on the energies of the secondary and backscattered electrons. The images produced as a result have a good

depth field and a high quality three-dimensional appearance (Billmeyer, 1984; Campbell and White, 1989). The basic layout of an SEM is shown by figure 2.19.

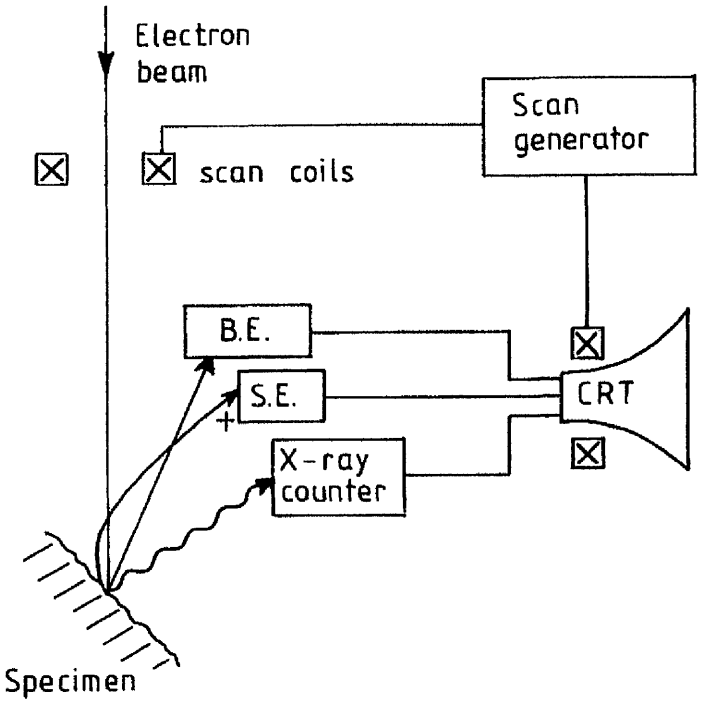

Figure 2.19: SEM schematic (Campbell and White, 1989)

To show the effect of different processing techniques on foam cell size and structure, small samples of foam were examined with a Phillips 525 scanning electron microscope (SEM). Foam samples approximately 10 mm square by 5 mm thick were cut with an extremely sharp knife to avoid deformation of the cut surface. The specimens were then fastened to SEM sample holders with double-sided adhesive tape. Care was taken to ensure that the side viewed by the microscope would be that parallel to the direction of foam rise.

Surface preparation of the sample surface consisted of a gold (a very good secondary electron source) sputter coating under vacuum in an argon atmosphere. Coating was carried for a total of two minutes performed in thirty second intervals with thirty second cooling periods in between to limit thermal damage to the sample. To ensure sufficient conduction between the gold-coated surface of the sample on the SEM sample holder, a thin line of conducting silver paint was applied between the two. Coated samples were then transferred to a Phillips SEM 505 scanning electron microscope. To allow direct comparison between images, a constant magnification of 3.9×10^1, a voltage of 10 kV and a spot size of 100 nm were selected.

The images of the foam cell structure obtained from the SEM allowed an estimation of the mean apparent cell size. The method used was a modification of a technique commonly used in industrial foam production (Sims and Khunniteekool, 1994). A transparent sheet was placed over the SEM micrograph and six reference lines were drawn as shown in figure 2.20 (the cells are omitted for clarity).

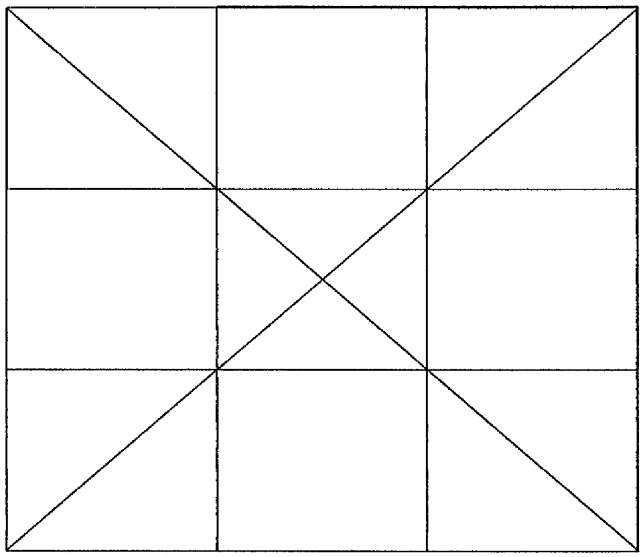

Figure 2.20: Micrograph measurement lines

The number of cells bisected by each line was then counted and the average cell size calculated by division of the total number of cells into the total length of the lines. The length of each line was calculated from the scale bar provided on the micrograph.

2.5.3: Mechanical Testing

2.5.3.1: Foam Compression Testing

Compression load deflection tests were carried out using an Instron 1122 universal testing machine equipped with a compression cage and a 2 kN load cell. Parallel sided samples of foam with dimensions of 50 × 50 × 15-20 mm were prepared in accordance with ASTM D 3575-00 (ASTM D 3575-00, 2000), and tested under a controlled environment maintained at 23 ± 2°C and 50 ± 5 % relative humidity. The samples, which were free from obvious defects such as large voids, were then placed in the compression cage and compressed at a crosshead speed of 20 mm min^{-1} using a chart speed of 100 mm min^{-1} and a full scale deflection of 500 N. The foam samples were compressed to a maximum of 80 %. Stress and strain values were then

calculated at 10 % compression increments from 10-60 % inclusive and also at 75 % compression using equations 2.12 and 2.13,

$$\sigma = \frac{F}{A_0}$$

(Eqn. 2.12)

$$\varepsilon = \frac{h_0 - h}{h_0}$$

(Eqn. 2.13)

where, σ is the stress, F_0 the force, A_0 the original cross sectional area, ε the strain, h_0 the original sample height and h the sample height at strain ε. The elastic modulus, E, was derived from the initial linear slope (elastic region) of the force deflection plots using equation 2.14.

$$E = \frac{\sigma}{\varepsilon}$$

(Eqn. 2.14)

2.5.3.2: Crosslinked Base Polymer Tensile Testing

Tensile testing of crosslinked EVA base polymer samples was carried out using an Instron 1122 universal testing machine. Crosslinked dumbbell shaped specimens with widths of approximately 4 mm and thicknesses of approximately 1.5 mm were tested under a controlled environment maintained at 23 ± 2°C and 50 ± 5 % relative humidity. The samples were tested at a crosshead speed of 20 mm min^{-1}, a chart speed of 100 mm min^{-1} and a gauge length of 25 mm. The elastic modulus was derived from the initial linear slope (elastic region) of the force deflection plots using equation 2.14.

2.6: Thermometry

One of the main problems associated with microwave heating is that of temperature measurement. Traditional wire thermocouples are unsuitable as they are made of metal and would cause arcing when placed in a microwave field. Two alternative methods of temperature measurement were used in this work. The methods used different principles of operation and were designed to be unaffected by microwave radiation.

2.6.1: Fluoroptic Thermometer

The temperature measurement equipment used for the waveguide foaming and microwave calorimeter was a four channel Luxtron 790 fluoroptic thermometer. The temperature probes used were fibre optic SFF wide range / fast response immersion type. The method of temperature measurement used by the system is based upon a temperature sensitive phosphorescent (which may be defined as slowly decaying fluorescence on removal of excitation source) sensor located at the tip of each temperature probe. The sensor is composed of a magnesium fluorogermanate (MFG), which is activated with tetravalent manganese). The technical specifications of the probes are given in figure 2.21.

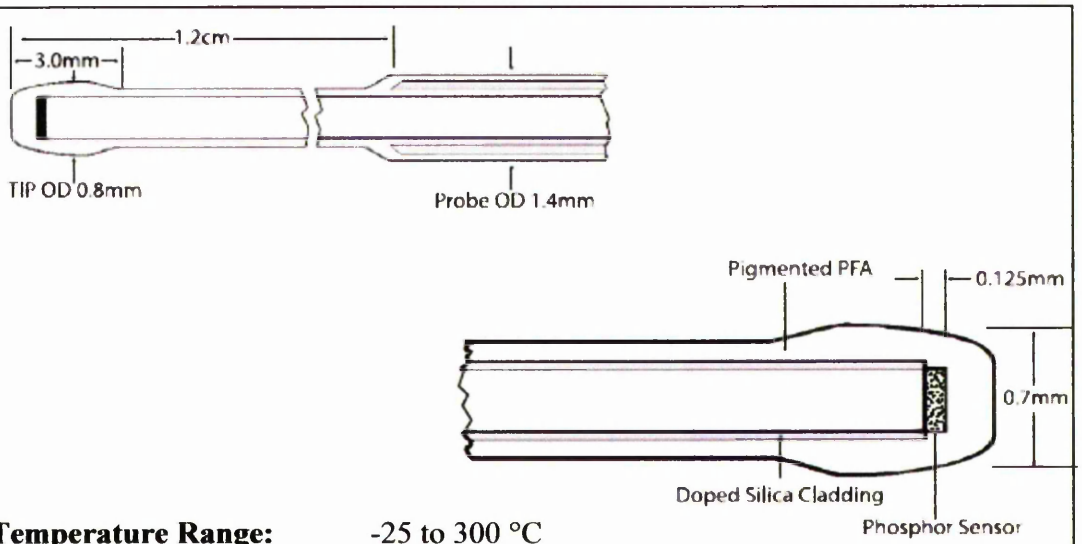

Temperature Range:	-25 to 300 °C
Response Time:	1.25 milliseconds in stirred water
Fibre Type:	200µm all silica, double PFA Teflon jacketed Kevlar cable fibre

Figure 2.21: Immersion type fluoroptic probe specifications (Luxtron, 2005)

The main instrument generates a blue-violet excitation light pulse, which travels down the fibre optic cable by internal reflections of the light pulse from the interface of the fibre optic core and the core cladding. On reaching the sensor, the light pulse causes it to glow red (fluoresce). The fluorescent signal then travels back down the fibre optic cable and is received by the main instrument. The decay rate of the fluorescence is precisely related to temperature.

The decay time is then calculated by multipoint integration of the decay curve, as depicted in figure 2.22, which is then related to temperature.

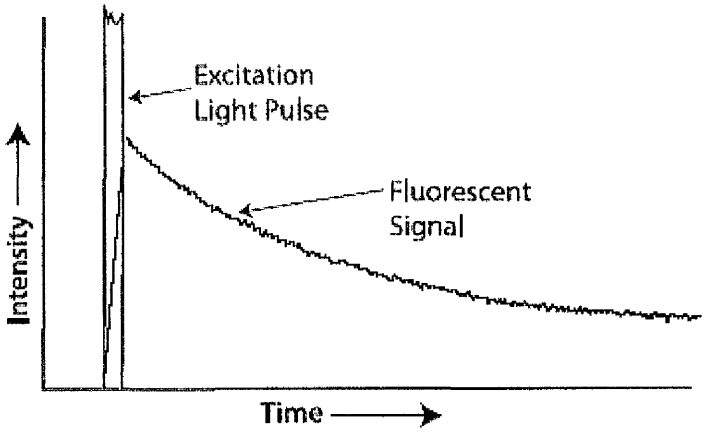

Figure 2.22: Fluorescence decay rate curve (Luxtron, 2005)

2.6.2: Fabry-Perot Based Thermometry

The temperature measurement system used for variable frequency microwave oven foaming was a Bus System manufactured by Fiso Technologies Incorporated. The Bus System is a multi channel, simultaneous reading signal conditioner. The signal conditioner used was a two-channel model with an independently controllable 10-volt analogue output per channel. The temperature probes were FOT-H models. In common with the Luxtron system, the Fiso temperature probes also utilised fibre optic technology. Instead of a chemical sensor the Fiso probes operated on the Fabry-Perot interferometer principle to measure temperature.

The Fabry-Perot interferometric principle is based on the interference of light rays. The probe sensor is a small cavity (gage) located a few millimetres from the end of the probe and is external to the fibre optic cable. The type of probe used is outlined in figures 2.23 and 2.24.

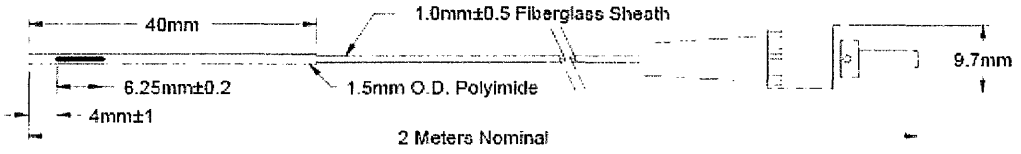

Figure 2.23: Fiso FOT-H temperature probe (Fiso, 2005)

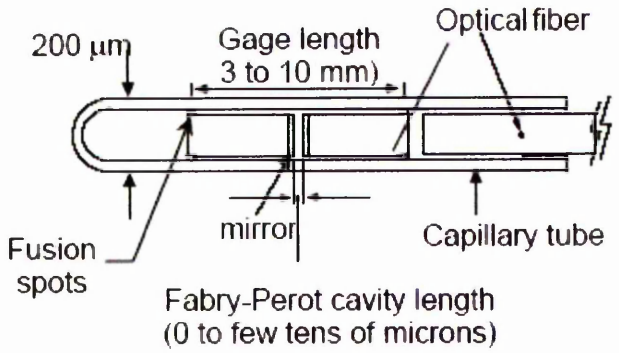

Figure 2.24: Fabry-Perot cavity (Choquet *et al.*, 2000)

The cavity is comprised of two semi-reflective mirrors facing each other. The mirrors are made by the deposition of a semi-reflective coating on the ends of optical fibres, which are then spot fused into a capillary. The air gap between the two mirrors is known as the cavity length, which varies with thermal expansion and contraction. The actual length of the cavity may vary between values of close to zero to a few tens of microns.

The light signal, produced by a white light emitting diode, is launched into one end of the fibre optic cable and travels by internal reflections within the cable to the cavity at the other end. Upon reaching the first semi-reflective mirror, a portion of the light signal is reflected back down the fibre optic cable. The remainder travels through the cavity and is partially reflected again by the second mirror. The light signals from these two reflections interfere resulting in the separation of the original white light into a number of wavelengths, which travel back to the signal conditioner. The signal conditioner then converts the reflected signal into a temperature reading using a Fizeau interferometer and a linear CCD (Charge Coupled Device) array combination. A schematic diagram of a Fizeau interferometer, which is also known as a white light cross correlator, is shown in figure 2.25.

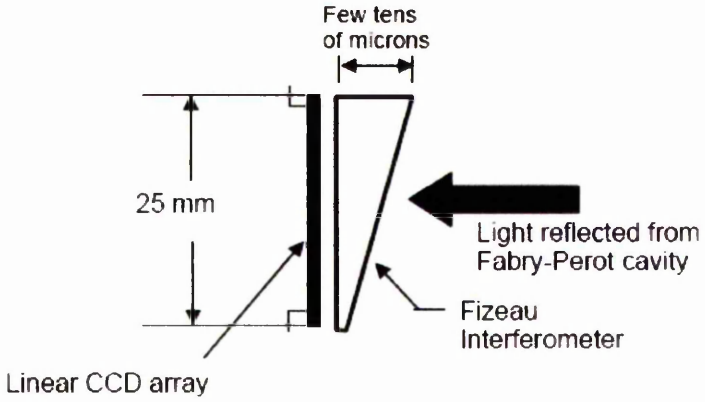

Figure 2.25: Fizeau interferometer and CCD array (Choquet *et al.*, 2000)

The Fizeau interferometer is comprised of a spatially distributed interferometer, the thickness of which varies between almost zero and a few tens of microns i.e. exactly the same as the limits of the cavity length. The reflected signal from the cavity illuminates the entire width of the interferometer. The light signal shows a power peak at the exact point where the thickness of the interferometer equals the length of the cavity. The CCD array behind the interferometer detects the position of the power peak along the interferometer thus the cavity length becomes known and is related to temperature (Choquet *et al.*, 2000).

CHAPTER 3: THERMAL CHARACTERISATION

Thermal analysis was performed to experimentally determine the thermal characteristics of the foam formulation components e.g. decomposition ranges, melting ranges etc. The techniques used included differential scanning calorimetry (DSC) and thermogravimetric analysis (TGA). A microwave calorimeter (which is analogous to conventional DSC) was used to determine the effect of microwave heating on the formulation components and allow comparison with results provided by conventional DSC (Nesbitt *et al.*, 2004).

3.1: Differential Scanning Calorimetry (DSC)

To enable accurate control of foam processing parameters it was necessary to obtain accurate information regarding the temperatures at which the thermally sensitive constituents of the formulation were active. DSC measurements were performed on the crosslinking and blowing agents to provide an independent assessment of their respective dissociation / decomposition ranges.

3.1.1: Azodicarbonamide

A power compensated DSC was used to experimentally verify the decomposition range of ADCE as shown in figure 3.1.

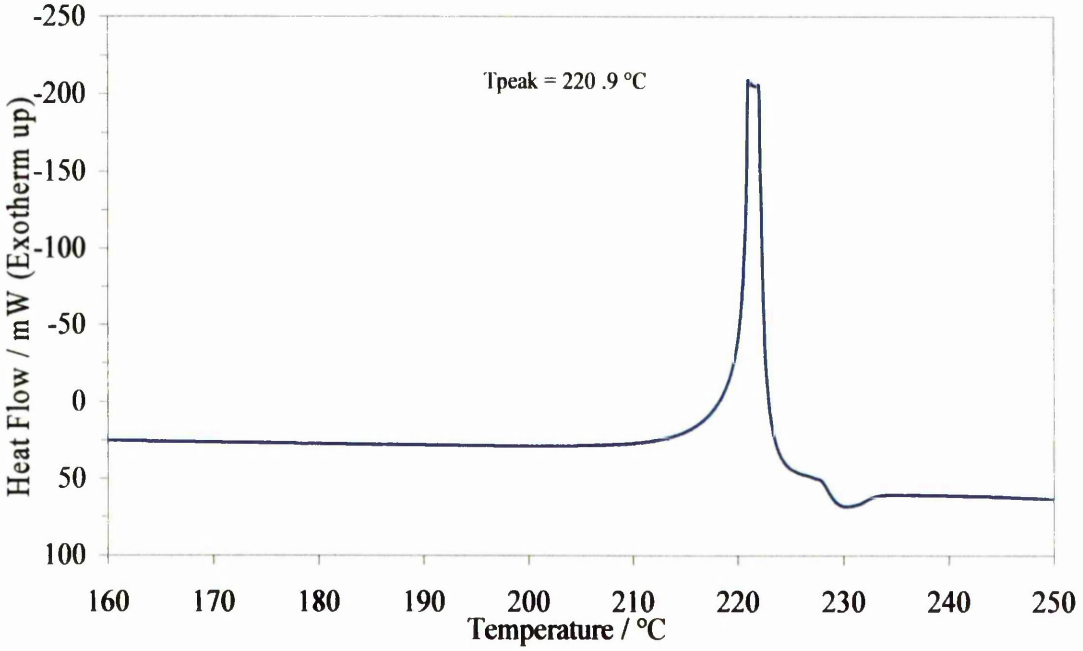

Figure 3.1: DSC data (power compensated) for ADCE heated at 15 K min^{-1}

Initially, measurements on the ADCE were made on a heat flux DSC. It was found that the extremely exothermic nature of the ADCE decomposition resulted in sharp slanted peaks which made determination of the peak temperature difficult. This was due to the inability of this type of DSC to compensate rapidly enough to the large heat changes involved.

The average of three runs was taken which gave an experimental decomposition peak error of ± 2.5 °C showing good repeatability. 10 ± 1 mg samples were used in each case. Figure 3.1 shows a large exotherm peak resulting from the exothermic decomposition of ADCE. This is followed by a smaller peak indicating a subsequent endothermic process. The decomposition mechanisms of ADCE are complex and may result in a number of different reactions and subsequent by products depending upon the conditions, these are outlined in section 1.8.3. The first exothermic peak was the largest and represented the largest energy change. It was therefore, attributed to the primary decomposition pathways. The second much smaller endothermic peak was assigned to the decomposition of by products formed during the primary decomposition mechanisms (Klempner and Frisch, 1991; Prakash *et al.,* 1975; Jaafar and Sims, 1994). These results suggest that blowing agent decomposition and foam expansion should ideally take place at temperatures in the region of 220 °C.

3.1.2: Dicumyl Peroxide

It is important to know the dissociation range of DCP to promote fast efficient crosslinking of the base polymer before the onset of blowing agent decomposition and cell formation. This is important as the uncrosslinked base polymer would not have sufficient melt strength to resist the internal cell pressure generated by the blowing agent gas. The rate at which DCP thermally decomposes is a time-temperature dependant process. In order to clarify the likely processing temperatures used experimentally, DSC measurements were made at a heating rate of 15 K min^{-1} to determine the exact dissociation temperature range of DCP. The results are reported in figure 3.2. An average of three runs was taken. These showed good repeatability. 10 ± 1 mg samples were used in each case.

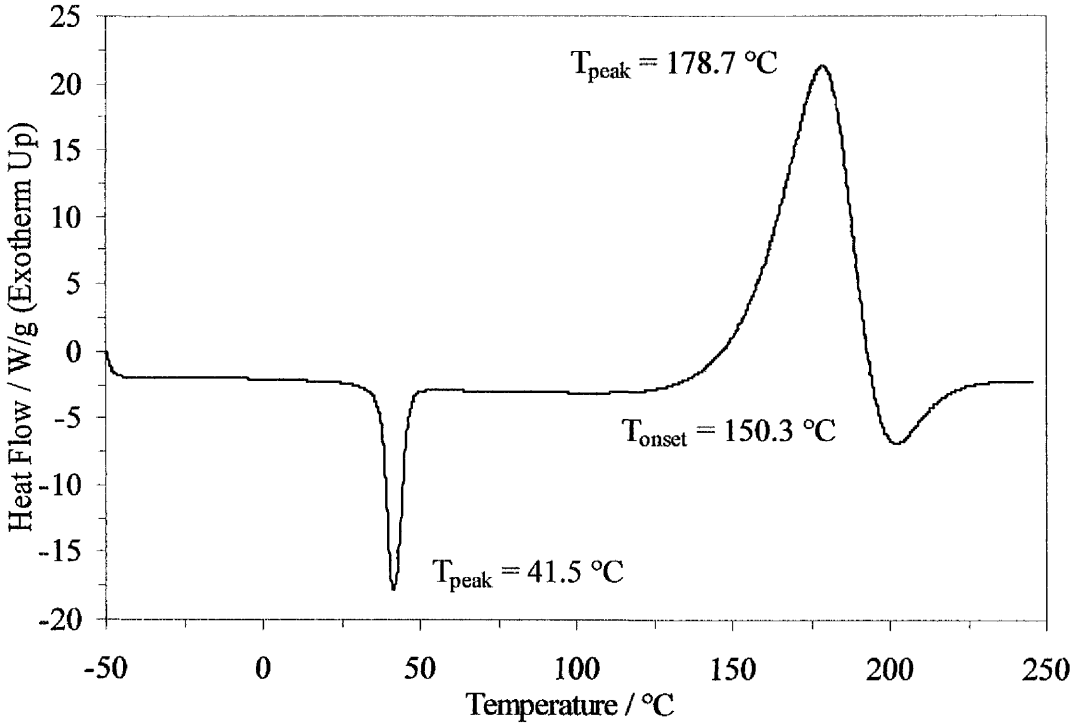

Figure 3.2: DSC data for DCP heated at 15 K min^{-1}

Figure 3.2 shows an endothermic peak at a temperature of 41.5 °C. This correlates well with the specified melting temperature of 39 °C (Akzo Nobel, 2001). The secondary larger exothermic peak was assigned to the dissociation of the DCP oxygen-oxygen bond and the generation of free radical species as shown by equations 1.29. The dissociation onset and peak temperature are shown in figure 3.2. These results indicate that for efficient crosslinking to take place within a reasonable timescale, temperatures between 150 and 179 °C should be used. DCP half life data (Akzo Nobel, 2001) show that at 150 °C, DCP half life is approximately 8 minutes. This would result in unacceptably long crosslinking times. For conventionally crosslinked samples, time would also have to be allowed for heat to conduct through the sample thickness. The calculated crosslinking time at 178 °C is less than 1 minute. It is important to remember that crosslinking should be complete or close to completion before the onset of blowing agent decomposition and foam expansion to prevent foam collapse. In order to examine the crosslinking and blowing agent decomposition separately, it was desirable to keep their decomposition processes separated. Although crosslinking at 178 °C would provide fast network formation it is very close to the decomposition range of ADCE (albeit the lower end and, therefore, any ADCE decomposition would be very slow). It was decided that crosslinking should be performed at 165 °C as a trade off between the two extremes.

3.1.3: Base Polymer Melting Point and Crystallinity Measurements

The EVA base polymer melting points and degrees of crystallinity were measured using DSC. All three grades were measured three times and the results were averaged. Typical DSC traces are shown in figure 3.3.

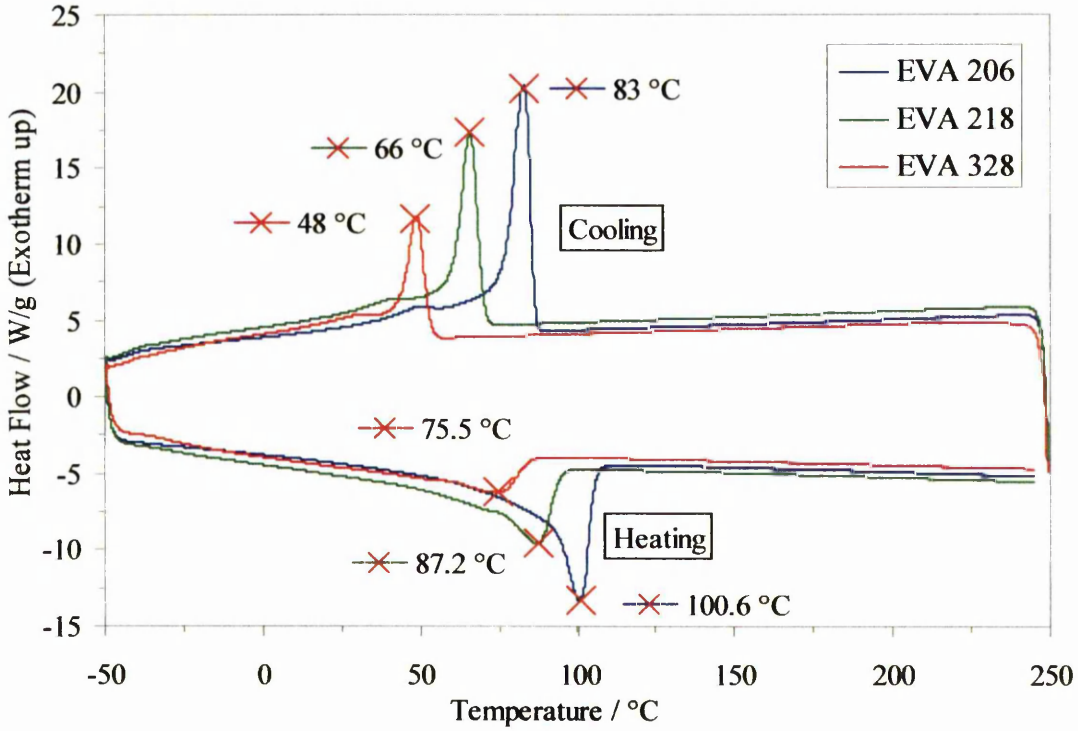

Figure 3.3: DSC data for three EVA base polymers heated at 15 K min^{-1}

In order to erase any thermal history and enable direct comparison with blended polymer formulations (since melting during milling and processing would have this effect), the thermal history of the polymer samples was erased by heating to above the melting point and cooling in the DSC before any measurements were taken. Melting enthalpy was taken as the area underneath each peak which deviated from the baseline. Measurements were taken of the pure base polymers and of the polymers blended with crosslinking and blowing agents. As figure 3.3 shows, a decrease in melting, recrystallisation temperature and melting enthalpy peak size with increasing polymer vinyl acetate content was observed. These trends were attributed to the effect of vinyl acetate on the polymer structures. The pendant vinyl acetate groups are large and bulky. As such, they disrupt polymer crystallinity by steric hindrance preventing efficient packing of the polymer chains and the formation of ordered crystalline regions. Thus, as vinyl acetate content increased, polymer crystallinity was reduced. Crystallinity was measured, using equation 2.4, for each of the three

pure polymers alone and for the polymers blended with crosslinking and blowing agents. The findings are reported in tables 3.1 and 3.2, respectively.

Table 3.1: Crystallinity data for the three EVA base polymers obtained using DSC

Polymer	Melting Point / °C	Melting Enthalpy / J g^{-1}	Crystallinity / %
EVA 206	100.6 ± 0.1	71.1 ± 3.6	24.8 ± 1.0
EVA 218	87.2 ± 0.6	44.2 ± 0.4	15.5 ± 0.5
EVA 328	75.5 ± 0.2	10.9 ± 0.2	4.6 ± 0.7

Table 3.2: Crystallinity data for the three EVA base polymers blended with 0.5 phr DCP and 8 phr ADCE obtained using DSC

Polymer + 0.5 phr DCP, 8 phr ADCE	Melting Point / °C	Melting Enthalpy / J g^{-1}	Crystallinity / %
EVA 206	100.3 ± 0.7	54.6 ± 3.5	19.0 ± 1.2
EVA 218	87.8 ± 0.2	20.2 ± 1.0	7.1 ± 0.4
EVA 328	74.3 ± 0.5	9.6 ± 1.6	3.4 ± 0.5

When the results in Table 3.1 are compared with those in Table 3.2 it may be seen that the incorporation of crosslinking and blowing agents into the polymer matrix had the effect of decreasing crystallinity. It would appear that the incorporation of fine particulates into the polymer matrix reduced the ability of the polymer chains to form ordered crystalline regions. Crystallinity often reduces the ability of a polymer system to interact with an alternating electric field as the crystalline regions limit the dipole and molecular vibrations (Chen *et al.*, 1993). It may be expected, therefore, that blending the base polymers with the additives necessary for foaming and disrupting the crystalline regions formation, would increase microwave heating efficiency. Data presented in subsequent sections does not support this argument, however.

3.2: Thermogravimetric Analysis (TGA)

The DSC results obtained for the dissociation and decomposition characteristics of the crosslinking agent and the blowing agent were supplemented by thermogravimetric measurements. Thermogravimetric analysis, which measures sample weight as a

function of time and temperature, was performed on each of the foam formulation components to help define processing conditions. This technique was also applied to the EVA base polymers to study the effect of oxidative degradation.

3.2.1: Azodicarbonamide

The decomposition range of ADCE is 200–220 °C (Sims and O'Connor, 1998). To clarify and support the results obtained by DSC measurements, further characterisation was performed using TGA. Figure 3.4 shows ADCE weight loss as a function of temperature. Three heating runs were performed (which gave a decomposition temperature range error of ± 3 °C) and averaged. The results are shown in figure 3.4.

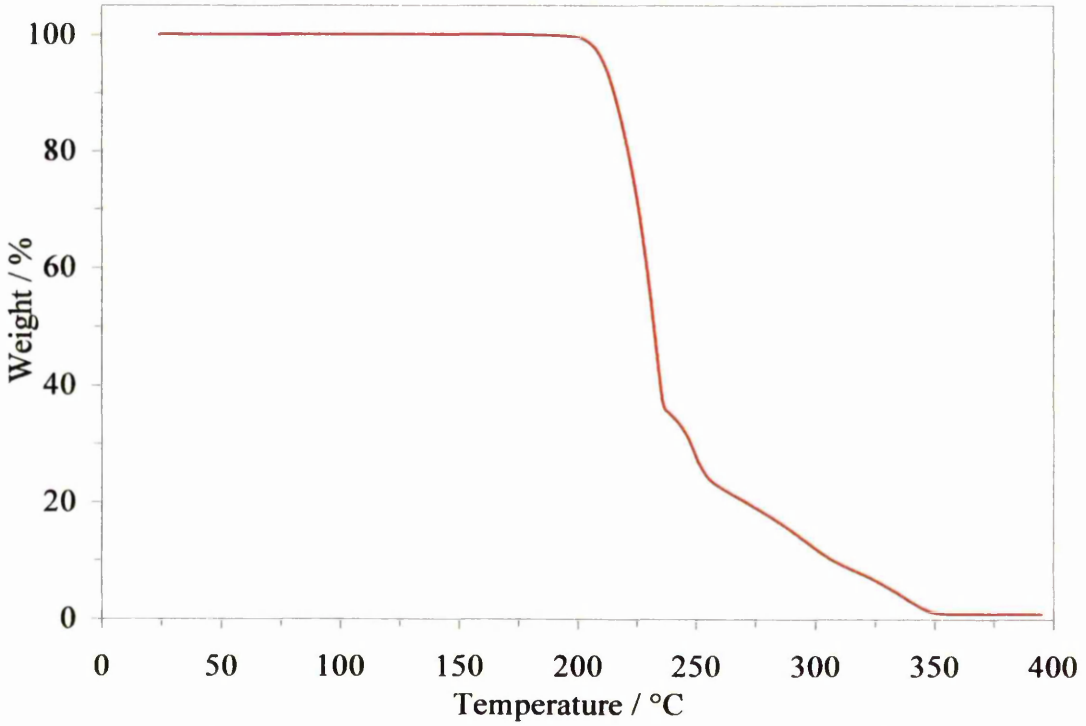

Figure 3.4: TGA data for ADCE heated at 15 K min^{-1}

During the heating cycle, the decomposition of ADCE appears to take place in three distinct stages. In the first stage, which occurred between approximately 199 and 236 °C, 64 % of the original mass was lost. This first decomposition stage represents the major decomposition phase of ADCE. The second and third decomposition stages occurred in the temperature ranges of 236 – 253 °C and 253 – 352 °C and represented mass losses of approximately 11 and 25 %, respectively. These were attributed to the decomposition of by products formed during the main ADCE decomposition reactions (O'Connor, 1999) as discussed in section 1.5.3. Samples of azodicarbonamide were

also heated isothermally at a range of temperatures over its specified decomposition range. The air assistance temperature used in the combination oven was 170 °C. Measurements were also taken at this temperature to predict the effect of the hot air assistance on the overall foaming process. The results are presented in figure 3.5.

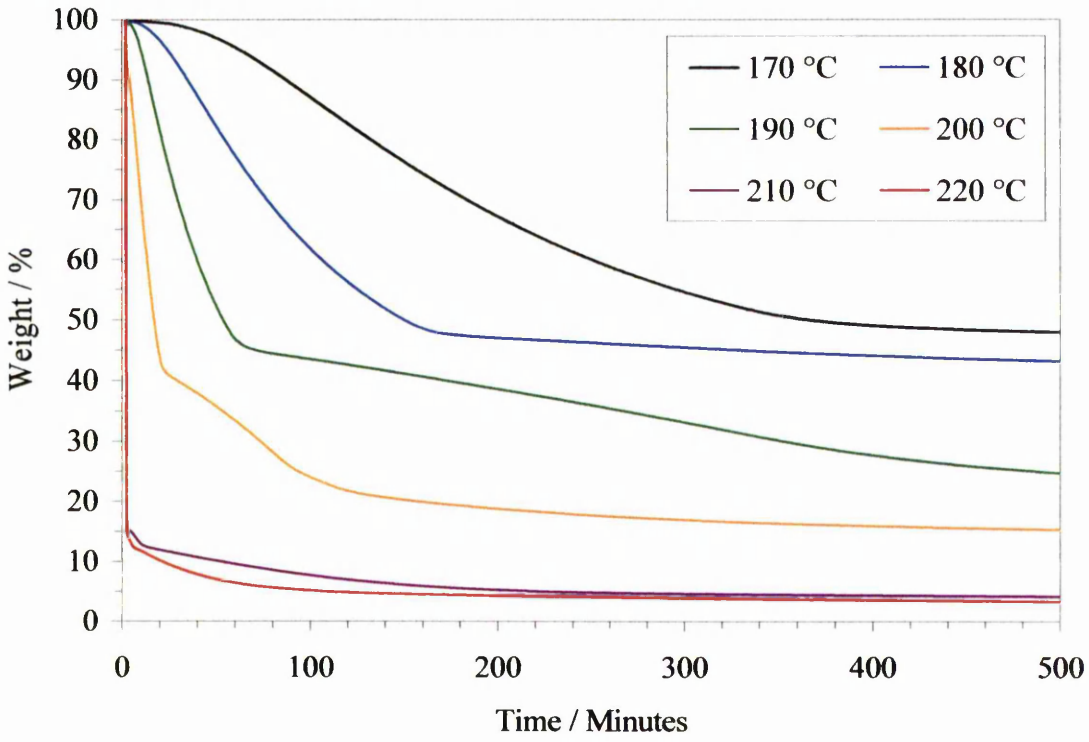

Figure 3.5: Isothermal TGA data for ADCE

Figure 3.5 shows that at the lower end of the temperature range studied, ADCE decomposition was relatively slow. At 170 °C there was very little weight loss (approximately 5 %) after 60 minutes heating time. After 100 minutes as little as 10 % of the original sample mass had been lost. This shows that foam production at this temperature would be extremely slow. The sample weight continued to decrease until approximately 50 % of the original mass was lost after approximately 400 minutes. As the decomposition temperature was increased, the rate of decomposition and final percentage weight loss increased. All decomposition profiles between 170 and 200 °C reach a plateau, beyond which, decomposition appeared to cease or progress at a negligible rate. Although the TGA data in figure 3.5 clearly demonstrated that ADCE decomposition took place at temperatures of 170, 180, 190 and 200 °C, it also shows that decomposition was very slow and did not proceed to completion. This is demonstrated by the residual sample mass, which remained at extended heating times. Figure 3.5 also shows that ADCE decomposition proceeded rapidly at 210 and 220

°C. Accurate determination of decomposition profiles at these two temperatures may be more clearly observed upon examination of figure 3.6.

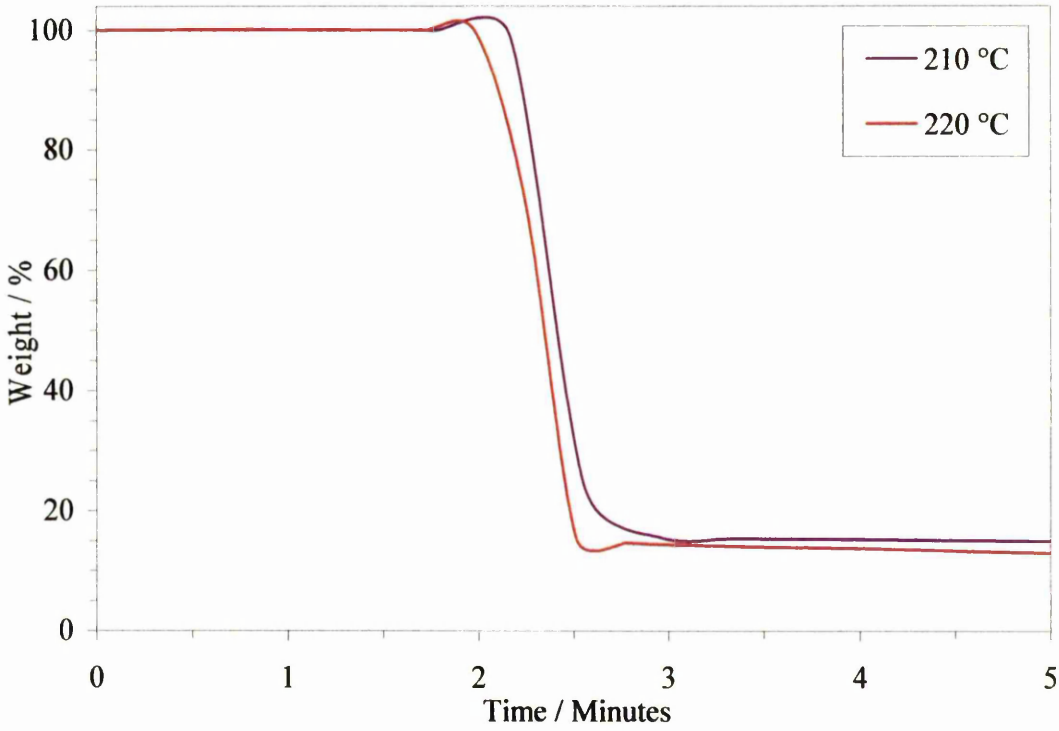

Figure 3.6: Expanded detail of isothermal ADCE TGA decomposition data at 210 and 220 °C

The data in figure 3.6 at 210 and 220 °C indicate that the samples underwent an initial small weight increase. This was attributed to sample pan buoyancy caused by rapid temperature rise. The decomposition profiles from 210 and 220 °C are only marginally different and show a rapid weight decrease over a period of 30-40 seconds. Total sample mass loss was in the order of 85 % for both temperatures.

These results indicated that at temperatures below 210 °C ADCE did not completely decompose. This would result in inefficient gas evolution and foam expansion would not be maximised. It has already been stated that the possible ADCE decomposition reactions are complex and involve the formation of numerous by products. Other workers have discovered that the volume of gas produced by ADCE is dependent upon heating rate (Sims and O'Connor, 1998). It is suggested that the incomplete decomposition of ADCE at temperatures below 210 °C is due to the formation of by products that are either thermally stable at these temperatures or decompose very slowly. Further investigation into the thermal decomposition pathways of ADCE is, however, beyond the scope of this work.

3.2.2: Dicumyl Peroxide

The thermally activated dissociation reaction of the peroxide crosslinking agent was also analysed using TGA. The results in figure 3.7 show the change in DCP sample mass with increasing temperature.

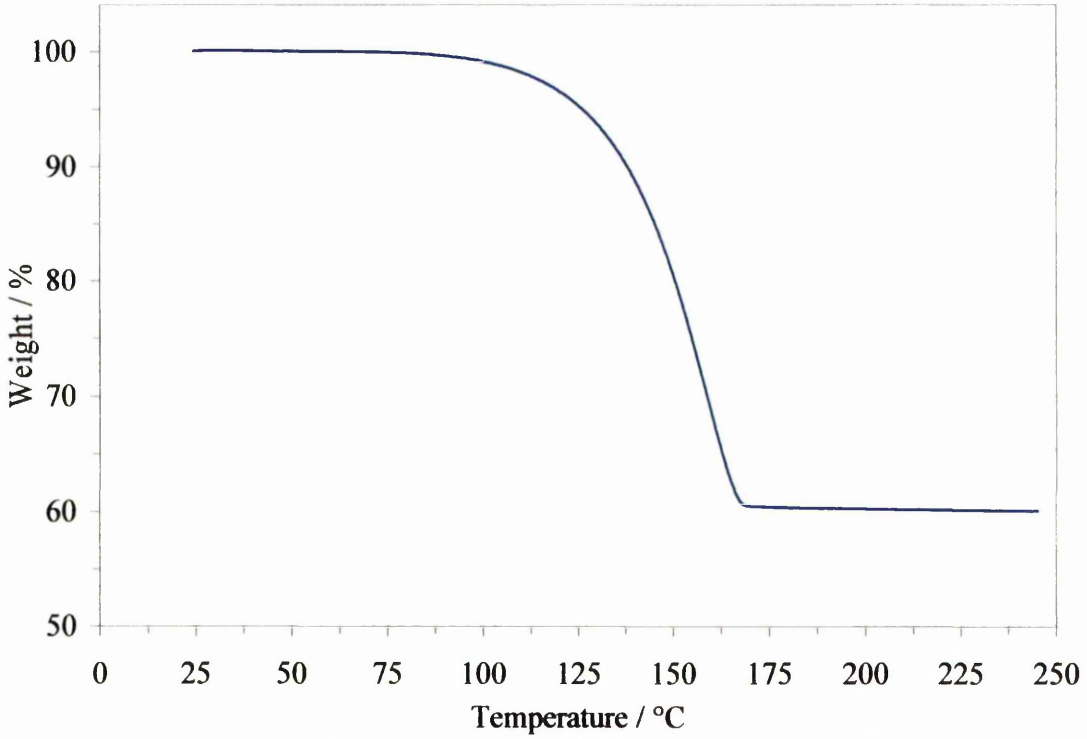

Figure 3.7: TGA data for DCP heated at 15 K min^{-1}

The TGA results in figure 3.7 showed significant DCP weight loss occurring in the region of ~90-165 °C. These results have a level of ambiguity as DCP melts at 39 °C and boils at 130 °C (Akzo Nobel, 2001). It is likely that the majority of the weight change may have been due to volatilisation. It was not possible, therefore, to directly attribute the observed weight loss to the dissociation reaction (although the decomposition temperature range was encompassed). Weight loss proceeded until 40 % of the total mass was lost. As the DCP was 40 % by weight on an inert clay substrate, the residual weight was attributed to the remaining support material.

The dissociation of DCP was also studied under isothermal conditions to study the effect of temperature on the rate of weight loss. The temperatures studied were chosen to encompass the dissociation range of DCP. The results are shown in figure 3.8.

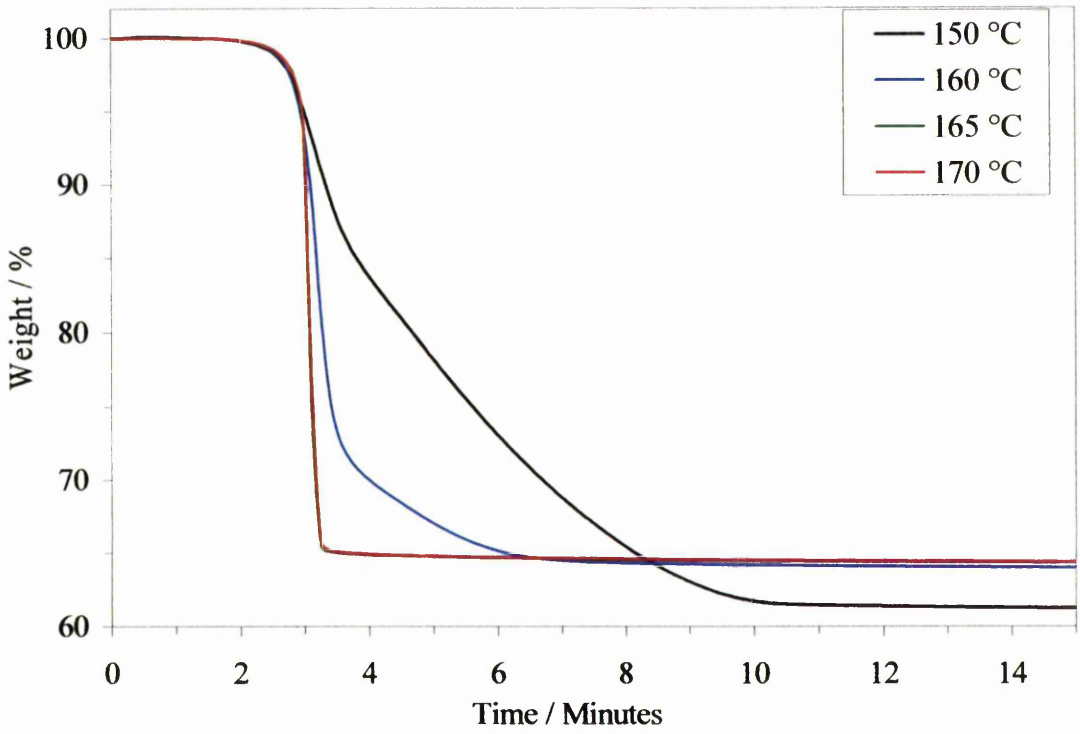

Figure 3.8: Isothermal TGA data for DCP

Figure 3.8 shows a trend of increasing mass loss rate with increasing isotherm temperature. This indicates that as the temperature was raised, the rate of DCP volatilisation, and hence mass loss, increased.

3.2.3: Base Polymers

The EVA base polymers were also analysed using TGA. Each was held at individual isotherm temperatures, applicable to this work, of 170, 180, 190, 200, 210 and 220 °C for 120 minutes to assess the effect of extended heating periods on polymer thermal degradation. The results are presented in figures 3.9 and 3.10. EVA 206 was not analysed using TGA as the results were not relevant to this work.

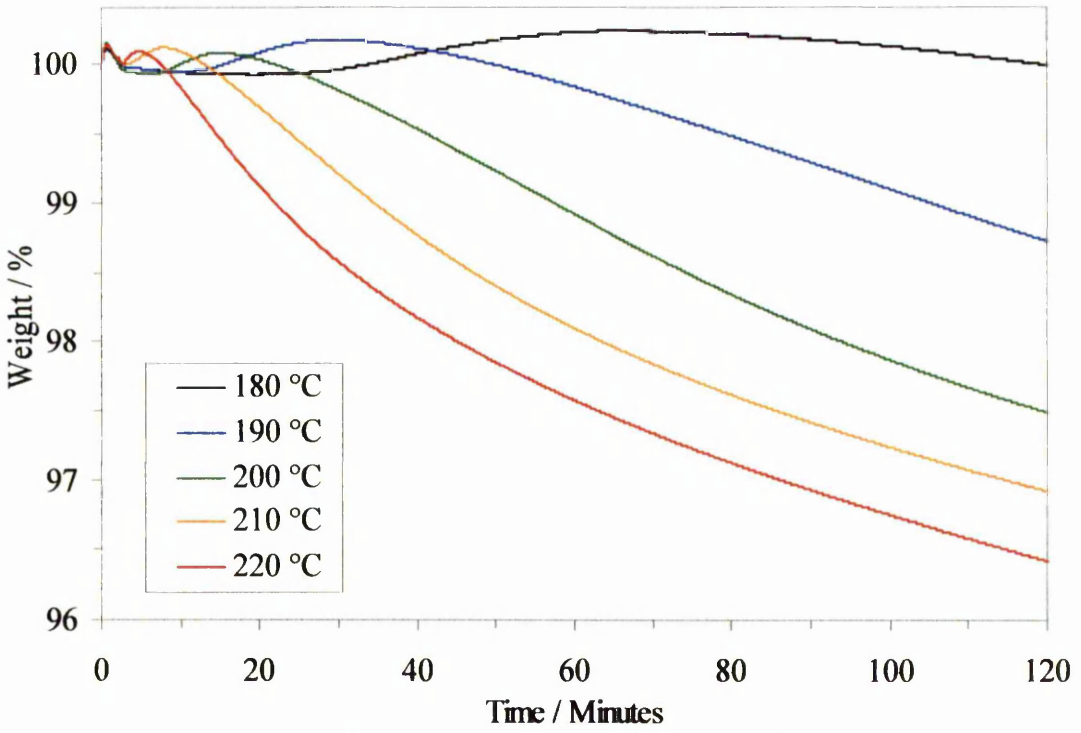

Figure 3.9: EVA 218 TGA variation of sample mass as a function of time and isotherm temperature

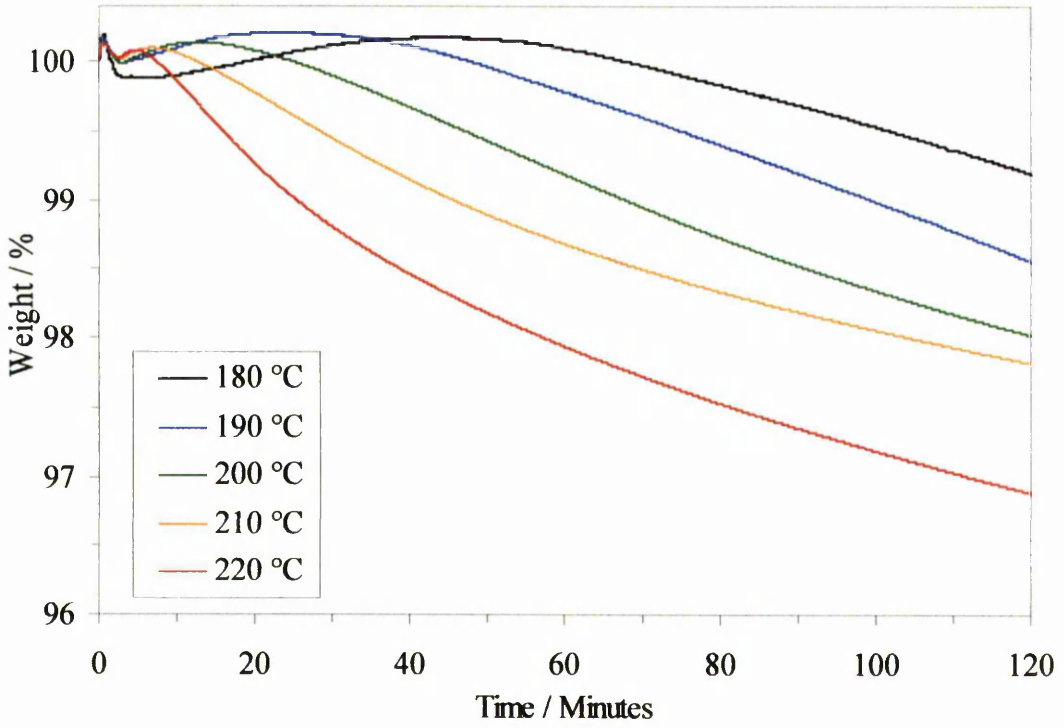

Figure 3.10: EVA 328 TGA variation of sample mass as a function of time and isotherm temperature

The results indicate that weight loss (in the order of 3 %) took place at the upper temperature and time limits and some sample yellowing was evident. Although small,

the mass lost represented 11 and 16 % of the vinyl acetate content (by weight) of EVA 218 and EVA 328, respectively. Figures 3.9 and 3.10 show that the mass lost at heating times less than 40 minutes was much reduced. This suggested that a small degree of thermal degradation during foam processing may occur.

3.3: Microwave Calorimetry

Although the production of polymer foams, using either conventional or microwave techniques, both rely on the thermal activation of the crosslinking and blowing agents there are two fundamental differences between the two techniques. Firstly, conventional hot air heating relies on the transfer of thermal energy from the surrounding air to the sample to be heated. Microwave heating on the other hand employs a direct conversion of electromagnetic energy to thermal energy within the sample. Secondly, conventional heating techniques rely upon the conduction of heat from the surface of a sample to its interior, whereas microwaves heat the sample bulk. Microwave calorimeter measurements were performed so that comparisons could be made with conventional DSC data in order to highlight any differences in the heating processes which may be attributed to the different heating techniques.

3.3.1: Azodicarbonamide

Unfortunately, it was not possible to obtain microwave calorimeter measurements of the decomposition of ADCE. As the ADCE decomposed, the majority of the material was converted to gas and lost to the atmosphere. Thus, as the reaction took place, the sample volume was rapidly reduced until there was very little material left to heat. Unlike a conventional DSC heating cell, the microwave calorimeter does not have a reference heating cell and, therefore, relies upon the microwave power necessary to maintain a fixed sample heating rate. If the sample is lost during the heating run the calorimeter is unable to compensate.

3.3.2: Dicumyl Peroxide

The effect of microwave heating on the dissociation of DCP was studied using the microwave calorimeter, and the data obtained was compared with the results for conventional DSC heating as presented in figure 3.2. To ensure that the complete DCP melting range was recorded, the samples were chilled in ice water to ~ 1 °C

before heating. Samples weighing 0.35g ± 0.05g were then prepared and heated at a rate of 15 K min^{-1}. The results are shown in figure 3.11.

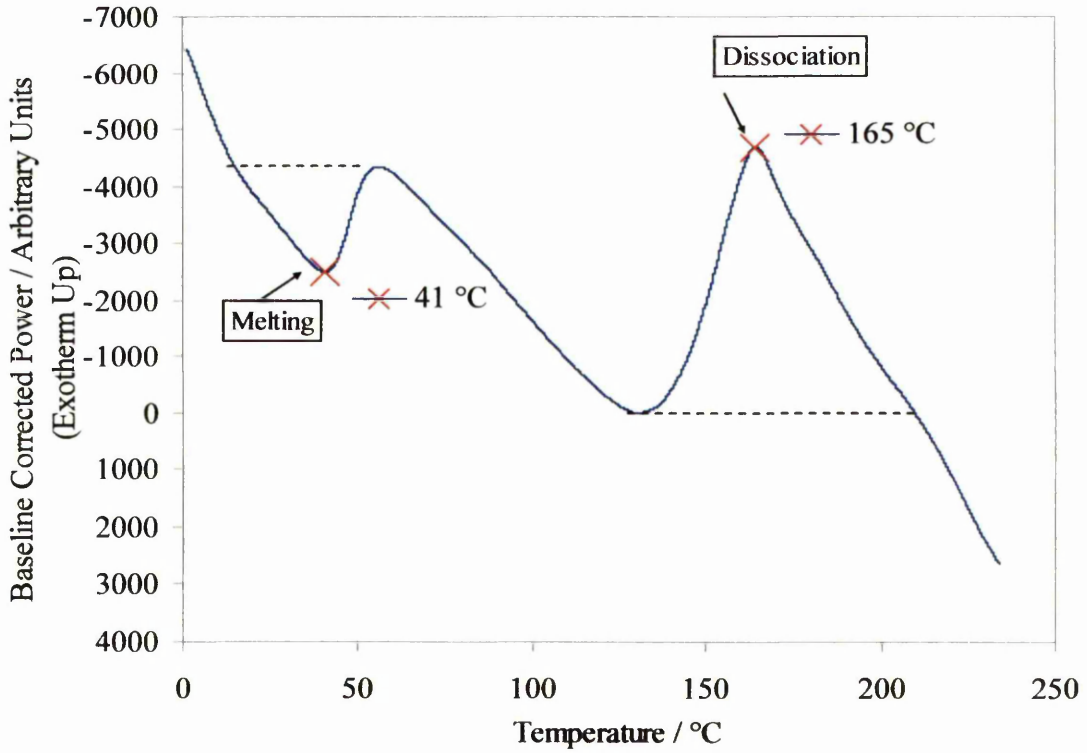

Figure 3.11: Microwave calorimeter data for DCP, heating rate 15 K min^{-1}

By comparison with conventional DSC data the first peak may be attributed to melting of DCP, this is further supported by the literature melting value of 39 °C (Akzo Nobel, 2001). The melting temperature was comparable to that obtained using conventional DSC. This was expected as melting is a physical process and, therefore, the heating method was not expected to have any effect on this value. The decomposition temperature was consistently lower when microwave heating was used. This may due to the electromagnetic field causing decomposition to occur at a lower temperature. This may also be due to a delay in thermal energy being transferred from the sample to the temperature probe.

3.3.3: Base Polymers

Each of the pure EVA base polymers were heated at 15 K min^{-1}. The samples used were heated to remove any thermal history then cooled and reheated. The base polymers were also cooled using microwave power to maintain a 15 K min^{-1} cooling rate. Each of the polymer samples weighed 0.35 ± 0.05 g. The results for EVA 206, 218 and 328 are shown in figures 3.12, 3.13 and 3.14, respectively.

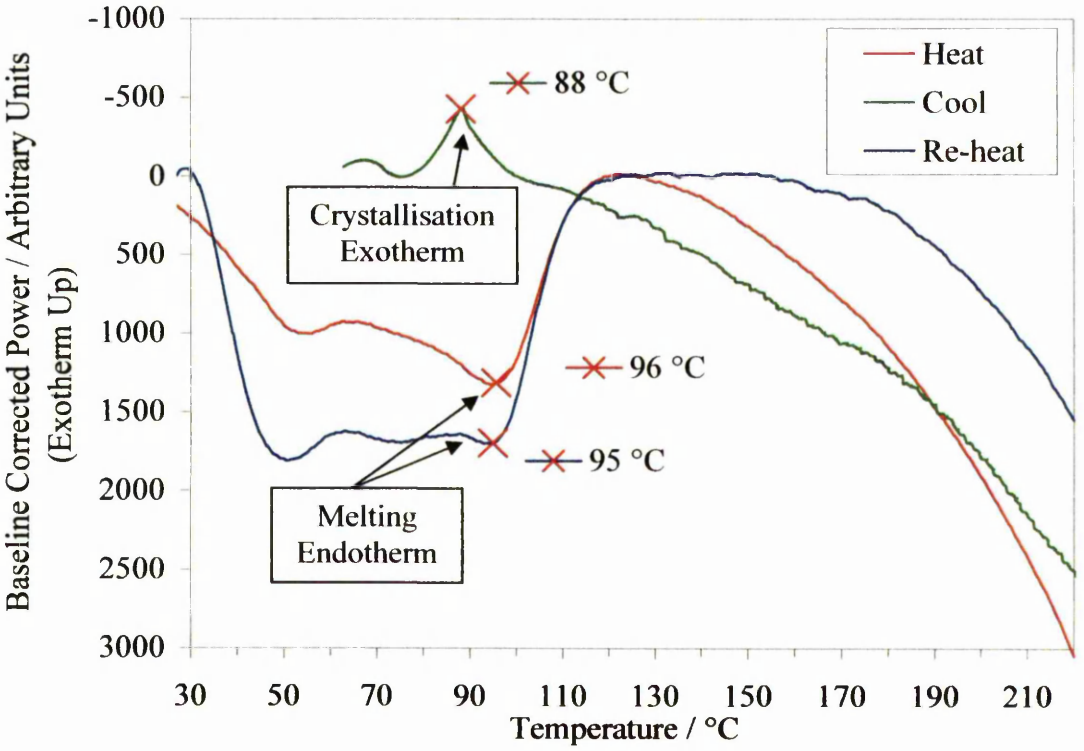

Figure 3.12: Microwave calorimeter data for 0.35 g pure EVA 206 heated at 15 K min^{-1}

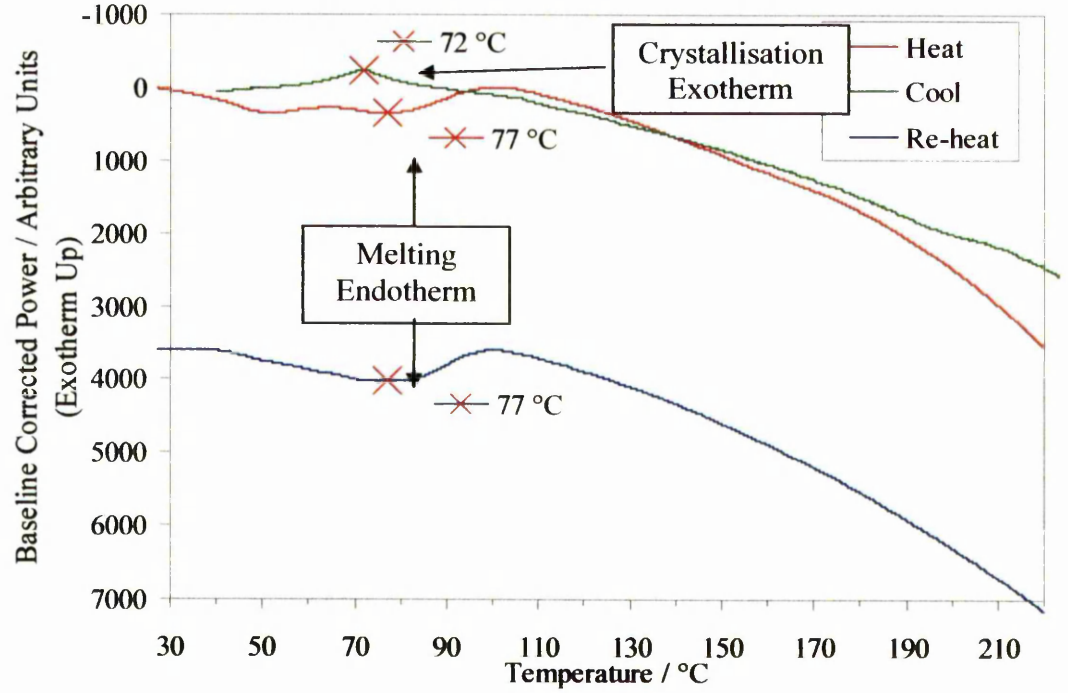

Figure 3.13: Microwave calorimeter data for 0.35 g pure EVA 218 heated at 15 K min^{-1}

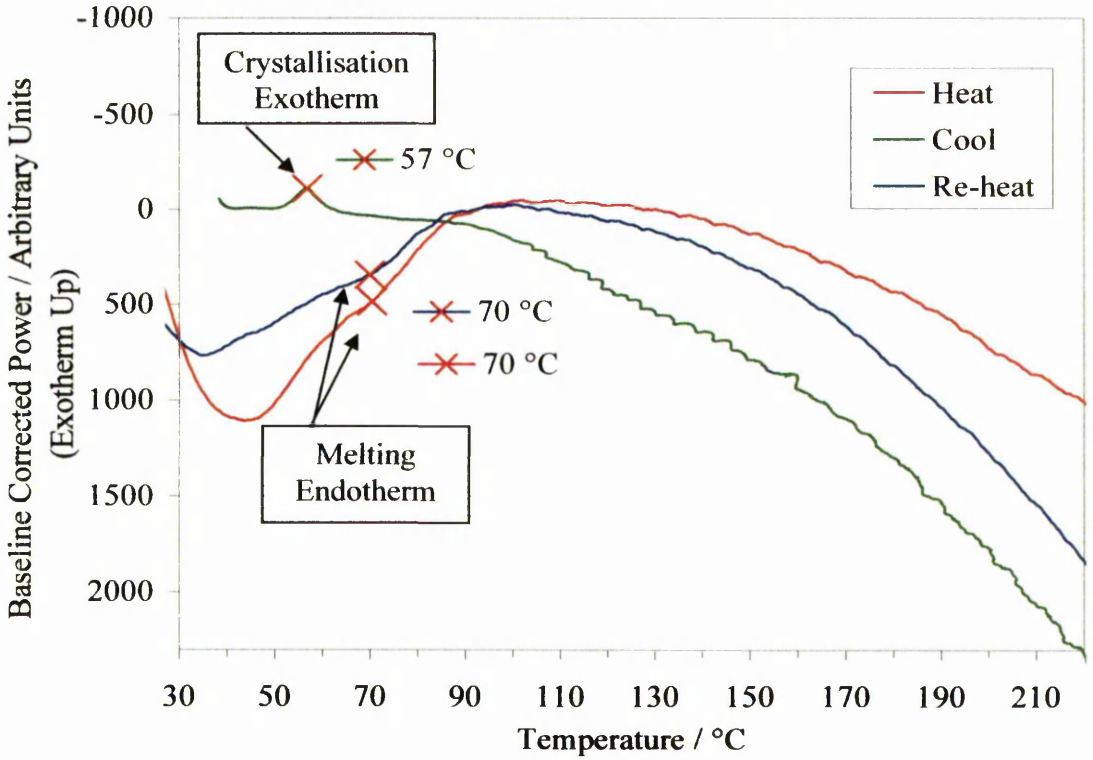

Figure 3.14: Microwave calorimeter data for 0.35 g pure EVA 328 heated at 15 K min^{-1}

When baseline normalisation was applied to figures 3.12, 3.13 and 3.14, the power values on the y axis became arbitrary. The original data corresponding to these figures is presented in appendices 5, 6 and 7 (shown with inverted y axis i.e. exotherm down). The microwave power levels corresponding to the crystalline melting peaks of the three EVA polymers (taken from the original data in appendices 5, 6 and 7) are presented in table 3.3.

Table 3.3: Melting peak microwave power levels for three EVA base polymers

EVA Polymer	Melting Peak Microwave Power Level / mW
206	7000
218	4100
328	3300

Table 3.3 shows that at the EVA crystalline melting points, the microwave power required to heat the samples decreased in the order EVA 206 > 218 > 328. This may be attributed to the increasing percentage of vinyl acetate groups in the polymers. The vinyl acetate groups contain dipoles and are, therefore, microwave active. The vinyl acetate dipole is able to alternate with the microwave field and convert the electrical

energy into heat. As the percentage of vinyl acetate groups was increased, the number of sites available for heat generation increased. This resulted in an increase in the efficiency of the microwave – material interaction and energy conversion. Thus, as the vinyl acetate content of the polymers increased, less energy was required to heat them.

The microwave calorimeter data for each of the base polymers showed two peaks on the initial heating trace. The first demonstrated a trend of increasing magnitude with increasing vinyl acetate content and disappeared on reheating. This was also observed in the conventional DSC data on the initial runs to remove thermal history. The second peak corresponded to the respective melting temperatures of 97, 79, and 71 °C for EVA 206, 218 and 328, respectively. These correlated well with the values obtained from conventional DSC and the values from the polymer datasheets. This was expected as melting is a physical process unlikely to be altered by the electromagnetic field. The melting peaks exhibited a trend of decreasing magnitude with increasing vinyl acetate content. As the vinyl acetate content of the polymer was increased the vinyl acetate side groups disrupted crystallinity by preventing efficient packing of the polymer chains which resulted in a decrease in crystallinity with increasing vinyl acetate content. A decreasing melting peak magnitude with increasing vinyl acetate content was, therefore, expected. The peak values were determined visually from the data and as such are open to a certain degree of interpretation. The peak for EVA 328, which has the lowest percentage crystallinity, was especially difficult to determine as the peak was small and poorly defined.

On cooling, a small exotherm peak was observed for each of the polymers. This peak was attributed to the recrystallisation process. As the polymer samples cool, ordered regions of the ethylene sections of the polymer are formed. The large bulky vinyl acetate groups are confined to the amorphous regions as they disrupt crystallinity by steric hindrance. The recrystallisation exotherm appeared to be higher in the samples heated and cooled in a microwave field. This suggests that the microwave field may have been having a favourable effect on the crystallization process within the polymers used.

After cooling, the polymer samples were then re-heated. It may be seen that the first peak was diminished. This was also seen during reheating of the conventional DSC

samples. This would indicate that it is some artefact of the polymer history and as such is not of great significance to this work.

3.3.4: EVA Base Polymers Blended with ADCE and DCP

EVA base polymer samples were blended with 0.5 phr crosslinking agent and 8 phr blowing agent (i.e. foam formulations). After chilling in ice water to ≈ 1 °C, 0.35g ± 0.005g samples were then heated in the microwave calorimeter to monitor the onset of foaming and its effect on the microwave power required to maintain a 15 K per minute heating rate. The results are presented in figure 3.15. The microwave power levels corresponding to the crystalline melting peaks of the three EVA polymers blended with 0.5 phr DCP and 8phr ADCE (taken from the original data in appendix 8) are presented in table 3.4.

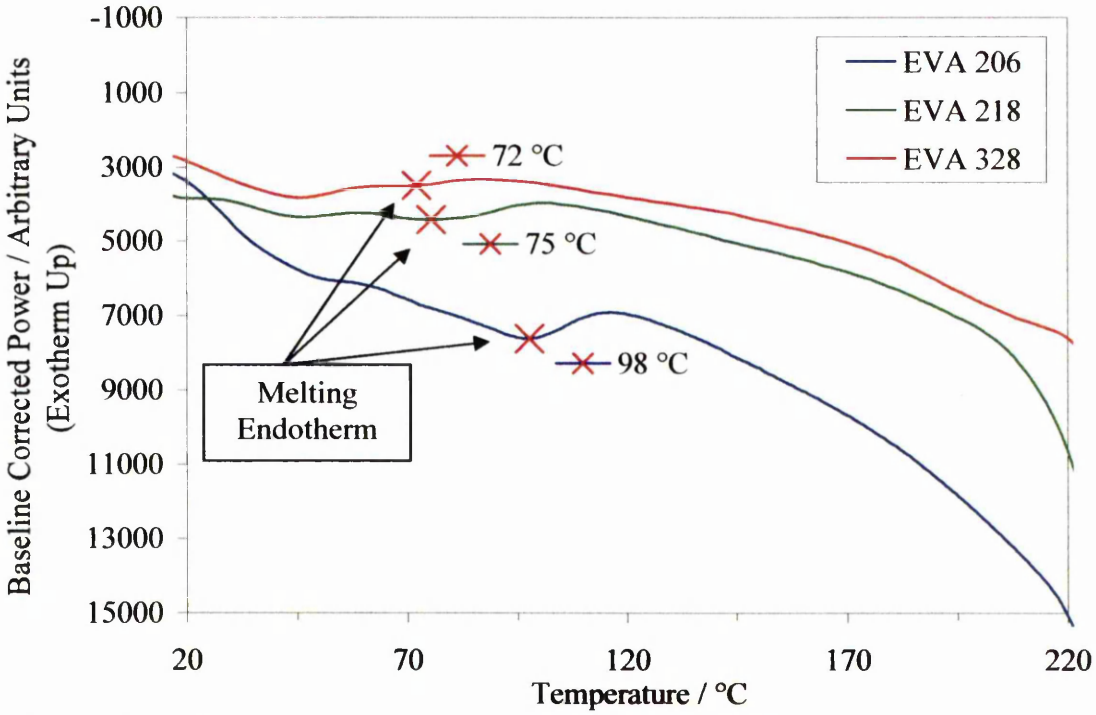

Figure 3.15: Microwave calorimeter data for three EVA base polymers blended with 0.5 phr DCP and 8 phr ADCE

Table 3.4: Melting peak microwave power levels for three EVA base polymers blended with 0.5 phr DCP and 8 phr ADCE

EVA Polymer	Melting Peak Microwave Power Level / mW
206	7800
218	4250
328	3800

When the data in table 3.3 is compared to the data in table 3.4, it may be seen that the microwave power levels at the melting peaks of the compounded polymers was greater than at the pure polymer melting peaks. This would suggest that inclusion of the blowing agent and the crosslinking agent reduced the loss factor of the system and as such rendered it harder to heat. The blowing and crosslinking agents occupy volume that would normally be occupied by polar EVA in pure polymer samples. Thus, their addition reduced the effective percentage polar groups in the system and reduced loss. There was a relatively small percentage of DCP and ADCE in the system so effect on loss was small. Figure 3.15 shows that the inclusion of blowing and crosslinking agent had negligible effect on the base polymer melting points.

As the decomposition temperature range of ADCE was reached the power required to maintain the set heating rate rapidly increased for all three polymers. As the ADCE decomposed, cells were formed within the polymer matrix which then began to expand as more blowing agent gas was liberated. The cells, which essentially contained air, may be considered to be loss free. As they grew, the fraction of lossy polymer per unit volume decreased. As a result, the power required to heat the foaming sample increased as the foaming process continued.

CHAPTER 4: DIELECTRIC CHARACTERISATION

The ability to heat a material using microwave energy and the ease of doing so is governed by the dielectric properties of the material. The dielectric properties are affected by a number of parameters including microwave field frequency, temperature and material composition. It is important, therefore, to make an assessment of a material's dielectric properties before attempting to heat it using microwaves. Dielectric measurements were performed on the EVA base polymers, blowing agent and crosslinking agent used in the foam formulations. The dielectric properties of the mixed crosslinkable, foamable formulation were also measured, since these are often not linearly related to the dielectric properties of the constituent materials.

4.1: Dielectric Properties as a Function of Frequency

The dielectric response of the formulation components as a function of frequency was measured using an open ended coaxial dielectric probe. This was performed to determine the frequency ranges at which heating would be possible and most efficient. A frequency range where the formulation components showed a high loss factor was desirable as this is important for efficient microwave heating to take place. The probe was designed primarily for measuring the dielectric properties of liquids by immersion of the probe within the sample, thus excluding any air between the probe face and the sample. When measuring solid samples, the probe face was pressed against the sample surface. Error was introduced when measuring solid samples as a small portion of air was present at the probe face / sample surface interface. The probe face and sample surface were arranged parallel to one another and pressed firmly together to minimise any air entrapment. The random error was minimised by taking five measurements for each sample and reporting the average. By doing so it was still possible to gain useful information regarding the dielectric property trends with increasing frequency using solid samples. Having set up and calibrated the probe as described in section 2.4.1.2, dielectric measurements were taken to ascertain the most efficient frequencies for microwave heating.

4.1.1: EVA Base Polymers

The dielectric probe used had a theoretical operating frequency range of 20 MHz to 20 GHz. Due to difficulty in establishing a calibration at higher frequencies, caused by minor damage to the probe, this range had to be reduced to 1 GHz to 10 GHz. The measurements were carried out to determine how each of the three EVA grades behaved over a broad frequency range which incorporated two ISM frequencies (2.45 GHz and 5.8 GHz) which are the most convenient for heating. The frequencies at which the polymers were most lossy and, therefore, gave the fastest heating rate could be determined. A solid polymer block was placed under the probe and a measurement was obtained using the method described in section 2.4.1.2. Variation between readings taken in different areas of the sample was encountered. This was presumed to be due to the presence of small amounts of air between the probe / sample interface. The results for the three different grades of EVA are shown by figure 4.1.

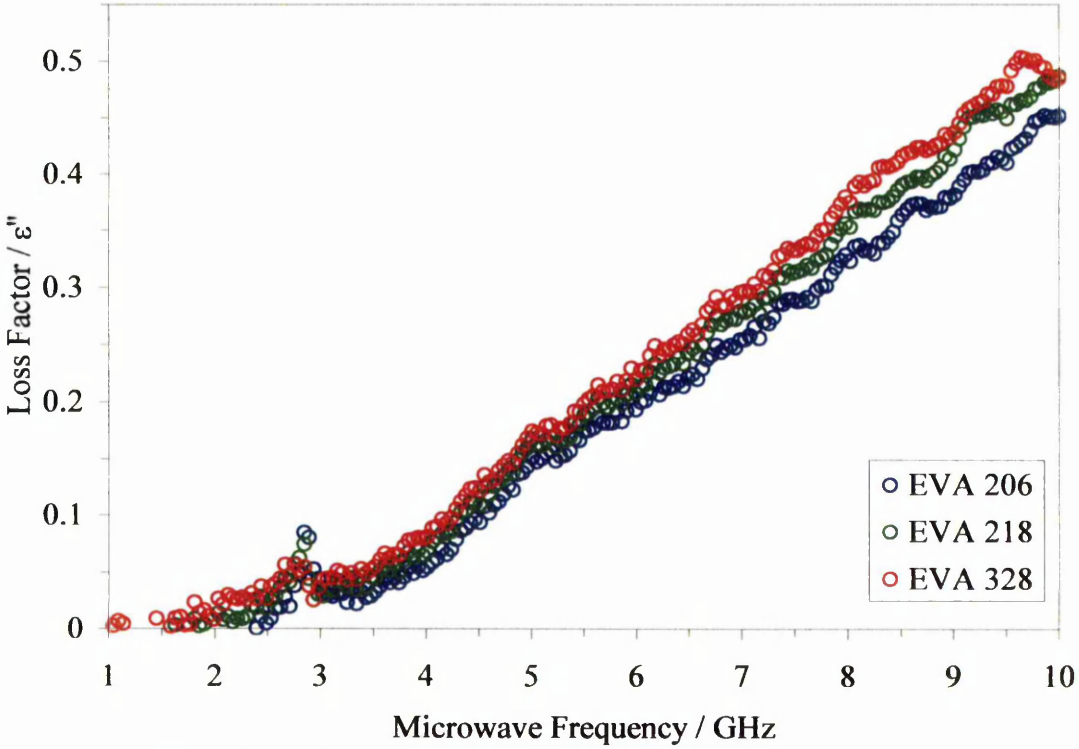

Figure 4.1: Variation of loss factor with frequency for three EVA grades (average of three runs)

A small general increase in loss factor with increasing vinyl acetate content is shown between the three EVA grades. This trend may be explained by consideration of the interaction of the polymers with the applied microwave field. Although there are a number of mechanisms that contribute to the dielectric response of a material such as

electronic and atomic polarisation, ionic conduction and Maxwell Wagner polarisation mechanisms, the most important heating mechanism (at the molecular level) at microwave frequencies arises from dipole polarisation (Thostenson and Chou, 1999; Chen *et al.,* 1993; Miijovic and Wijaya, 1990). In a dielectric material, local charge moves in response to an applied electric field. It is the movement of the bound charge such as dipoles, with the electric field, that results in polarisation. Restriction of this motion within a material creates a lag between the dipole orientation and the alternating electric field. It is this lag, which is known as the dipole relaxation time that converts and dissipates the electric field within the material as heat.

EVA has a greater interaction with microwaves when compared to non-polar polymers such as PE because of the polar vinyl acetate groups present. When an alternating electric field is applied, these dipoles constantly re-orientate themselves. As the amount of vinyl acetate increases, more sites that are capable of interacting with the microwave field are created and the more electrical energy may be converted to heat and distributed throughout the material. As a result an increase in loss factor, which is a measure of ability of a material to convert microwave energy into heat, with increasing vinyl acetate content is observed, as there are more groups lagging behind the field which in turn leads to more friction and, therefore, more heat.

Another factor that must be considered is crystallinity. Polymers that have a degree of crystallinity greater than 45 % are in essence microwave transparent due to the restrictive forces acting on the dipoles (Thostenson and Chou, 1999). Thus, as the degree of crystallinity increases, a corresponding decrease in loss factor may be observed (Chen *et al.,* 1993). Side groups, large bulky ones in particular, have the effect of disrupting crystallinity as they prevent the alignment of polymer chains necessary to form crystallised regions (Young and Lovell, 1991). It would be expected, therefore, that as the percentage of vinyl acetate (side groups) increases in the order EVA 206 < 218 < 328 there would be a corresponding decrease in crystallinity as the rising vinyl acetate content progressively disrupts the ability of the EVA to crystallise. As the polymer becomes more amorphous in nature an increase in loss factor would also be expected as the restrictions on dipole movement are reduced.

It was expected that the three EVA grades would show a trend of increasing loss factor with increasing vinyl acetate content for any given frequency.

The loss factor results suggest that heating at the ISM frequency of 2.45 GHz is possible as the loss factor values are greater than 10^{-2}. This has been reported as the minimum value at which microwave heating is possible (Osswald and Menges, 1996). Heating at frequencies around 2.45 GHz is likely to be slow particularly at low microwave power, however, as the loss is relatively low in this region, suggesting that conversion of microwave energy into heat is likely to be low. The results show (over the frequency range studied) that heating would be more efficient at frequencies greater than 3.5 GHz as the loss factor begins to increase at this point. The dielectric properties of the pure polymers are likely to differ from those of the blended foamable samples. This would be due to contributions to the overall dielectric properties of the system from the blowing agent and crosslinking agent incorporated in the polymer matrix. It is reasonable to assume however, that as the base polymer is present in the greatest quantity, its dielectric properties are likely to dominate. This hypothesis is examined further in section 4.1.4.

The most valuable information that may be obtained from these results is the response of the dielectric loss factor to increasing frequency. As figure 4.1 shows, for EVA 328, the loss factor remained relatively unchanged up to around 3.5 GHz, EVA 218 and 206 showed a small increase. From approximately 4-8 GHz all three EVA grades became increasingly lossy. The observed increase in loss factor with increasing frequency may be explained by consideration of the interaction of the microwave field and the polar vinyl acetate groups joined to the polymer chain. The loss factor is a measure of the phase lag of the polar groups behind the alternating microwave field. As the frequency of the alternating electromagnetic field increases, there is a corresponding increase in the lag of the dipoles. As a result more energy is dissipated within the system and, therefore, an increase in loss factor occurs.

This work used microwave processing frequencies close to 2.45 GHz as this is a widely used ISM heating frequency. The dielectric response of the EVA, which is the main component of the foaming formulation, (and, therefore, likely to be the

dominating material as far as heating is concerned) would indicate, however, that higher frequencies would be more efficient for heating.

The trend of increasing dielectric properties with increasing frequency does not however, continue indefinitely. Figure 4.2 displays the effect of increasing frequency on the dielectric constant, which is a measure of the material polarisability.

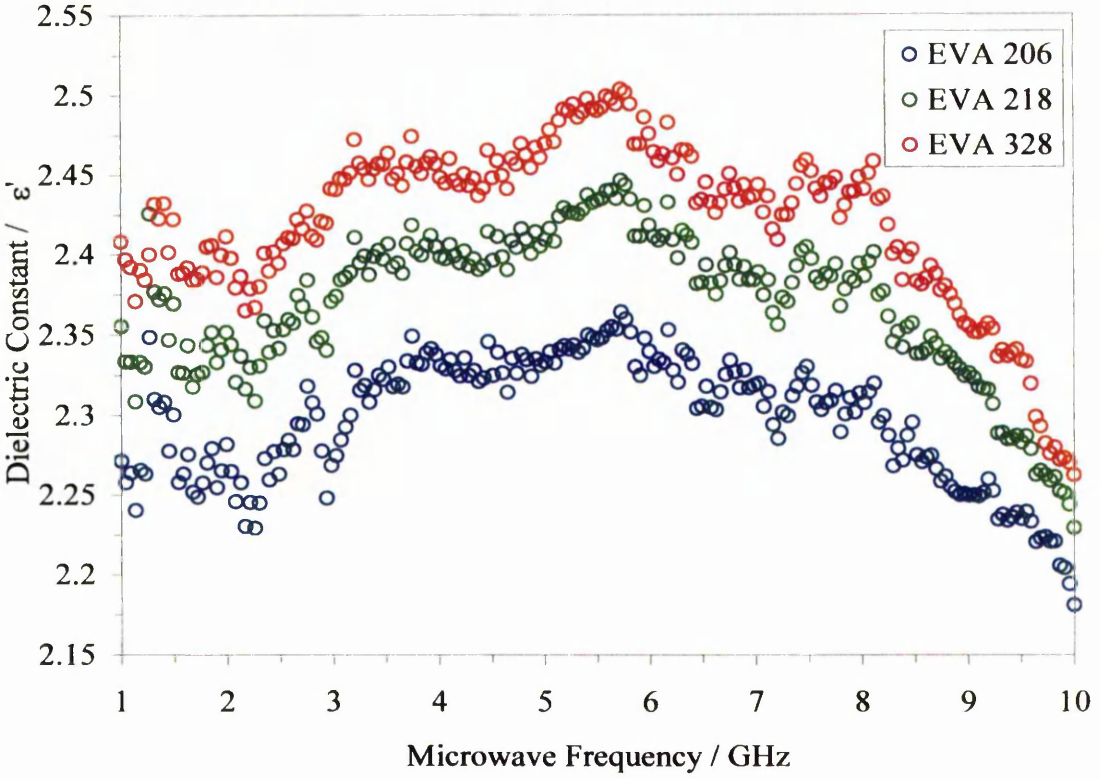

Figure 4.2: Variation of dielectric constant with frequency for the three EVA grades

Although the difference in dielectric constant between each of the polymers appears to be small there is a trend of increasing dielectric constant with increasing vinyl acetate content. Generally, the dielectric constant reaches a maximum value at 4.5-5 GHz and then decreases. The reason for this decrease may be attributed to a decrease in polarisability at higher frequencies. Initially, polar groups that are capable of aligning themselves with the alternating field do so and alternate back and forth with the field. At higher frequencies the polar groups lag further and further behind the field until they are eventually no longer able to keep up. At this point they can alternate less and less with the microwave field and, therefore, suffer a decrease in polarisability and hence a reduction in dielectric constant is observed.

4.1.2: Dicumyl Peroxide

The dicumyl peroxide used in this work was supplied as a fine powder, which facilitated homogeneous dispersion within the polymer matrix during milling. Powders are not well suited to dielectric measurements using the dielectric probe, as there will be a significant amount of air between the individual particles. This would introduce error into any measurement of the dielectric properties. Thus, compacted DCP samples were prepared by pressing circular DCP tablets using a cylindrical mould and hydraulic press (14 MPa). The tablets had a diameter of 50 mm and a height of 35 mm. It was assumed that some air would still remain within the sample although this would be reduced to such a degree to allow reasonable measurements to be taken. The specified density of DCP is 1110 kg m^3 (Akzo Nobel, 2001) and the density of the Kaolin clay carrier was 2600 kg m^3 (Wu, 2001). The density of the pressed sample was calculated as 1510 kg / m^3. Given that DCP is 40 % by weight adsorbed onto a clay carrier, the volume of the air remaining within the sample was estimated as 25 %. Air has a dielectric loss of zero and a dielectric constant of 1, its presence would, therefore, result in an underestimation of the dielectric properties. Thus, the results for loss factor and dielectric constant in figures 4.3 and 4.4 are corrected for the presence of air.

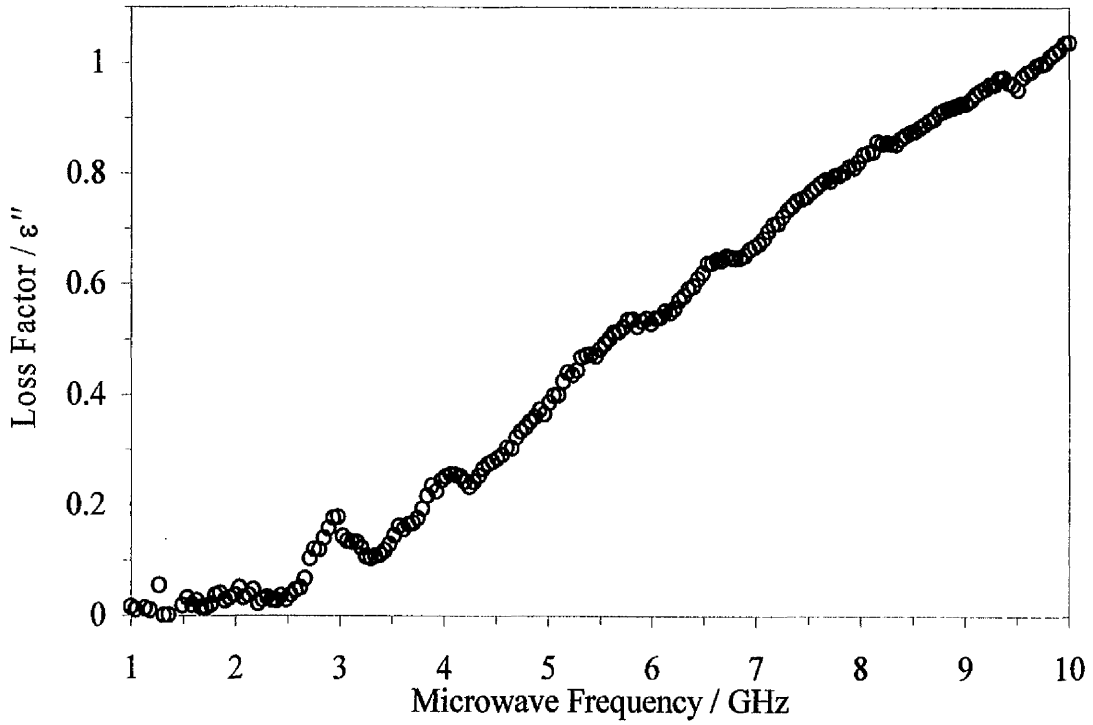

Figure 4.3: Variation of loss factor with frequency for DCP

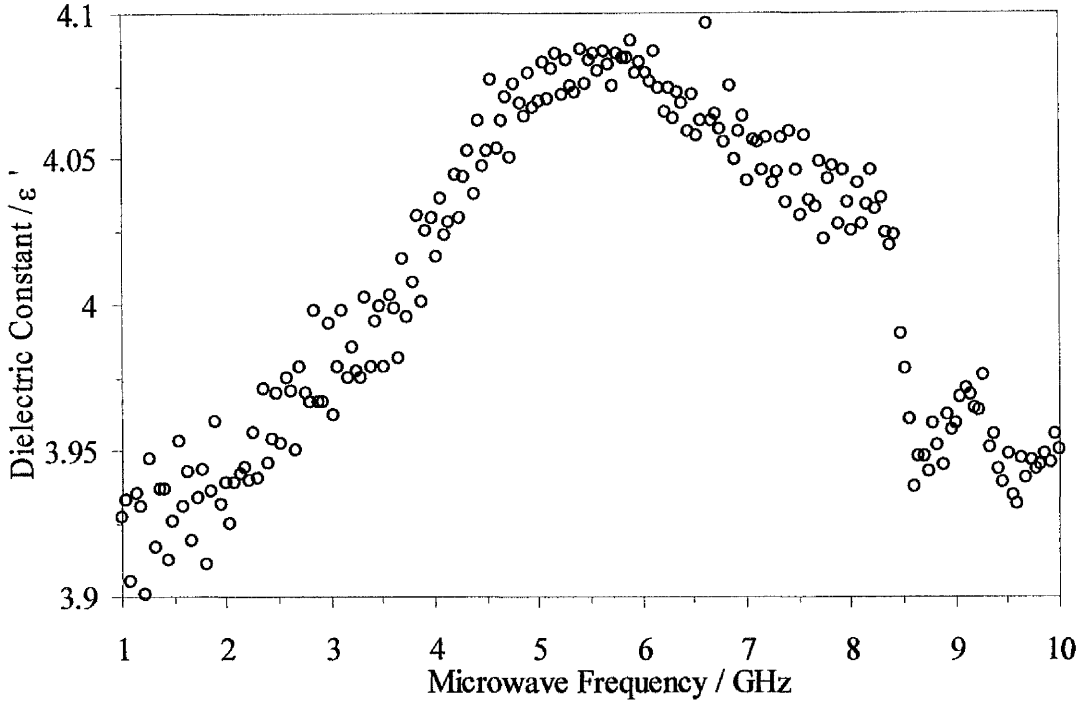

Figure 4.4: Variation of dielectric constant with frequency for DCP

It may be seen that the trend of loss factor with increasing frequency follows a similar pattern to that of the pure EVA polymers although the results indicate that the overall loss factor and, therefore, polarity was higher for DCP than the EVA polymers. At the lower end of the frequency range (1-2.5 GHz) the loss value remained below 0.05. In the region of 2.5 GHz the loss began to increase and continued to do so until the upper frequency range limit was reached. Although the loss was low in the region of 2.45 GHz, it was above 10^{-2}. The dielectric constant results presented in figure 5.4 show an increase between 1 and 5.5 GHz, after which they begin to fall. This trend suggested that at frequencies higher than 5.5 GHz, the polar regions within DCP were unable to alternate fast enough with the applied electric field which resulted in a decrease in the dielectric constant. These results are not applicable to DCP in its pure form. The DCP tested was present as 40 % by weight on an inert clay substrate. The results, therefore, are due to a combination of the dielectric responses from both these components. However, the results shown are applicable to this work as DCP was used in this form.

4.1.3: Azodicarbonamide

The ADCE blowing agent was also supplied in a powder form. Samples were prepared and corrected for the presence of air in the same way as the DCP samples.

The results for loss factor and dielectric constant are presented in figures 4.5 and 4.6.

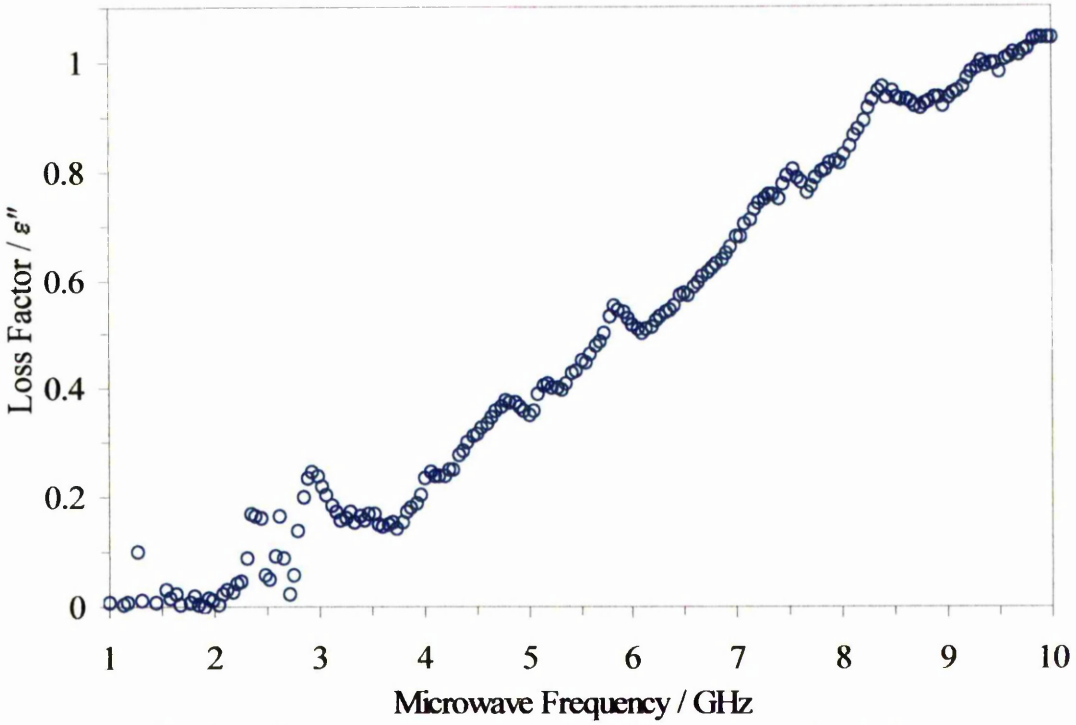

Figure 4.5: Variation of loss factor with frequency for ADCE

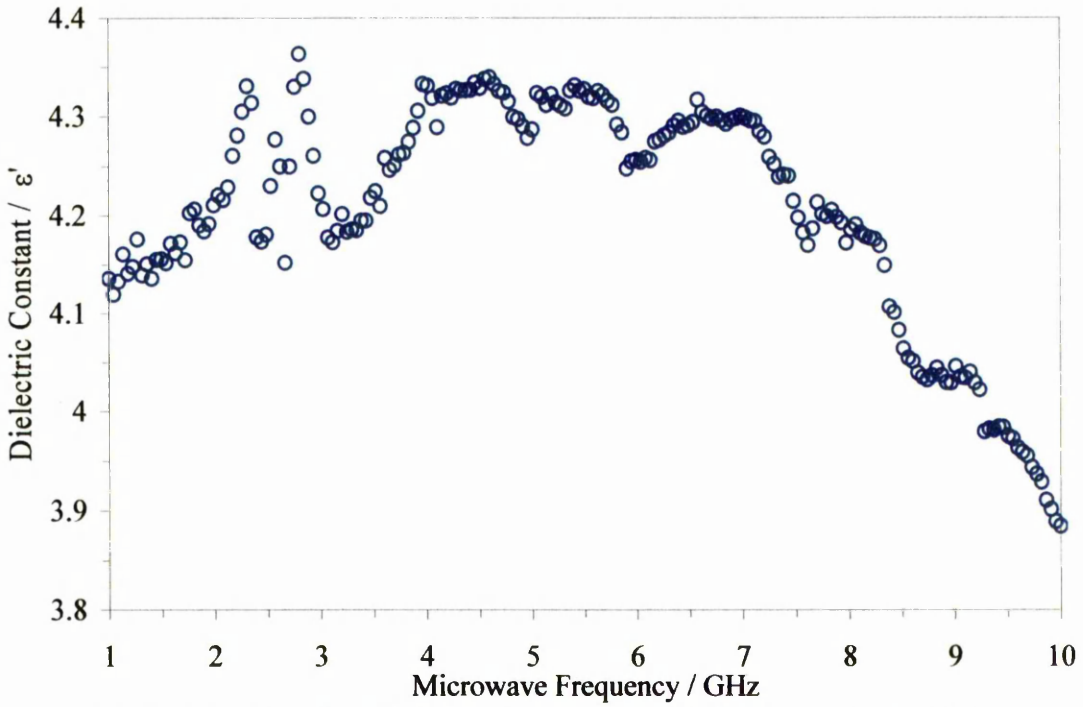

Figure 4.6: Variation of dielectric constant with frequency for ADCE

The dielectric properties of the ADCE blowing agent followed a similar pattern to the DCP crosslinking agent and the EVA base polymers. The loss factor remained low up to the region of 2 GHz and then began to increase with increasing frequency. Like

DCP, the loss factor appeared to be higher at any given frequency than for the pure base polymers indicating a higher degree of polarity. The dielectric constant results displayed in figure 5.6 show a degree of oscillation which introduced a degree of uncertainty although a general trend was apparent. The general trend, however, was similar to those shown by the EVA base polymers and DCP. Unfortunately no suitable data could be found in the literature to compare with these results although additional measurements showed good data repeatability.

4.1.4: Blended Crosslinkable-Foamable Compound

Having established the frequency response of the individual formulation components dielectric properties it was necessary to examine the dielectric properties of the system as a whole. Crosslinkable-foamable samples were prepared by mixing each of the EVA base polymers with 0.5 phr DCP crosslinking agent and 8 phr blowing agent. Figures 4.3, 4.4, 4.5 and 4.6 indicate that DCP and ADCE have marginally higher values of loss and dielectric constant at a given frequency (between 1 and 10 GHz) than the EVA base polymers. To reveal the effect of the additive's dielectric properties on the overall system, the dielectric properties of the blended polymers were measured and are presented in figures 4.7 and 4.8.

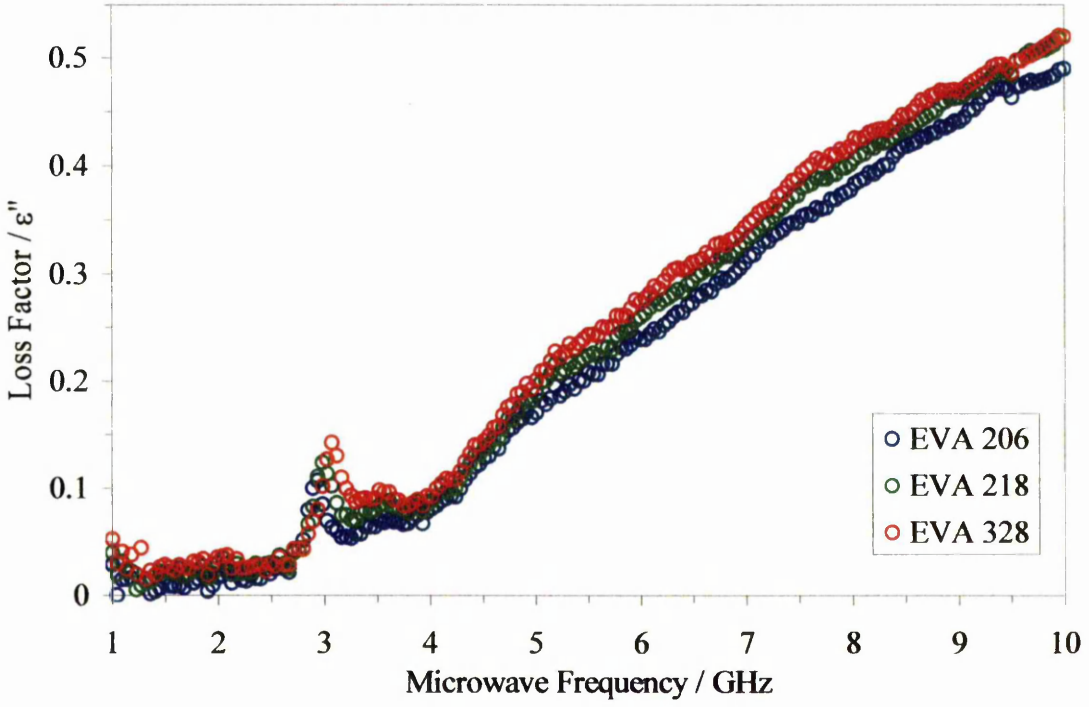

Figure 4.7: Variation of loss factor with frequency for three EVA grades blended with 0.5 phr DCP and 8 phr ADCE

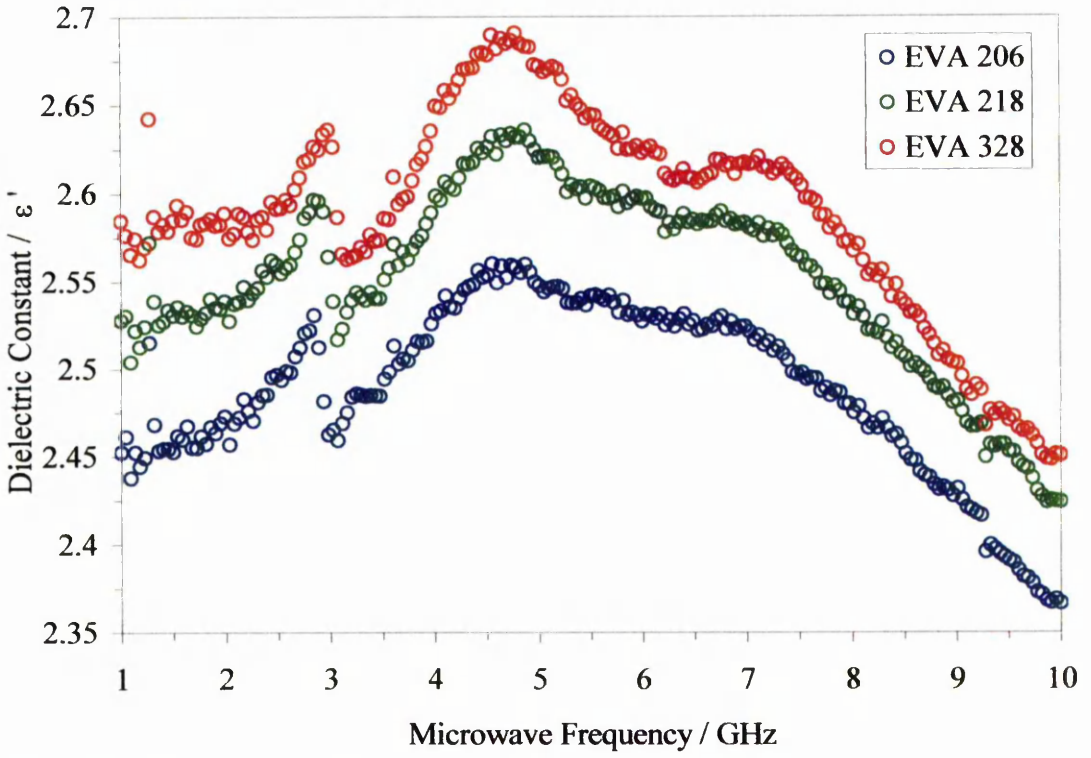

Figure 4.8: Variation of dielectric constant with frequency for three EVA grades blended with 0.5 phr DCP and 8 phr ADCE

It would appear that the incorporation of crosslinking and blowing agent into the polymer had little effect on the overall loss factor when compared to the results from the pure polymer samples. This would suggest that because the polymer was by far the greatest formulation constituent, it was the dominating component with regards to the overall dielectric loss factor. The dielectric constants for the blended foam formulations were marginally higher than that of the pure polymers. This suggests that the blended system was more polarisable than the pure polymers alone, thus the decrease in polymer crystallinity caused by the incorporation of crosslinking and blowing agents into the polymer matrix (as presented in tables 3.1 and 3.2) had a small effect on the overall dielectric properties

The dielectric properties of the pure polymers blended with DCP alone and ADCE alone were also measured. The results were found to be similar to those for the pure base polymers and the complete blended system. These are shown in appendices 1, 2, 3 and 4.

4.1.5: Crosslinked Base Polymers

As a polymer system becomes crosslinked, thermosetting systems in particular, a general decrease in the dielectric loss is usually observed (Chen *et al.*, 1993; Chen *et al.*, 1995). As crosslinks form between adjacent molecules their movement becomes restricted as the network grows. This physical restriction detrimentally affects the movement of dipoles within the polymer chain when exposed to a microwave field, thus reducing the loss factor.

It was expected that the dielectric properties of the crosslinked base polymers would be lower than those of the pure base polymer due to the reasons outlined above, i.e. the crosslinks formed between adjacent polymer chains would restrict their interaction with microwaves. The loss factors and dielectric constants for the crosslinked base polymers (no blowing agent) are shown in figures 4.9 and 4.10, respectively

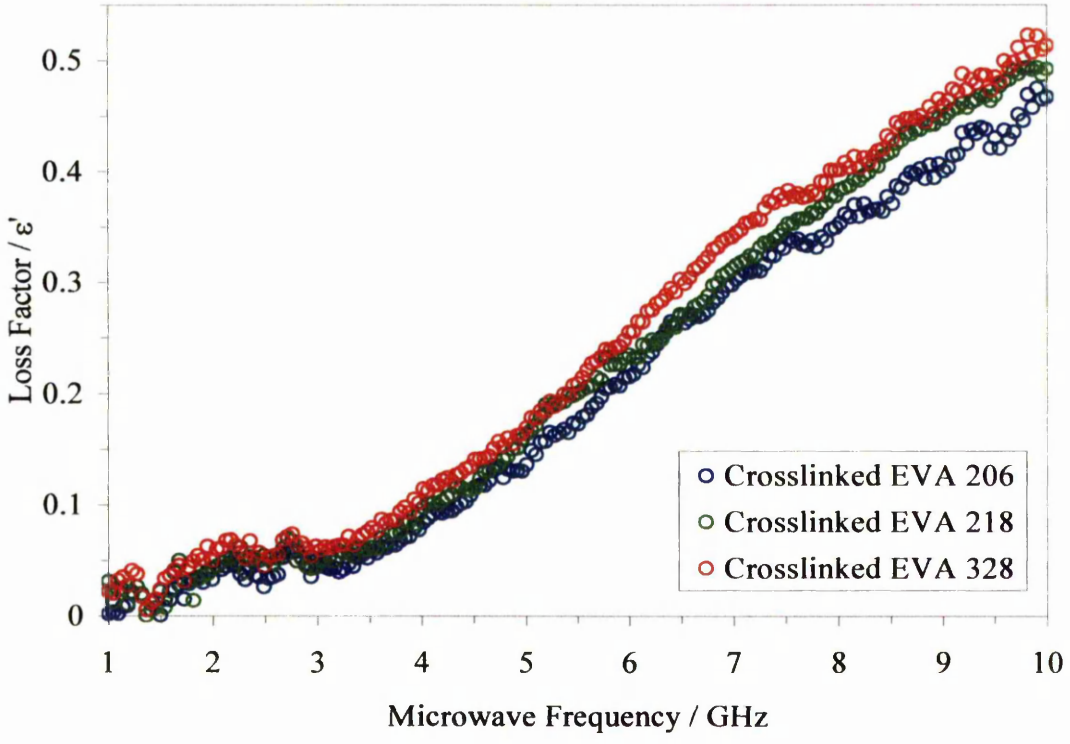

Figure 4.9: Variation of loss factor with frequency for three EVA grades crosslinked with 0.5 phr DCP (compression moulded for 25 minutes at 165 °C)

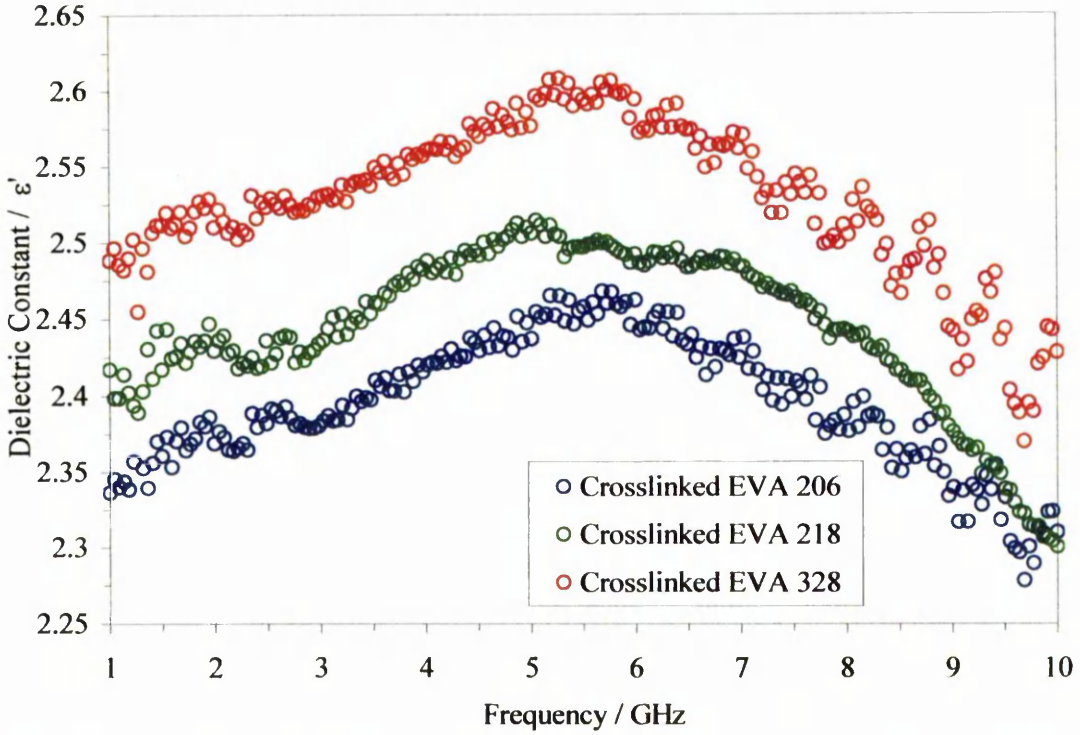

Figure 4.10: Variation of dielectric constant with frequency for three EVA grades crosslinked with 0.5 phr DCP (compression moulded for 25 minutes at 165 °C)

As figures 4.9 and 4.10 show, the expected decrease in the dielectric properties was not observed. The results showed a slight increase in the dielectric loss compared with the pure EVA base polymers at lower frequencies. This may be explained by consideration of the effects of crosslinking on crystallinity. Crosslinking disrupts crystallinity by preventing efficient packing of the polymer chains. This would, therefore, decrease the dipole motion restriction caused by crystallinity. The polar vinyl acetate groups would be able to interact with the microwave field more easily and hence increase the loss factor. The majority of crosslinking takes place between tertiary hydrogen sites between adjacent polymer chains (Kircher, 1987). The polymer chains themselves are not polar and, therefore, do not contribute significantly to the dielectric loss. Although the polymer chains are linked together, the vinyl acetate groups (which have the greatest interaction with the microwave field) remain free, unrestricted and are still able to oscillate with the microwave field.

4.2: Dielectric Properties as a Function of Temperature at 2.45 GHz

During heating the loss factor of materials may change. These changes may be brought about by physical and chemical changes within the material. Physical

changes such as melting are often accompanied by increases in loss factor as molecular freedom is increased and any dipoles present are able to interact more readily with the alternating field. Chemical reactions such as crosslinking may also have an effect, if molecular motion is increasingly restricted as crosslinking takes place, then a decrease in loss factor will take place. During a heating cycle, new species may be generated and others consumed. Depending on their dielectric properties and concentrations these may also affect the overall system properties.

The principle behind microwave processing is that the dielectric power absorption is proportional to the dielectric loss factor, which determines the conversion rate of electrical energy into heat (DeMeuse *et al.,* 1991). It is, therefore, important to monitor the dielectric properties of a material during heating to identify and explain any changes that occur.

Dielectric measurements were made as a function of temperature, using the microwave calorimeter equipment outlined in section 2.4.4 and a microwave frequency of 2.45 GHz. This provided information on the dielectric properties of the material as it was heated in a microwave field in an applicator designed to resonate at a frequency of 2.45 GHz. The actual resonant frequency was dependant upon the sample size and dielectric properties. As heating progressed, regular frequency sweeps were made in order to determine the resonant frequency and Q factor of the cavity from which the dielectric properties of the sample could be calculated using equations 2.6 and 2.7. The results were normalised to the dielectric probe data as described in section 2.4.4.3. Small changes to the input frequency were necessary due to the resonant frequency shifting slightly as the sample temperature changed. The assumption was made that although foam production used frequencies in the region of 2.45 GHz and would, therefore, involve loss factor values that were marginally different, the dielectric property changes would follow a similar pattern.

4.2.1: EVA Base Polymers

The results from the dielectric probe measurements made in section 4.1 indicated that the EVA base polymer was the dominant material (in the foam formulation) in terms of dielectric properties. The probe measurements were taken at room temperature. During heating, however, EVA undergoes physical changes such as melting and viscosity reduction that may influence the dielectric properties. The dielectric loss

factor and dielectric constant results for the three pure EVA grades as a function of temperature are shown in figures 4.11 and 4.12.

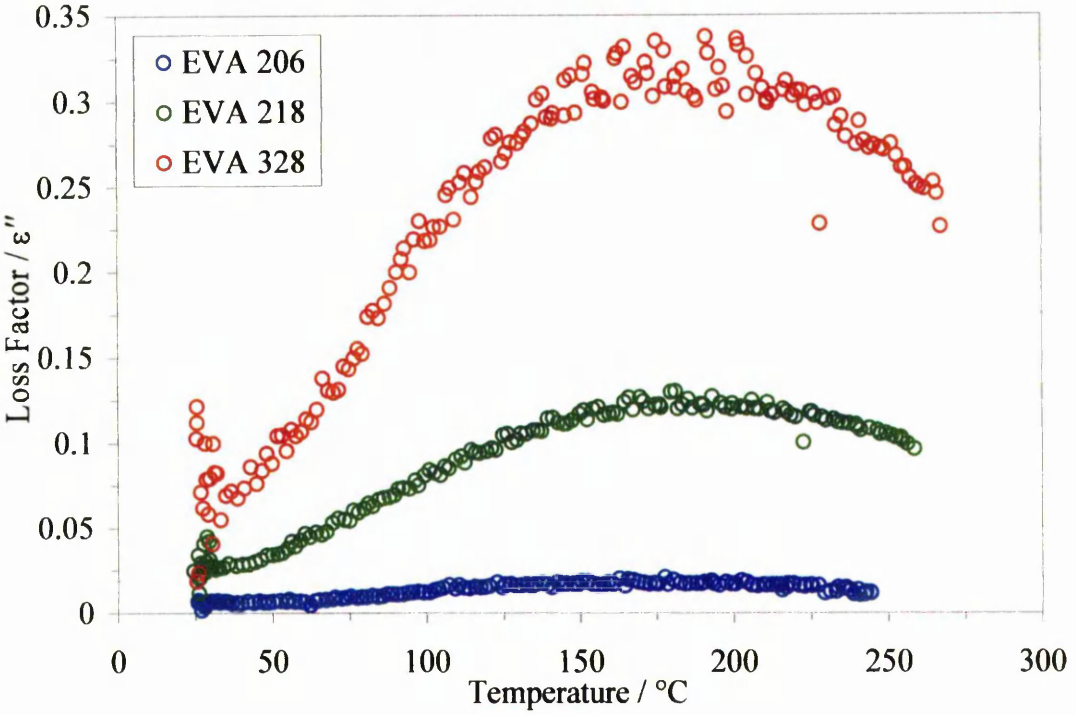

Figure 4.11: Variation of loss factor with temperature for three EVA grades

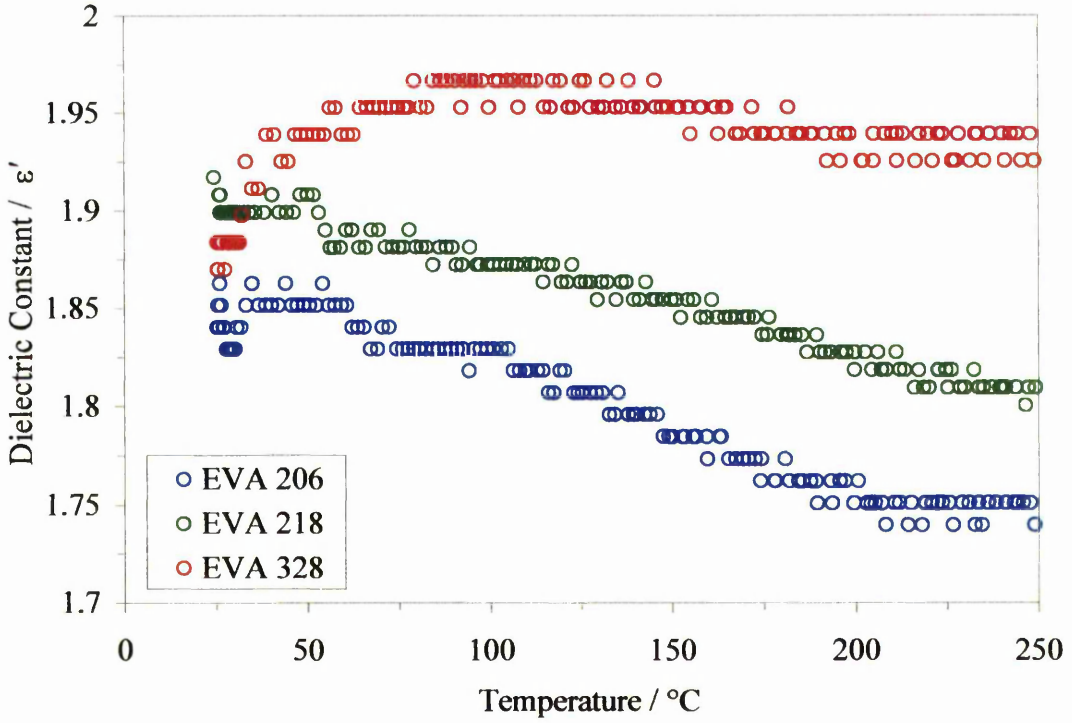

Figure 4.12: Variation of dielectric constant with temperature for three EVA grades

Figure 4.11 shows that there was a trend of increasing loss factor with polymer vinyl acetate content at any given temperature. This is consistent with the trend shown by the results from the dielectric probe measurements in figure 4.1. This was expected as the dielectric loss of these copolymers is principally due to the presence of polar groups (ester groups) within the pendant vinyl acetate groups attached to the main ethylene chain (Cassagnau and Michel, 1994). Microwave energy may be directly absorbed by these groups resulting in localised heating. As the percentage of these polar groups is increased in the order EVA 206< EVA 218 < EVA 328, so a corresponding increase in the loss factor is observed as the sites available for energy absorption and subsequent conversion are increased. The percentage vinyl acetate group difference between EVA 206 and EVA 218 is marginally greater than the difference between EVA 218 and EVA 328. It was expected that this would be reflected in the difference between the loss values at any given temperature. Figure 4.11 shows a greater difference in loss values between EVA 218 and EVA 328 which suggested other mechanisms may have influenced the dielectric properties such as percentage crystallinity and viscosity.

Generally, increased crystallinity tends to decrease polymer dielectric loss (Chen *et al.,* 1993), as the crystalline regions progressively restrict dipole mobility. Of the three EVA grades, EVA 206 has the lowest vinyl acetate content and therefore, the highest percentage crystallinity. If the dielectric properties of EVA were affected by the degree of crystallinity, EVA 206 should have showed the greatest change in loss factor during melting. Figure 4.11 indicates that the loss factor of EVA 206 changed very little over the temperature range studied. This would suggest that the melting of the crystalline regions had a negligible effect on the loss factor. This may be explained by the location of the dipoles within EVA. The bulky polar vinyl acetate groups disrupt crystallisation as steric hindrance prevents close packing of the polymer chains. They are, therefore, located on segments of the polymer chain that form the amorphous regions of the polymer (Baird and Houston, 1975). The crystalline regions are composed of closely packed non polar ethylene segments of the polymer chains. Crystallinity greatly restricts the motion of dipoles, such as those incorporated directly within the polymer backbone that may be located directly within the crystalline regions. As the EVA polar groups are located with the amorphous

regions of the polymer, their motion is unlikely to be greatly affected by the percentage crystallinity.

Effect of viscosity on dipole motion is more likely to have a greater influence over loss factor that crystallinity. As the amorphous regions soften, their viscosity drops. This leads to an increase in dipole mobility and a corresponding increase in loss factor.

The loss factor for all three polymers showed an increasing trend with increasing temperature. The loss factor for all three polymers reached a maximum value in the approximate temperature range of 175 – 180 °C and then began to decrease. The decrease in loss was thought to be due to vinyl acetate loss. Other work (Sultan and Sorvik, 1991) has shown that degradation of EVA by the loss of vinyl acetate as acetic acid by volatilisation can begin at temperatures as low as 150 °C. Furthermore, vinyl acetate loss was more pronounced in EVA copolymers with higher initial vinyl acetate contents. It is suggested therefore that the decrease in loss factor observed in figure 4.11 is due to the loss of vinyl acetate which are the main sites for microwave energy conversion to heat. This argument is supported by the observation that the decrease in loss appears to increase with increasing vinyl acetate content. Although this suggests that the efficiency of EVA microwave heating decreases with increasing temperature, the TGA results in appendices 5 and 6 indicate that the loss of vinyl acetate is slow and unlikely to affect the microwave foaming process.

4.2.2: Dicumyl Peroxide

As DCP is heated it undergoes physical and chemical changes such as melting and dissociation of the peroxide bond and free radical formation. The dielectric response of DCP was measured as a function of temperature to establish the effect of heating upon its dielectric properties. The results are presented in figure 4.13 and 4.14.

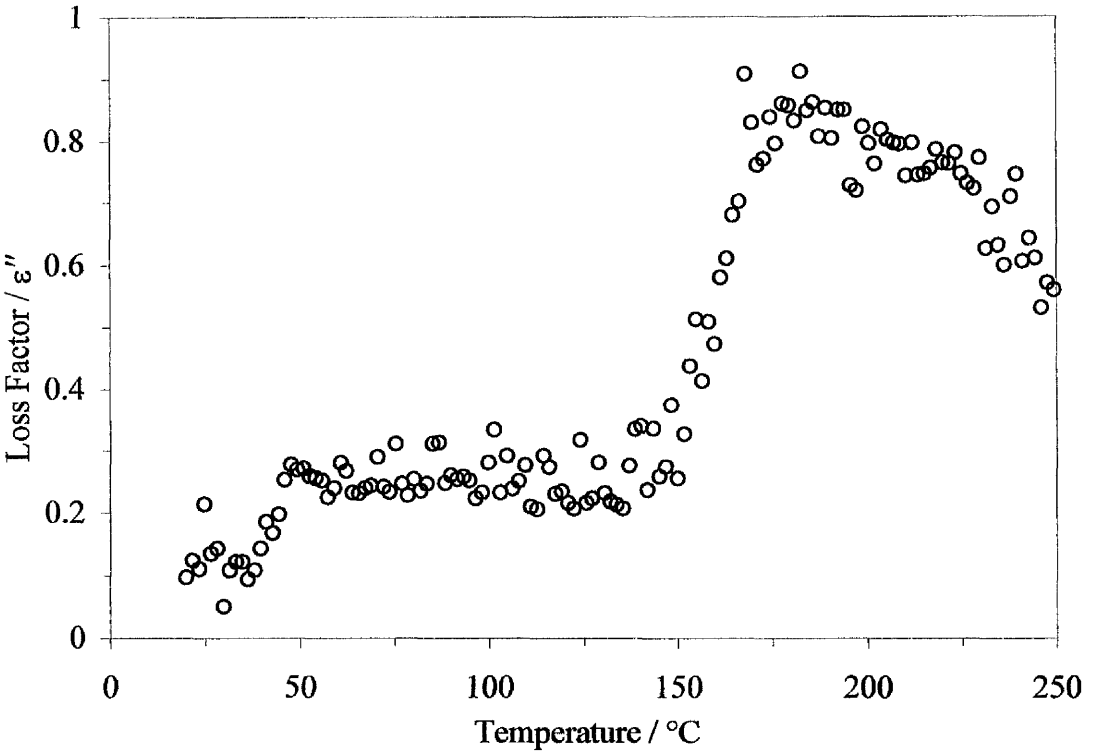

Figure 4.13: Variation of loss factor at 2.45 GHz with temperature for DCP

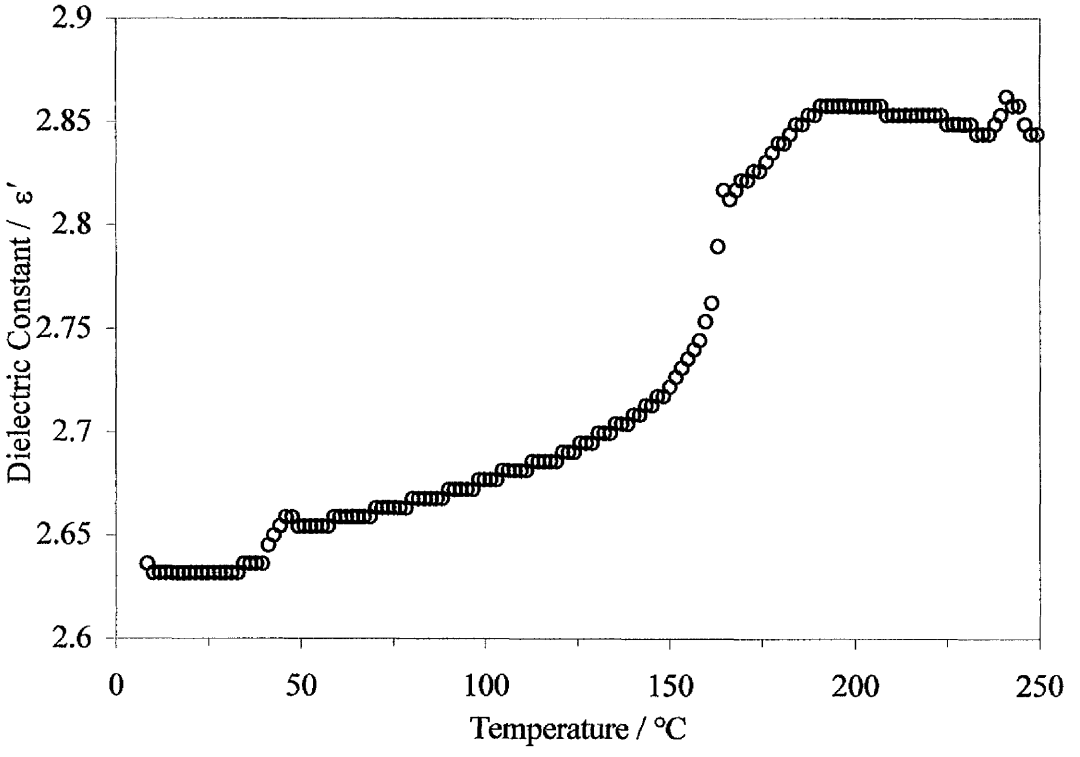

Figure 4.14: Variation of dielectric constant at 2.45 GHz with temperature for DCP

Chen (Chen *et al.*, 1993) reports that DCP has little microwave activity. This was attributed to the fact that DCP is a symmetrical, non polar molecule. However, figure

4.13 shows that heating DCP (as supplied) using microwave energy is possible. The DCP as supplied consisted of 40 % DCP on an inert clay carrier. The microwave heating of ceramics is well documented (Chatterjee *et al.,* 1998; Thostenson and Chou, 1999; Xie *et al.,* 1999; Bykov *et al.,* 2001). If DCP is not heated directly by the microwave energy it may be that the clay carrier is heated instead which is then able to transfer heat to the adsorbed DCP. Closer examination of figure 4.13 would suggest however, that that some of the observed changes in dielectric loss may be attributable to DCP alone. Figure 4.13 shows an initial increase in DCP loss factor from approximately 0.1 to 0.3 in the temperature region of 40 - 50 °C. Although there is a large degree of scatter this increase in dielectric loss corresponds to the melting temperature of DCP. The observed increase in loss may be attributed to the increase in molecular freedom resulting from the melting of DCP. Melting would decrease the physical restrictions on the DCP molecule and allow more efficient interaction with the microwave field.

After the initial increase, the dielectric loss remains reasonably constant until the temperature approaches 150 °C. The loss then increases to values in the region of 0.9. This large increase in loss falls within the same temperature range as the thermal dissociation of DCP and may be explained by considering the DCP dissociation mechanism. It would appear that the increase in loss is due to the dissociation of the peroxide bond generating highly reactive peroxy radicals. The dissociation of the non polar symmetric DCP molecule generates two identical peroxy radicals which each have one unpaired electron generated by the homolytic cleavage of the peroxide bond. The lone electrons are located on the oxygen atoms of the free radical moieties. The reaction is represented by equation 4.1.

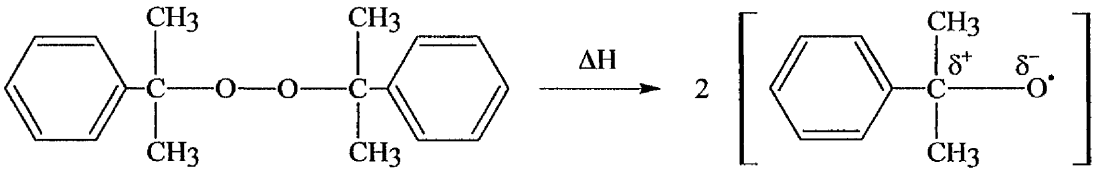

(Eqn. 4.1)

Dissociation of the DCP molecule in this way may increase the loss factor in two ways. Firstly, the dissociated radical molecules are not symmetrical which would

result in a degree of molecular polarity. Oxygen is more electron withdrawing than carbon (more electronegative); therefore electron density will accumulate at the oxygen atom. This will result in a build up of negative charge on the oxygen atom and leave the carbon atom, to which it is bonded, electron deficient and positively charged. Hence a dipole is generated which allows the peroxy radicals to alternate with the microwave field and convert its electrical energy into heat. The DCP dissociation generates two polar radicals / per peroxide molecule which results in an increase in the number of microwave active sites which may also increase the dielectric loss.

The second contribution to the dielectric loss may be due to the decrease in molecular weight that takes place during dissociation. The dissociated radicals are half the molecular weight of the original DCP molecule. They are therefore, able to interact with the applied microwave field more efficiently thus, increasing dielectric loss.

As the temperature was increased further, the dielectric loss reached a maximum and then began to fall slowly when a temperature of approximately 190 °C was reached. The decrease in dielectric loss may be explained by the evaporation of these free radicals. Furthermore, one of the main by products of DCP dissociation is acetophenone which is formed by rearrangement of the radicals. In common with its radical precursor acetophenone possesses a dipole and so it is reasonable to assume that it would also be heated by microwaves. However, the boiling point of acetophenone is 202 °C (Chemfinder, 2005), hence, as the temperature is increased further acetophenone and any remaining radical molecules are lost through volatilisation. The contribution to the dielectric loss decreases as they are lost, therefore a decrease in loss factor was observed.

During the DCP reaction, dissociation products were lost to the atmosphere. The DCP as supplied comprised 40 % (by weight) DCP on a clay carrier. It may therefore, be assumed that approximately 40 % of the sample mass was lost during dissociation (as shown in figure 3.7). As the dielectric property calculations take into account sample volume, any change in this parameter could affect the results. It was assumed that, although the decomposition products were lost, the bulk of the material was represented by the clay carrier onto which the DCP was adsorbed and that the

loss of dissociation products did not significantly alter the sample volume. This was confirmed by visual examination of the sample after heating.

4.2.3: Azodicarbonamide

It was only possible to measure the dielectric properties of ADCE effectively, at temperatures below its decomposition range. The main decomposition product of ADCE is nitrogen, which upon evolution was released to atmosphere. Consequently, as ADCE decomposed the sample volume rapidly decreased as nitrogen and other gaseous by products were formed and lost. As mentioned in the previous section, a decrease in sample volume was not taken into account in the dielectric property calculations. Thus, upon decomposition the dielectric data for ADCE became increasingly erroneous and unreliable. The dielectric properties for ADCE as a function of temperature up to the beginning of decomposition are presented in figures 4.15 and 4.16.

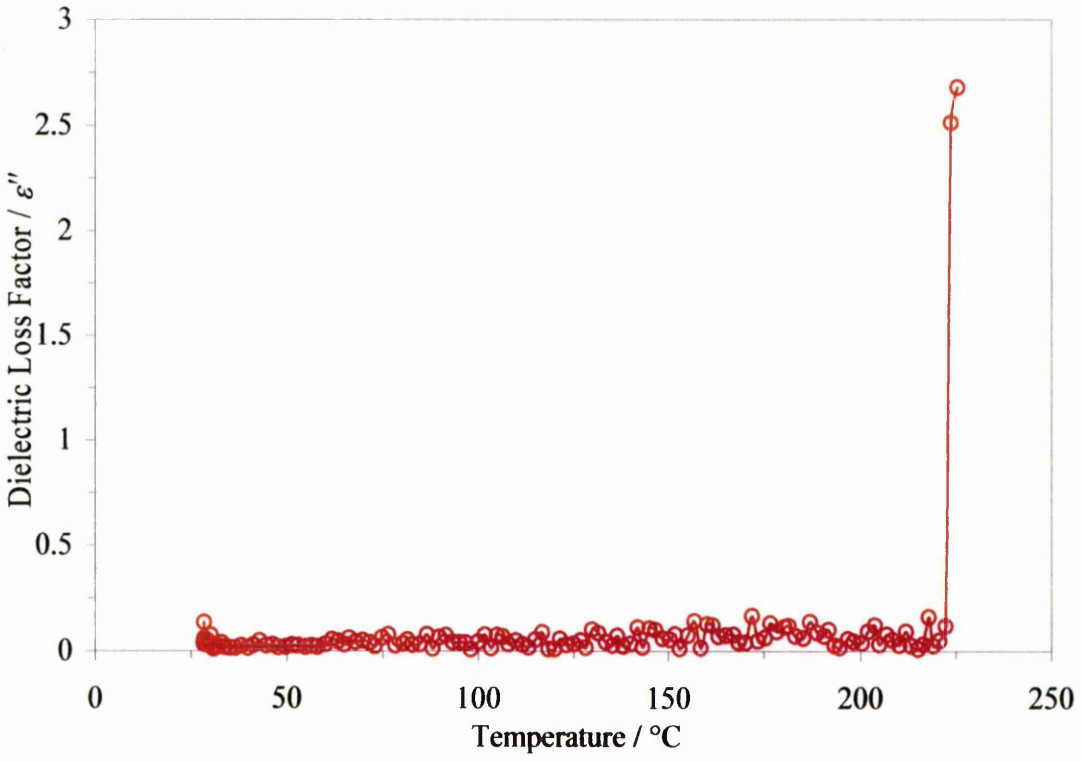

Figure 4.15: Variation of loss factor at 2.45 GHz with temperature for ADCE

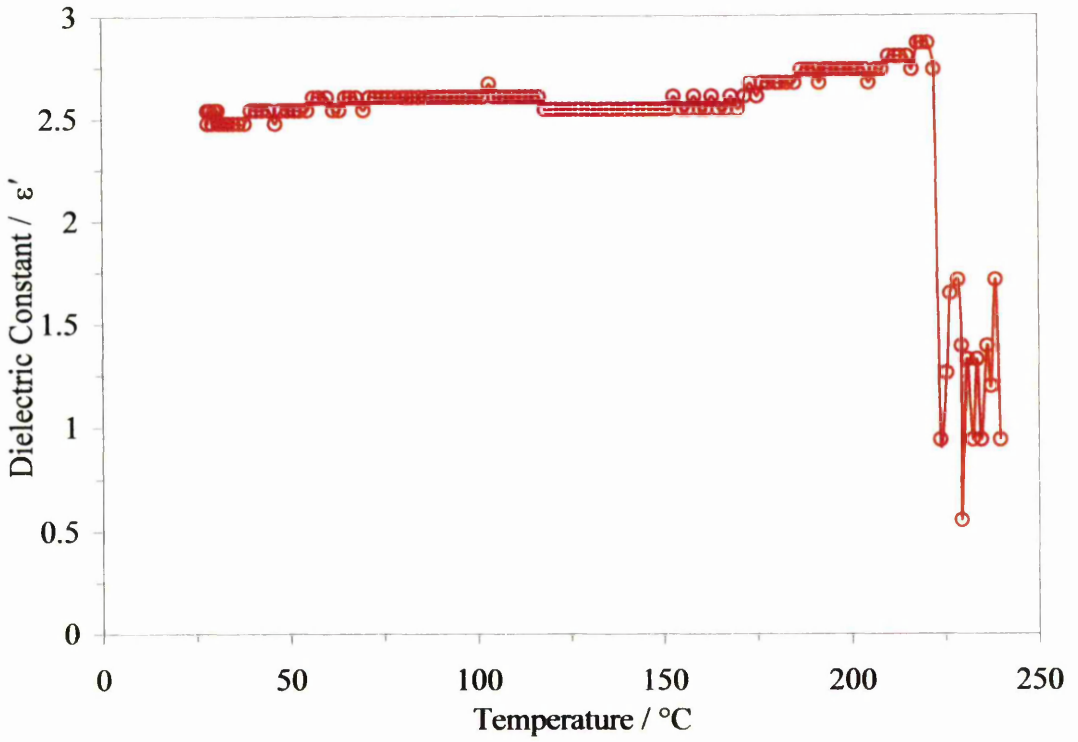

Figure 4.16: Variation of dielectric constant at 2.45 GHz with temperature for ADCE

It was expected that the dielectric properties of ADCE would show little variation during heating until decomposition took place. The DSC results shown in figure 3.1 demonstrate that ADCE does not undergo any thermal transitions until decomposition where it sublimed. In the absence of events such as melting where loss factor is often increased due to increases in molecular freedom it was thought unlikely that the dielectric properties would change significantly. Figure 4.15 indicates that the dielectric loss of ADCE increases marginally when heated from room temperature to approximately 225 °C. When the temperature reached ~ 225 °C, a large increase in the dielectric loss and constant was observed. This suggested that upon decomposition, ADC formed polar compounds in addition to the major gaseous reaction products. However, after the initial decomposition, the data for the dielectric loss and constant became erratic as the blowing agent was converted to gas and its volume rapidly decreased.

4.2.4: Foamable Formulation

Unfortunately, it was not feasible to determine the dielectric properties of the polymer samples blended with blowing and crosslinking agents. The reason for this was, as the samples reached the blowing agent decomposition temperature they began to

foam. Foaming was accompanied by a large change in volume size. The equations used for the determination of dielectric properties assume a fixed sample volume, therefore, changes in sample volume during heating would have caused significant error in the calculations. It was assumed that the dielectric properties of the blended polymers would follow a similar trend to the data presented in figure 4.11 for the pure base polymers until the onset of blowing agent decomposition and foam expansion.

4.3: Summary

The results showed that heating the individual foam formulation components alone and as a whole using microwave energy was feasible. The results strongly suggested that foaming using microwave energy would be possible. The three EVA base polymers all had dielectric characteristics suitable for microwave heating although the loss factor observed at 2.45 GHz for EVA 206 was only marginally above the lower limit of 10^{-2} required for feasible microwave heating. This suggested that foaming EVA 206 would be possible, although, given the power limits of the available equipment (200 W), increasing vinyl acetate further may be necessary. EVA 218 and 328 had much greater loss values at 2.45 GHz and might, therefore, prove to be more suitable as base polymers for use in this work.

CHAPTER 5: INITIAL FOAMING STUDIES WITH EVA 206

5.1: Ethylene Vinyl Acetate

To allow efficient interaction between a microwave field and a material, it is important that there are polar structures present within the material. The polar groups of a material are able to interact with the electric component of the microwave field and convert the electrical energy to heat via the mechanisms described in section 1.11.2 and 1.11.3. Previous work involving the heating of polyolefin polymers using microwave energy has clearly demonstrated that heating pure polyethylene is not feasible (Curran, 1998; Osswald and Menges, 1996). This was due to the minimal polarity of the polymer chain, resulting in dielectric properties which make it unsuitable for microwave heating in the pure form.

It is for this reason that the initial section of this study concentrated on ethylene vinyl acetate copolymer, subsequently referred to as EVA, as the base polymer. This initial small scale study was necessary to obtain information which could then be used to perform a larger scale study and to construct the equipment required. EVA is a random copolymer of ethylene and vinyl acetate and is essentially a polyethylene polymer backbone with pendant vinyl acetate groups. A number of EVA grades are available with different vinyl acetate concentrations. Polarity is introduced at the points along the polymer chain where the vinyl acetate groups are located as shown in figure 5.1.

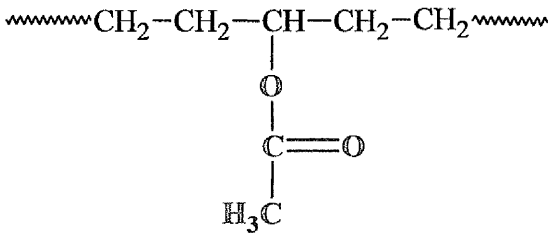

Figure 5.1: Section of EVA polymer chain (vinyl acetate group shown in red)

For the initial part of this work EVA 206 was used which has 6 % by weight vinyl acetate content.

5.2: Conventional Crosslinking

Crosslinking of the EVA base polymer was required in order to stabilise the matrix during foaming (expansion) and to increase the resistance of the foamed polymer to thermal collapse. During these initial studies, all crosslinking was carried out in the press during sample moulding. The reactivity of a peroxide crosslinking agent is usually defined by its half life at various temperatures. A range of half life times for DCP is displayed in table 5.1.

Table 5.1: Half life times for DCP BC-40k-pd (Akzo Nobel, 2001)

Half Life ($\tau_{1/2}$) / Minutes	**Temperature / °C**
720	110
22	140
1.7	165
0.4	180

Although the theoretical half life times are a useful guide to processing conditions, in practice there will be a temperature profile through the sample. To gain information on the crosslinking time necessary to provide the required degree of crosslinking within an acceptable time scale, gel content determinations were carried out (ASTM D 2765-90, 1990) on non foamable crosslinked samples of EVA 206 compounded with 0.5 phr (parts per hundred resin) DCP. Crosslinking was carried out at 165 °C for various time periods using the compression moulding technique described in section 2.2.2.2. It was important that the crosslinking temperature was high enough to complete crosslinking in an acceptable time period. It was necessary that the temperature was sufficiently low to prevent premature blowing agent decomposition in the mould. The gel content (%) results as a function of press dwell time and associated errors are shown in figure 5.2.

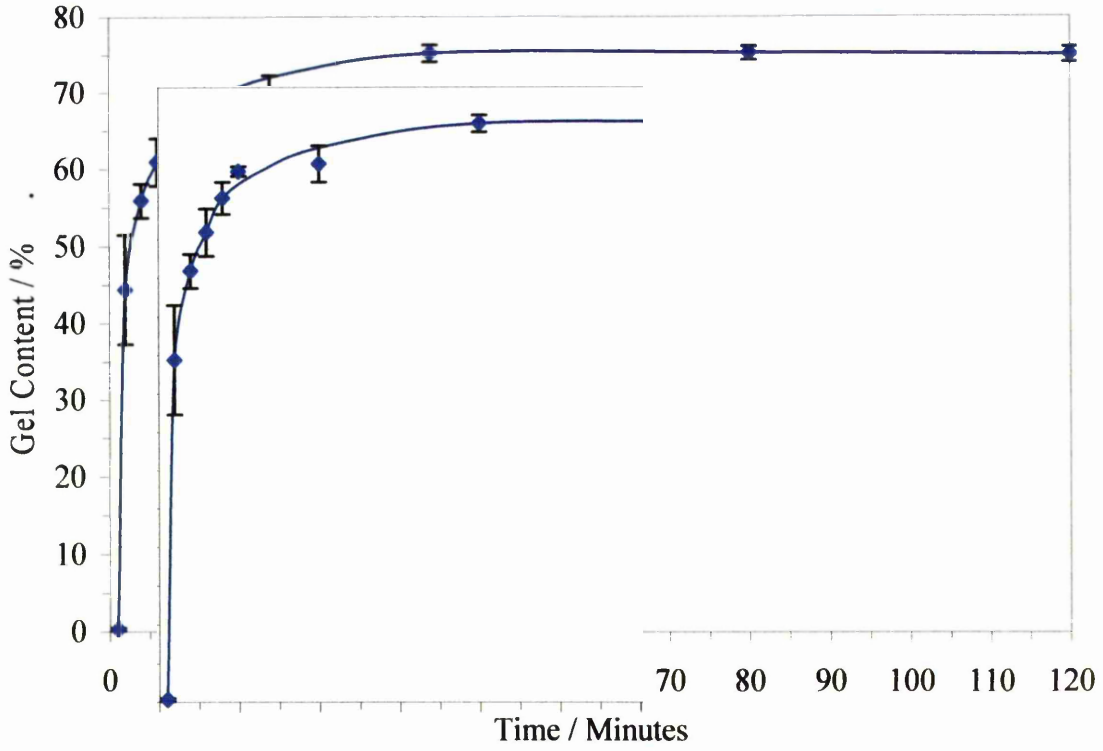

Figure 5.2: Variation of EVA 206 gel content with mould dwell time at 165 °C (0.5 phr DCP)

Crosslinking in EVA takes place predominantly at the tertiary hydrogen carbon site (to which the vinyl acetate group is also bonded) as this is the most energetically favourable. The results in figure 5.2 show trends of increasing gel content with mould dwell time. They show that increasing dwell time allowed further DCP reaction and increased network formation. Previous work (Clarke, 2000) indicated that a minimum gel content of 50 % was necessary to provide sufficient reinforcement to the melt strength, thus maintaining the gas pressure generated by the decomposition of ADCE during the expansion phase of the foaming process. Figure 5.2 shows that 50 % network formation is achieved in approximately 2.5 minutes and that the majority of network formation is complete after 25 minutes (although a small percentage increase does occur at extended time periods). It is also noticeable that as mould dwell time increased, the associated errors exhibited a decreasing trend overall. This is presumably due to extended mould dwell times allowing time for heat conduction through the sample thickness and more uniform crosslinking to take place thus reducing the variability between individual samples. These results show that 25 minutes at 165 °C will be sufficient to perform the necessary degree of base polymer crosslinking.

5.3: Conventional Foaming

5.3.1: Conventional Oven Foaming

Industrial foam production techniques often use multi zone hot air ovens to achieve the crosslinking and expansion phases of the process separately (Asaaka *et al.*, 1968; Hosoda and Shina, 1972). Foams based on EVA 206 using 0.5 phr DCP and 8 phr ADCE were produced using hot air convection ovens to provide conventionally foamed specimens for comparison with those produced by subsequent microwave heating. The polymer, blended with crosslinking and blowing agent, was heated in a mould at 165 °C for different times to perform various levels of crosslinking. This was done to simulate the effect of the first zone of a foaming oven where crosslinking is initiated but not always completed before the expansion phase and to determine the effect of various pre-crosslinking levels on foam density. The crosslinking stage is necessary to increase the polymer melt strength to the required level such that foam collapse and blowing agent loss through cell wall rupture is avoided. Samples with dimensions of 30 × 20 × 5 mm were then heated at a second, higher, temperature (220 °C) in a circulating hot air oven, in order to effect blowing agent decomposition and foam expansion thus emulating a second oven zone. The completion of expansion was determined visually and found to be complete after 6 minutes. The samples were then removed from the oven and conditioned in a temperature and humidity controlled lab for 24 hours prior to density measurement, the results are presented in table 5.2.

Table 5.2: Variation of foam density with initial gel content

Gel Content / %	Foam Density / kg m^{-3}
0	54.4 ± 3.4
15	56.6 ± 2.8
47	53.3 ± 3.6
49	55.5 ± 2.9
60	57.7 ± 2.2

It was expected, that at low levels of crosslinking, there would be very little enhancement provided to the melt strength. Thus high-density values were expected as it was thought that the melt strength would not be sufficient to retain the blowing

agent gas and that foam collapse would follow. At higher crosslinking levels, sufficient foam stabilisation was expected such that the melt strength increase would be great enough for retention of blowing agent gas and stable foam formation, hence lower density values. The results shown in table 5.2 do not, however, indicate the expected trends and the density values for each foam sample are similar with the margins of experimental error. Although the pre-crosslinked foamable samples had different initial gel fractions, it is proposed that crosslinking had reached similar levels in each sample before the onset of blowing agent decomposition and foam expansion. A drawback to this method is that the samples had to be cooled to allow their removal from the press. As such it was necessary to reheat them in the oven prior to expansion. It is proposed that during the reheat process crosslinking was completed before expansion took place. Industrial methods use multi zone ovens which move the polymer instantly from lower temperature crosslinking zones to higher temperature expansion zones thus avoiding any reheating.

5.3.2: Twin Oven Foaming

The method described above was modified using two ovens instead of the mould, thus eliminating the need for cooling in between the two processes. In an attempt to more closely model the perceived action of a commercial convection oven (i.e. crosslinking and expansion at atmospheric pressure) the samples were crosslinked in one oven at a lower temperature for a set time. The samples were then immediately transferred to a second oven at a higher temperature for blowing agent decomposition and expansion. Density values were again similar, however, suggesting the completion of crosslinking before expansion.

Significant problems were encountered during the crosslinking phase of this technique. Whilst crosslinking in the first oven, the polymer reached its melting point before crosslinking could take place. As a result, the polymer samples tended to flow and stick to the oven shelf. As a result, considerable time was lost removing the samples from the oven. It was thought that during this time (and the time taken to transfer the polymer from one oven to the other) crosslinking progressed to similar levels for all samples. During industrial polyethylene foam production, the polymer sheet is floated on jets of hot air or molten salts in order to prevent sticking and flowing of the polymer as it melts before crosslinking. The ovens used in this

investigation were standard laboratory ovens and as such did not have these capabilities.

5.4: Microwave Heating and Foaming

Microwave heating was initially carried out on a small scale using the equipment outlined in section 2.3.2.1. This section of the work concentrated on heating polymer samples in the pure form and foaming pre-crosslinked samples. To avoid the problems encountered with polymer flow when crosslinking samples in the conventional oven, samples were pre-crosslinked in the press and then cooled to ambient temperature. A rectangular section of brass waveguide, as shown in figure 5.3, was used as the microwave applicator.

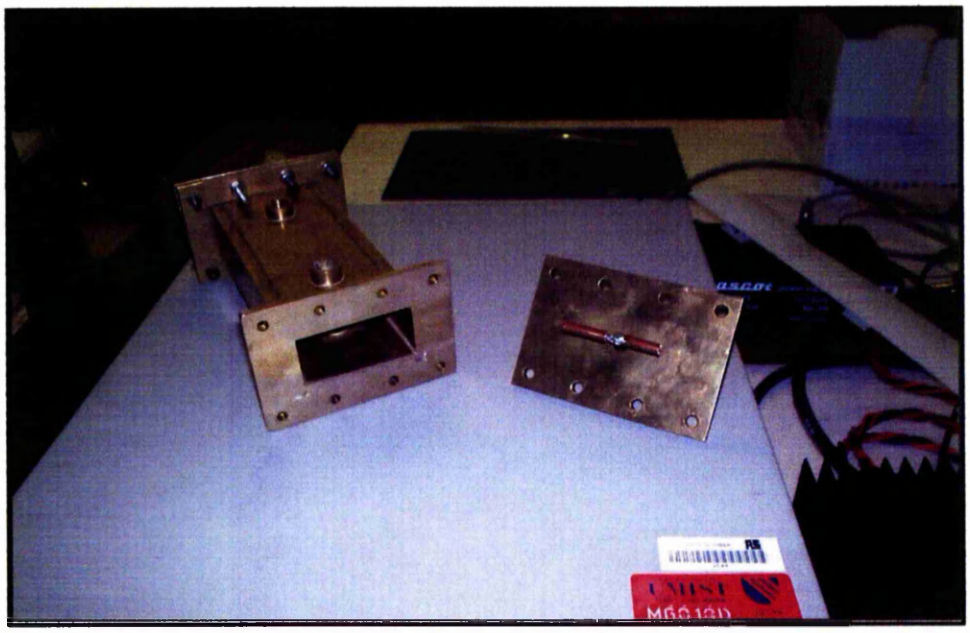

Figure 5.3: Rectangular brass waveguide applicator and antenna

The waveguide was designed to resonate at a fixed frequency of 2.45 GHz with the microwave field localised at known positions. The area of maximum field intensity was localised between two holes (previously used for the insertion of stub tuners) located in the top and bottom surfaces of the wave guide. The holes allowed insertion of the glass tube which housed the fluoroptic thermometer probe and also acted as a sample support during heating. The field distribution was simulated using Agilent HFSS (High Frequency Structure Simulation) software and is presented in figure 5.4.

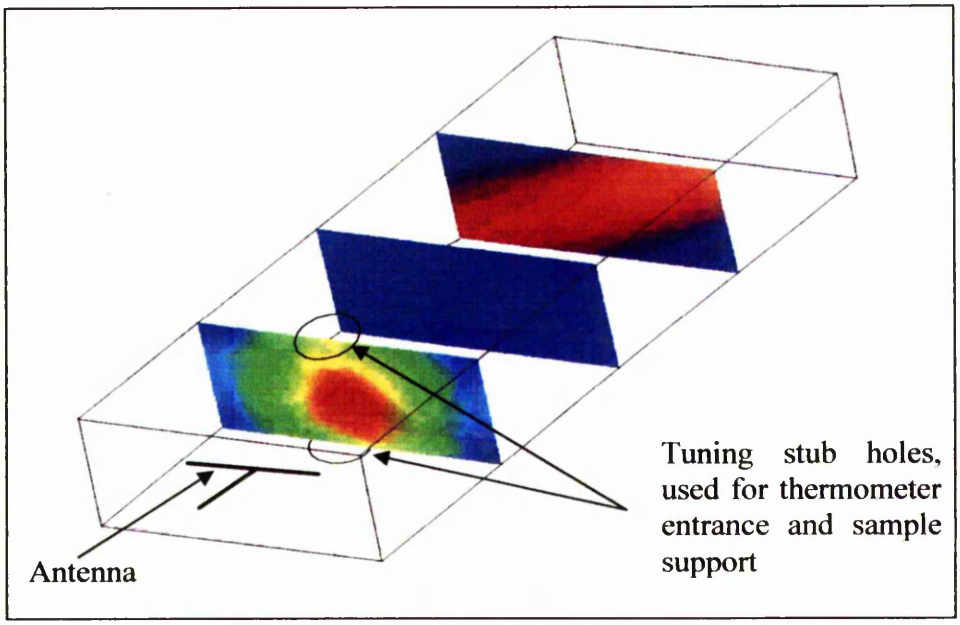

Figure 5.4: Waveguide microwave field distribution (electric component 2.45 GHz)

As the microwave field simulation in figure 5.4 shows, the waveguide applicator was designed such that the area of maximum field intensity was located directly above one of the sample insertion apertures. This allowed the sample to be placed directly into an area of known high field intensity. The sample was supported in the wave guide by a glass tube which also served to house the fluoroptic thermometer probe.

5.4.1: Heating Power

To determine the power level required to heat the EVA polymer, crosslinked samples (no blowing agent) of the same volume (30×20×5 mm) were heated at different power output levels to a set point of 160 °C. As the microwave amplifier operated at a fixed gain level, the power level was modified by adjustment of the output power from the network analyser to the microwave amplifier (0.1-1 mW). The temperature increase in the samples was recorded with a fluoroptic thermometer and plotted against time taken. The amplifier output powers were calculated using equation 5.1,

$$Power\,Gain\ (dB) = 10Log_{10}\left(\frac{RF\,Output\ Power\ /\ W}{RF\ Input\ Power\ /\ W}\right)$$

(Eqn. 5.1)

where RF output power is the power level after amplification and RF Input Power is the power level output by the VNA. Using the specified amplifier gain of 44.5 dBm

(assumed to be constant) the amplified power levels were calculated and are listed in table 5.3.

Table 5.3: Calculated variation of microwave amplifier output power with VNA output power based on a microwave amplifier specified gain of 44.5 dBm

Network Analyser Output Power / mW	Theoretical Microwave Amplifier Output Power / W
0.4	11.3
0.5	14.1
0.6	16.9
0.7	19.7
0.8	22.5
0.9	25.4
1.0	28.2

The heating rates for EVA 206 for each power level were plotted as a function of time to more clearly evaluate the effect of varying the input power and to help determine the most suitable power level for general usage. The results are shown in figure 5.5.

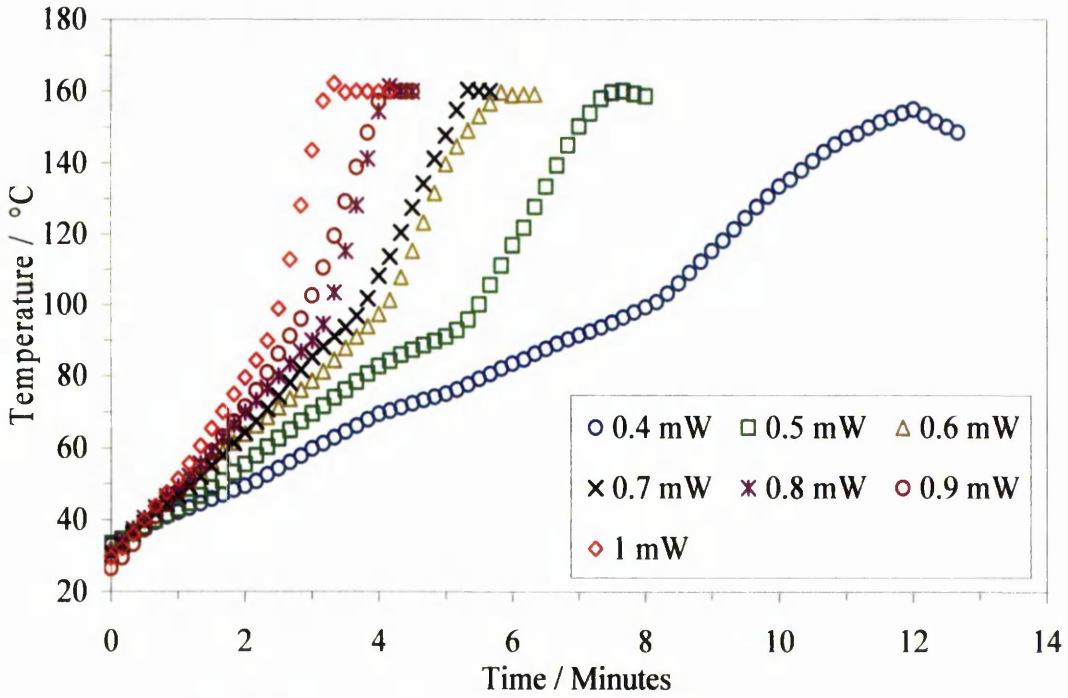

Figure 5.5: Heating rates for EVA 206 at different network analyser power outputs

The results show an increase in heating rate with increasing power output. It is also noticeable from figure 5.5 that, in each case, the heating rate showed a marked

increase when temperatures of around 90-100 ^{0}C were reached. This may be attributed to an increase in the dielectric loss factor. As the temperature increased the polymer matrix began to soften and the crystalline areas eventually melted. This resulted in a greater degree of polymer chain mobility and hence greater mobility of dipoles present within the polymer chain. This in turn allowed greater interaction of the microwave energy with the polymer matrix, thus an increase in heating rate was observed. A power output of 1 mW gave the fastest heating rate. This power setting was, therefore, used for all subsequent microwave heating using the waveguide. Curran (Curran, 1998) successfully foamed polyethylene using microwave heating techniques. However due to the low loss factor of PE (6.75×10^{-4} at 3×10^9 Hz, (Curran, 1998) hybrid heating and the presence of microwave active additives such as silica were necessary. The additives converted the electrical energy of the microwave field to heat which was then transferred to the polyethylene base polymer. It was thought that producing foam from EVA base polymer would be less problematic than using PE as the pendant acetate groups create polar regions along the polymer chain, which are microwave active. Samples of low density polyethylene (Stamylan LDPE 1808, 30×20×5 mm) and EVA 206 were heated in the waveguide for comparison. The results are shown in figure 5.6.

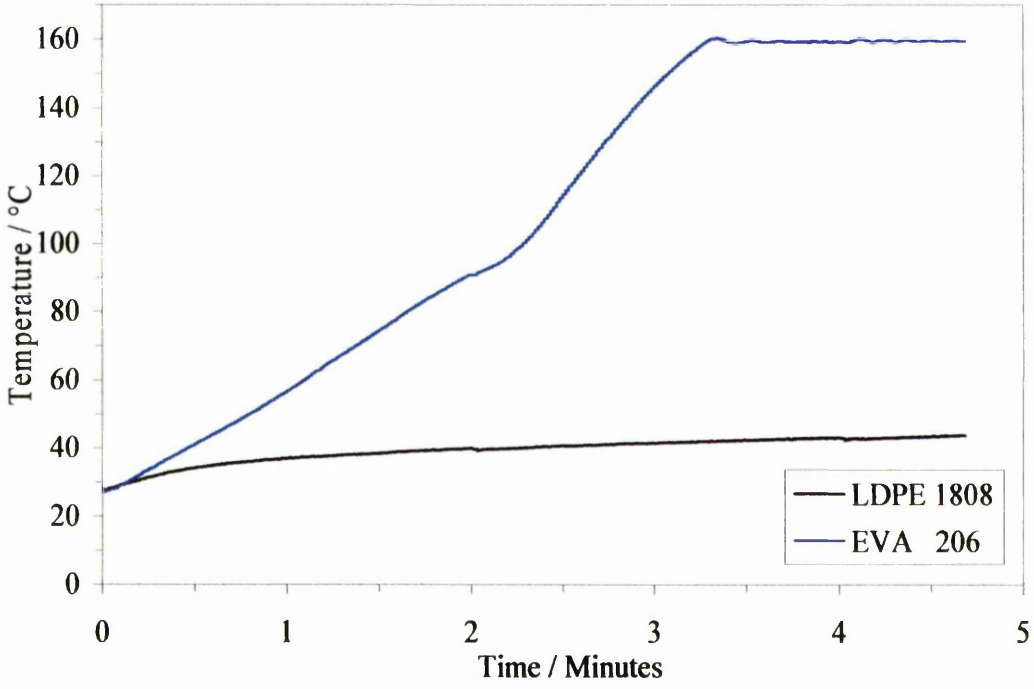

Figure 5.6: Heating rate comparison of EVA 206 and LDPE 1808 (1 mW network analyser output power ≈ 30 W heating power)

Figure 5.6 clearly demonstrates the effect of including a relatively small percentage of vinyl acetate into the polymer chain. The EVA 206 temperature increased to the set point within 3.5 minutes whereas LDPE 1808 only showed a marginal increase from room temperature to approximately 40 °C after almost 5 minutes heating time. The EVA profile also shows a distinct increase in heating rate in the 100 °C region. This was attributed to the melting of the polymer crystalline regions and the increase in loss factor due to the increased molecular freedom.

5.4.2: Microwave Foaming

It was necessary to use relatively small samples for the microwave foaming studies for two main reasons. Firstly the aperture of the waveguide was small and the increase in volume of the sample during foaming had to be taken into consideration in order that the sample could be removed on completion of the cycle. Secondly the sample had to be accurately placed inside the waveguide to ensure that it was located in the area of maximum field intensity. Using large samples would lead to the possibility that as the sample foamed and expanded, it would expand outside the area of maximum field strength. This would cause a microwave field strength gradient through the specimen, which may result in uneven foaming.

The samples were placed in the waveguide and located on the glass tube housing the fluoroptic thermometer. The control algorithm used two user defined temperature limits to control heating. Firstly the desired foaming temperature was defined as the maximum temperature limit. Secondly, a low temperature limit was entered. On commencement of heating the temperature was read by a Luxtron fluoroptic thermometry system. This output an analogue voltage signal, which was proportional to sample temperature, to the computer via an analogue – digital converter. The temperature was read by the computer which set the power output of the VNA (Vector Network Analyser) accordingly via a GPIB. On reaching the low temperature limit the VNA output power was progressively reduced to avoid setpoint overshoot. When the setpoint limit was reached the power was adjusted to maintain the setpoint temperature. It was found, however, that although the reaction of ADCE is exothermic (Sims and O'Connor, 1998) it did not result in significant overshoot of the temperature set point. The minimum power setting was, therefore, set just below the target temperature. It was also found that the resonant frequency of the loaded cavity

changed negligibly during the process. The settings for the heating cycle were as shown in table 5.4.

Table 5.4: Microwave heating cycle settings

Maximum VNA Output Power / mw	1
Minimum Output Power / mw	0
Temperature Set Point / °C	220
Minimum Temperature / °C	219
Frequency Span / MHz	200
Centre (Heating) Frequency / GHz	2.560
Time Between Frequency Sweeps / s	60

Initial Heating of the foamable samples took place at an acceptable rate (~30 ^{0}C / minute). However when sample temperatures approached 90-100 ^{0}C, a significant increase was observed in the heating rate. At these temperatures it was most unlikely that the temperature increase would be due to ADCE exothermic decomposition as the unactivated grade of ADC used decomposed in the range of 180-220 ^{0}C. The most likely explanation for this is that melting of the crystalline regions of EVA 206 allowed greater molecular freedom and coupling of the material with microwave energy became more efficient. Samples are shown *in situ* before and after foaming in the waveguide by figures 5.7 and 5.8, respectively.

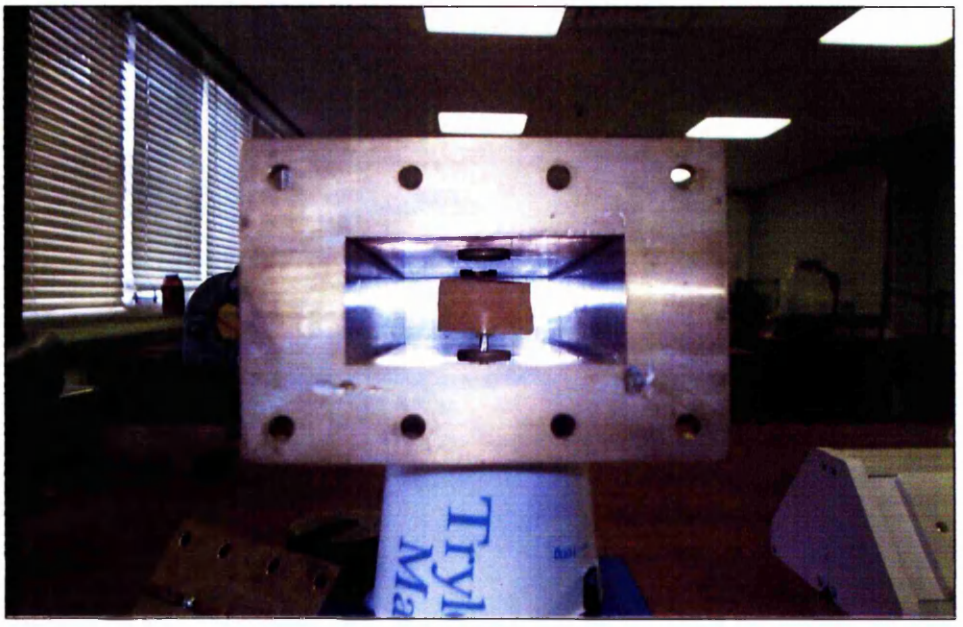

Figure 5.7: Crosslinked foamable EVA 206 in waveguide applicator

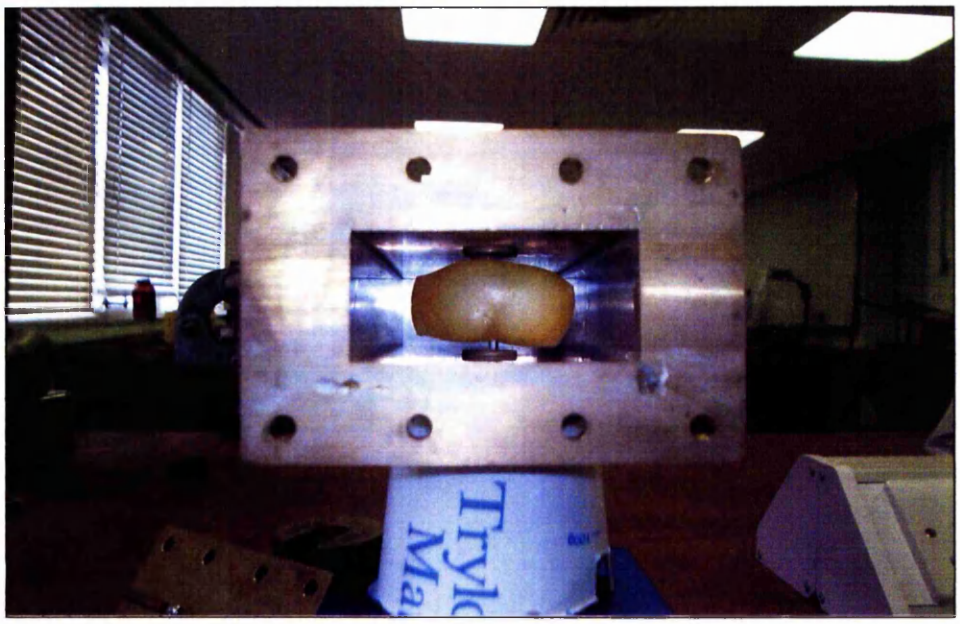

Figure 5.8: EVA 206 after heating and foaming in waveguide applicator

Although the density of the foams produced by thermal heating methods were consistent, indicating the completion of crosslinking before blowing agent decomposition, it was thought a trend would be observed with microwave heating. This was expected as the heating rates using microwave energy are generally faster and, therefore, expansion may begin before the completion of the crosslinking reaction. The density of the foams produced by microwave heating showed a great deal of variation and no clear trend was observed. It was thought that the faster heating rates achievable with microwave heating may require some pre-crosslinking in order to prevent cell rupture and foam collapse. As with the thermally foamed samples various levels of pre-crosslinking were performed before foaming. Due to the limitations on sample size, it was necessary to use the method of pycnometry to determine the sample densities. It may be argued that this technique is not directly comparable with the standard cutting and weighing technique as the cut foam surfaces have exposed open cells. The water used in this method can occupy these voids causing an underestimation of sample volume and subsequent overestimation of density. It was necessary, therefore, to re-measure the density of the foams produced by convection heating using pycnometry to ensure that any comparisons were valid. Samples of foam were cut from the centre of the foamed specimen. The skin was removed as its density was inconsistent with that of the sample bulk. The density

results are reported in table 5.5 and are accompanied by a typical heating rate profile in figure 5.9.

Table 5.5: Density of foams produced by thermal and microwave heating methods

Initial Gel Content / %	Thermally Expanded Foam Density / kg m^{-3}	Microwave Expanded Foam Density / kg m^{-3}
0	62.5 ± 10.0	83.9 ± 3.5
15	57.4 ± 1.2	112.1 ± 41.3
47	68.8 ± 9.6	60.4 ± 8.9
49	61.0 ± 3.6	79.1 ± 29.5
60	62.5 ± 6.2	118.2 ± 48.2

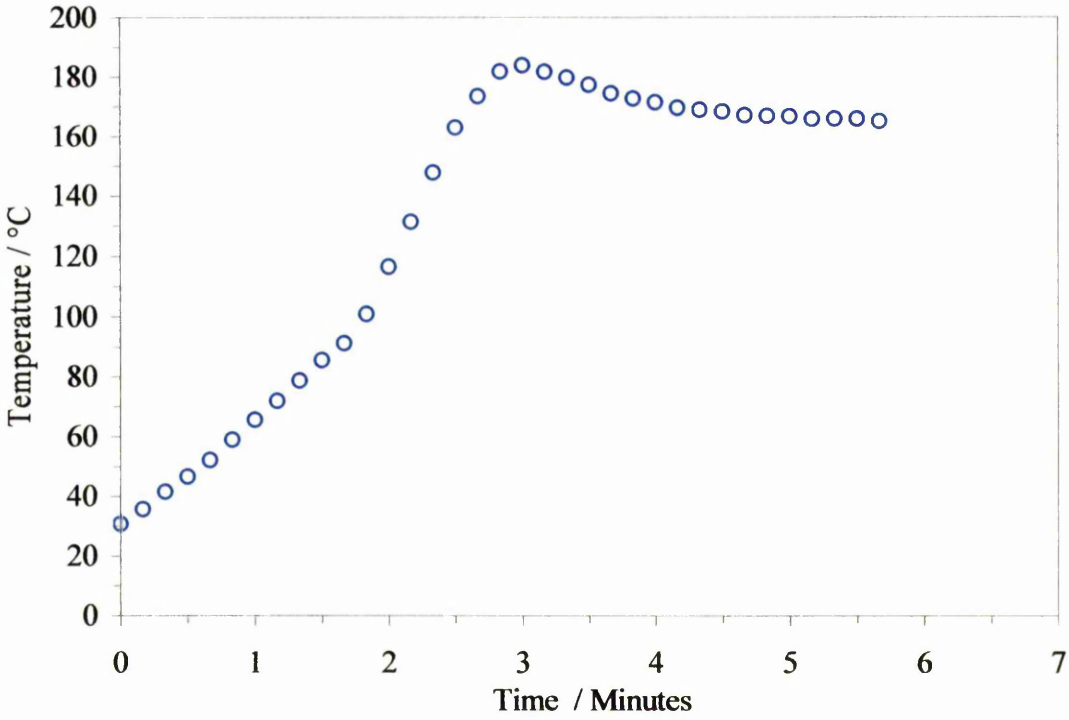

Figure 5.9: Heating profile for pre-crosslinked foamable EVA 206 blended with 0.5 phr DCP and 8 phr ADCE, heating power 30 W (1 mW VNA output power)

If the results for the thermally expanded foams shown in table 5.5 (measured by pycnometry) are compared with those shown in table 5.2 it may be observed that the results obtained by pycnometry are slightly greater than those obtained from cut samples. This was thought to be caused by water entering the bisected open cells on the sample surface resulting in a marginal overestimation of overall density. As with

the thermally cured samples, no clear variation of density with pre crosslinking level is evident. This would suggest that the samples had been fully crosslinked before blowing agent decomposition began. On examination of the microwave heated sample, considerable density variation was encountered. This would suggest that foaming was inconsistent between samples. It was evident upon visual inspection that an area of unfoamed polymer was present surrounding the samples. Although this unfoamed skin was removed prior to density measurement (as were the conventional foams) it appeared that the presence of the skin was restricting expansion particularly around the sample extremities. If foaming was restricted, full expansion of the sample would not take place and would result in the higher microwave foam density values observed.

During the heating cycle, the temperature of the crosslinked foamable samples increased at a similar rate to the non foamable crosslinked (no blowing agent) samples. Furthermore, the increase in rate observed with the crosslinked samples at 90-100 ^{0}C was present. It was generally found, however, that after temperatures had reached 180-210 ^{0}C, the heating rate slowed and the sample temperature began to fall despite microwave heating power being maintained. The foaming of polymers has been shown to decrease losses at microwave frequencies. The incorporation of voids, which can be considered loss free, in a dielectric material lowers the dielectric loss and permittivity leading to a significant drop in microwave activity (Reed and Lunk, 1985; Wilkenloh *et al.*, 1978). Previous heating of pure EVA 206 samples (no crosslinking or blowing agent) had shown that a temperature of 220 °C could be reached and maintained. The introduction of air into a polymer matrix has the effect of significantly lowering the dielectric loss especially at microwave frequencies (Reed and Lunk, 1985). The cells generated during foaming, which essentially contain air, may be considered to be loss free, hence, as foaming progressed, both the dielectric loss and dielectric constant were reduced. Furthermore, upon foaming the sample turned from a solid to a cellular material with very thin walls. The cell walls would have had high heat loss and increased the effective surface area of the sample. As foaming continued, the sample became progressively harder to heat until a point was reached where there was insufficient microwave power available to maintain the heating rate and the sample began to cool.

As there was no appreciable difference in the heating rates of crosslinked EVA and crosslinked EVA blended with ADCE, it would appear that the incorporation of cells into the polymer is the dominant factor for the observed decrease in temperature and not the loss of ADCE through decomposition. This is supported by the fact that EVA was the largest formulation component and, therefore likely to be the dominant materials with regards to loss factor.

5.5: Scanning Electron Microscopy

Micrograph images were used to compare the cellular structures of foams produced by microwave and conventional techniques. This allowed a broad comparison of the foam structures to be made, as well as highlighting any regions of unfoamed material within the specimens. The samples were fully crosslinked in the press and foamed for 6 minutes at 220 °C (6 minutes at full power due to temperature decrease) (microwave and conventional). Comparison of foams produced by microwave and thermal heating methods may be made by examination of figures 5.10-5.13. The magnification was the same in each case to allow direct comparison.

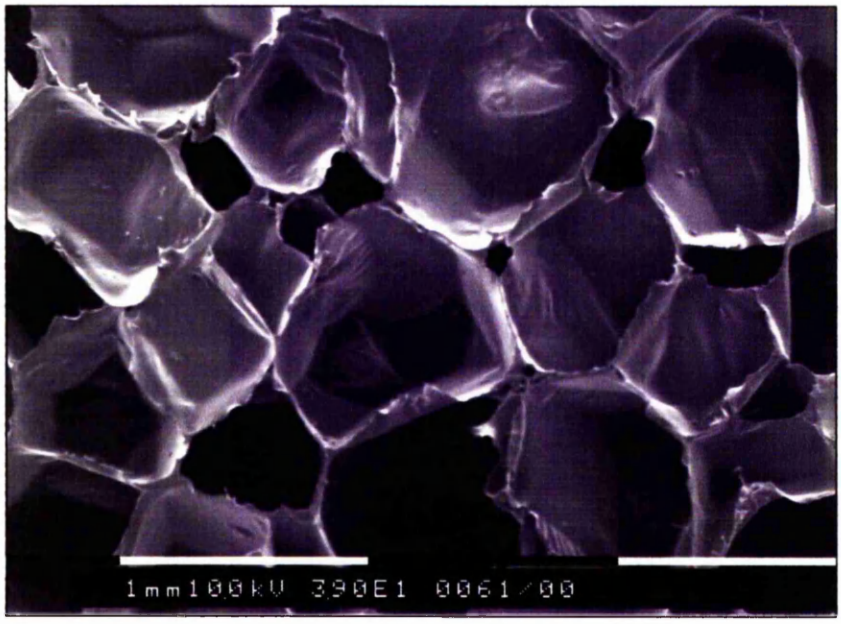

Figure 5.10: Foam (centre) produced by convection heating

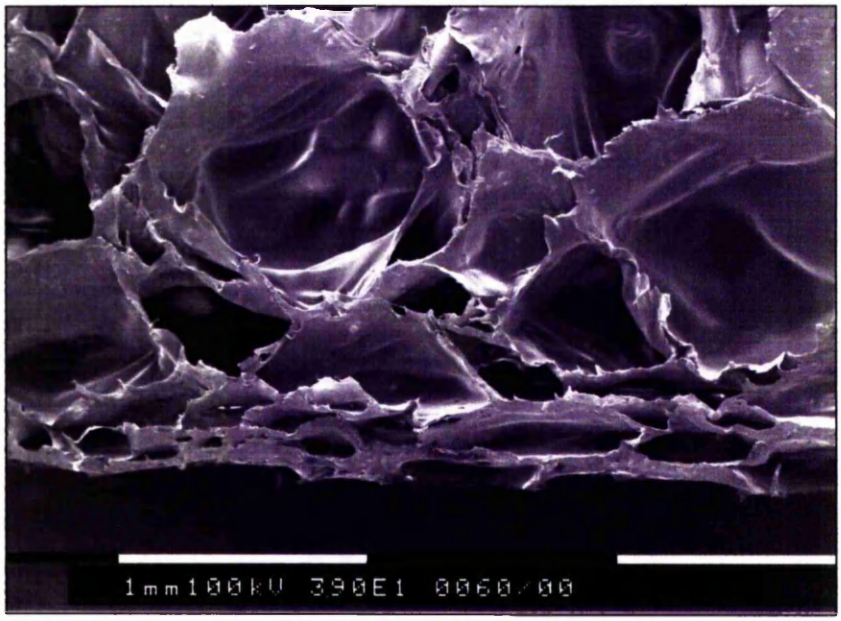

Figure 5.11: Foam (edge) produced by convection heating

Figure 5.12: Foam (centre) produced by microwave heating

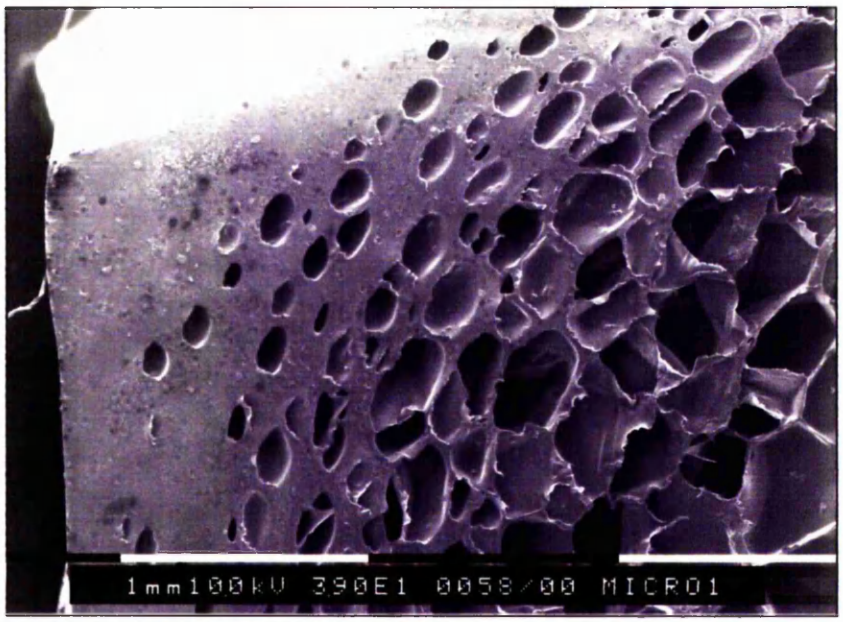

Figure 5.13: Foam (edge) produced by microwave heating

The foam samples produced using conventional hot air methods exhibited well formed closed cells that were in the region of 1 mm. Upon examination of the sample edge it was evident that foaming had taken place throughout the entirety of the sample with the exception of a very thin skin on the sample surface. This was expected as the edges of the samples were heated first and were, therefore, the regions of the sample that foamed first. Heat was then conducted from the sample surface to the centre to complete foaming.

The SEM images of the microwave heated samples would suggest that their cells were considerably smaller than those produced by convection heating. It was noticed that the foams produced by microwave heating had a significantly thicker skin than thermally produced foams. The surface of these foams also showed a distinct yellow discolouration. Whilst this may be attributed in part to thermal oxidative degradation, it also indicated the presence of un-reacted blowing agent which itself is an intense yellow colour. To provide confirmation of this, images of the foam skin were obtained.

Figure 5.13 shows, the corner and edge of one of the foam samples produced by microwave heating in the wave guide. It may be seen that there was a significant area of unfoamed polymer skin surrounding the foamed core of the specimen. This was

attributed to two factors. Firstly, as the polymer sample was being heated, heat was continually lost from the surface of the sample to the surrounding air which was at ambient temperature. This would lead to a significantly lower temperature at the surface of the sample, which was not sufficiently high to cause blowing agent decomposition and foaming to occur. Secondly, as the core of the sample foamed and expanded, the sample extremities migrated from the area of high microwave field intensities towards the wall of the waveguide, where, as the field simulation shows, the microwave field was relatively weak. The microwave field may not, therefore, have had sufficient intensity in these areas to raise the skin temperature to the level required for blowing agent decomposition and subsequent foaming. Foams expanded in the oven avoid this as heat conduction takes place from the sample surface inwards therefore making the sample extremities the hottest areas. The skin on these foams may also help explain the variable nature of the density values. The thick areas of unfoamed skin show that these regions did not achieve sufficiently high temperatures to effect blowing agent decomposition. At these lower temperatures, the modulus of the polymer would be significantly higher than that of the sample centre where foaming occurred. These cooler regions would effectively oppose the expansive forces of the blowing agent gas within the foam cells. As a result the cells in the centre of the sample may not have expanded to their maximum potential.

5.6: Summary

The results from this section show that although heating EVA 206 using microwave energy was possible there were some technical issues to be addressed when considering a scale up study. The specimens foamed by microwave heating exhibited good cellular structure and density reduction comparable with conventionally produced material. However, the thick unfoamed exterior portion of the samples demonstrated that there was a need for a supplementary heat source required to complete the foaming process in these regions. Furthermore, it is evident that the samples produced in the waveguide were far too small for mechanical property measurements. A new applicator was necessary to produce larger foam specimens that could be used for mechanical property tests in addition to more reliable SEM and density measurements. In order to achieve these goals, the remainder of this work will concentrate on the design and construction of suitable heating equipment and the analysis of the foamed specimens it produced.

CHAPTER 6: COMBINATION OVEN DESIGN, CONSTRUCTION AND DEVELOPMENT

The small samples of foam produced using a waveguide section as the microwave applicator were useful for providing some initial data on the nature and feasibility of the foaming process using microwave radiation. One of the most significant findings was the need for some supplementary heating (i.e. hot air) to alleviate the drawback of the unfoamed sample surfaces. The necessity for larger samples was also highlighted. It was possible to obtain good SEM images but it was difficult to obtain reliable values for density from the small samples produced in the section of waveguide. It was also unfeasible to obtain any mechanical testing data from these small sections of foam.

The aim of this part of the work was the construction and development of a foaming oven, capable of producing larger foamed samples. The waveguide applicator was resonant at 2.45 GHz only and the field was localised in a small region. This was acceptable for the production of small samples of foam where the sample could be accurately placed within the area of maximum field intensity. Such field localisation was undesirable in the production of larger samples as this would lead to areas of localised heating within the sample and result in an unevenly foamed specimen. The oven needed to be much larger to allow larger samples to be produced. The oven was also to include additional air heating capabilities to supplement microwave heating, with the intention of foaming the surface of the samples.

6.1: Electric Field Simulation

After choosing main cavity dimensions of 500 × 500 × 100 mm which would allow the production of suitable sized samples, microwave simulations were carried out using Agilent HFSS (High Frequency Structure Simulation) software to predict the distribution of the microwave field within the cavity. The software was based on the finite element method and allowed electromagnetic modelling of passive three dimensional structures. The programme produced three dimensional representations of the electric field thus facilitating rapid evaluation of field uniformity and the prediction of any areas of high or low field intensity.

6.1.1: Simulation at 2.45 GHz

One of the main drawbacks to microwave heating is the presence of hotspots caused by localised areas of high field intensity. In an effort to reduce this problem, two antenna designs were evaluated and compared, a simple monopole and a spiral antenna designed to more evenly distribute the microwave field throughout the oven. Figures 6.1 and 6.2 show the effect of antenna type on the empty cavity.

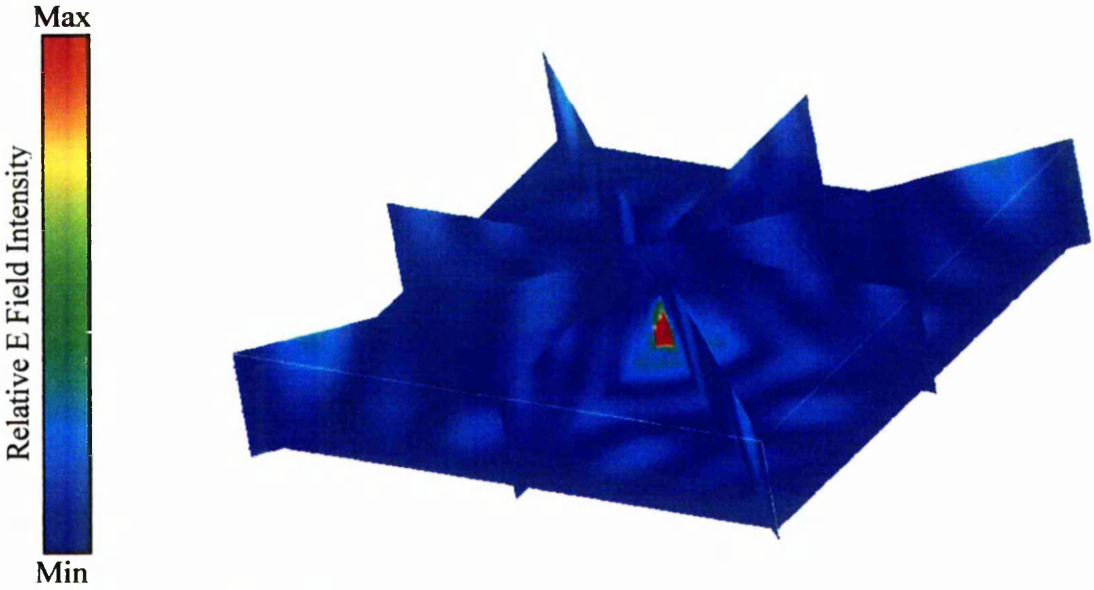

Figure 6.1: Electric field distribution at 2.45 GHz for oven cavity (monopole antenna)

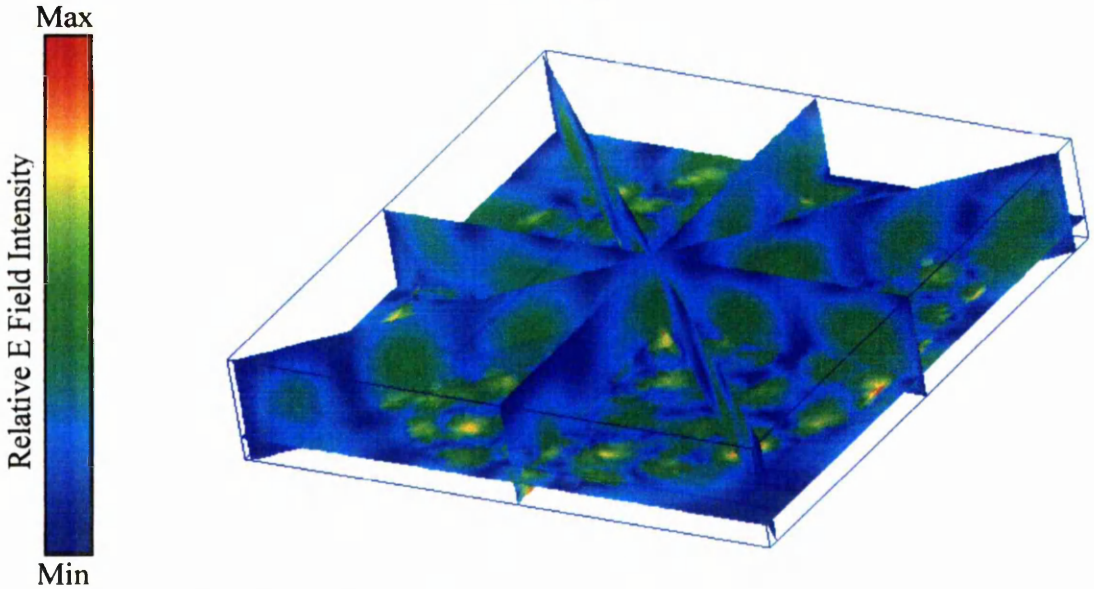

Figure 6.2: Electric field distribution at 2.45 GHz for oven cavity (spiral antenna)

Figure 6.1 shows the electric field distribution at 2.45 GHz using a simple monopole antenna. The field appears to be heavily localised around the antenna, resulting in a

region of high electric field intensity in this region. The remainder of the cavity volume shows low field intensity further suggesting that the majority of the power is distributed in close proximity to the antenna. For a sample placed in the centre of the cavity this would result in an undesirable localised heating effect in the centre of the sample leading to uneven foaming throughout the sample. Placement of the sample off centre may reduce this problem but on foaming and subsequent expansion, it is likely that the foam would expand into this region. Furthermore, as the majority of the electric field appears to be concentrated around the antenna, there may be insufficient power distributed in the extremities of the cavity to heat and foam the sample. Figure 6.2 shows the electric field distribution at the same frequency as figure 6.1 but using a spiral antenna instead of a monopole. It is evident that the electric field distribution is greatly improved throughout the cavity. The more evenly distributed field would result in a more uniformed heating profile throughout the sample and reduce areas of localised heating.

Although much improved, the field still displays some large areas of high field intensity. Using a single frequency for heating may still have resulted in undesirable localised heating. The effects of these localised areas may be reduced somewhat by the foaming process. As the sample began to foam and expand it would pass through these areas thus aiding the distribution of heat. It is likely however, that localised heating would still cause non-uniform foaming. This in turn may have a detrimental effect on the uniformity of the foam properties as foaming takes place in the hotter areas before the cooler regions. To further alleviate this problem, it was decided that a range of microwave frequencies should be used during heating in order to constantly redistribute the high field intensity regions and therefore even out temperature profiles within the sample. Further simulations were performed once the oven was completed and suitable heating frequencies could be chosen from the microwave reflection characteristics of the cavity loaded with a foamable sample.

6.1.2: Simulation at 8 GHz

The results from the dielectric probe presented in chapter 4 indicated that heating at higher frequencies than 2.45 GHz would be more efficient. Simulations were, therefore, carried out at 8 GHz. At higher frequencies the electric field becomes more uniform as a greater number of modes are possible compared with lower frequencies. Figures 3.4 and 3.5 show the effect of antenna type at 8 GHz.

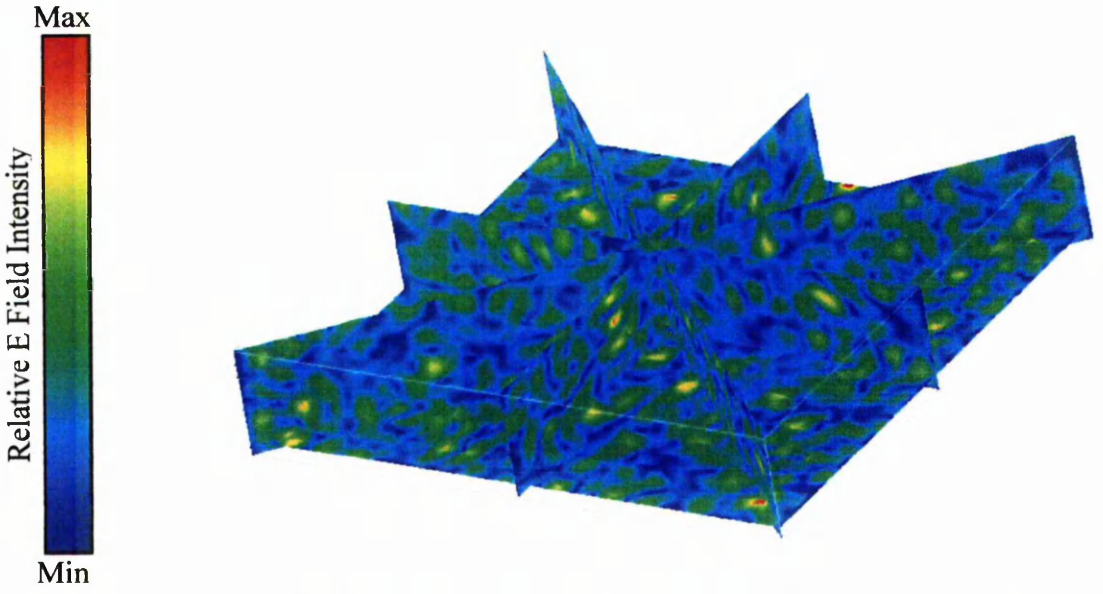

Figure 6.3: Electric field distribution at 8 GHz for oven cavity (monopole antenna)

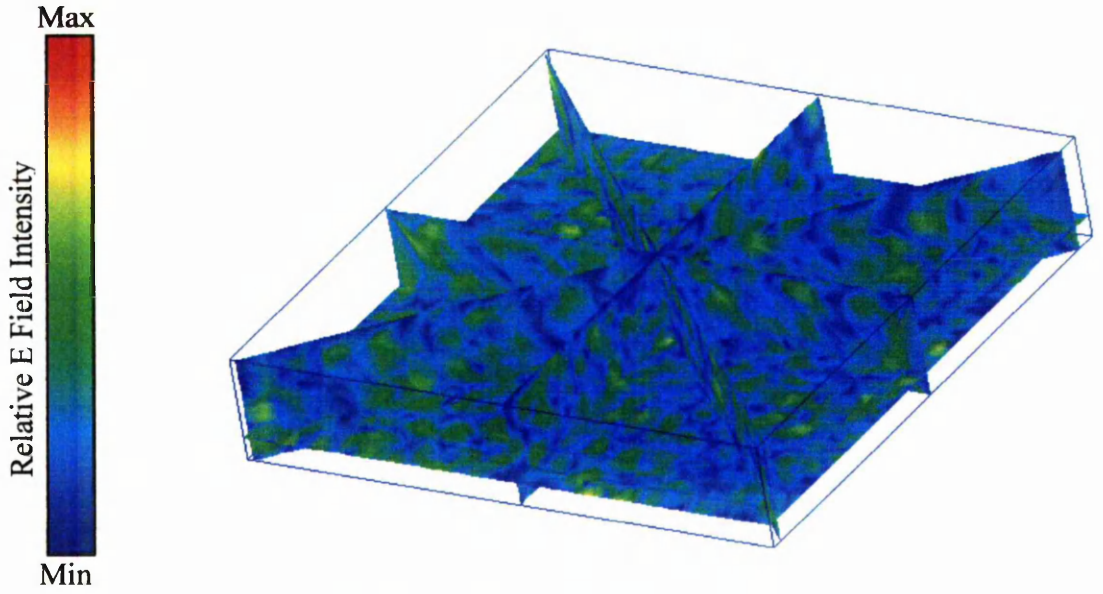

Figure 6.4: Electric field distribution at 8 GHz for oven cavity (spiral antenna)

By comparison of figure 6.3 with 6.4, it would appear very little difference between using the monopole and the spiral antenna in the higher frequency ranges. Both simulations show that the electric field is well distributed throughout the cavity, which is desirable for uniform heating. This would suggest that the greater number of modes possible in the higher frequency range distribute the electric field more evenly and that the antenna design becomes less critical with regards to field uniformity.

The frequencies used for the simulation were based on the available equipment frequency capabilities and ISM frequencies. The maximum frequency that could be

generated by the TWT amplifier was 8 GHz. Although heating at higher frequencies would be more efficient (based on the dielectric data in chapter 4), 8 GHz is not an ISM frequency and leakage problems could be encountered if this frequency was used in an industrial process. Furthermore, there were serious concerns regarding the reliability of the TWT amplifier as it frequently had to be sent away for repairs to faults that occurred during operation. Thus, simulations were also performed for 2.45 GHz, which is a commonly used ISM frequency (Ku *et al.*, 2002).

6.2: Oven Construction

To allow heating to be conducted at variable frequencies, a new variable frequency cavity was constructed based on the simulations. A drawback associated with microwave heating is heat loss from the sample surface. Foams produced using the waveguide section showed that such heat losses resulted in the formation of a thick unfoamed skin. For this reason, a hot air facility was included to aid sample surface foaming. Brass was chosen for the main oven body material, as it is a very good electrical conductor. The main oven body was constructed from 5mm thick brass plate sections. The heating cavity had dimensions of 500 × 500 × 100 mm and was covered by a hinged lid. The main oven body and lid are shown pictorially by figures 6.5, 6.6 and schematically by figure 6.7.

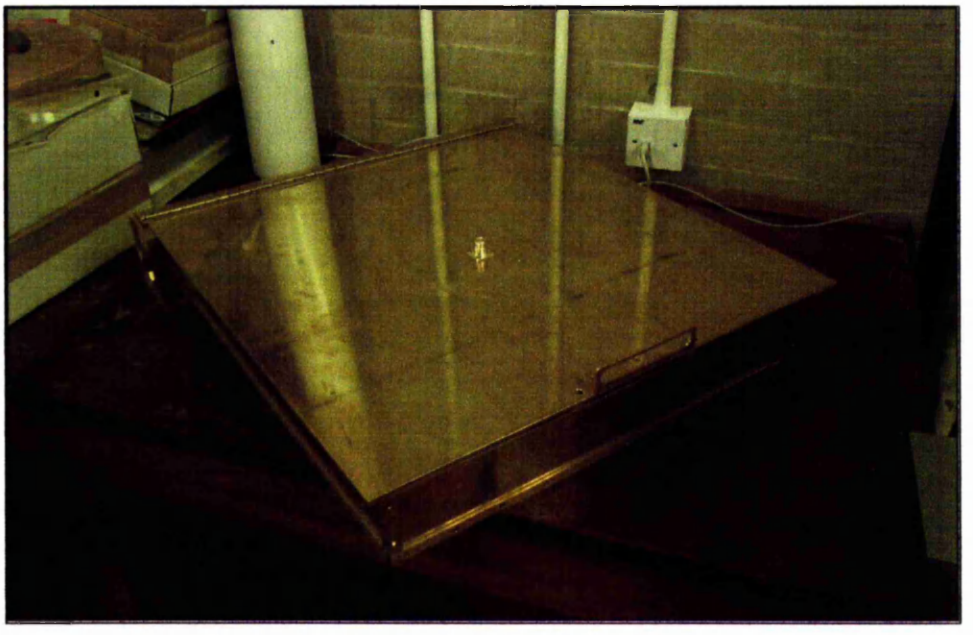

Figure 6.5: Combination microwave / hot air oven main body

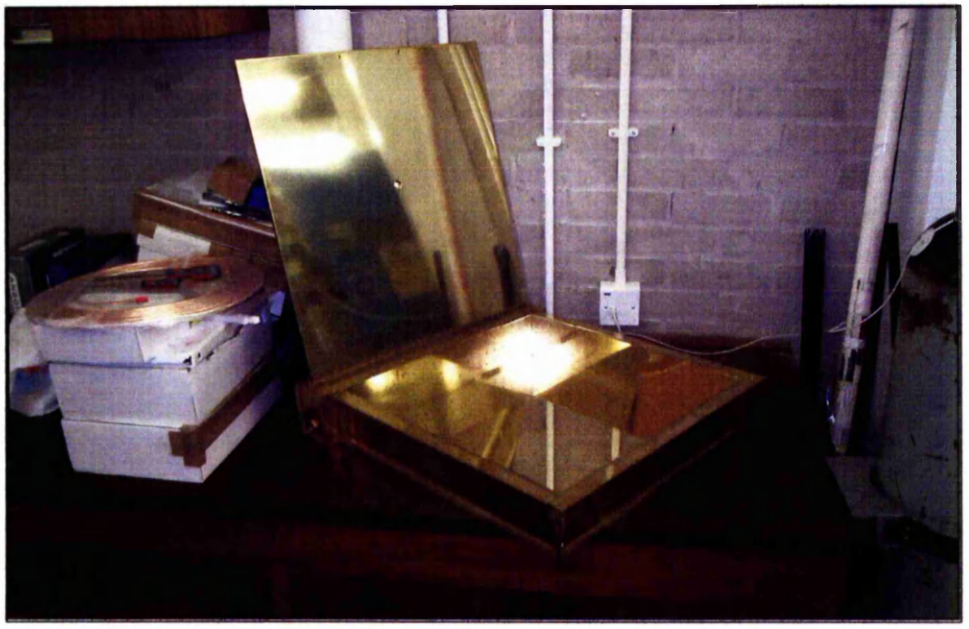

Figure 6.6: Combination microwave / hot air oven interior

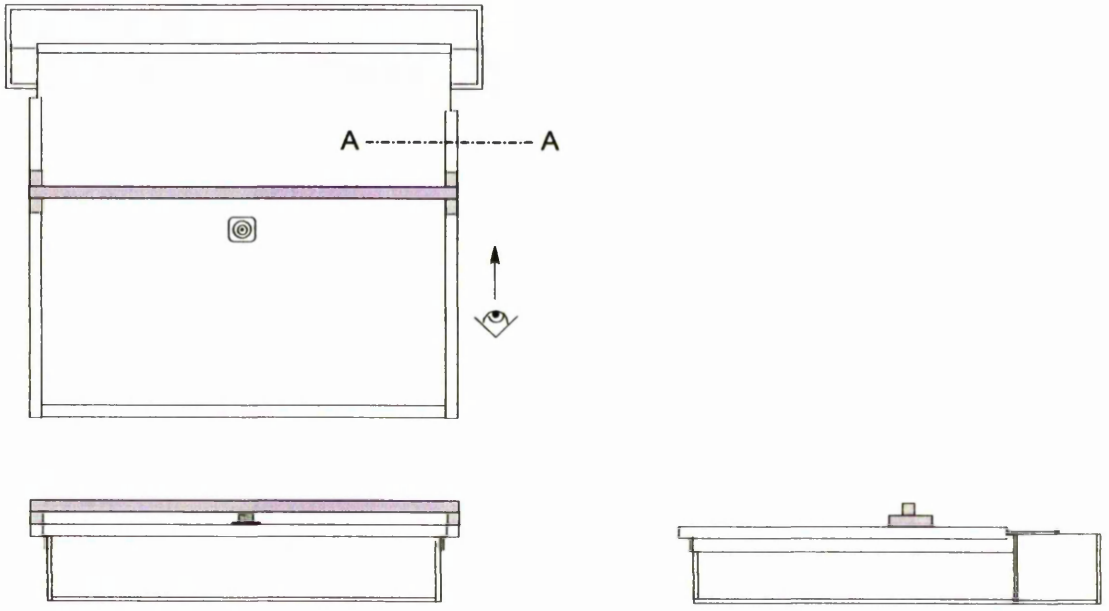

Figure 6.7: Oven plan, front and side elevations (section A-A relates to figure 6.18)

It was initially planned to continuously join all the brass sections by brazing. A continuous joint was desirable in order to obtain continuous electrical conductivity between all the mating surfaces, which is important to obtain a high Q value, which is necessary for efficient heating, and to help prevent microwave leakage. However, on consideration of the high temperatures involved during brazing, this method was ruled out due to the high probability of serious distortion of the brass sections. As an

alternative, laser welding was also investigated. A trial sample of the brass sheet was welded using this method. It was found that the weld was of poor quality and very low strength. It was determined that during the welding process, the Zinc present in the alloy was reacting with atmospheric oxygen and the resulting oxide was preventing the formation of a good weld.

The method of jointing finally used involved screwing lengths of brass angle to the external edges of the oven. The brass angle covered the joints between the brass plates, thus guarding against leakage. However, this method did not produce the desired continuous conduction between the brass plates. Seams in microwave applicators may be caulked with conducting fillers such as a resin heavily loaded with silver particles (Meredith, 1998). Thus, silver DAG paint (a suspension of fine silver flakes) was applied over the joints between the mating surfaces to improve electrical conductivity.

A mobile frame was constructed to support the oven at a convenient working height. The frame was made from 25 mm square section steel tubing. Castors (with brakes) were fitted to the frame to facilitate movement of the oven.

6.3: Fittings

6.3.1: Hot Air Facility

One of the problems highlighted by the foam samples produced in the waveguide was that heat losses from the surface resulted in a thick unfoamed skin. In order to house the necessary components for air heating, a small secondary compartment was formed by a partition across the rear of the oven. Two 750 W air process heaters (depicted in figure 6.8) were installed inside the compartment. The heaters were fed from a pressure and volume regulated compressed air supply. Numerous holes were drilled in the rear wall of the oven to allow the heated air to pass into the main oven cavity. The air was routed such that after entering the cavity it could circulate and the exit though an exhaust. The air process heaters used are shown in figure 6.8 and the perceived internal oven airflow by figure 6.9.

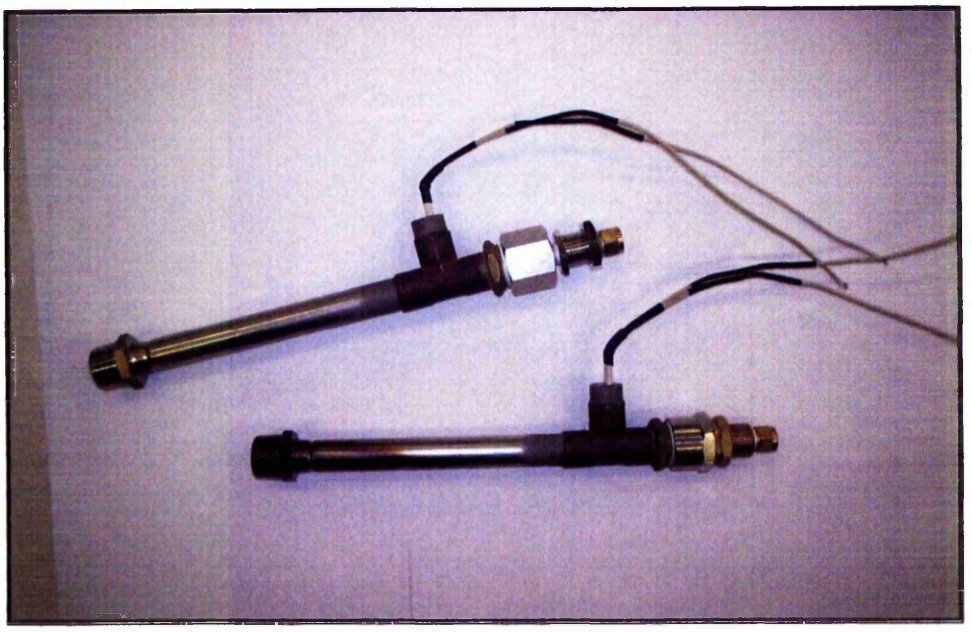

Figure 6.8: Air process heaters

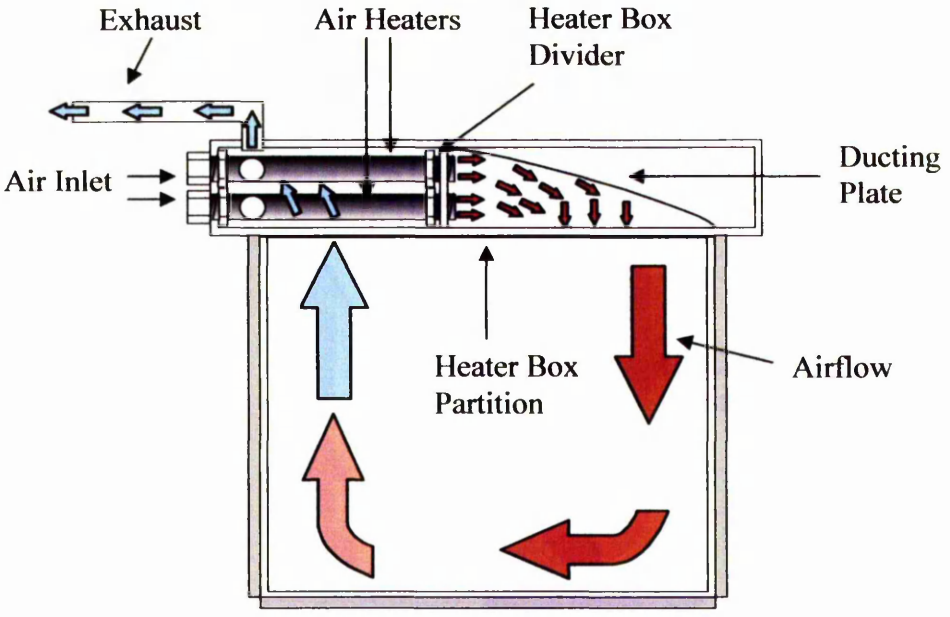

Figure 6.9: Oven airflow

6.3.2: Insulation

It was necessary to ensure that the oven was sufficiently insulated to prevent heat loss from the external oven surfaces and personal injury by contact with the hot oven. Firstly, the oven was lagged with a thin layer (~ 3mm) of alumina cloth. The oven body was then enclosed by thick sections (~ 25 mm) of insulation board. The lid was

insulated with only the alumina cloth to avoid adding to its already considerable weight.

6.3.3: Antenna

A spiral antenna (attached to the inside of the lid) design was chosen in an effort to achieve as uniform distribution of the microwave field throughout the cavity as possible. Figures 3.4 and 3.5 indicate that there would be little advantage, with regard to field uniformity, in using a spiral type antenna at frequencies between 6 and 8 GHz However, the spiral antenna would appear to be much more effective at 2.45 GHz than a monopole thus providing the facility to use both high and low frequencies for foaming. The antenna was formed from 3mm (outside diameter) copper tubing and held in shape by clipping it into four PTFE supports which, were then attached to the lid with a silicone adhesive. Although this method of attachment was successful initially there were doubts about its long-term reliability as PTFE is an inherently non-stick material. The inner end of the copper spiral was then soldered to the connector stub of an N-type connector that entered through an aperture in the centre of the cavity lid. The antenna spiral is shown in figure 6.10.

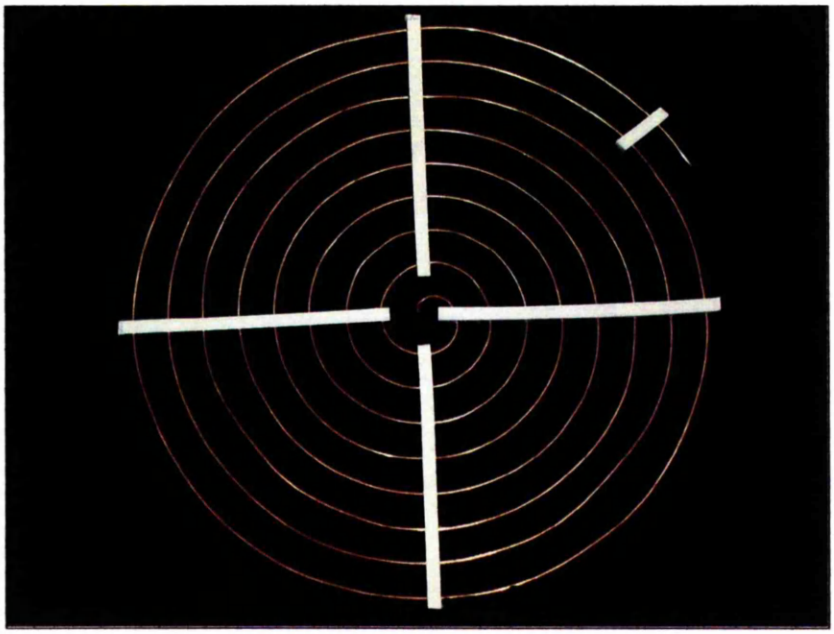

Figure 6.10: Spiral antenna and PTFE supports

6.4: Oven Development

6.4.1: Heater Modification.

Initial heating trials, using the hot air facility alone, revealed that the air process heaters were not sufficiently powerful and did not have the necessary air throughput to heat the cavity at a reasonable heating rate. Although the specifications for the heaters indicated that they should easily be able to generate the required temperatures, heating the cavity to temperatures above 100 °C proved to be slow and problematic. It appeared that this was due to the heaters having to continually heat cold compressed air. As it was not feasible to re-circulate the air back into the heaters, an alternative method was required.

The oven was modified by removal of the air process heaters and the installation of 2 1kW heating elements supplied by RS. The elements were supplied as straight lengths. They therefore needed to be bent and formed into shapes suitable to fit into the oven heater box. The connector ends of the heating elements were routed through one end of the heater box and connected to a mains electrical supply via a cal temperature control unit. A tangential blower fan (also supplied by RS) was installed next to the heaters. The heating element components and fans are shown in figures 6.11 and 6.12 respectively.

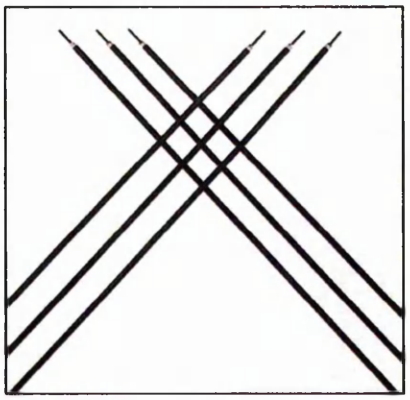

Figure 6.11: Heater elements

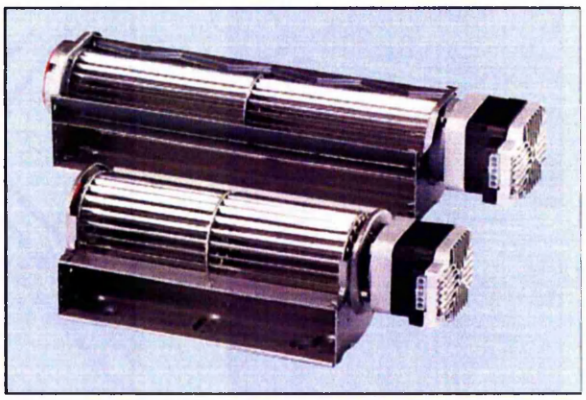

Figure 6.12: Tangential blower fans

Before installation, the fan needed to be modified to fit the oven. As figure 6.12 shows, the fan motor is mounted directly to the fan chassis. The motor could not be placed in the heater box due to the elevated temperatures inside. Thus, the motor was removed and bolted to the end of the heater box (sections of insulation were used to isolate the motor from the oven body). A steel drive shaft was made to connect the

output shaft of the fan motor to the fan blade cylinder. The opposite end of the fan cylinder was mounted in a rubber / nylon bush assembly. This was replaced by a plain brass bush bearing. The fan and heating elements are shown in figure 6.13.

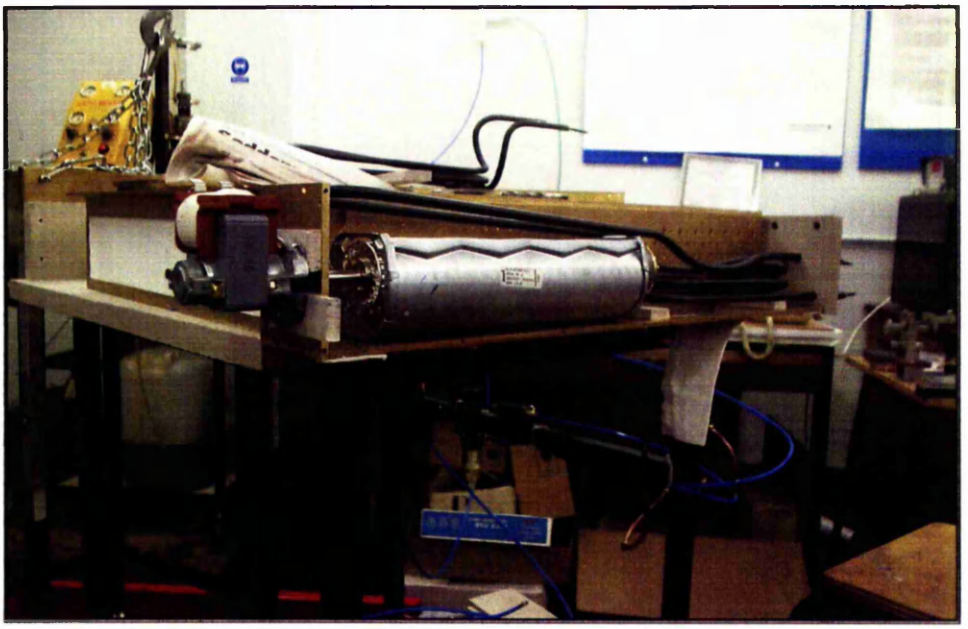

Figure 6.13: Heating elements and fan *in situ*

The fan motor and the live ends of the heating elements were then enclosed in aluminium housings to cover the exposed electrical terminals. A slot was cut into the rear wall of the oven to allow the fan to blow the heated air from the heater compartment into the oven cavity. The air could then circulate within the cavity before re-entering the heater cavity via the original air holes. The slot cut for the fan was covered with a fine steel mesh (reclaimed from a domestic microwave oven door) to prevent leakage of microwave radiation into the heater box. The re-circulating airflow within the oven is represented in figure 6.14.

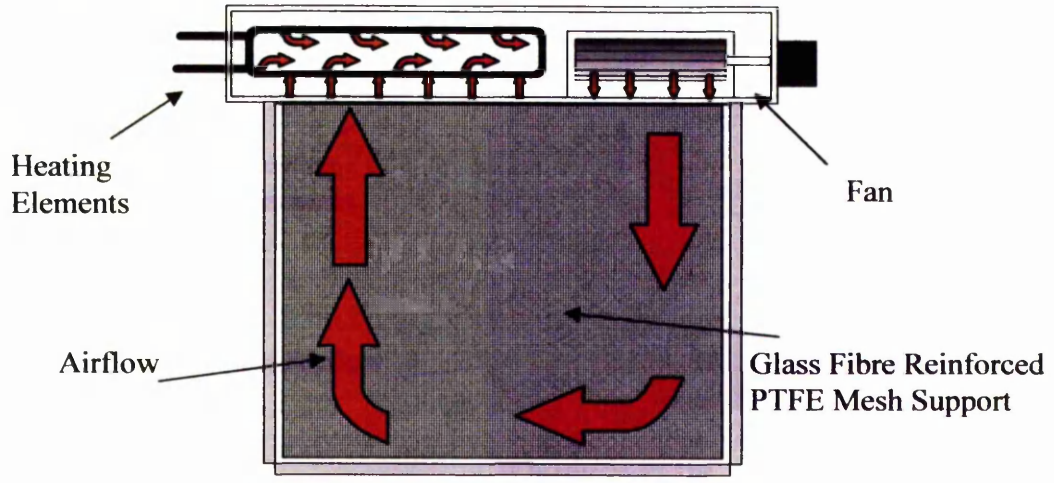

Figure 6.14: Oven re-circulating airflow

The improved heating arrangement resulted in reasonable heating rates. The fan motor housing needed to be adapted to accept a 240 V AC 80 mm fan to cool the motor as it had a tendency to overheat and seize at high temperature. Doubts concerning the silicone adhesive attaching the antenna were confirmed when the antenna assembly became detached during an initial hot air heating test. The PTFE supports were re-attached to the lid using PTFE screws.

6.4.2: Heating Control System

A system was developed to allow controlled heating using hot air and microwave heating simultaneously. The system is outlined in figure 6.15

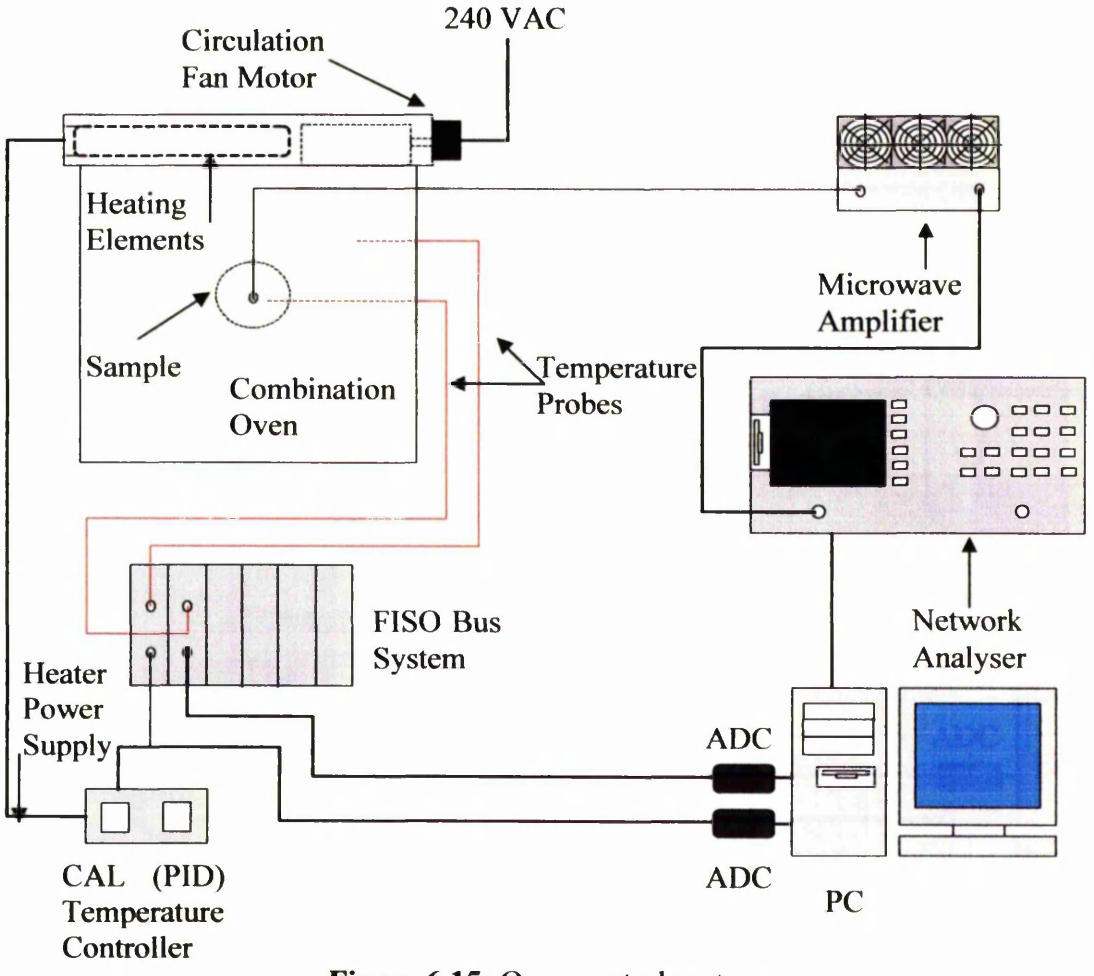

Figure 6.15: Oven control system

Two 1 kW heating elements and a re-circulating fan arrangement were used to heat and re-circulate the air. Air temperature was controlled using a PID process controller (CAL Controls Ltd). The required temperature was programmed into the PID, which then supplied current to the heating elements via a solid-state relay. The current supplied to the elements by the controller was varied to achieve and maintain the

desired air temperature. The air temperature was recorded using one channel of a two channel FISO Bus system equipped with fibre optic temperature probes (shown as red lines in figure 6.15). The temperature probe connected to the first channel of the Fiso Bus system was placed directly in the air stream where it entered the oven. An analog output voltage proportional to the air temperature was supplied by the Bus system to a PC through an analogue-digital converter (ADC), and to the PID process controller. The air circulation fan was independently connected to a mains electricity supply.

Microwave heating was controlled using a feedback loop between the source power and the sample temperature. The primary microwave signal source was a Hewlett Packard network analyser. A process control programme on the PC was used to set the microwave frequency and power. After entering the frequencies to be used and their respective powers into the control programme, adjustment of the network analyser output power and signal frequency was achieved via a GPIB. The output / reflection port of the network analyser was connected to the input port of a solid state 200 W microwave amplifier. The amplified signal was fed though a microwave cable connected between the output port of the amplifier and the N-type connector of the oven antenna.

The sample temperature was recorded using the second channel of the Fiso Bus system. The temperature probe connected to the second channel was contained within a thin walled glass tube embedded in the sample. Sample temperature was supplied as an output voltage to the PC through an analog-digital converter.

6.4.3: Sample Support

To allow the circulation of hot air around the sample, a support was built so the specimen could be placed directly in the centre of the oven cavity. The support comprised lengths of glass tubing and glass fibre reinforced PTFE mesh. A section of glass tubing was cut to the diagonal length of the cavity. Two smaller glass tube sections that were a close fit inside the diagonal tube were cut to the height of the cavity, heated (using an oxy-acetylene torch) and bent at their centres to form 90° angles. These were then slotted into the ends of the diagonal tube to act as legs and support the diagonal tube at halfway height within the cavity. A second support was constructed in a similar manner with the addition of a U shaped junction in the middle

to clear the other support tube. A 500 × 500 mm section of glass fibre reinforced mesh was then cut and placed over the glass support tubes as shown by figure 6.16,

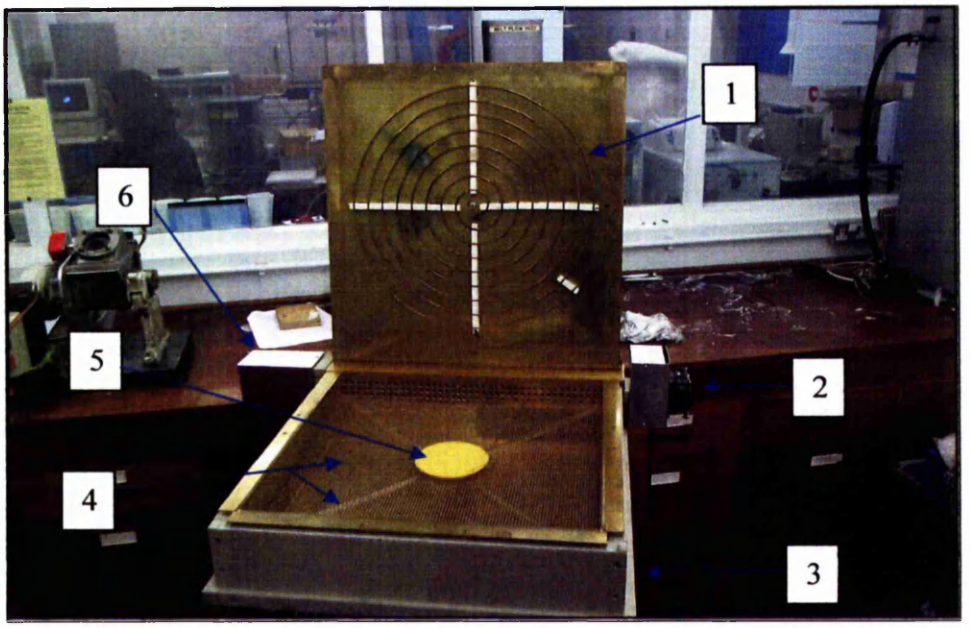

Figure 6.16: Completed oven

where 1 is the spiral antenna, 2 is the fan motor housing, 3 is the insulation board, 4 is the glass fibre reinforced PTFE mesh and glass tube sample support, 5 is the sample and 6 is the heater element live ends enclosure.

6.4.4: Lid Frame

To prevent microwave leakage from around the oven lid during microwave heating a lip was formed around the top of the oven cavity using 3mm thick 90° brass angle section. The lip extended out to the same distance as the lid overlap. A frame was then made from U section brass bar that could then be slotted over the lid / lip edge. Two functions were served by the frame cross piece. The first was as a handle to push the frame onto the oven. Secondly, the handle was designed to just clear the N-type coaxial connector on the oven lid. This prevented the lid from being opened whilst the power cable was still connected and hence prevented exposure to microwave radiation by accidental lid opening. The frame is shown by figure 6.17. Figure 6.18 shows section A-A of figure 6.7 and illustrates the fitment of the frame around the lid.

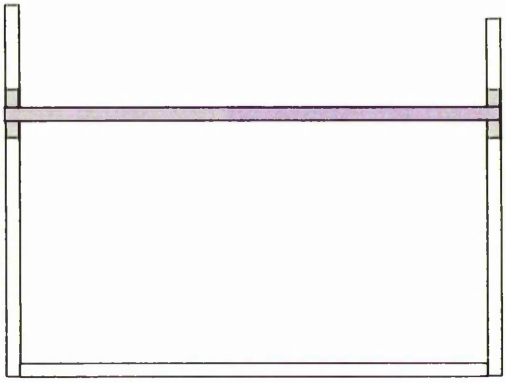

Figure 6.17: Oven lid frame

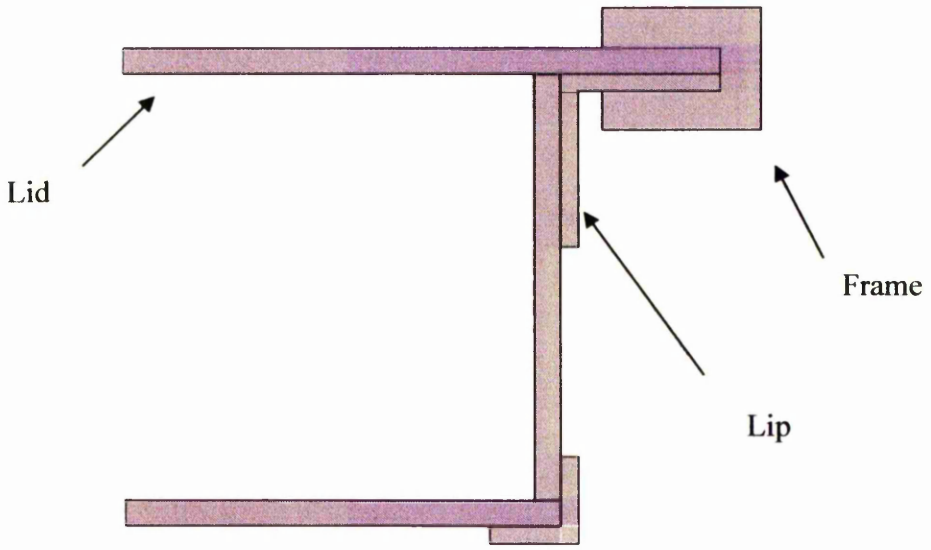

Figure 6.18: Section view of oven wall and lid frame (section A-A of figure 6.7)

6.5: Microwave Heating Frequency Simulations

Before heating and foaming using microwave energy could take place it was necessary to determine a number of suitable microwave heating frequencies. The pattern of microwave field distribution was affected by materials within the cavity. Hence, all objects, i.e. sample, sample support structure and PTFE mesh support, which would be present during microwave processing, were placed in the oven. The reflection response of the oven as a function of frequency was then measured using a network analyser. A number of frequencies that showed strong absorption (little reflected microwave power) were chosen and their field distributions were simulated using Agilent HFSS software. Simulations of heating frequencies in the range 2.3-2.45 GHz are presented in figure 6.19; frequencies in the range 6-8 GHz are shown in figure 6.20.

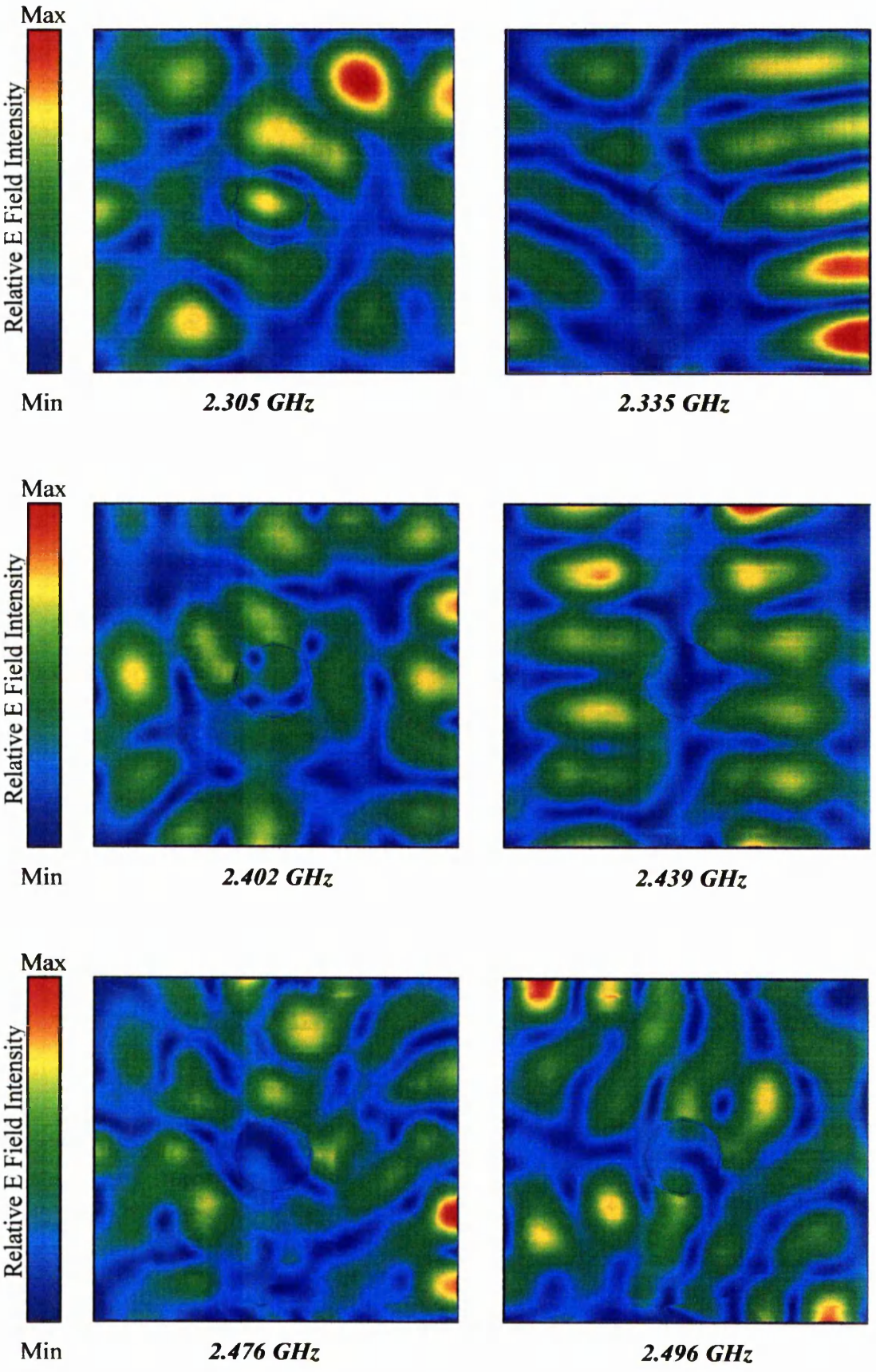

Figure 6.19: Electric field distribution at frequencies in the range of 2.3-2.45 GHz (spiral antenna), EVA 328 sample is shown as a faint circle

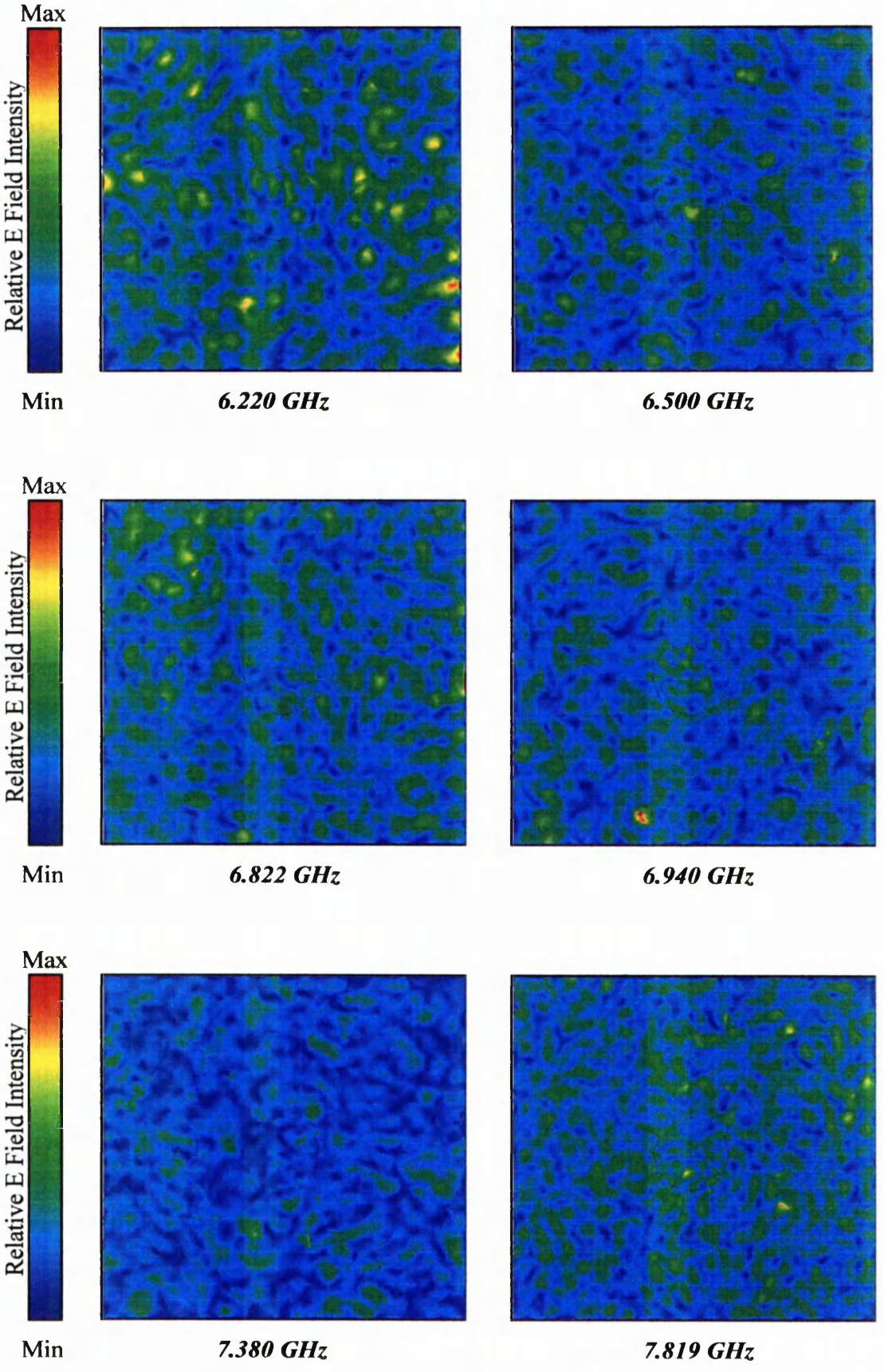

Figure 6.20: Electric field distribution at frequencies in the range of 6-8 GHz (spiral antenna), EVA 328 sample is shown as a faint circle

Figure 6.19 depicts the microwave field distribution in the cavity 30 mm up from the bottom of the cavity i.e. in a flat plane midway through the cavity and sample depth. The frequencies displayed were chosen as they had good absorption characteristics and low levels of power reflection (the frequencies in figure 6.19 were subsequently used for processing). Although the field distribution still consists of large localised areas of high electric field intensity, it can be seen that these are constantly redistributed throughout the cavity and sample as the frequency is changed. This would help alleviate the problems associated with localised hot spots being generated within the sample by moving areas of high field intensity through the sample.

Figure 6.20 shows the effect of varying frequency between 6 and 8 GHz. As the frequency is changed the areas of high field intensity are again rearranged throughout the cavity in a similar manner to the lower frequency range (figure 6.19). However the effect of increasing frequency is clear. A greater number of high intensity regions are observed compared with the lower frequency range. This would aid heating uniformity throughout the sample as a greater number of smaller high field intensity areas exist and would, therefore, more evenly heat the sample..

CHAPTER 7: FURTHER FOAMING STUDIES WITH EVA 218 AND EVA 328

Having completed construction of the new variable frequency combination oven, scaled up conventional foaming studies were performed to understand the action of the microwave oven and to refine the processing conditions. Microwave and combination microwave / hot air foaming studies were then carried out and the results were compared with the conventionally produced material. The remainder of this work will largely concentrate on the foaming of EVA 218 and 328 base polymers. It was found that EVA 206 was unsuitable for heating in the combination oven for reasons which will be discussed later. The results for EVA 206 obtained so far are, however, still important as they help to highlight some of the experimental trends associated with vinyl acetate content.

7.1: Base Polymer Crosslinking

Crosslinking studies were performed to determine the most appropriate times and temperatures required to effect crosslinking of the base polymer and to compare the effectiveness of conventional and microwave crosslinking. The primary motive for the study was to determine the feasibility of using microwave radiation to crosslink the base polymer before the onset of blowing agent decomposition and foam expansion. Given the difficulties encountered in chapter 5 where polymer flow and adhesion during crosslinking in the conventional oven was encountered, significant problems were expected when attempting similar trials in the combination microwave oven. Thus, microwave crosslinking trials were carried out on small crosslinkable samples (blowing agent included), using the microwave calorimeter as an applicator. Identical sized samples were subjected to the same heating profiles in a conventional oven for comparison. It is important that crosslinking is performed before the onset of blowing agent decomposition so that the base polymer melt strength is sufficiently enhanced and is, therefore, able to withstand and contain the pressure generated by the blowing agent gas. If sufficient crosslinking is not achieved before blowing agent decomposition and foam expansion, the pressure generated by the blowing agent gas will lead to cell wall rupture and foam collapse. Conventional and microwave heating

trials using small samples of crosslinkable base polymer (base polymer blended with 0.5 phr DCP) were carried out to determine any differences in level and speed of crosslinking achieved that may be associated with the different heating mechanisms.

From a processing perspective it is desirable to complete crosslinking as quickly as possible in order to maximise production rate. This would suggest that the highest temperature possible should be used. However it is important that the temperature used is not so high that premature blowing agent decomposition may take place before crosslinking completion. Thus the temperature used for crosslinking was 165 °C. The temperature was also sufficiently below the decomposition temperature range of ADCE (180-220 °C) that the risk of blowing agent decomposition was minimised.

Three EVA grades were used in the study, EVA 206, 218 and 328 with 6, 18 and 28 % by weight vinyl acetate content, respectively. The base polymers were blended with 0.5 phr dicumyl peroxide crosslinking agent, 8 phr ADCE blowing agent and compression moulded into flat 5 mm thick sheets. The moulding temperatures were kept low enough (115 °C) to prevent any crosslinking to take place but high enough to allow melting and shaping of the polymer.

To enable a direct comparison between polymer samples using conventional and microwave heating to be made, the sample sizes and heating rates used in the two techniques were the same. This was done to ensure that any crosslinking that took place during the heating period before reaching the isotherm temperature of 165 °C was the same for both methods. It was important that the heating rate be as fast as possible to minimise crosslinking during the heating ramp. The maximum heating rate that the conventional oven could maintain was measured and calculated to be 12 K min^{-1}. The microwave calorimeter was equipped with a programmable PID controller which was used to maintain the same heating rate. The microwave calorimeter could only practically heat small samples (5 × 5 × 12 mm); therefore this sample size was used for both heating methods.

The crosslinkable polymer samples were placed in the oven on a sheet of glass fibre reinforced PTFE. They were then heated to the isotherm temperature of 165 °C. Samples were removed at the desired time intervals and immediately quenched in cold water to halt the crosslinking reaction. The gel content of each sample was then

measured using the technique described in section 2.4.2 and reported as the mean of five readings.

To study the effect of microwave heating on crosslinking, crosslinkable samples, with same dimensions as the conventional samples, were cut longitudinally and placed in a small Pyrex glass tube with a small glass capillary tube between them to house the temperature probe. As with conventional heating, the samples were heated to 165 °C using the same heating rate and removed at specific time intervals. They were also immediately quenched in cold water. The gel contents were then measured and reported as a mean of five readings. The results for conventional and microwave crosslinked samples of EVA 206, 218 and 328 are presented and compared in figures 7.1, 7.2 and 7.3 respectively.

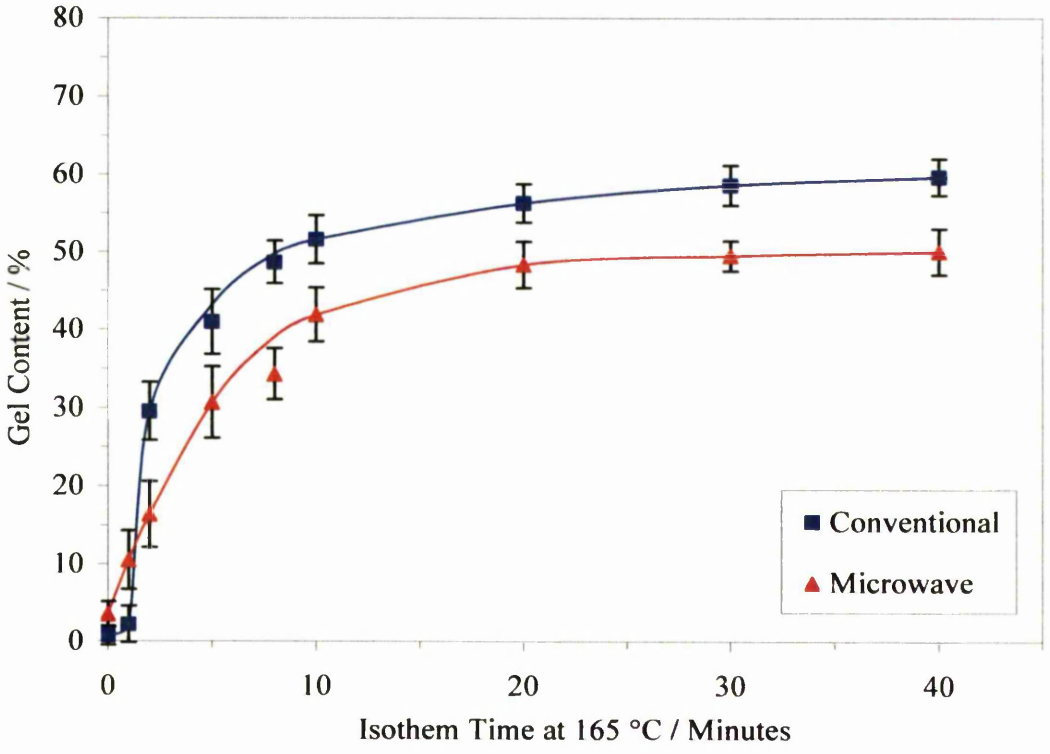

Figure 7.1: Gel content values for EVA 206 blended with 0.5 phr DCP, 8 phr ADCE and crosslinked isothermally at 165 °C for different time periods

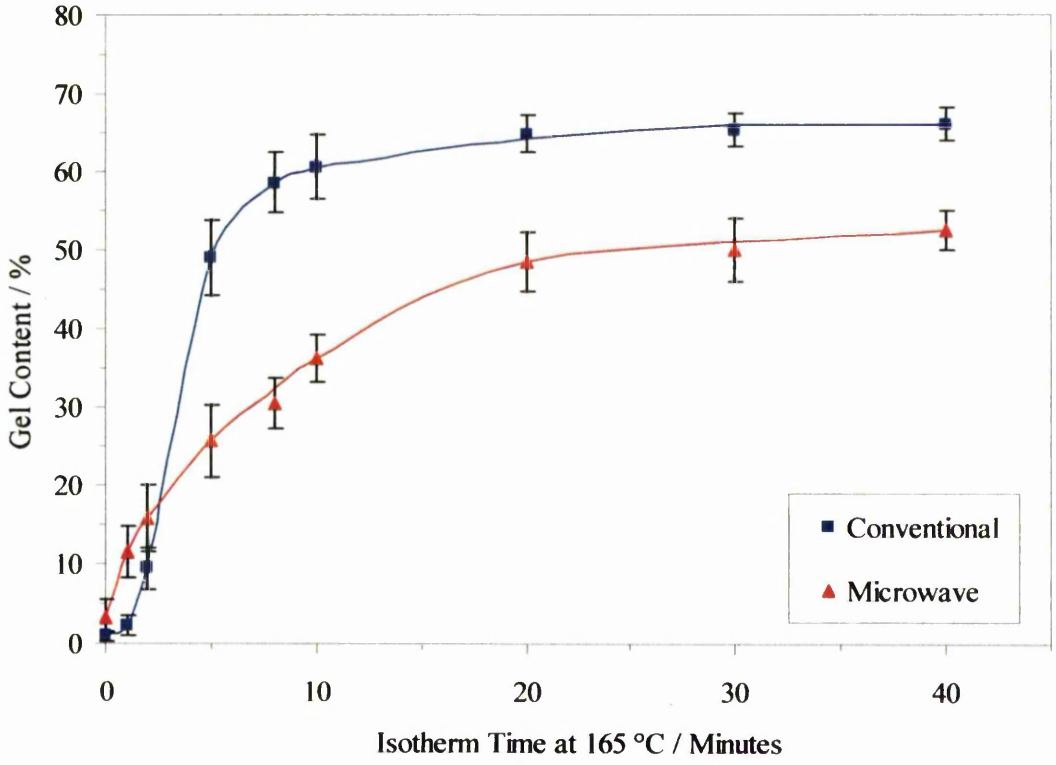

Figure 7.2: Gel content values for EVA 218 blended with 0.5 phr DCP, 8 phr ADCE and crosslinked isothermally at 165 °C for different time periods

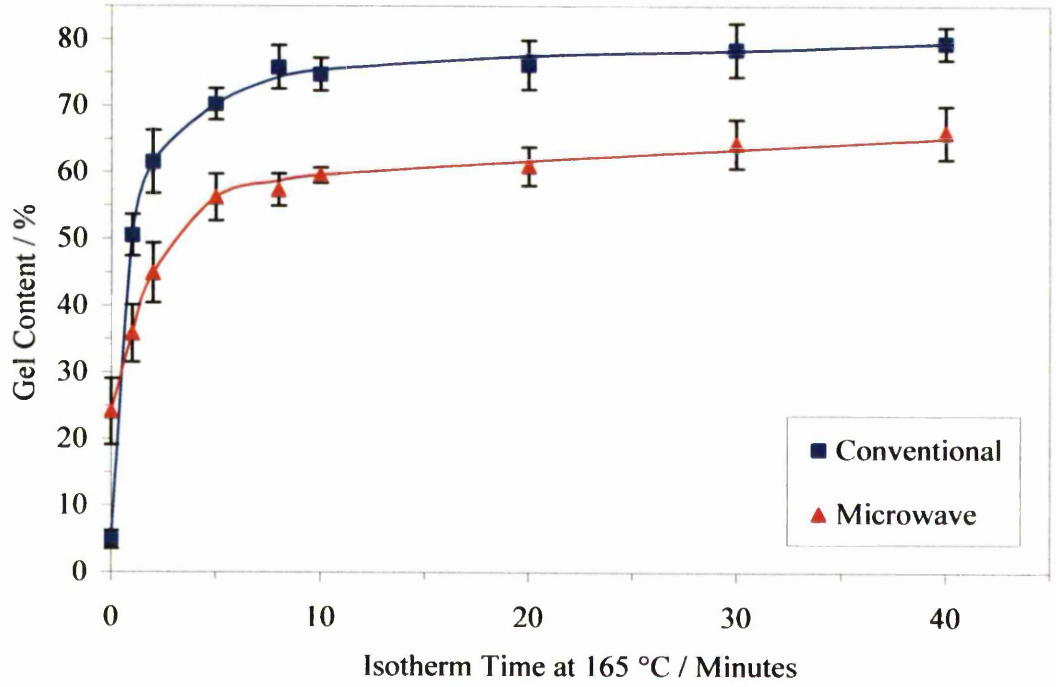

Figure 7.3: Gel content values for EVA 328 blended with 0.5 phr DCP, 8 phr ADCE and crosslinked isothermally at 165 °C for different time periods

The results for all three base polymers demonstrate a trend of increasing gel fraction with increasing isotherm time. This trend is followed by both the microwave and conventional heating methods. The longer the sample is held at the isotherm temperature, the greater the DCP dissociation. This increased the number of peroxy radicals available to react with tertiary hydrogens to form polymer chain radicals. Adjacent polymer chain radicals could then react together to form crosslinks.

A secondary trend common to both the microwave and conventional processing methods was (within experimental error) one of increasing gel content with increasing vinyl acetate content. The most energetically favourable route to polymer chain formation is by the extraction of a low bond energy tertiary polymer chain hydrogen atom by the peroxy radical (Kircher, 1987). In EVA copolymers, tertiary hydrogen atoms are located on polymer main chain carbon atoms to which the pendant vinyl acetate groups are also attached. Thus, as the vinyl acetate content was increased, EVA 206 < 218 < 328, the number of tertiary hydrogen atoms was increased by the same amount. This increased the crosslinking efficiency and resulted in higher crosslinking levels at higher vinyl acetate contents.

It was expected that overall, a greater gel content for microwave samples would be observed. The volumetric nature of microwave heating allows the bulk of a sample to be heated at once. Unlike conventional hot air heating, the process is not reliant upon the poor thermal conductivity of the polymer to transmit heat from the surface of the sample to the interior, which often leads to an initial temperature gradient through the sample thickness (particularly problematic in thick sectioned samples). The data presented in figures 7.1, 7.2 and 7.3 shows that in the early stages of heating this would appear to be true as the gel contents for the microwave heated samples were significantly higher than the conventional samples. This would indicate that the volumetric heating was taking place within the microwave samples leading to faster initial crosslinking. The conventional samples, on the other hand, showed lower crosslinking levels which were attributed to the presence of a thermal gradient. This resulted in crosslinking taking place at the sample surface first whilst the bulk of the sample was still sufficiently below the isotherm / decomposition temperature to prevent significant network formation. It is clear, however, that microwave crosslinking was faster than conventional crosslinking at short time periods although the conventional values soon matched and then exceeded the microwave values.

It is postulated that the apparent lower level of microwave crosslinking was due to the following reasons. Firstly, the method assumes that the temperature within the microwave heated sample was uniform. In practice, the temperature was measured in only a small area in the centre of the sample. There may have been cooler regions within the samples which did not crosslink as fast or to the sample extent as the area where the temperature was measured, thus lowering the overall gel content. Secondly, lower gel content may be a manifestation of lower sample surface temperatures. It has already been shown in chapter 5 that surface heat losses significantly affect the foaming uniformity of EVA 206 when heated using microwaves. It is likely, therefore, that heat losses from the surface of the crosslinkable samples result in lower sample skin temperatures and lower the sample gel fraction.

Previous work (Clarke, 2000) found that gel fractions greater than 50 % are necessary for successful foam formation when using blowing agent levels in the region of 8 phr. The crosslinking results cast some doubt upon the feasibility of crosslinking using microwave radiation in this study. The microwave crosslinked EVA 206 and 218 samples demonstrate gel fractions lower than this level even at extended time periods which suggests that foam collapse would be a strong possibility due to low polymer melt strength. EVA 328 demonstrated higher crosslinking levels which may be attributed to a greater microwave heating efficiency due to its increased polarity and an increased proportion of energetically favourable tertiary hydrogen crosslinking sites.

7.2: Dicumyl Peroxide Kinetic Study

A small scale reaction study was performed on the dissociation of DCP to determine the effect of heating method, i.e. conventional and microwave, on the decomposition kinetics and overall conversion. A conventional power compensated DSC using an air purge was used for the conventional studies and the microwave calorimeter, as described in section 2.4.4, was used to obtain the microwave heating data. The activation energies associated with the two heating techniques were also calculated according to the Kissinger technique (Kissinger, 1957) and compared to literature values. It was hoped that the study would help explain some of the differences between the conventional and microwave gel contents presented in section 7.1.

Differential scanning calorimetry is commonly used to measure the reaction kinetics of thermosetting polymers (Sun *et al.,* 2002; Nam and Seferis, 1993) but has also been applied to the dissociation of DCP (Brazier and Schwartz, 1980). Reaction kinetics may be determined using isothermal and non – isothermal conditions. Isothermal conditions are, however, unsuitable for, and are beyond the limits of the microwave calorimeter, therefore a non – isothermal (dynamic) method was used.

An assumption made when using DSC to determine reaction kinetics is that the reaction rate, $d\alpha/dt$, and the rate of heat evolution, dH/dt, are proportional as shown by equation 7.1,

$$\frac{d\alpha}{dt} = \frac{1}{\Delta H_T}\frac{dH}{dt}$$

(Eqn. 7.1)

where ΔH_T is the total heat generated to reach full conversion (Hedreul *et al.,* 1998). The fractional conversion, α, at any given temperature, T, during the dynamic process may be determined by equation 7.2 (Karkanas and Partridge, 2000),

$$\alpha = \frac{\int_{T_0}^{T_1} \frac{dH}{dT} dT}{\Delta H_T}$$

(Eqn. 7.2)

where the lower bound of the integration, T_0, is the lowest temperature at which heat evolution begins. The total heat of reaction, ΔH_T, may be derived by integration of the area under the DSC thermogram. It is assumed that this represents the total heat of reaction and that the reaction proceeds to completion by the end of the run and that 100 % conversion is achieved at all heating rates (Karkanas and Partridge, 2000).

When integrating the area under a DSC thermogram, particular attention should be paid to the baseline used. A baseline is necessary to account for the changes in specific heat capacity that take place in a material as it is heated and thermal transitions such as melting, curing and dissociation take place. Baseline correction was particularly important for the microwave calorimeter traces as, although they were reasonably linear, they were not perfectly flat. An expression exists that corrects the baseline by using the thermal response of a material preceding and succeeding any

thermal event to incorporate changes in the specific heat of the system during reaction. This is shown by equation 7.3 (Bandara, 1986),

$$F(t) = \alpha\{P_2(t) - P_1(t)\} + P_1(t)$$

(Eqn. 7.3)

where $F(t)$ is the sample background, t is the time coordinate which is proportional to temperature for constant heating rates, α is the partial concentration of the product and is defined as being equal to the current degree of conversion, $P_2(t)$ is the DSC signal for the product only and may be estimated by linear extrapolation of the portion of the total curve after a thermal event, $P_1(t)$ is the DSC signal for the initial substance in the absence of the event and may be estimated through linear extrapolation of the portion of the curve prior to the thermal event. The current fractional conversion, α is defined by equation 7.4 (Bandara, 1986),

$$\alpha = \frac{\int_0^t \{G(t) - F(t)\}dt}{\int_0^{t_n} \{G(t) - F(t)\}dt}$$

(Eqn. 7.4)

where $G(t)$ is the total signal corrected for the instrumental background and t_n is the termination time of the thermal event. By substituting equation 7.4 into 7.3 equation 7.5 is obtained,

$$F(t) = \frac{\int_0^t \{G(t) - F(t)\}dt}{\int_0^{t_n} \{G(t) - F(t)\}dt}\{P_2(t) - P_1(t)\} + P_1(t)$$

(Eqn. 7.5)

7.2.1: Conventional Dicumyl Peroxide Dissociation

DCP samples (10 ± 0.5mg) were heated in a conventional power compensated DSC. Air was used as the purge gas as the microwave calorimeter was not equipped with gas purge facilities and the samples were open to the atmosphere. Four heating rates, 5, 10, 12 and 15 K min^{-1}, were used. Three runs were carried out at each heating rate and the variability between peak temperatures was found to be ± 1 °C. Typical examples of the conventional heating curves are shown in figure 7.4.

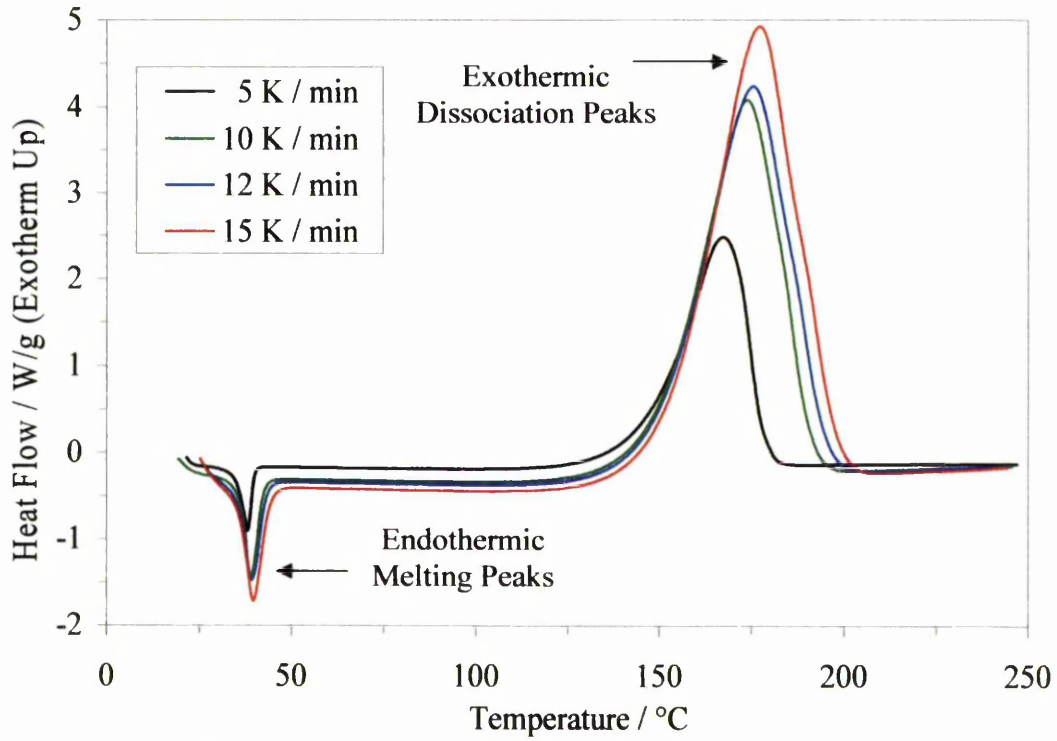

Figure 7.4: Conventional DSC data for DCP at four heating rates

Figure 7.4 shows two distinct thermal events on each heating rate curve. The first lower temperature endothermic peak was attributed to the DCP melting transition and, for the purposes of the study, was ignored. The second higher temperature peak was attributed to the exothermic dissociation of the DCP peroxide bond. It is obvious that as the heating rate was increased, the peaks shifted to higher temperatures. This effect was a result of smaller thermal lags at slower heating rates. Furthermore, as the heating rate was increased, the reactions terminated at higher temperatures. The heat of reaction was calculated at each heating rate by integration of the area under each exothermic peak. The peak temperatures for each heating rate, their respective calculated heats of reaction and the fractional conversion at each peak temperature (from figure 7.6) are presented in table 7.1.

Table 7.1: Conventional DSC data for the dissociation of DCP at four heating rates

Heating Rate (K min^{-1})	**Peak Temperature (°C)**	**ΔH_T (J/g)**	**Fractional Conversion (α) at Peak Temperature**
5	167	689	0.59
10	174	675	0.55
12	176	624	0.55
15	177	581	0.51

Using equations 7.1 and 7.2, the data obtained from the different DSC heating rates was used to derive the reaction rate, $d\alpha/dt$, and the fractional conversion, α as a function of temperature. The results are shown in figures 7.5 and 7.6, respectively.

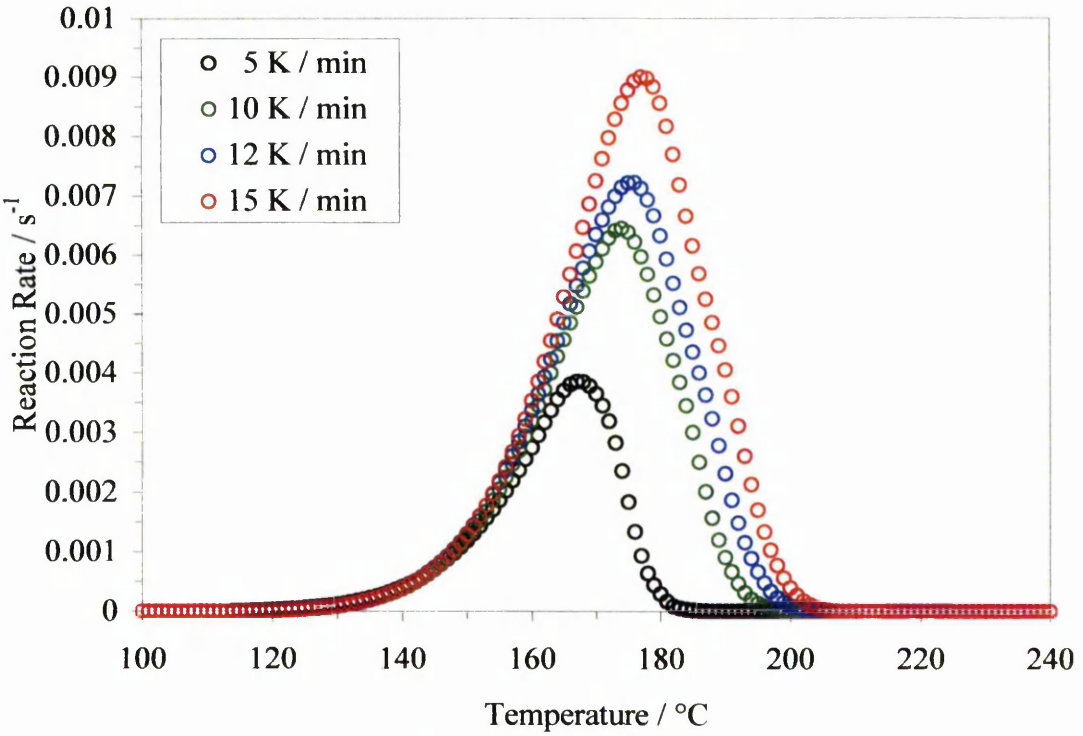

Figure 7.5: Conventional DSC reaction rates for DCP at four heating rates

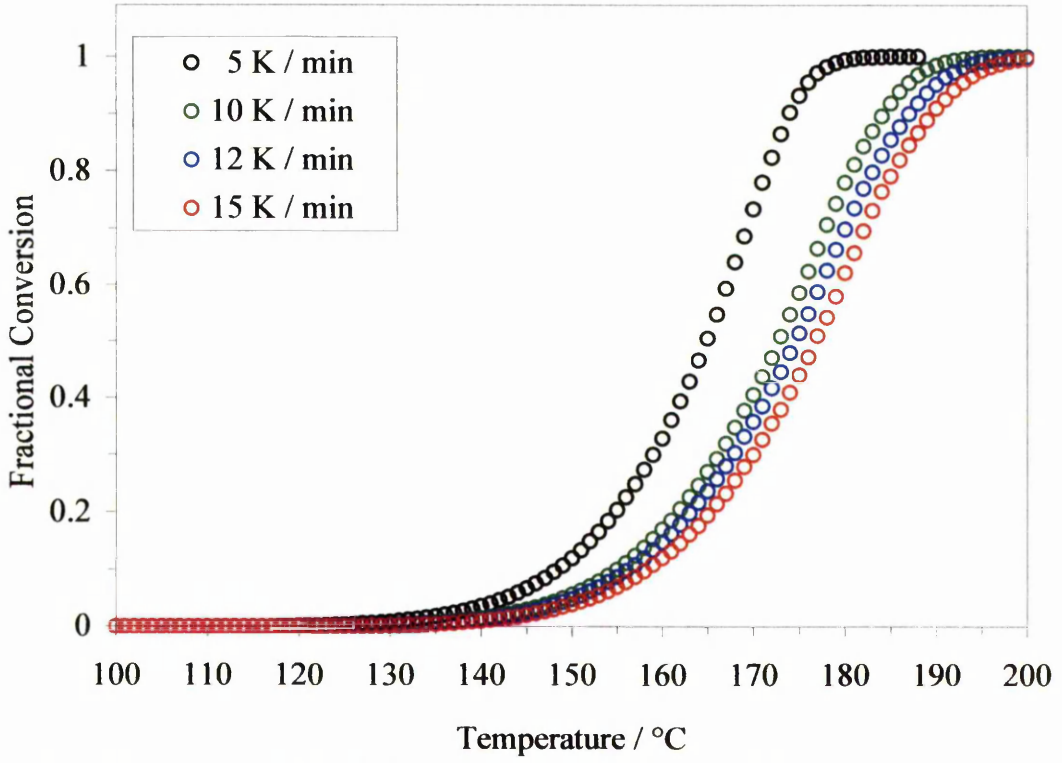

Figure 7.6: Conventional DSC conversion data for DCP at four heating rates

The data presented in table 7.1 suggest that the heat of reaction decreased as the heating rate was increased. Vented pans and an air purge were used in the conventional DSC to ensure, as far as possible, that the data were comparable with those obtained from the microwave calorimeter where the samples were open to the atmosphere during heating. It was thought that as the heating rate was increased, small amounts of DCP (boiling point 130 °C) were being lost from the vented pans through volatilisation before dissociation took place, thereby reducing the apparent heat of reaction. On observation of figure 7.5, a trend of increasing peak reaction rate with increasing heating rate is apparent. The reaction rate peaks shifted to higher temperatures as the heating rate was increased.

Figure 7.6 shows the fractional conversion as a function of temperature. The fractional conversions at the peak exotherm temperatures are summarised in Table 7.1. It may be seen that the fractional conversion at each peak temperature was reasonably constant regardless of the heating rate although the exotherm peak position increased with increasing heating rate. Different fractional conversions at the heating rate exotherm peaks indicated that the reaction pathway was dependant upon the heating rate. As the fractional conversion at each exotherm peak was the same it is suggested that the reaction pathway was the same for each heating rate. This would be expected as the reaction involves the homolytic cleavage of the peroxide bond only and does not involve any other chemical species. It may be assumed, therefore, that other reaction pathways would have been unlikely. Figure 7.6 also shows that the fractional conversion was higher at any given temperature as the heating rate was decreased.

The reaction rate was also plotted as a function of fractional conversion. The resulting trends are shown in figure 7.7.

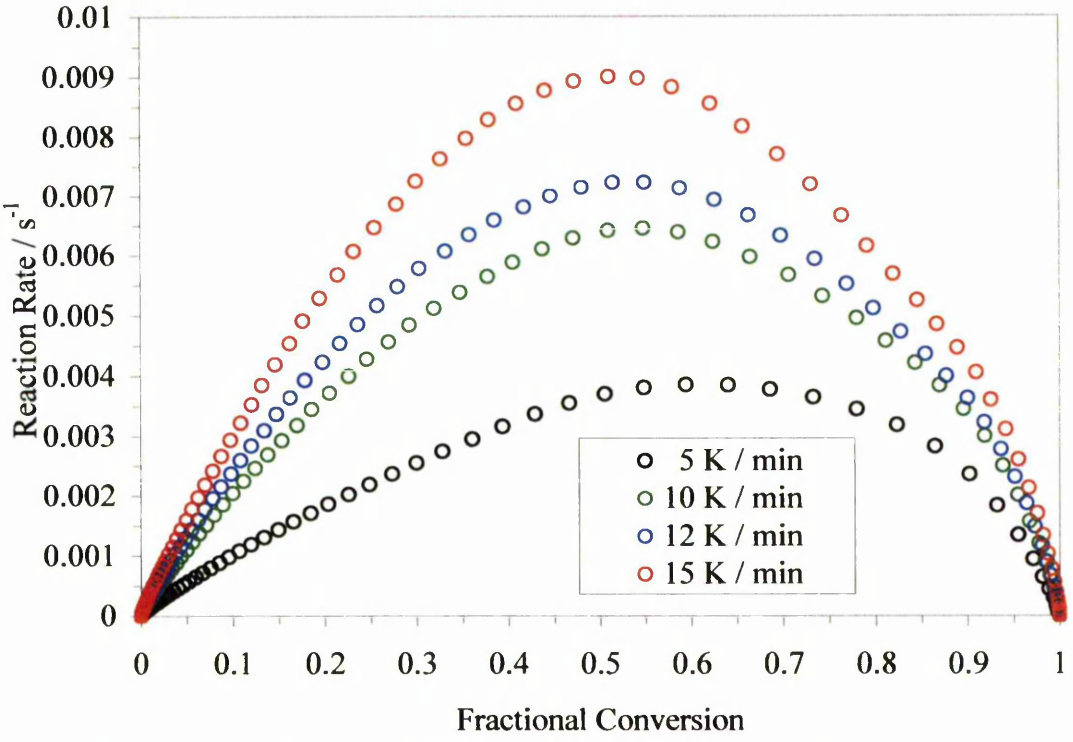

Figure 7.7: Reaction rate versus fractional conversion for conventionally heated DCP at four heating rates

The data in figure 7.7 show that the maximum reaction rate for DCP dissociation using conventional heating occurred when the fractional conversion was in the region of 0.5. The maximum rate was achieved at similar conversions for each heating rate although the maximum rate for 5 K min^{-1} appeared to take place at a slightly higher fractional conversion of 0.55.

7.2.2: Dicumyl Peroxide Dissociation Using Microwave Heating

Microwave heating was performed using the microwave calorimeter equipment, as described in section 2.4.4, to provide data analogous to that obtained using conventional DSC methods. The microwave calorimeter maintained a given heating rate by variation of the heating power. Thus, exothermic thermal events were recorded and shown as a decrease in input power (less power required to maintain heating rate) whereas endothermic events were shown as an increase in input power (more power required to maintain heating rate). It was necessary to use much larger samples in the microwave calorimeter (0.35 ± 0.05g) to ensure that the temperature probe sensor was adequately covered by the sample. The conventional DSC data in figure 7.4 shows two distinct thermal events that occur in DCP over the studied

temperature range, therefore, a similar result was expected from the microwave heated samples. Figure 7.8 shows the microwave data.

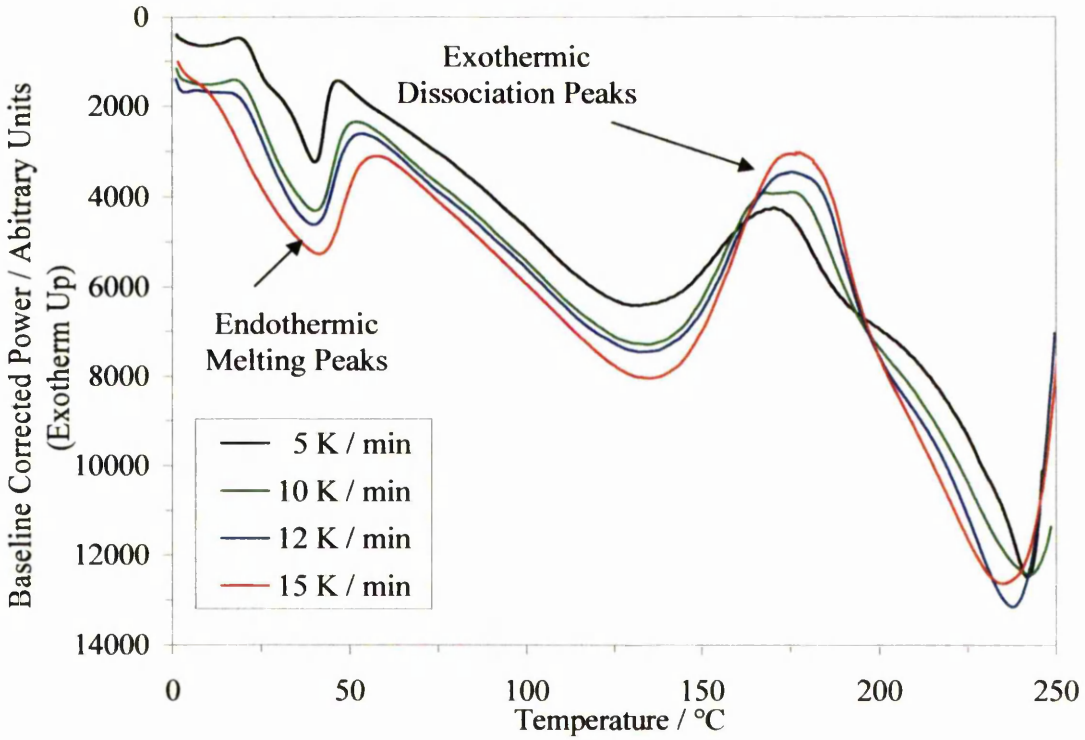

Figure 7.8: Microwave calorimeter traces for DCP at four heating rates

Data was recorded at the same heating rates as the conventional DSC. The results shown in figure 7.8 indicate that the thermal events that occur during microwave heating of DCP are similar to the conventional results. Two peaks are clearly evident and were assigned to the same events as the conventional data. The peak temperatures were determined for each heating rate and are shown in table 7.2.

Table 7.2: Microwave calorimeter data for the dissociation of DCP at four heating rates

Heating Rate (K min^{-1})	**Peak Temperature (°C)**	**Fractional Conversion (α) at Peak Temperature**
5	170	0.76
10	174	0.75
12	177	0.73
15	179	0.76

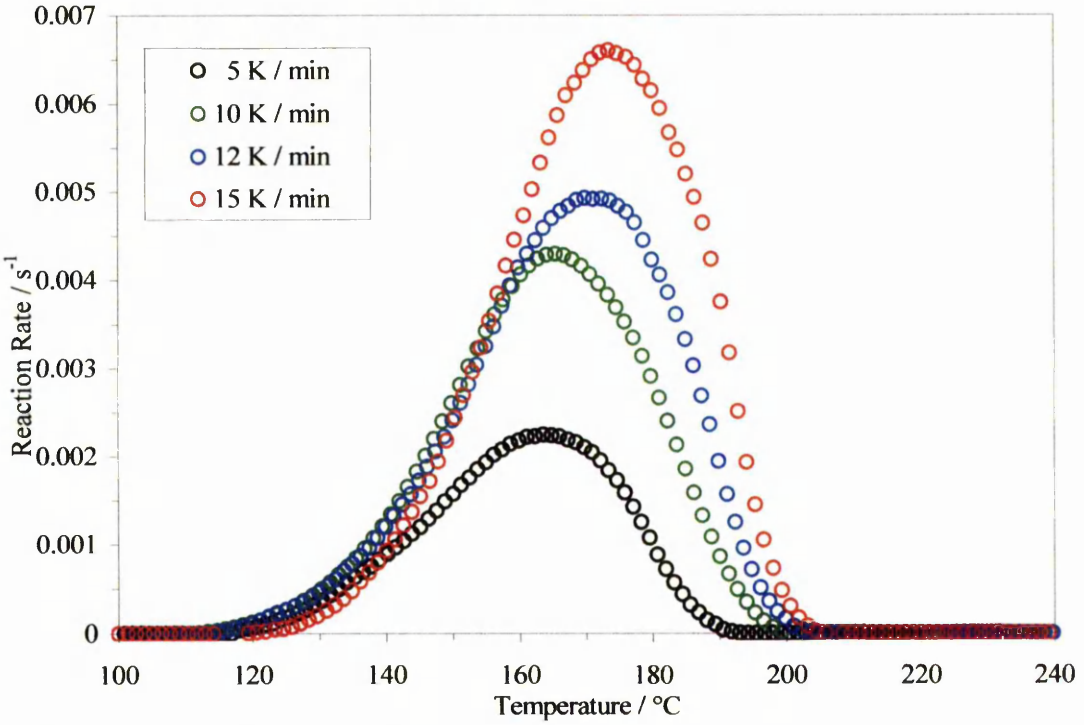

Figure 7.9: Microwave calorimeter reaction rates for DCP at four heating rates

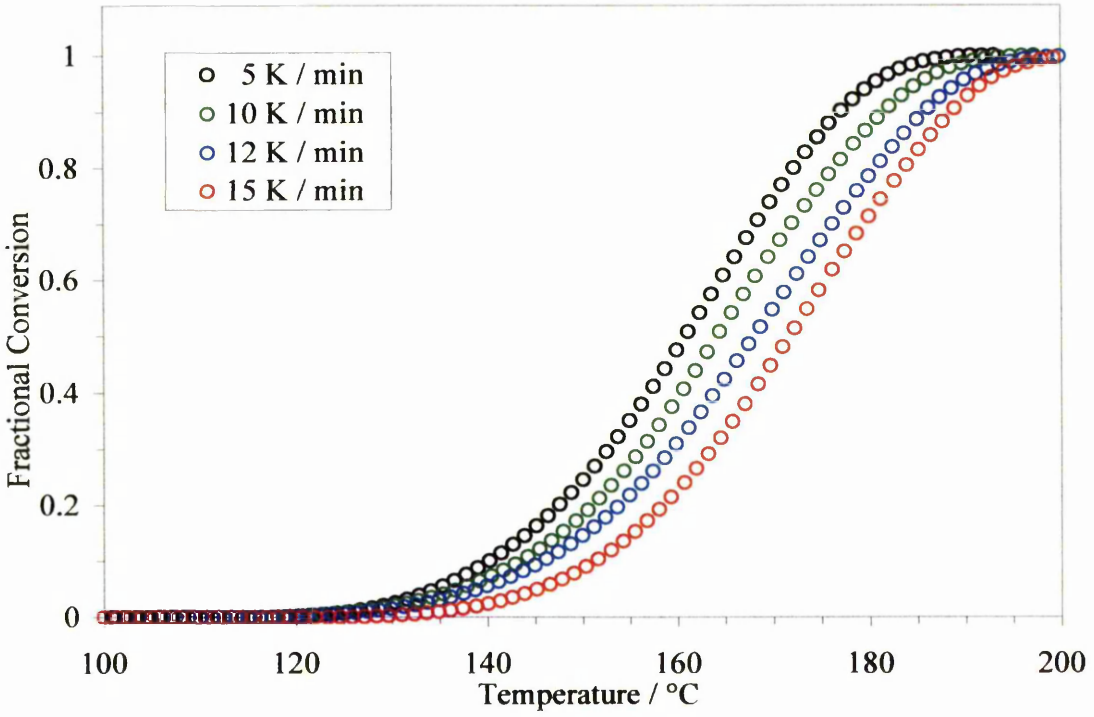

Figure 7.10: Microwave calorimeter conversion data for DCP at four heating rates

Unfortunately, it was not possible to determine the total heats of reaction from the microwave data. At present there is no way of calibrating the calorimeter and converting the power signal to heat flow values (Nesbitt *et al.*, 2004).

The results in table 7.2 show that the for the microwave heated DCP samples, the peak exotherm temperature reaction rates were reasonably constant. The results indicated that the peak temperature fractional conversions, for the microwave heated samples, were higher than the conventional DSC values, although the peak temperatures themselves were slightly higher than the conventional results.

Figure 7.9 shows the microwave heated reaction rate as a function of temperature. The results indicate that the maximum reaction rate at each heating rate occurred at a similar temperature to the conventional data shown in figure 7.5. It may be noticed, however, that the reaction rates for the microwave heated samples appear to be slower than the conventional rates. However, the reaction rate curves appear to begin approximately 10 °C earlier, they are also marginally broader which may help explain similar conversion but slower rate. As with the conventional data shown in figure 7.6, the microwave data presented in figure 7.10 shows that at a specific temperature, the conversion was higher as heating rate was decreased.

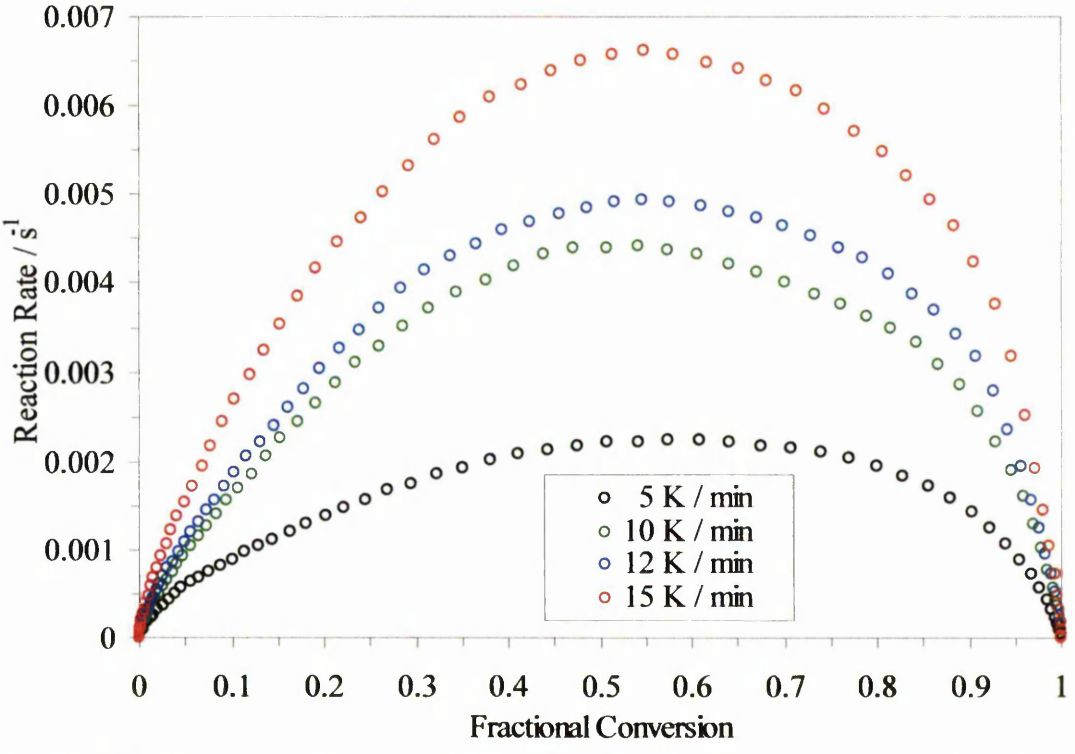

Figure 7.11: Reaction rate versus fractional conversion for microwave heated DCP at four heating rates

Figure 7.11 shows that for the microwave heated samples, the maximum reaction rates occurred when the fractional conversion was ~0.55. This is similar to the conventional data.

In general, the kinetic study results suggest that the dissociation of DCP proceeds in a similar manner regardless of the heating method although there do appear to be some differences. The results for both techniques indicated that the maximum reaction rate took place at approximately 0.5-0.55 fractional conversion. The conversion at the exotherm peak temperatures appeared to be constant for each method regardless of heating rate although the peak positions and fractional conversion differed between the two techniques. The main difference observed between the two methods was that the maximum reaction rates for the microwave heated samples at each heating rate were lower than the conventionally heated samples. The maximum rate peaks were at the same temperatures for both microwave and conventional samples, however it was apparent that the reaction rate curves for the microwave samples began approximately 10 °C lower than the conventional samples. It was surmised therefore, that the differences in gel contents observed in section 7.1 were as a result of thermal gradients with the sample during crosslinking rather than differences resulting from the direct dissociation of DCP by the different heating techniques. It may be argued that differences may have been observed if the kinetics studies had been performed on polymer samples blended with DCP rather than DCP alone. Although this was possible using the highly sensitive conventional DSC, the energy changes involved were so small when small quantities of DCP were dispersed in a relatively large volume of polymer that they were well beyond the sensitivity of the microwave calorimeter.

7.2.3: Activation Energy

The activation energies associated with the conventional and microwave heating methods were calculated according to the Kissinger method (Kissinger, 1957). This method, which is based on the assumption that the exothermic peak coincides with the maximum reaction rate (Salla and Ramis, 1996), uses an *n*th order equation for the reaction rate and is shown by equation 7.6,

$$r = \frac{d\alpha}{dt} = q\frac{d\alpha}{dT} = A\exp\left(\frac{-E}{RT}\right)(1-\alpha)^n \qquad \textit{(Eqn. 7.6)}$$

where r is the reaction rate and q is the heating rate. The maximum rate occurs when $dr/dt = 0$, therefore if equation 7.6 is differentiated with respect to time and the result

equated with zero equation 7.7 is generated (Navabpour *et al.*, 2005) which may then be rearranged and written in natural logarithm form giving equation 7.8,

$$q\frac{E}{RT_p^{\,2}} = An(1-\alpha_p)^{n-1}\exp\left(\frac{-E}{RT_p}\right) \qquad \textit{(Eqn. 7.7)}$$

$$-\ln\left(\frac{q}{T_p^{\,2}}\right) = \ln\left(\frac{E}{RAn}\right) - (n-1)\ln(1-\alpha_p) + \frac{E}{RT_p} \qquad \textit{(Eqn. 7.8)}$$

where T_p is the exotherm peak temperature. A straight line plot with a slope equalling E/R may then be constructed by plotting $-ln(q/T_p^2)$ versus $1/T_p$. The activation energies calculated for the conventional and microwave processes are shown in table 7.3

Table 7.3: Activation energies of DCP heated conventionally and using microwaves

Heating Method	Activation Energy E_a (kJ mol^{-1})
Conventional	168 ± 2
Microwave	189 ± 6

The activation energy results presented in table 7.3 compared reasonably well with a literature value of 152.7 kJ mol^{-1} (Akzo Nobel, 2001) although they appeared to be slightly higher. The results tend to suggest that the microwave heated samples had higher activation energies than those heated conventionally. This may be a result of the vastly different sample sizes required by the two methods.

7.3: Conventional Oven Foaming of Ethylene Vinyl Acetate

Foamed material produced in previous sections was based on EVA 206 base polymer. It was decided that all subsequent foaming should concentrate on an additional two EVA copolymer grades so that the effect of vinyl acetate content on the foaming processes could be investigated. Before any microwave foaming was attempted in the newly constructed variable frequency combination oven, additional conventionally foamed material was produced for comparison with microwave foamed samples. Foams were produced by compounding the base polymers with crosslinking and

blowing agents then crosslinking in a heated hydraulic press at 165 °C as described in sections 2.2.1 and 2.2.2.2. The crosslinked foamable samples were then transferred to a conventional hot air convection oven where they were heated at temperatures in the blowing agent decomposition range under atmospheric pressure to allow expansion to take place. Various expansion temperatures were used to investigate the process parameters required to produce fully expanded foams where the optimum foam density was reached. Optimum foam density (maximum density reduction) is attained when full decomposition of the blowing agent has been achieved and retention of the blowing agent gas by the expanded matrix is maximised. These processing conditions could then be applied to subsequent microwave foaming studies and direct comparisons between the foams produced using the different heating methods could be made.

The results from chapter 3 show that when ADCE was decomposed at temperatures at the lower end of its decomposition range, decomposition was slow and incomplete. A range of temperatures over the decomposition range of ADCE were investigated to determine if microwave foaming was more efficient at lower temperatures than conventional heating.

7.3.1: Conventional Foam Characterisation

Conventional thermal foaming relies on conduction of heat from the heated air to the sample. As a result, the sample surface heats first before heat may be transferred to the internal bulk of the sample. This may result in foaming occurring at the sample surface before taking place in the rest of the sample. The higher the expansion temperature the greater the thermal gradients become and the problem is exacerbated.

Although it is possible to determine the extent of foaming visually with reasonable accuracy, foam density as a function of time was monitored to remove any doubt. Successful foaming is mainly dependant upon the complete decomposition of the blowing agent and the generation of the gas necessary for expansion. The decomposition of ADCE is a time–temperature dependant process. Thus foaming was carried out in the oven over a range of temperatures that were appropriate to the decomposition temperature range of ADCE (180–220 °C). The pre-crosslinked foamable samples were heated at a rate of 12 K min^{-1} to the selected foaming

temperature. Foaming was performed using a range of time periods at each selected temperature. The extent to which foaming had occurred was then measured by visual inspection and density calculations. Figures 7.12 and 7.13 show examples of conventionally produced foam and demonstrate some of the thermal conduction effects associated with conventional foaming.

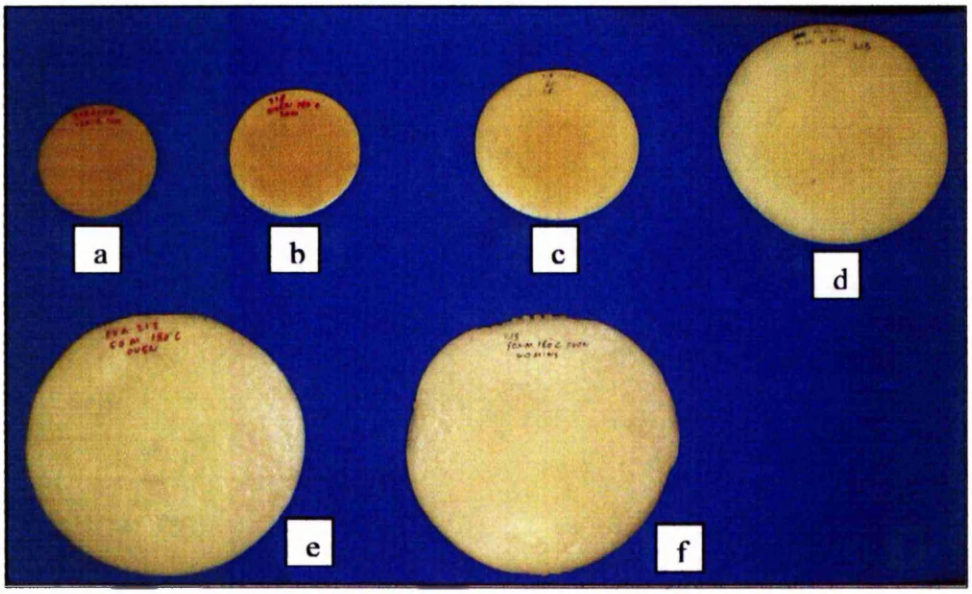

Figure 7.12: EVA 218 conventionally foamed at 180 °C for 10 (a), 20 (b), 25 (c), 30 (d), 40 (e) and 50 (f) minutes

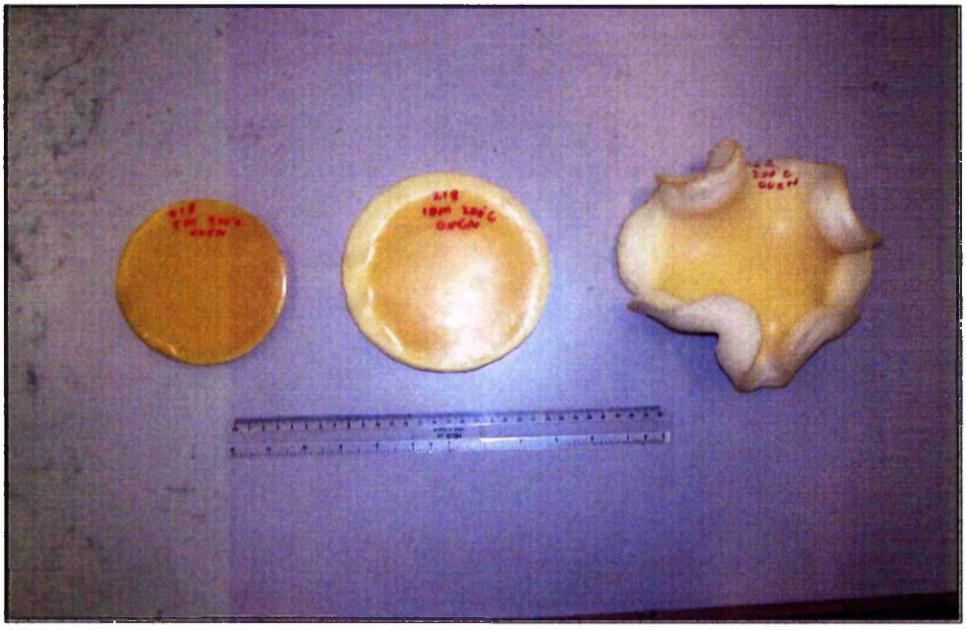

Figure 7.13: EVA 218 conventionally foamed at 200 °C for 5, 10 and 15 minutes (left to right)

Figure 7.12 shows EVA 218 foams expanded at various times at 180 °C. This is at the lower end of the decomposition range of ADCE, therefore foaming was very slow. After 10 minutes isotherm at 180 °C the sample (top left) showed no obvious signs of foaming. If the TGA data in figure 3.5 is referred to it may be seen that negligible blowing agent decomposition would have taken place. As expansion took a long time, the effects of thermal gradients within the foam would have been small as the heat had sufficient time to uniformly conduct through and heat the whole sample before significant foaming took place. The samples in figure 7.12 therefore, appear to foam uniformly and do not show any distinct demarcations between foamed and unfoamed areas at any of the heating times. Surface yellowing was attributed to mild polymer degradation due to the extended heating periods necessary to complete foaming at this temperature rather than residual blowing agent. The data in figures 3.9 and 3.10 indicate that a small amount of EVA degradation occurs at the lower expansion temperatures.

Figure 7.13 demonstrates the effects of heat conduction during the early stages of foaming EVA 218 at a higher temperature (200 °C). After 5 minutes at the isotherm temperature, little obvious foaming occurred, however after 10 minutes the onset of foaming was more obvious. It may be seen that the edges of the sample began to foam before the interior of the foam reached temperatures high enough to induce blowing agent decomposition. As the circular sample edge foamed it expanded and warped the sample as shown by the specimen on the far right. The samples regained their flat circular shape on completion of foaming. As the surface of the sample foamed first this would have the effect of insulating the interior of the sample. The foam cells were filled with the blowing agent gas which is an extremely poor conductor of heat. This would slow the conduction of heat from the surrounding air further and slow the overall foaming process.

7.3.2: Conventional Foam Density Measurements

The densities of the foam specimens were measured at various time intervals during the foaming process to physically evaluate the extent of foaming as a function of time at each expansion temperature. Foams were removed from the oven at various times and their average densities were measured. The results for EVA 218 and EVA 328 are presented in figures 7.14 and 7.15.

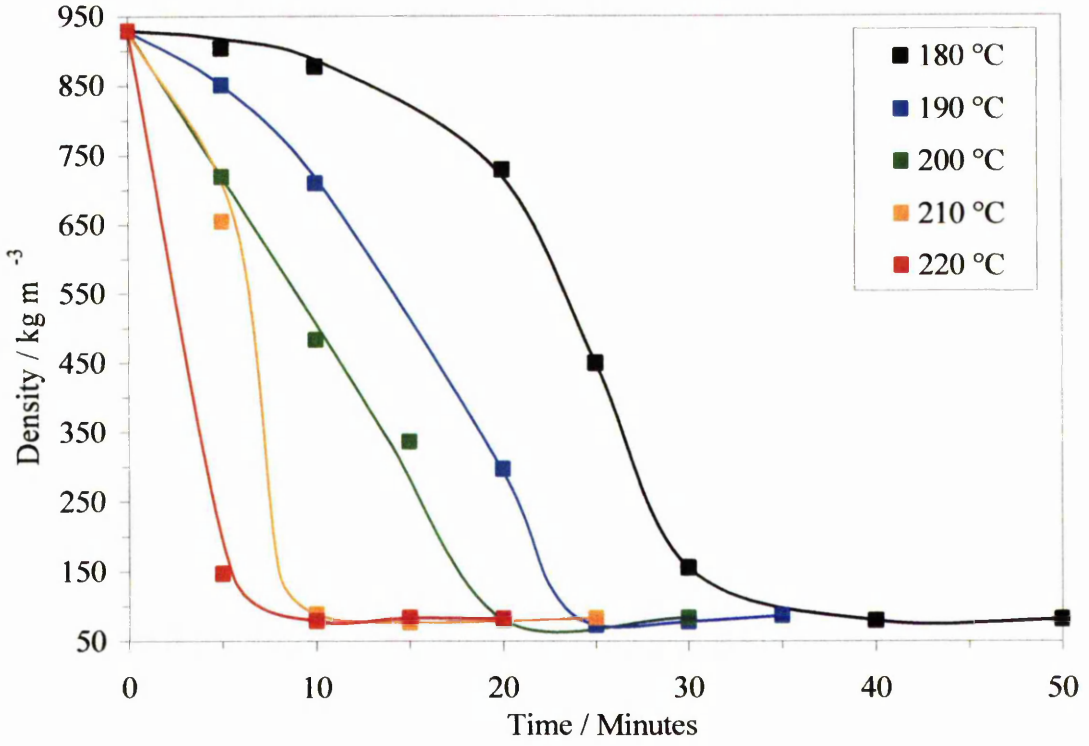

Figure 7.14: Conventional EVA 218 densities (including foam skin)

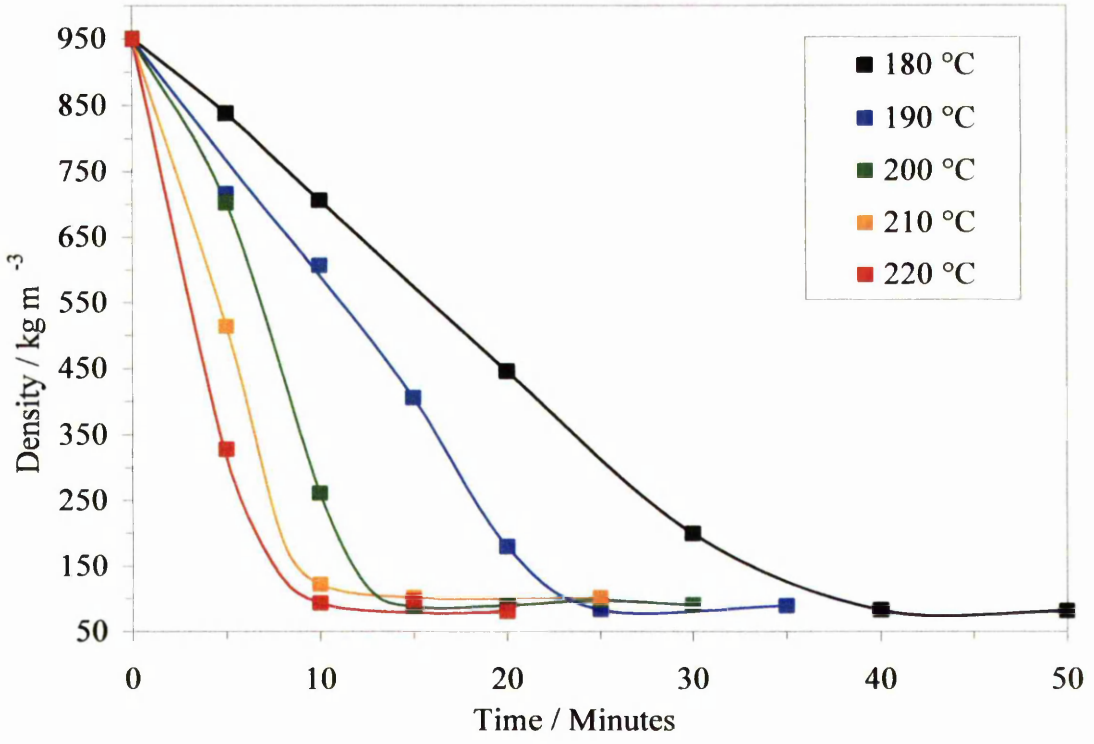

Figure 7.15: Conventional EVA 328 densities (including foam skin)

It should be remembered that the density values quoted include the foam skin, the density of which was inconsistent with the bulk of the sample. Foam density is more accurately reported by samples where the skin has been removed. However, the skin was left intact to allow comparisons with the microwave heated samples. It was not always possible to define where the skin on the microwave foamed samples ended and the fully foamed areas began. The microwave heated samples heated from the inside out which resulted in a smooth transition between foamed and non foamed areas with no clear boundary between the two. Conventionally heated samples heat from the surface inwards which resulted in a skin that was in the order of 0.25 – 0.5 mm thick and could easily be removed with a suitable knife. High density variation was encountered across individual sample diameters at short foaming times. Foaming took place at edge first, therefore, samples taken from the sample edges were fully foamed whereas those taken from areas nearer the centre were almost entirely unfoamed. This was particularly noticeable at high temperature, low heating time samples where rapid surface foaming occurred. The repeatability between individual average sample densities was, however, reasonable with errors within ± 12 % of the mean average.

Figures 7.14 and 7.15 show a trend of decreasing sample density with increasing isotherm time at each of the isotherm temperatures. Each of the foam samples decreased in density until a minimum density value was achieved where full expansion had taken place and the most efficient usage of the blowing agent gas had been made. After this point the results suggested that a marginal density increase occurred. This may be attributed to accelerated diffusion of gas from the foam cells as the foam remained at elevated temperature levels. This would result in progressive collapse of the foam cells and densification of the system overall. It may also be observed that as the isotherm temperature was increased, the rate of density decrease accelerated. This may be explained by consideration of the effect of temperature on the decomposition rate of ADCE. In section 3.2.1, TGA studies regarding the effect of isotherm temperature on the decomposition rate of ADCE show that as temperature was increased the decomposition of ADCE increased. The density values reported in figures 7.14 and 7.15 at zero minutes are the densities measured for the unfoamed, uncrosslinked base polymer compounded with 0.5 phr DCP and 8 phr ADCE. The density of the samples at this point was likely to be lower however, as although they

have not experienced any residence time at the isotherm temperature, they had been subjected to the temperature ramp. It is likely that some degree of foaming would have taken place before the relevant isotherm temperature was reached, thus reducing density by a small amount. This would be most noticeable for the higher isotherm temperature samples as they experienced the longest ramp time period and at elevated temperatures.

The reported density values appear to conflict with the TGA data shown in figure 3.5 which indicates that after 40 minutes at 180 °C only mass in the region of 15 % was lost from the ADCE. Figures 7.14 and 7.15, however, indicate that the foams reached a similar minimum density value to those foamed at higher temperatures. This may be explained by consideration of the highly exothermic nature of ADCE. The small sample in the TGA had its temperature accurately controlled and the very small sample size made it easier to maintain the temperature level. The oven temperature was less well controlled and the ADCE generated its own heat on exothermic decomposition. Previous work (O' Connor, 1998) demonstrated that the interior of the foam sample can reach temperatures at least 20 °C higher than the external isotherm temperature applied to the sample. This would have the effect of raising the internal temperature and significantly increase the rate of ADCE decomposition. As the surrounding base polymer is a very poor conductor of heat, the excess heat generated by the blowing agent decomposition was effectively sealed in.

7.4: Variable Frequency Microwave Foaming (2.3-2.5 GHz)

The conventional foam densities presented in figures 7.14 and 7.15 showed the times at each foaming temperature where the foams achieved maximum density reduction. These processing conditions were then used for microwave foam production to allow direct comparison between the two processes. A photograph of the variable frequency combination oven and associated heating equipment is shown in figure 7.16

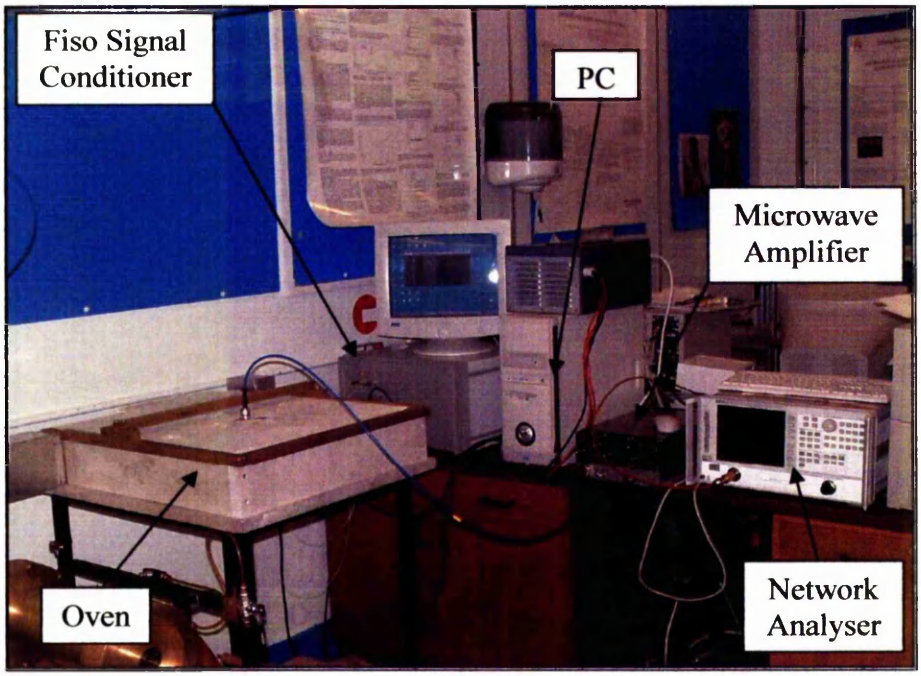

Figure 7.16: Variable frequency microwave heating apparatus

The microwave heating equipment used in this section of the work differed significantly from that used in chapter 5 for the wave guide foaming of EVA 206 and is described in greater detail in chapter 6. Instead of a small, single mode applicator using as low power amplifier, a large multimode, variable frequency microwave oven using a higher power amplifier was used. The oven also had an added circulating hot air facility. A vector network analyser was used to generate the microwave signal which was then routed via a coaxial microwave cable to a solid state microwave amplifier. The amplifier was then connected to the oven via a second coaxial microwave cable.

Before heating using microwaves, it was necessary to determine which frequencies within the amplifier operating frequency range would be most easily absorbed by the sample and, therefore, most suitable for heating. This was done by connecting the network analyser directly to the oven loaded with a foamable sample (using the amplifier to oven cable) and measuring the reflected signal response. Typical frequency – reflected power plots are shown for EVA 218 and 328 by figures 7.17 and 7.18.

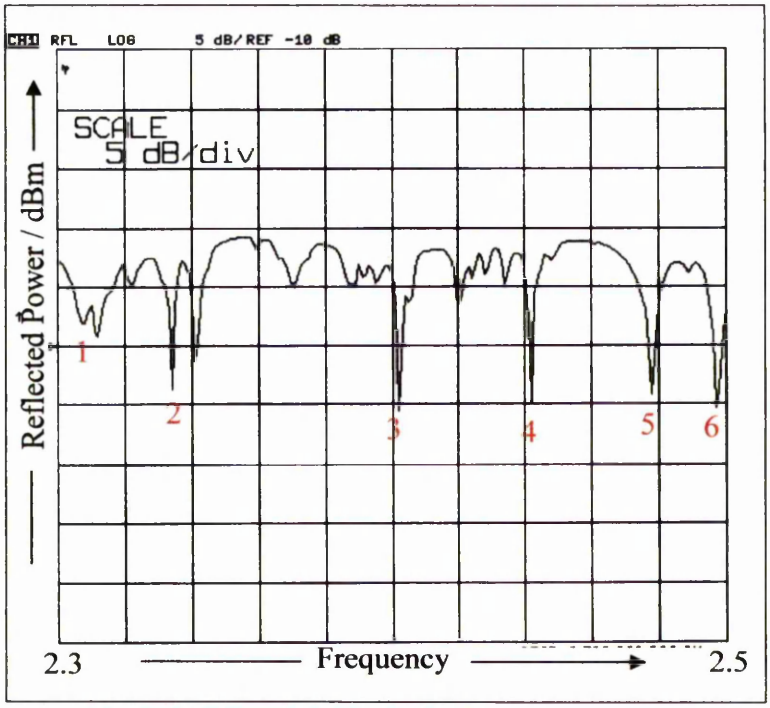

Figure 7.17: Reflected signal as a function of frequency for multimode oven loaded with EVA 218 blended with 0.5 phr DCP and 8 phr ADCE (sample dimensions, diameter 110 mm tapering to 100 mm, depth 10 mm)

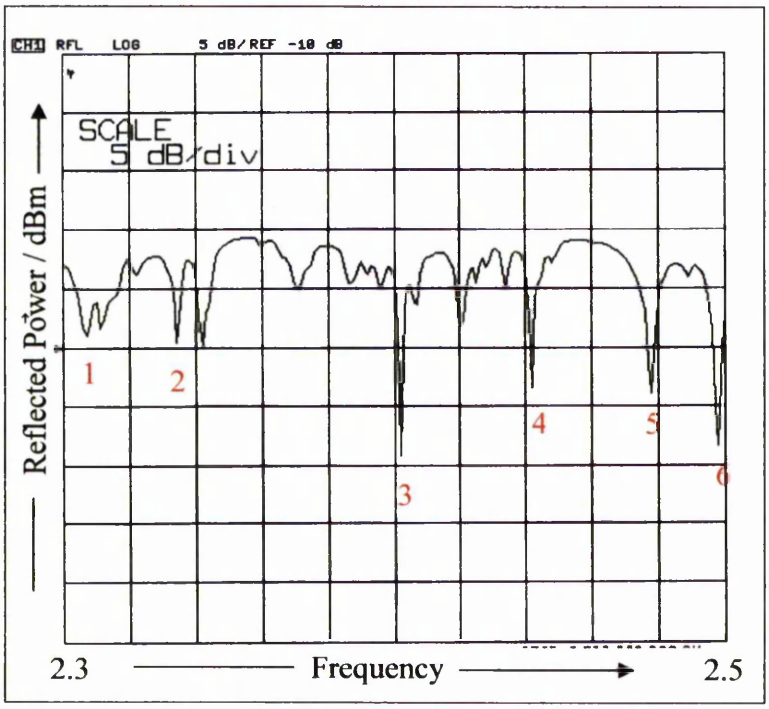

Figure 7.18: Reflected signal as a function of frequency for multimode oven loaded with EVA 328 blended with 0.5 phr DCP and 8 phr ADCE (sample dimensions, diameter 110 mm tapering to 100 mm, depth 10 mm)

The excitation frequencies used for heating were chosen from the minimum reflection peaks. Six excitation frequencies were chosen for the heating process to promote even distribution of the microwave field throughout the sample. Although the frequency peaks varied from sample to sample the variation was small and of the order of 4 %. Typical examples of the frequencies used are shown by the numbered peaks in figures 7.17 and 7.18. The frequencies were kept as close as possible between individual samples.

The density results presented in figures 7.14 and 7.15 also indicate that to achieve rapid foam production, 220 °C was the most suitable blowing agent decomposition temperature. This was supported by the TGA data in figure 3.5 and 3.6 which showed that at this temperature, blowing agent decomposition was rapid and largely complete. In order to determine the most suitable parameters for foam production, process variables were determined individually. Initially, EVA 218 and 328 foams were produced using microwave heating only. Subsequent processes used different microwave heating temperatures, variable air assistance temperatures and different heating times. The densities of the foams were then calculated by cutting samples of foam into uniform parallel sided samples and accurately measuring their dimensions using digital callipers (to 0.01 mm) and weights using an analytical balance (to 0.0001 g). The maximum power output of the amplifier (specified as 200 W) was used to heat the samples as quickly as possible to the preset foaming temperature of 220 °C.

Microwave foaming times were chosen by selecting the shortest conventional foaming time where minimum density had been reached and the error had been reduced to $\leq$ 12 % of the mean. The shortest time chosen to minimise the risk of thermal collapse and degradation and to minimise processing time.

7.4.1: Foaming Using Microwave Energy Alone

Significant problems concerning polymer flow during the conventional oven crosslinking of EVA 206 were encountered. Initially microwave crosslinking of the larger multimode oven samples was attempted. However, upon subsequent blowing agent decomposition and expansion, the foam samples appeared to undergo catastrophic cell rupture and foam collapse. This indicated that the crosslinking process was largely incomplete resulting in an insufficient polymer melt strength

enhancement necessary to retain the blowing agent gas pressure. Although the samples appeared to have foamed upon first inspection, examination of the sample interiors revealed that the cellular structure had undergone catastrophic collapse indicating insufficient crosslinking and melt strength reinforcement. As such, no significant data could be obtained from these samples. This problem was recurrent even at extended crosslinking times and temperatures higher than the previously determined crosslinking temperature of 165 °C. On the basis of these and the crosslinking and kinetics results discussed previously, it was decided that microwave crosslinking of the foamable polymer samples using the equipment available was not feasible within the time constraint of this work. The samples used for all heating were, therefore, pre-crosslinked in the press taking care that no blowing agent decomposition occurred. Although this meant that crosslinking was performed conventionally, the main phase of foam formation (i.e. decomposition of the blowing agent and cell formation) would still be carried out using microwave heating. Crosslinking in this way had the added benefit of allowing complete separation of the crosslinking and expansion phases of the process.

The heating temperatures used were based on the findings from the conventionally produced foams. The times at which maximum density reduction for both base polymers were determined and are shown in table 7.4

Table 7.4: Foaming time required to achieve maximum density reduction at individual conventional foaming temperatures based on figures 7.14 and 7.15

Foaming Temperature / °C	180	190	200	210	220
Foaming Time / Minutes	40	25	20	15	10

Crosslinked, foamable samples were then placed in the combination oven and heated at full power (to achieve maximum heating rate) to the relevant isotherm temperature and foamed for the specified time. Typical time temperature data are shown for the three EVA base polymers in figure 7.19 (220 °C set point).

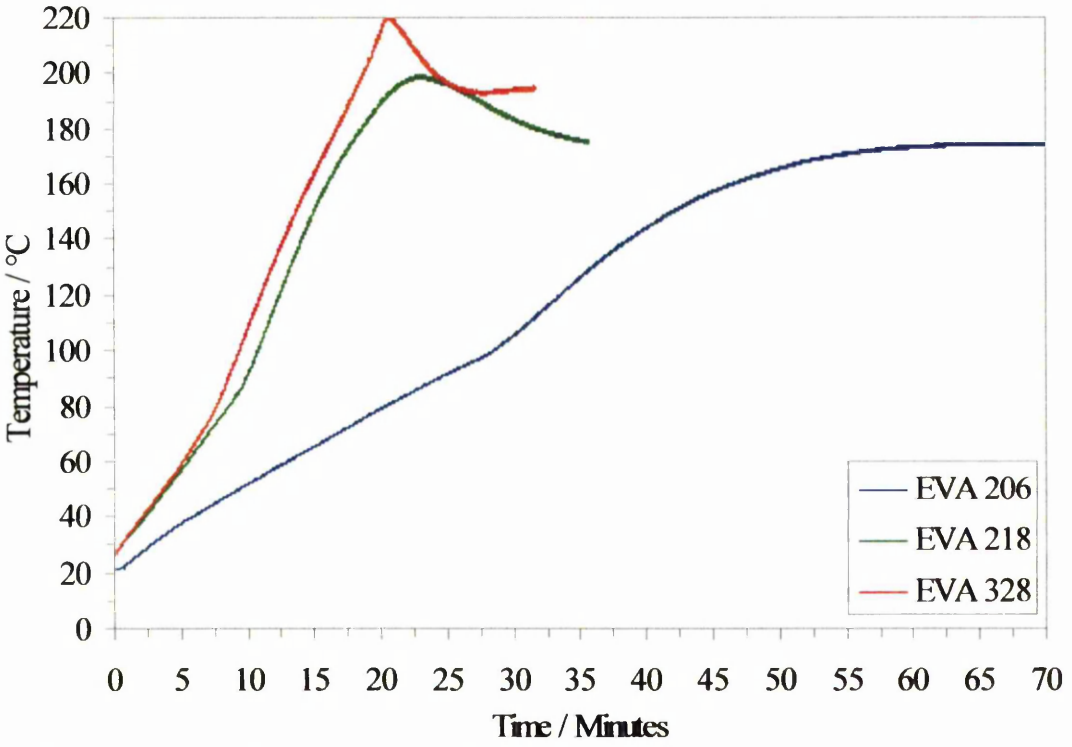

Figure 7.19: Temperature versus time for heating of EVA 206, 218 and 328 (sample dimensions, diameter 110 mm tapering to 100 mm, depth 10 mm) using microwaves only (200 W) and a set point temperature of 220 °C

Figure 7.19 shows the heating profiles for the three EVA grades during heating using microwave radiation alone in the combination oven. The same microwave power (200 W) and set point temperatures (220 °C) were used for each of the profiles shown. Each sample was the same size, weight and geometry and care was taken to ensure that the temperature sensor was located in the same place in each sample. A linear heating profile was obtained for EVA 206 between ambient temperature and approximately 80 °C. When this temperature was reached the trend line started to level off which suggested that any further heat increase would be small and the profile would plateau. Upon reaching an approximate temperature of 100 °C, however, the heating profile showed a pronounced increase. This supports the heating profile results from the waveguide heated samples and indicates that melting of the polymer crystalline regions has the effect of increasing the efficiency of microwave material interactions. It may be seen that the maximum temperature achieved by EVA 206 was in the region of 173 °C at which point the heating profile forms a flat plateau. This was not high enough for blowing agent decomposition to occur and, therefore, it was not possible to foam the EVA 206 sample under these conditions. Successful

EVA 206 foam production was achieved using microwave heating and a waveguide applicator as discussed in chapter 5, and would appear contradictory to these results. However, this may be explained by the differences in microwave applicator, sample sizes, microwave field distribution and EVA 206 loss factor. Firstly, the specimens foamed in the waveguide were much smaller than the variable frequency oven samples. The samples were located directly within a known localized area of high field intensity. Although the power input to the variable frequency oven was much greater than the waveguide (200 W and 28 W, respectively) the former was much larger. The microwave power would, therefore, be distributed over a much larger area and, by design, distributed among numerous areas of high field intensity or hot spots. The simulations in figure 6.19 show that many of these hot spots were located in unoccupied regions of the oven and, therefore, did not contribute to sample heating. The dielectric loss factor results for EVA 206 showed that its loss factor was only marginally in excess of the minimum value required for feasible microwave heating. It would appear, therefore, that the output power of the variable frequency microwave amplifier was insufficient to heat the samples to temperatures where blowing agent decomposition occurs.

The initial linear heating trends were present in the heating profiles for both EVA 218 and 328. They also demonstrated an increase in heating rate around their respective melting points, the increase became less pronounced as vinyl acetate content was increased and crystallinity decreased correspondingly. Both showed sudden increases in temperature when the dissociation range of ADCE was reached. These were attributed to the highly exothermic nature of the ADCE decomposition. The set point was rarely reached and maximum temperatures in the region of 210 °C were more common. After the EVA 218 and 328 peak temperatures were reached the temperature profiles began to fall, this was a direct result of the foaming process. As the samples foamed they became harder to heat because the voids (foam cells) introduced during the foaming process contained a gas phase (mainly nitrogen) and were, therefore, essentially loss free. Introduction of a loss free phase reduced the overall sample loss factor which resulted in the temperature drop. The profile for EVA 206 remained constant after it reached its maximum indicating that no foaming had taken place to reduce the loss factor and thus, cause a similar temperature change.

Examples of the foams made using microwave heating are shown complete in figures 7.20 and 7.21 and in cross section in figures 7.22 and 7.23.

Figure 7.20: EVA 218 samples produced using microwave heating only, top left to bottom right, 180, 190, 200, 210, 220 °C microwave set point temperatures (bottom right unfoamed sample for comparison)

Figure 7.21: EVA 328 samples produced using microwave heating only, top left to bottom right, 180, 190, 200, 210, 220 °C microwave set point temperatures (bottom right unfoamed sample for comparison)

Figure 7.22: Cross sections of EVA 218 foams produced using microwave heating only (180, 190, 200, 210, 220 °C set point temperature top to bottom). A cross section of an unfoamed sample is shown on the right for comparison

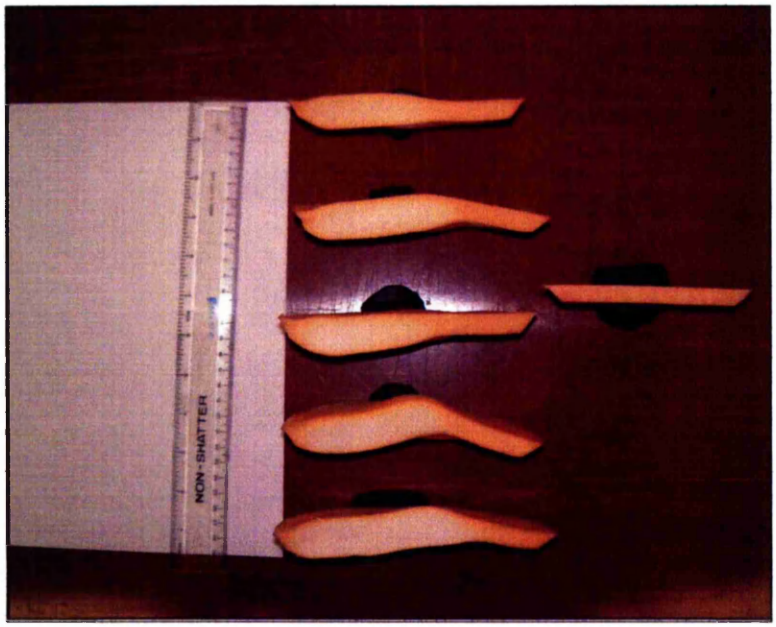

Figure 7.23: Cross sections of EVA 328 foams produced using microwave heating only (180, 190, 200, 210, 220 °C set point temperature top to bottom). A cross section of an unfoamed sample is shown on the right for comparison

When the samples had been heated to their individual isotherm temperatures for the times periods determined from the conventional foaming trials, they were allowed to

cool and condition in a temperature and humidity controlled lab for 24 hours. Their densities were then determined by measuring the volume and mass of samples cut from a 3 cm wide strip taken from across the sample diameters. The densities are reported in table 7.5.

Table 7.5: Microwave processed foam densities

Foaming Temperature / °C	Foam Density / kg m^{-3}	
	EVA 218	EVA 328
180	409 ± 50	317 ± 39
190	399 ± 36	345 ± 27
200	327 ± 22	373 ± 35
210	389 ± 44	366 ± 28
220	378 ± 46	292 ± 41

The results in table 7.5 show that although some degree of foaming and subsequent density reduction had taken place, the density values were considerably higher than those of the conventionally processed samples. The density variations across individual samples was large as foamed and non foamed areas were present, the error values reported in table 7.5 are the errors between individual sample average densities. By visual examination of the foams produced by microwave heating alone and measurement of their densities (and error margins) it was clear that foaming was only partial and showed high variability between individual samples. Foams produced by microwave heating alone showed clear signs of foaming when cut across their diameters. Expansion had taken place predominantly in the vertical direction, however overall expansion was considerably less than conventionally produced foams. When cut sections of the foams were examined, it was discovered that the central cores of the samples had foamed well. However the foamed cores were surrounded by a thick (3 – 4 mm) unfoamed skin which was at its thickest (approximately 10 mm) around the circumference of the foams. This observation led to the conclusion that microwave energy was heating the centre of the samples and causing foaming to take place. It would appear that heat loss from the external surfaces of the sample to the surrounding atmosphere (at ambient temperature) was resulting in a greatly reduced temperature at the sample surface. As a consequence

the skin did not reach the temperature range required for decomposition of the blowing agent to take place which resulted in incomplete, uneven foaming. These results corroborate the findings in chapter 5 where poor surface foaming was linked to heat loss from the sample surface. From the cross sections of the foam specimens it would appear that foaming did not take place uniformly throughout the sample at the same time. This cast some doubt upon the uniformity of the microwave field distribution throughout the cavity.

The temperature of the sample skin was measured to confirm whether lower surface temperatures were partly responsible for the poor surface foaming. Temperature measurements were made in four different locations on the foam sample. The locations chosen are shown schematically in figure 7.24.

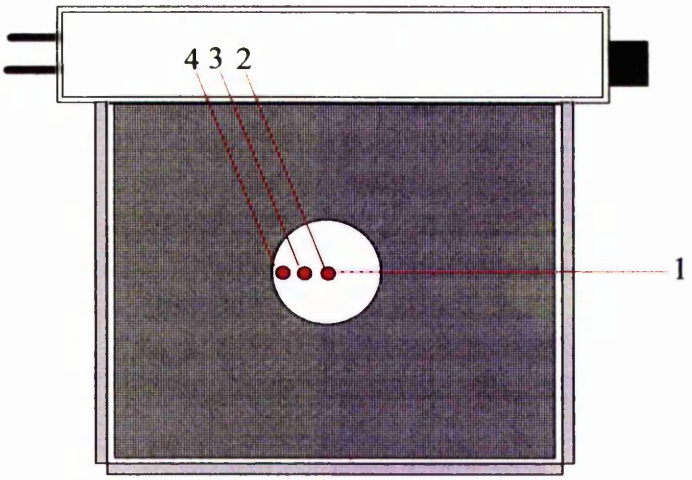

Figure 7.24: Top view schematic of an EVA sample in the oven (lid not shown for clarity) showing the temperature sensor positions used to record sample internal, (1), and surface, (2), (3) and (4), temperatures.

The first temperature sensor (1) was placed directly within the sample and measured the central internal temperature of the specimen. The second, third and fourth temperature sensors all measured sample surface temperatures in the middle of the sample (2), half way between the sample centre and the outer edge (3) and the very outer edge (4). The Fiso temperature measurement system available at the time was equipped with two channels. This necessitated two runs to obtain the four

temperature profiles. The temperature profiles recorded at these positions are shown in figure 7.25.

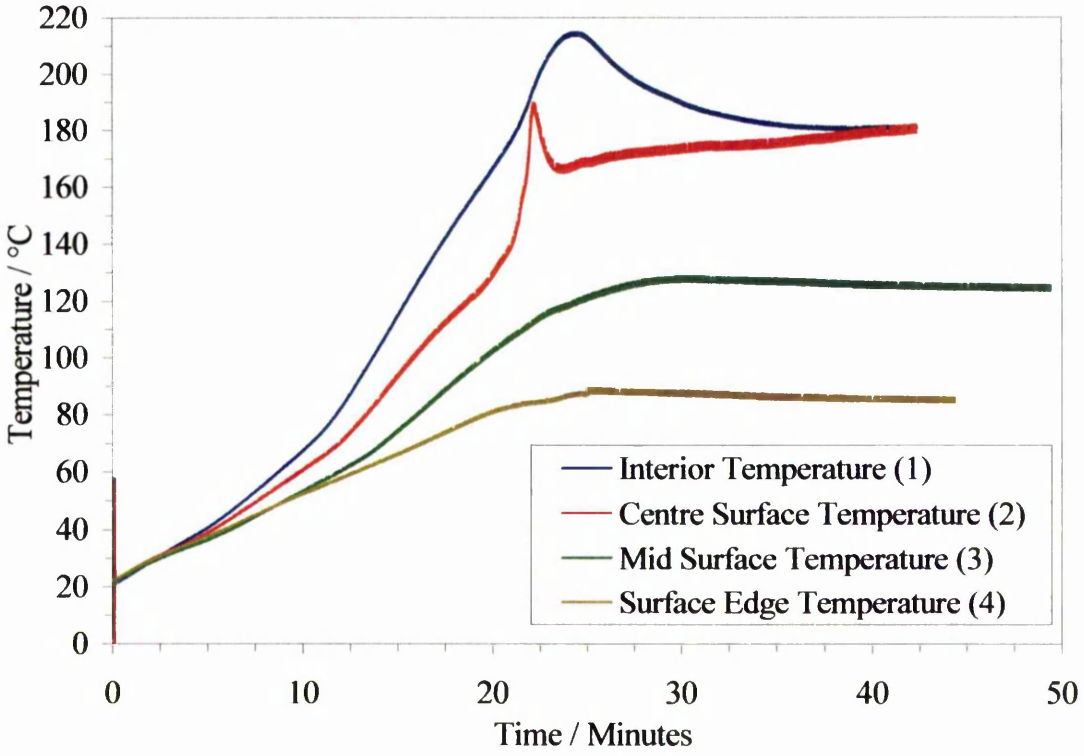

Figure 7.25: Variation of EVA 328 sample temperature according to temperature sensor location

The temperature sensor located centrally inside the sample showed the fastest and largest temperature increase. It was noticeable from profile 1 that there was an increase in heating rate as the internal temperature reached approximately 180 °C. This was attributed to the exothermic decomposition of the ADCE blowing agent generating heat within the sample (O' Connor, 1998) and accelerating the heating rate. This rise in heating rate was also observed from the centrally mounted surface temperature probe (2). The exotherm occurred at a similar time but at a lower temperature. This would indicate that the heat was generated within the sample and then passed to the surface by conduction. The temperature measured at position (2) diminished faster than at position (1) indicating rapid heat loss from the sample surface. The heating profiles from midway point (3) and the sample edge (4) are much lower that the data from the central probes. This suggests that although the antenna was designed to distribute the microwave energy uniformly throughout the cavity interior, much of the energy was localised in the centre of the cavity where the

antenna was connected. The maximum surface temperatures recorded by probes (2) and (3) were 125 and 90 °C, respectively. It would appear that although these areas were heated by the microwave energy they received less energy than the sample centre and were not heated as efficiently. Secondly, the effect of surface heat losses became more pronounced as the extremities of the sample were reached limiting the maximum achievable temperatures in these regions given the power available. These results show that some degree of hot air assistance would be required in combination with the microwave heating for successful foam production.

7.4.2: Foaming Using Microwave Energy and Hot Air Assistance

The results from the samples heated by microwave energy alone further support the requirement for supplemental hot air heating of the sample to help counteract the heat losses from the sample surface and reduce the thermal gradients between the centre of the sample and its extremities. In addition to the reduced surface heat losses, supplemental hot air heating would also have a beneficial effect on the dielectric properties of the polymer samples. The dielectric results presented in section 4.2.1 show that as the temperature of the base polymer was increased the dielectric loss factor also increased due to an increased degree of molecular freedom allowing more efficient dipole – microwave interaction. Thus, heating using hot air in conjunction with microwave radiation would help to increase the microwave heating efficiency in areas of the sample which foam poorly using microwave heating alone. Although it was not possible to heat EVA 206 to the required temperatures using microwave heating alone, heating using microwaves and hot air was also attempted. It was thought that the increase in sample temperature caused by the hot air assistance might elevate the dielectric loss sufficiently to couple more efficiently with the microwave field and allow heating to the required levels.

For the hot air assistance runs, a fixed microwave set point temperature of 220 °C was used as this provided the greatest density reduction in the microwave only trials. Heating time was limited to 10 minutes isotherm temperature (or 10 minutes after maximum temperature if the set point was not reached) plus the temperature ramp period. For the hot air assistance, it was decided that temperatures above the melting points of the base polymers should be considered as temperatures below this level would have been unlikely to benefit the process. Temperatures between 100 and 170

°C were used in 10 °C increments. These limits were defined by the polymer and blowing agent. A temperature of 100 °C was selected as the lower limit as this was close to the softening point of the polymer and, therefore, any lower was unlikely to have any significant benefit. 170 °C was selected as the maximum as temperatures higher than this would start to contribute to the decomposition of the blowing agent and, therefore, it would be difficult to ascertain the contribution to foaming from the microwave heating effect. A range of foams base on EVA 218 and 328 and heated using microwaves and the air assistance temperatures described above are shown in figures 7.26 and 7.27. The density values for these foams are subsequently reported in figures 7.28 and 7.29.

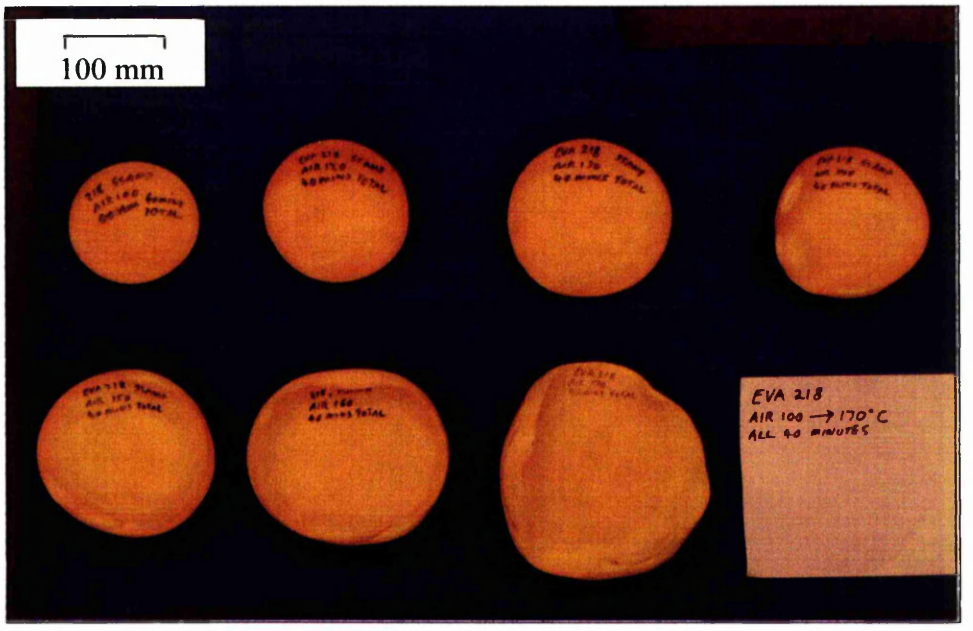

Figure 7.26: EVA 218 foams produced using microwave heating (maximum power) with hot air assistance temperatures of 100, 120, 130, 140, 150, 160 and 170 °C

Figure 7.27: EVA 328 foams produced using microwave heating (200 W) with hot air assistance temperatures of 100, 120, 130, 140, 150, 160 and 170 °C

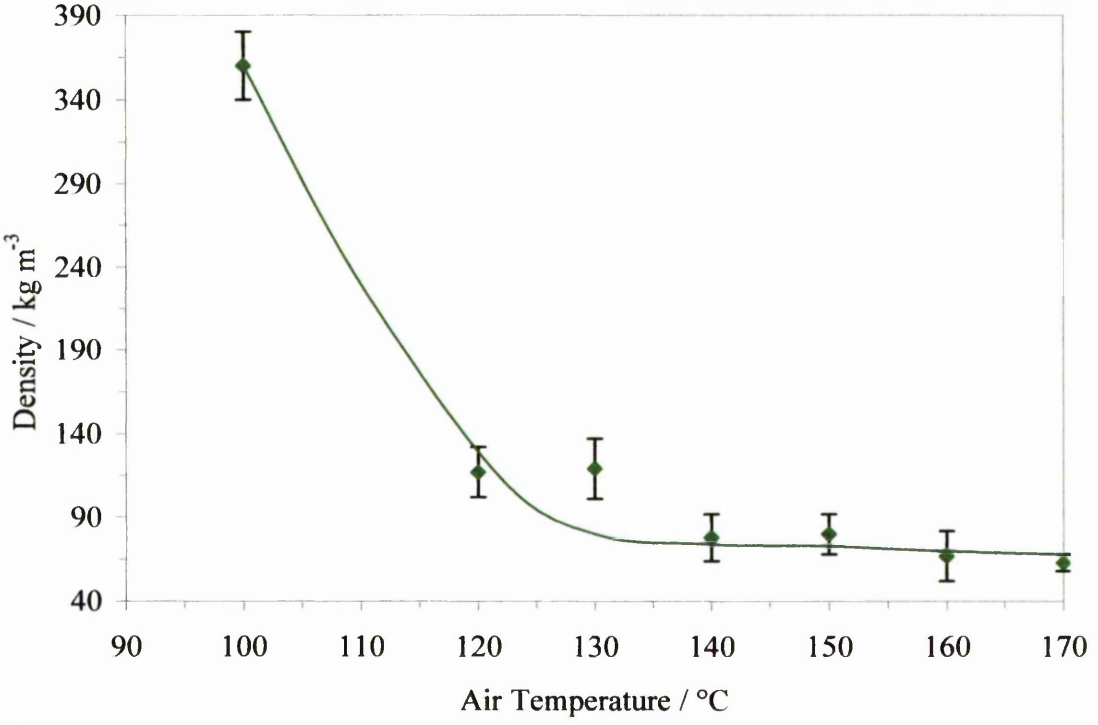

Figure 7.28: Variation of microwave heated EVA 218 foam density as a function of hot air assistance temperature. All samples heated for 40 minutes using 200 W microwave power and a series of hot air assistance temperatures (220 °C set point)

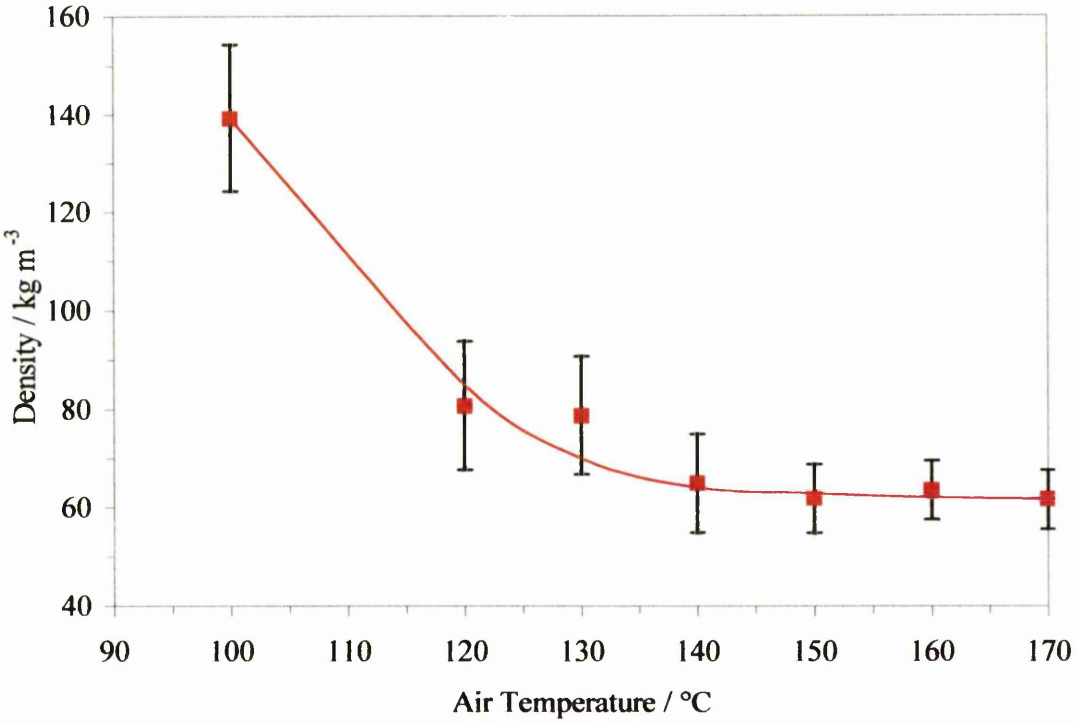

Figure 7.29: Variation of microwave heated EVA 328 foam density as a function of hot air assistance temperature. All samples heated for 40 minutes using 200 W microwave power and a series of hot air assistance temperatures (220 °C set point)

The foams pictured in figures 7.26 and 7.27 show a clear increase in expansion as air assistance temperature was increased. This indicated that as the surrounding air temperature increased, the outside of the sample was progressively softened. This in turn lowered the resistance of the sample surface to expansion (by lowering its viscosity) and allowed the foam generated in the sample interior to expand more easily. Furthermore the density values and associated errors shown in figures 7.28 and 7.29 show that the samples achieved a much lower density value than those heated with microwave radiation alone. Whereas the microwave only samples had large areas of unfoamed materials and thick skins enclosing the foamed core, the foams produced using hot air assistance showed a progressive reduction of these undesirable features as the air assistance temperature was raised. It is proposed that this was due to the hot air raising the loss factor (by increasing sample temperature) in the sample extremities which facilitated microwave heating and uniform sample foaming. When using the lower air assistance temperatures of 100-120 °C, it was noted that the preset microwave foaming temperature of 220 °C was not being reached even in the centre of the sample (where temperature measurement took

place). It was surmised that at this lower air temperature, the circulating air flow was having the inverse effect to that desired. Rather than aiding expansion by increasing the external sample surface temperature, the air movement within the oven was actually having a cooling effect on the sample and exacerbating the problem of heat loss from the sample surfaces. It was thought that the foams produced using microwave heating alone heated the air locally around them and the skin insulated the foamed core allowing greater internal temperatures.

From figures 7.28 and 7.29, it may be observed that as the air assistance temperature was increased, the average density of the foam samples decreased. As the air temperature was increased, the heat loss from the surface of the samples was reduced. This allowed foaming to progress from the centre of the sample to the surface thus greatly reducing the thickness of the skin and decreasing overall density.

In addition to the localised skin thickness reduction in the centre of the foamed specimens, the supplemental hot air also greatly reduced the portion of unfoamed material around the circumference of the samples. This was beneficial to the process in two ways. Firstly overall foam density was greatly reduced as the hot air increased the loss factor of the base polymers (as demonstrated by figure 4.11) and, therefore, increased the efficiency of the microwave material interaction. This had the effect of reducing the large density variation across the sample and lowered overall density. Secondly, the increase in sample surface and edge temperature reduced the polymer viscosity. Figure 7.25 strongly suggests that when using microwave heating alone, the temperatures at the sample extremities were in the region of the base polymer melting ranges. The viscosity of the base polymers in these regions would be sufficiently large to resist the expansive forces of the blowing agent gas and thus greatly impede expansion. The use of supplementary hot air greatly reduced the viscosity of the base polymer around the sample extremities and facilitated expansion in the horizontal plane.

On the basis of the results presented in figures 7.28 and 7.29 and their associated error values, 170° C was chosen as the air assistance temperature for all subsequent microwave foaming. The density values show that 170 °C allowed efficient expansion and reduced the error between individual samples. In addition, foaming as a direct result of hot air heating at this temperature would be minimised as it is below

the decomposition range of ADCE which has been confirmed by TGA and DSC analysis. It is unlikely, therefore, that air assistance at this temperature would directly result in significant blowing agent decomposition and sample foaming. Its role would be limited to the increase of base polymer loss factor and the assistance of expansion by base polymer viscosity reduction. The foam – skin boundary was much easier to identify in the microwave foams with hot air assistance, this greatly facilitated its removal which was necessary for processes such as mechanical testing.

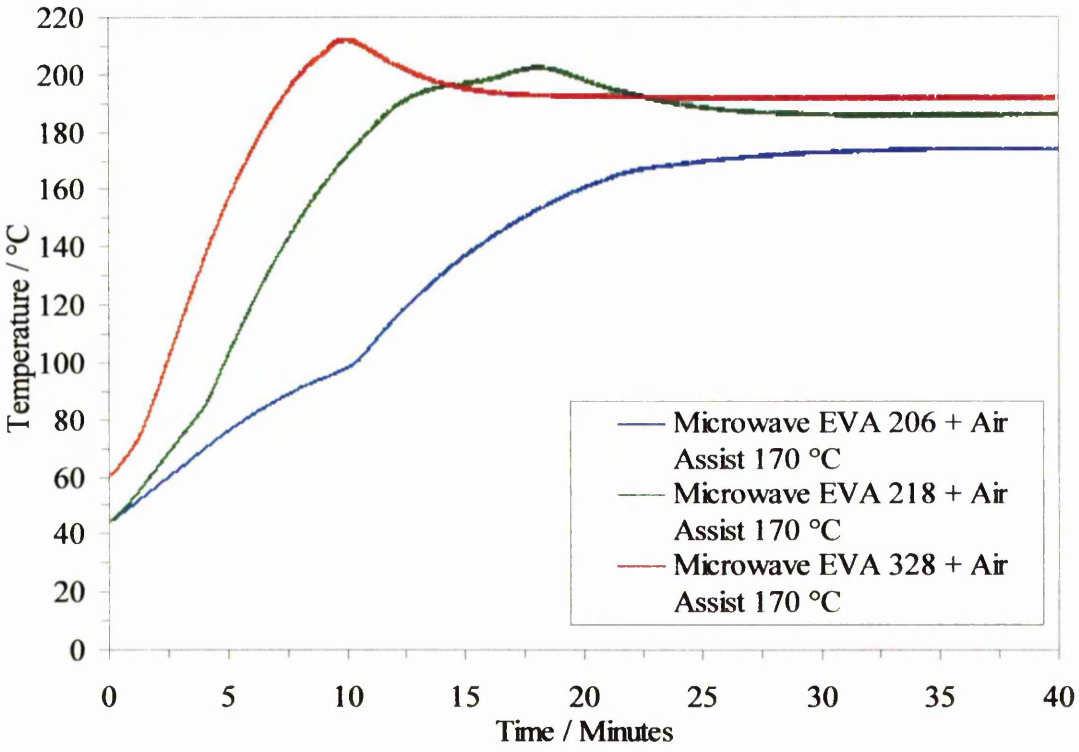

Figure 7.30: Typical temperature versus time data for EVA 206, 218 and 328 using microwaves (set point temperature of 220 °C) and an air assistance temperature of 170 °C

Figure 7.30 shows typical temperature versus time data for the three EVA base polymers. When compared to the profiles in figure 7.19 it is noticeable that the trends follow similar patterns and may be explained in the same way. However the heating rates were considerably faster when hot air assistance was used. The increase in heating rate was attributed to a combination of conduction of heat, by the sample, from the surrounding air and an increase in loss factor in each case due to elevated sample temperature.

Having set the air assistance level at 170 °C, microwave foams using hot air assistance were produced at each of the temperatures and times used for the

conventional foam trials. These were produced so that a range of foams expanded at different isotherm temperatures could be tested and compared. The density results for these microwave (with hot air assistance) foams are presented in tables 7.6 and 7.7; the density results for the respective conventional foams are also included for comparison. Results for foams with skin intact and skin removed are both shown.

Table 7.6: Conventional and microwave foam (with 170 °C air assistance) densities including foam skin

Expansion Temperature / °C	**EVA 218 Foam Densities / kg m^{-3}**		**EVA 328 Foam Densities / kg m^{-3}**	
	Conventional	***Microwave***	***Conventional***	***Microwave***
180	80 ± 3	107 ± 15	83 ± 4	125 ± 40
190	73 ± 3	88 ± 5	83 ± 2	94 ± 13
200	81 ± 4	86 ± 7	88 ± 5	95 ± 5
210	77 ± 2	83 ± 9	97 ± 5	83 ± 3
220	79 ± 2	88 ± 7	94 ± 5	83 ± 5

Table 7.7: Conventional and microwave foam (with 170 °C air assistance) densities foam skin removed

Expansion Temperature / °C	**EVA 218 Foam Densities / kg m^{-3}**		**EVA 328 Foam Densities / kg m^{-3}**	
	Conventional	***Microwave***	***Conventional***	***Microwave***
180	65 ± 2	78 ± 10	71 ± 6	76 ± 12
190	57 ± 1	64 ± 3	66 ± 4	67 ± 4
200	49 ± 6	63 ± 7	63 ± 9	64 ± 5
210	54 ± 3	64 ± 6	65 ± 8	63 ± 5
220	52 ± 1	62 ± 5	69 ± 5	60 ± 7

Table 7.6 shows that for the microwave foams, where the skin was left intact, the density values were generally higher than those of the conventionally heated foams. This suggested that the microwave heated samples were still marginally cooler at their

surfaces despite the supplemental hot air assistance. The results for the conventionally foamed EVA 328 samples at 210 and 220 °C are slightly higher than the microwave heated samples. It was noticed that, although the TGA results suggested minimal EVA weight loss, these samples had undergone some thermal degradation (oxidative surface yellowing) and were thinner than the lower temperature foams. The surface yellowing was indicative of degradation of the foam skin due to the high expansion temperature and thermal sensitivity of EVA 328. Furthermore, the reduced foam thickness may have been due to a degree of cell gas loss and partial foam collapse due to the extreme expansion temperatures. It is proposed that the microwave heated samples were able to achieve lower densities in this case as the higher expansion temperatures are only reached in the foam interior. The surface of the microwave samples were subjected to temperatures no greater than 170 °C which may have helped to prevent degradation. The presence of the skin may also have helped to reduce gas loss through diffusion.

Table 7.7 shows the foam density results after the surface skin had been removed from each foam sample, this entailed cutting ~0.5-1 mm from the exterior surfaces of each specimen. After skin removal it may be observed that the density results for the microwave heated EVA 218 foam samples were still greater than the respective conventional samples. It would appear, therefore, that in addition to the thicker skin, the bulk of the EVA 218 foam produced using microwave heating was denser than the bulk of the conventional foam. This suggested that the minimum foam density achievable by this formulation was not being reached and that sample was not fully expanded. However, the density values from the two processes were reasonably close especially when the experimental error was considered which indicated that the vast majority of expansion had taken place. Table 7.7 also shows that the density results for the microwave EVA 328 foam samples (free of skin) were approximately the same as the conventional samples. This indicated that the bulk of the microwave EVA 328 foams had fully expanded and reached the minimum possible density values.

The density results for the bulk of the foam samples presented in table 7.7 (skin removed) highlight differences in the expansion efficiency of the two base polymers when microwave heating was used. The differences may be attributed to the difference in vinyl acetate content. EVA 218 had 10 % less vinyl acetate content by

weight than EVA 328. It has fewer polar groups than EVA 328 and is not as lossy. As a result, EVA 218 does not heat as well as EVA 328 when using microwaves. It may be surmised that the EVA 218 foams had not reached maximum expansion and density reduction and foaming was less uniform compared to EVA 328. This is reflected in the higher error in the density values for microwave heated EVA 218 foams than conventional 218. The densities for the microwave and conventional EVA 328 foams were comparable suggesting that expansion was complete for microwave process. This may be because of the higher vinyl acetate content allowing more efficient microwave-material interaction which in turn resulted in more even heating, maximised density reduction and expansion.

7.5: Summary

The microwave crosslinking and DCP kinetics studies in this chapter showed that, given the equipment available, microwave crosslinking was unlikely to be feasible for foam production although some network formation was achieved. Heating pre-crosslinked foamable samples using microwave radiation alone met with limited success. Samples foamed well in the sample interior but were surrounded by unexpanded areas and a thick unfoamed skin which were attributed to sample surface heat losses and less than ideal microwave field uniformity. The introduction of hot air assistance greatly improved the quality of the foam specimens particularly at higher assistance temperatures.

The EVA 218 foams produced using microwave heating and hot air assistance had higher density values than the corresponding conventionally foamed material. In contrast, the densities of the microwave heated EVA 328 foams (with hot air assistance) had densities that were comparable with the comparable conventionally foamed specimens. This was attributed to the increased vinyl acetate content of EVA 328 allowing more efficient interaction with the microwave field.

CHAPTER 8: MECHANICAL TESTING

Polymer foams are commonly used in applications were they undergo compression. Compression testing was used to characterise the foams made using conventional and microwave (with hot air assistance) processing methods.

8.1: Modelling of Closed Cell Foam Compressive Properties

The compressive properties of the foams made using both conventional and microwave heating methods were predicted using the equations developed by Gibson and Ashby presented in sections 1.6.2.1-1.6.2.3 (Gibson and Ashby, 1997; Gibson and Ashby, 1982). Three events that take place during the compression of elastic – plastic foams were predicted, these were: Young's modulus; plastic yield; and the plastic collapse plateau region. Modelling of these regions was performed to assess the validity of the experimental results as no data were available in the literature for the compressive properties of microwave foams. The predicted results for plastic collapse are presented with the experimental results in figures 8.1 to 8.10. The predicted values of compressive modulus and plastic yield stress are shown with the experimental data in tables 8.1-8.4.

8.2: Compression Load Deflection

Foam samples were compression tested using the method described in section 2.5.3.1. Figures 8.1 to 8.5 show compressive stress as a function of strain for EVA 218 conventional and microwave foams (with 170 °C hot air assistance) at the expansion temperatures used. Figures 8.6 to 8.10 show the data for EVA 328 foams. The plots also show the predicted values of collapse stress at strain values of 0.3, 0.4 and 0.5 calculated using equation 1.21.

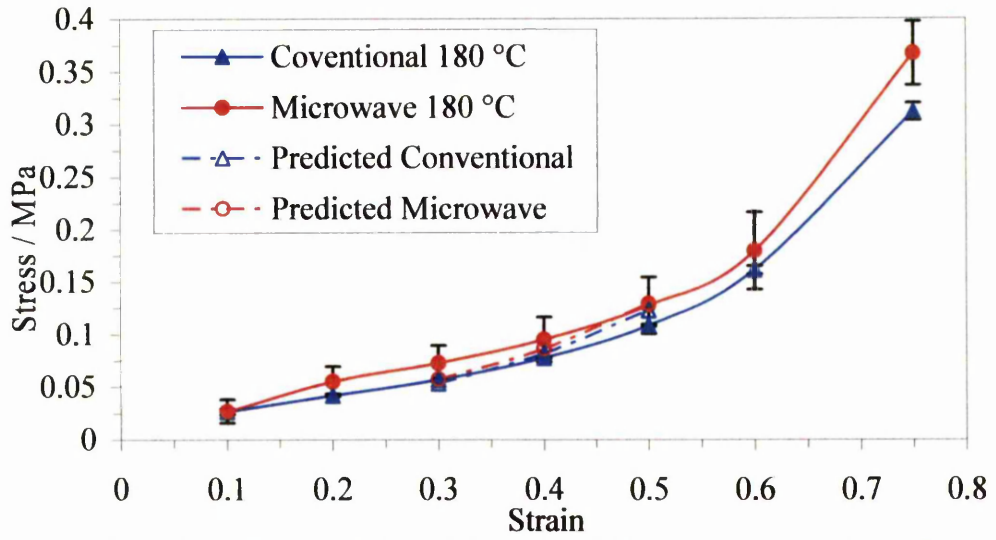

Figure 8.1: Stress - strain response for EVA 218 foamed at 180 °C

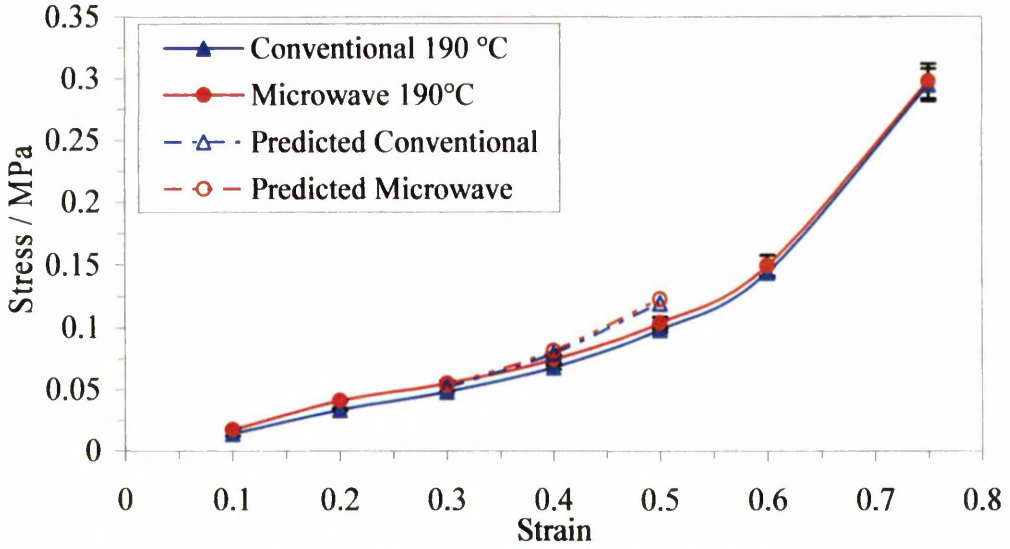

Figure 8.2: Stress - strain response for EVA 218 foamed at 190 °C

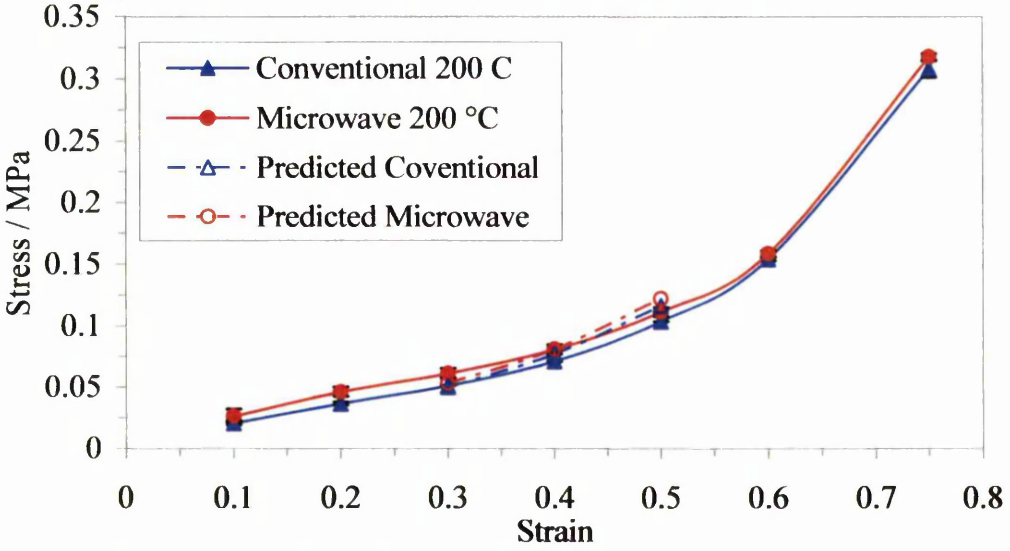

Figure 8.3: Stress - strain response for EVA 218 foamed at 200 °C

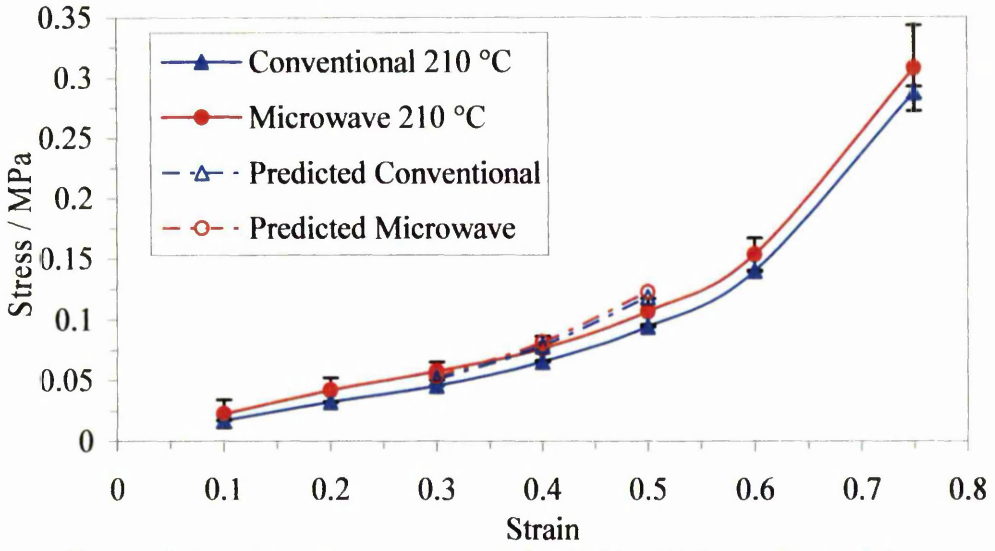

Figure 8.4: Stress - strain response for EVA 218 foamed at 210 °C

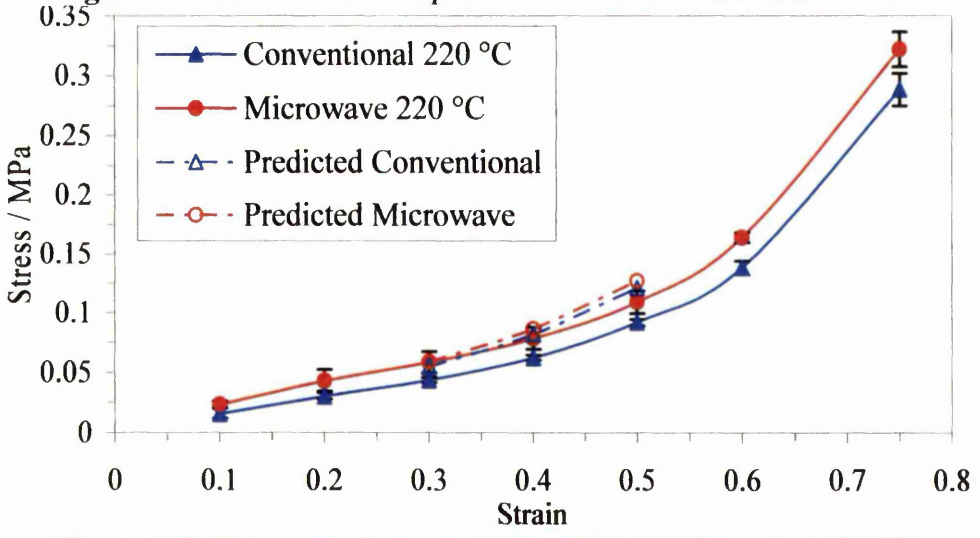

Figure 8.5: Stress - strain response for EVA 218 foamed at 220 °C

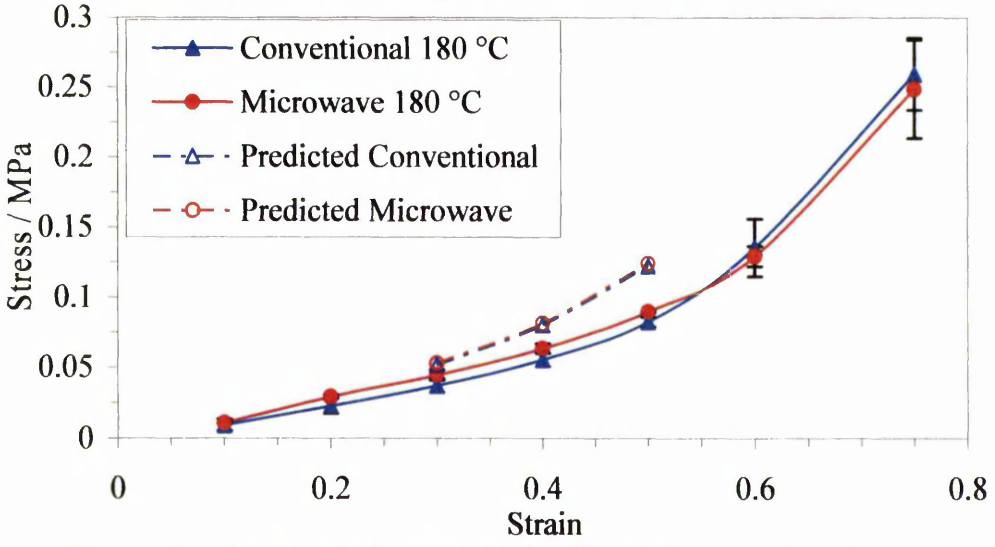

Figure 8.6: Stress - strain response for EVA 328 foamed at 180 °C

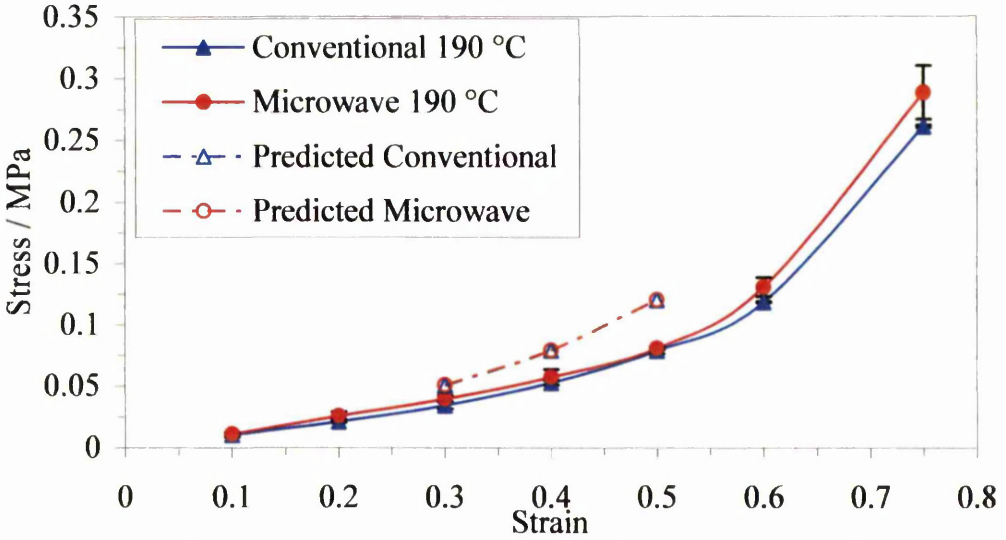

Figure 8.7: Stress - strain response for EVA 328 foamed at 190 °C

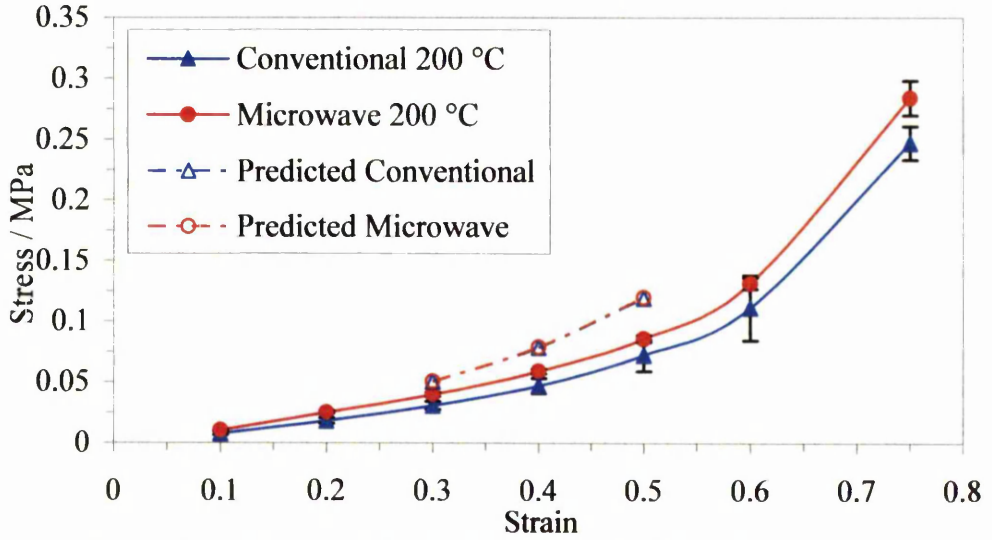

Figure 8.8: Stress - strain response for EVA 328 foamed at 200 °C

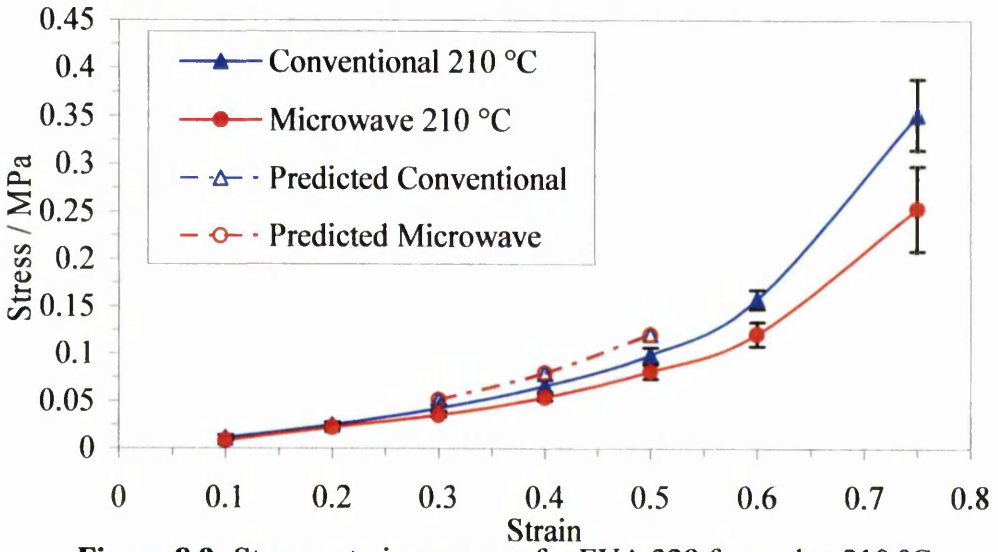

Figure 8.9: Stress - strain response for EVA 328 foamed at 210 °C

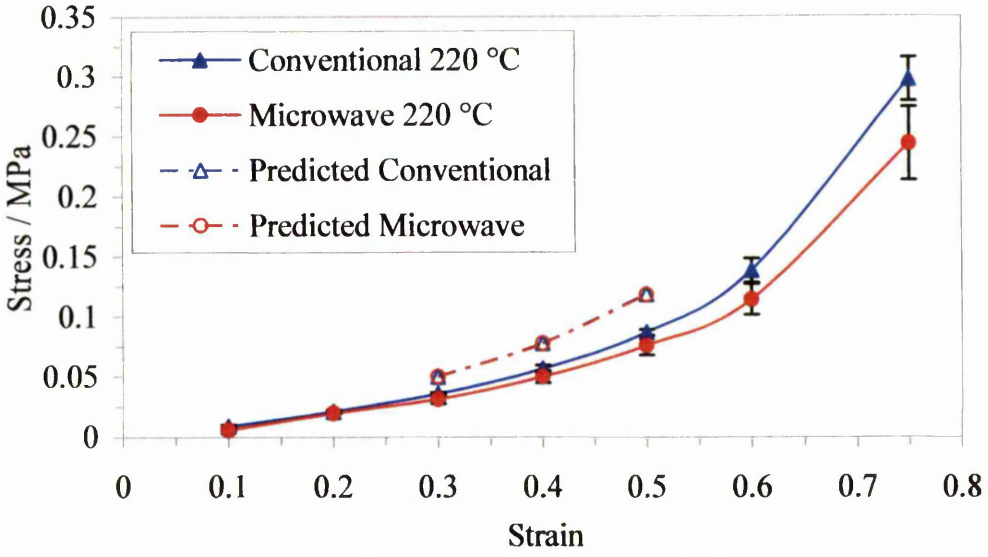

Figure 8.10: Stress - strain response for EVA 328 foamed at 220 °C

The original data was in the form of force-deflection charts. These had to be manually converted to stress-strain plots by calculating the stress at a number of strain values. The force deflection plots for EVA 218 showed clear initial linear regions (similar to area 1 in figure 1.8) from which Young's modulus was calculated directly. Much of the definition of the initial elastic straight line section of the plots was lost when they were converted from force – deflection curves to stress strain curves. The linear elastic region of the EVA 328 force deflection plots was very poorly defined which made determination of Young's modulus particularly difficult. This was attributed to the lower crystallinity of EVA 328. Young's modulus, elastic yield point and their associated predicted values are presented in tables 8.1, 8.2 (conventional), 8.3 and 8.4 (microwave + 170 °C air assist).

Table 8.1: Predicted and experimental values of Young's modulus and elastic yield stress for ***conventionally*** heated EVA 218 foam, 0.5 phr DCP and 8 phr ADCE

Expansion Temperature / °C	Predicted Young's Modulus (E^*) / MPa	Experimental Young's Modulus (E) / MPa	Predicted Plastic Yield Stress (σ_{el}^*) / MPa	Experimental Plastic Yield Stress (σ_{el}) / MPa
180	0.249	0.282 ± 0.061	0.006	0.030 ± 0.001
190	0.219	0.225 ± 0.009	0.004	0.029 ± 0.001
200	0.188	0.254 ± 0.019	0.003	0.027 ± 0.002
210	0.207	0.205 ± 0.011	0.004	0.022 ± 0.006
220	0.199	0.189 ± 0.017	0.004	0.023 ± 0.003

Table 8.2: Predicted and experimental values of Young's modulus and elastic yield stress for ***conventionally*** heated EVA 328 foam, 0.5 phr DCP and 8 phr ADCE

Expansion Temperature / °C	Predicted Young's Modulus (E^*) / MPa	Experimental Young's Modulus (E) / MPa	Predicted Plastic Yield Stress (σ_{el}^*) / MPa	Experimental Plastic Yield Stress (σ_{el}) / MPa
180	0.142	0.139 ± 0.007	0.0034	0.035 ± 0.005
190	0.132	0.111 ± 0.003	0.0030	0.027 ± 0.002
200	0.125	0.107 ± 0.014	0.0027	0.016 ± 0.006
210	0.130	0.129 ± 0.012	0.0029	0.025 ± 0.002
220	0.121	0.117 ± 0.011	0.0024	0.019 ± 0.004

Table 8.3: Predicted and experimental values of Young's modulus and elastic yield stress for ***microwave*** heated EVA 218 foam, 0.5 phr DCP and 8 phr ADCE

Expansion Temperature / °C	Predicted Young's Modulus (E^*) / MPa	Experimental Young's Modulus (E) / MPa	Predicted Plastic Yield Stress (σ_{el}^*) / MPa	Experimental Plastic Yield Stress (σ_{el}) / MPa
180	0.301	0.479 ± 0.138	0.008	0.051 ± 0.038
190	0.246	0.321 ± 0.020	0.006	0.034 ± 0.005
200	0.242	0.403 ± 0.074	0.005	0.036 ± 0.002
210	0.246	0.333 ± 0.115	0.006	0.035 ± 0.004
220	0.238	0.307 ± 0.033	0.005	0.037 ± 0.003

Table 8.4: Predicted and experimental values of Young's modulus and elastic yield stress for ***microwave*** heated EVA 328 foam, 0.5 phr DCP and 8 phr ADCE

Expansion Temperature / °C	Predicted Young's Modulus (E^*) / MPa	Experimental Young's Modulus (E) / MPa	Predicted Plastic Yield Stress (σ_{el}^*) / MPa	Experimental Plastic Yield Stress (σ_{el}) / MPa
180	0.151	0.163 ± 0.050	0.004	0.025 ± 0.017
190	0.133	0.153 ± 0.014	0.003	0.019 ± 0.001
200	0.128	0.161 ± 0.011	0.003	0.018 ± 0.003
210	0.126	0.128 ± 0.010	0.003	0.018 ± 0.004
220	0.120	0.123 ± 0.005	0.003	0.013 ± 0.001

The theoretical modulus was calculated for all foams using equation 1.18. Although plots of E^*/E_s versus ρ^*/ρ_s showed reasonable linearity, the degree of error made the estimation of ϕ, the polymer fraction in the cell struts, uncertain. Thus, a literature value of 0.85, used previously by others (Zhang *et al.*, 2003) in the modelling of closed cell polyethylene foams by this method, was used. The tensile Young's modulus of crosslinked base polymer samples was determined using the method described in section 2.5.3.2. The experimental values for EVA 218 and 328 were 23.78 ± 1.63 MPa and 12.31 ± 0.98 MPa, respectively.

Generally, the results for the experimental and predicted values for Young's modulus show reasonably good agreement. The experimental values tended to be marginally higher than the predicted values although the results for the EVA 328 conventional foams are marginally lower than predicted. However, within the limits of experimental error, it is suggested that the results are the same. Comparing the modulus results in table 8.1 with 8.3 it may be seen that the experimental and predicted values of Young's modulus were higher for the microwave foamed EVA 218 material than for the conventionally produced EVA 218 foams. This indicated that the microwave foams were stiffer than the comparable conventional foams and offered more resistance to compression. This may be explained by comparison of the density of the foams produced using the two processes. Upon examination of the density results shown in table 7.7, it may be seen that generally, the microwave foams have a higher density than the conventionally produced material. This suggests that the EVA 218 microwave foams had a greater polymer fraction per unit area. As a result, the microwave foams would have thicker struts and cell membranes which in turn would increase the stiffness and compression resistance of the foam, hence the observed increase in modulus. The experimental Young's modulus values for the microwave heated EVA 328 foams appeared to be slightly higher than their respective conventional values. They were, however, closer than the EVA 218 values. Table 7.7 shows that the microwave and conventional EVA 328 foam densities were similar which would explain the closer modulus values. This is supported by the observation that at the highest two expansion temperatures (where expansion may have been more complete) the results for conventional and microwave modulus values were close.

The Young's modulus for EVA 218 was greater than for EVA 328. EVA 218 has a smaller percentage of vinyl acetate groups than EVA 328. The pendant vinyl acetate groups inhibit crystallite formation, thus EVA 328 has a lower degree of crystallinity which adversely affects its mechanical properties (Khunniteekool *et al.,* 1994). The lower crystallinity lowers overall stiffness and thus reduces the modulus. The generally higher error values for the microwave foams suggested that the greater variation in foam density resulted in areas with variable polymer fraction, thus increased variability in compressive modulus was observed.

The predicted values of plastic yield stress were calculated according to equation 1.20, assuming that the internal cell gas pressure was equal to atmospheric pressure. The results were significantly lower than the experimental values. The reasons for this are unclear although it may suggest that there is some stress contribution from the internal cell gas pressure at this point. However, this was thought highly unlikely as these types of man made foams generally have internal cell gas pressures that are less than atmospheric pressure so the contribution to the yield stress can be safely ignored (Zhang *et al.,* 2003; Gibson and Ashby, 1997).

Tables 8.1 and 8.3 show that, the experimental yield point for conventionally foamed EVA 218 was lower than the microwave heated material. With reference to table 7.7, it may be seen that the EVA 218 microwave foam density was slightly greater that the conventional value at each expansion temperature suggesting that expansion was incomplete. The greater polymer fraction per unit area would result in an increased resistance to compressive collapse and would explain the higher microwave yield point. In contrast, the experimental yield point results for conventionally and microwave foamed EVA 328 show reasonably good agreement. If the data in table 7.7 is examined, it may be seen that the foam densities from both heating methods were very similar. This would indicate that the processes produced foams with similar polymer fractions per unit area, hence the similarity in yield stress.

Figures 8.1 – 8.10 show that the experimental values for the cell collapse plateau stress values fit reasonably well with the data predicted using equation 1.21. Generally the predicted values are marginally higher than those determined experimentally and were a closer fit for the EVA 218 data than the EVA 328. This may be attributable to the contribution from internal cell gas pressure being lower

than predicted and would indicate that initial gas pressure was marginally lower than atmospheric pressure (throwing further doubt upon gas pressure stress contributions during the plastic yield phase).

8.3: Summary

Overall, the mechanical properties of the foams decreased as expansion temperature was increased and were greatly influenced by foam density. At higher expansion temperatures, the blowing agent generated gas more efficiently and the viscosity of the polymer decreased allowing greater foam expansion and density reduction. As a result the polymer fraction per unit area was reduced and a consequential reduction in the mechanical performance was observed.

The results for compressive stress as a function of strain presented in figures 8.1 – 8.10 show that foams produced using microwave heating generally had slightly higher stress values at a given strain. This may be attributed to the slightly higher density values of the microwave foams and their increased polymer fraction increasing overall foam stiffness.

CHAPTER 9: SCANNING ELECTRON MICROSCOPY

9.1: Cell Size Measurement

Scanning electron microscopy (SEM) was used to obtain micrograph images of foam samples produced using conventional and microwave techniques. The micrographs were used to determine the mean average cell sizes of the foam samples to determine the effect of processing conditions and method on cell size. Furthermore, the effect of processing temperature on foam skin thickness was also studied. SEM images were studied in preference to optical microscope images for the following reasons. Firstly, the SEM images were extremely well defined with a high depth of field and could be stored electronically for future reference. Secondly, high magnifications were possible that facilitated examination of the cellular structure and calculation of the mean average cell sizes using the scale bar provided on each micrograph.

Great care was needed during the sputter coating process to avoid thermal damage to the foam specimens. EVA 328 samples needed particular care and had to be coated using 5 second intervals with 30 second cooling periods in-between as it was particularly susceptible to thermal damage due to its low melting point. A cross section through the diameter of each foam was taken and five equally spaced samples were taken from each cross section as shown in figure 9.1.

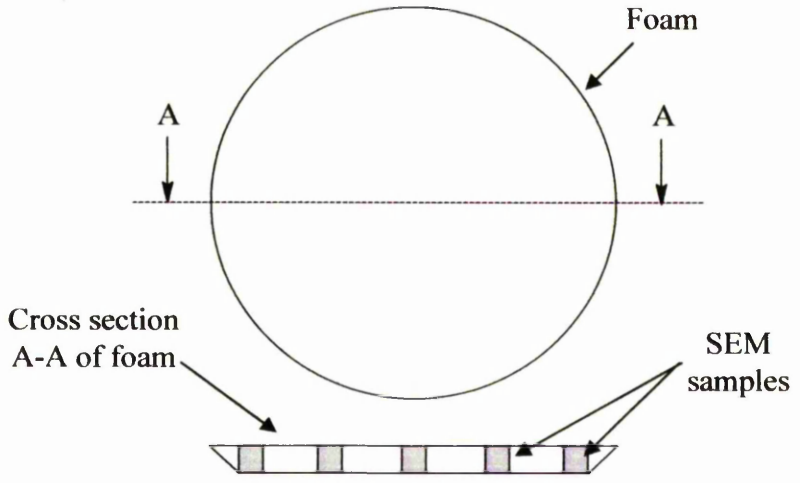

Figure 9.1: Foam sample selection for SEM studies

Samples were taken in this way to provide average cell sizes across the width of the foam samples. Of the five samples, three images were obtained from each. The mean average cell size was then obtained for each polymer, expansion temperature and processing method. The average number of cells counted and size averaged for each foam type was approximately 850. It should be remembered that, although developed standard procedures were followed (Sims and Khunniteekool, 1994), cell size may be considered as a misnomer. When cutting a foam sample, the true cell size or diameter will only be revealed if the cell is cut exactly along its equator. Bisection at any other point will give an apparent cell size that is lower than the actual value. As a result all average cell sizes are always underestimated. Example micrographs for each polymer, expansion temperature and processing method are shown in figures 9.2 and 9.3.

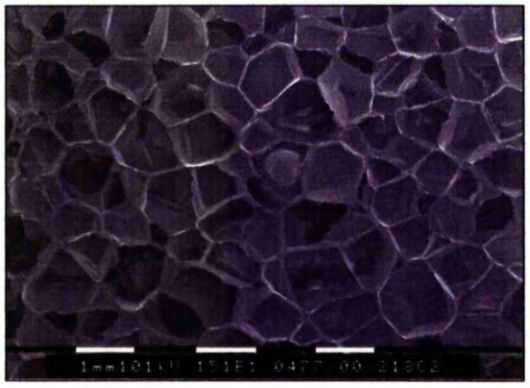

EVA 218 conventional 180 °C

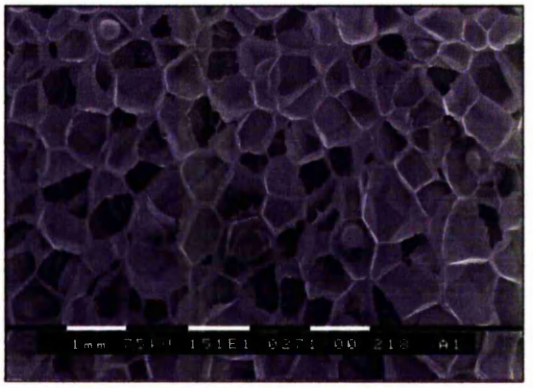

EVA 218 microwave 180 °C

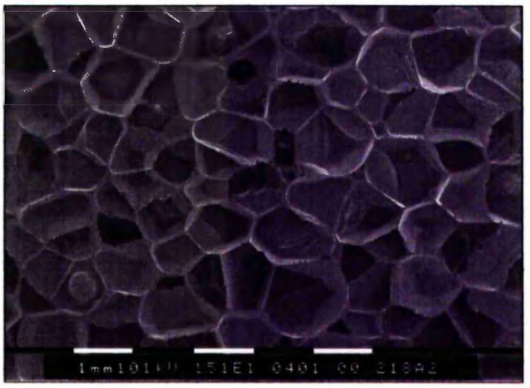

EVA 218 conventional 190 °C

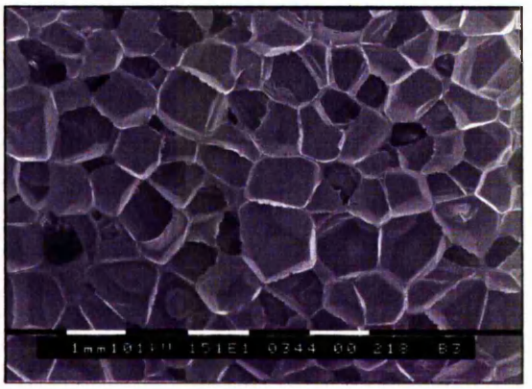

EVA 218 microwave 190 °C

Figure 9.2: EVA 218 foams produced using conventional (left) and microwave techniques (right) at different expansion temperatures (continued overleaf)

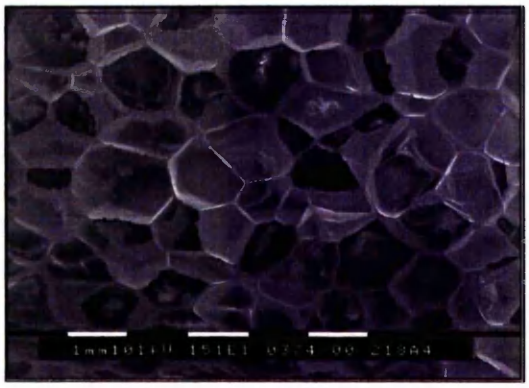

EVA 218 conventional 200 °C

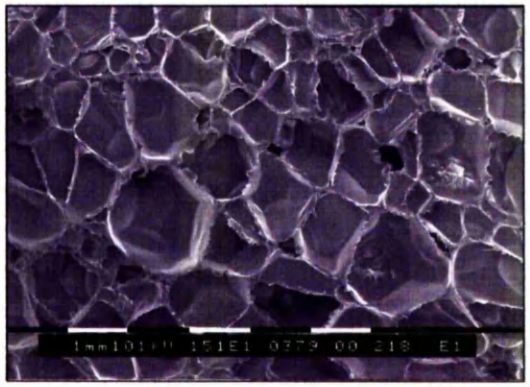

EVA 218 microwave 200 °C

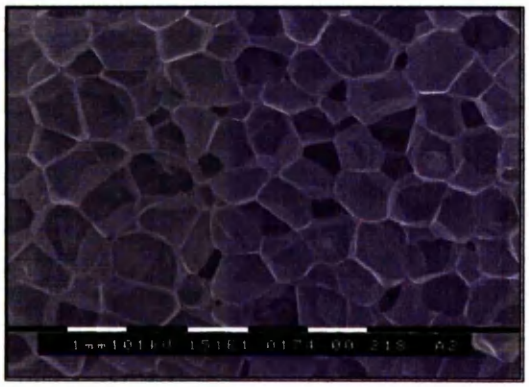

EVA 218 conventional 210 °C

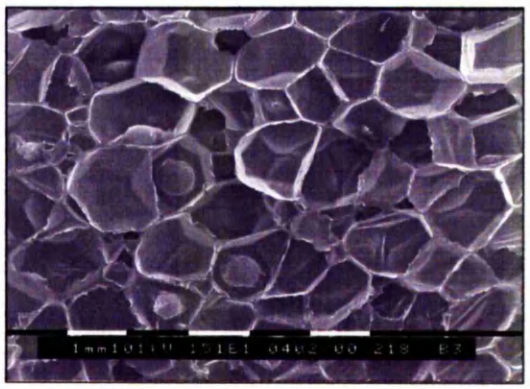

EVA 218 microwave 210 °C

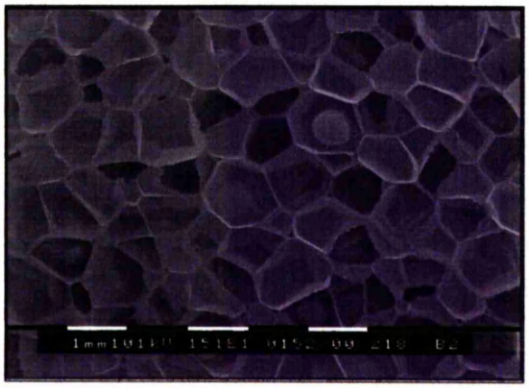

EVA 218 conventional 220 °C

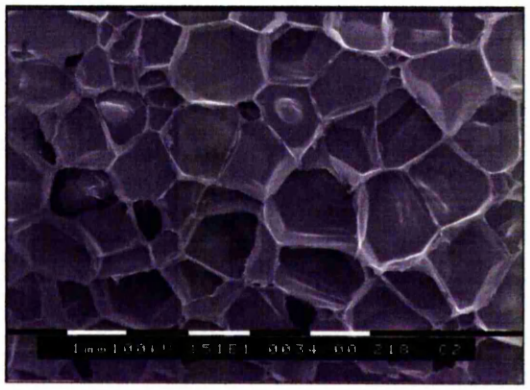

EVA 218 microwave 220 °C

Figure 9.2: EVA 218 foams produced using conventional (left) and microwave techniques (right) at different expansion temperatures (continued)

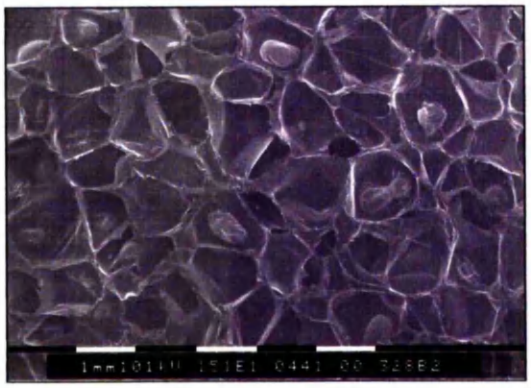

EVA 328 conventional 180 °C

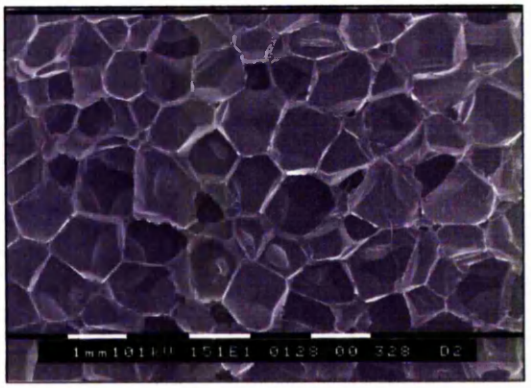

EVA 328 microwave 180 °C

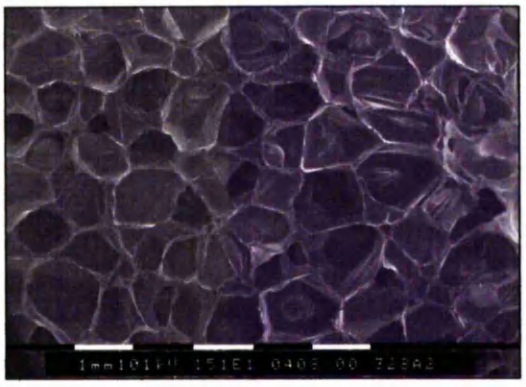

EVA 328 conventional 190 °C

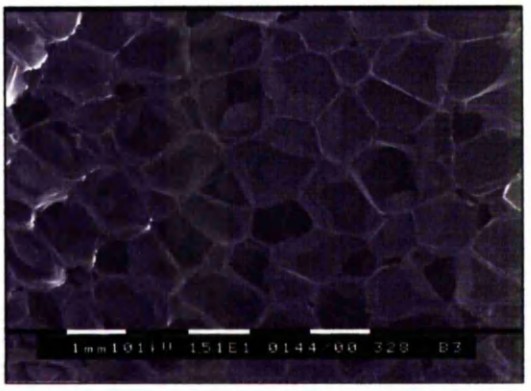

EVA 328 microwave 190 °C

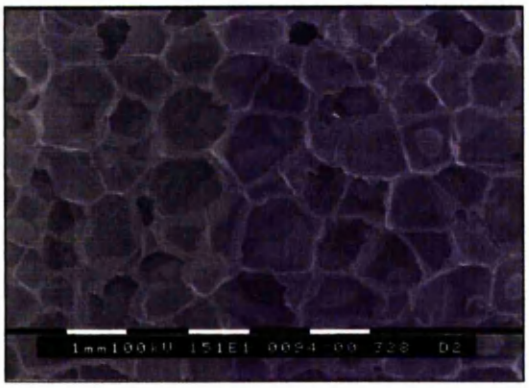

EVA 328 conventional 200 °C

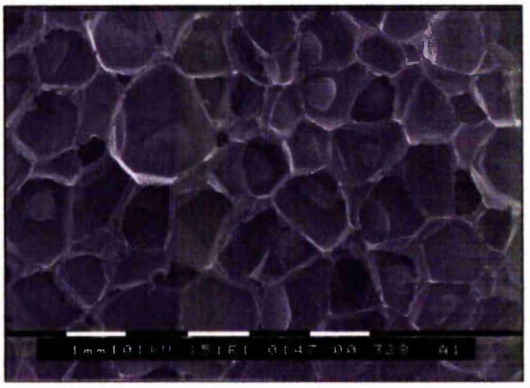

EVA 328 microwave 200 °C

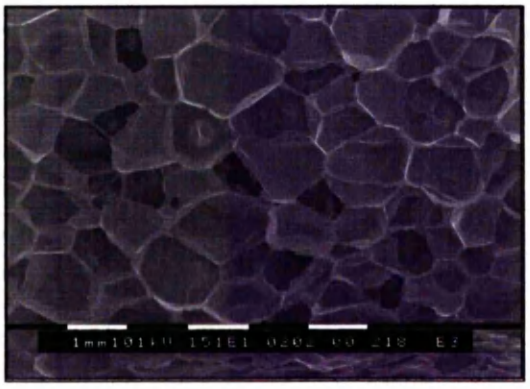

EVA 218 conventional 210 °C

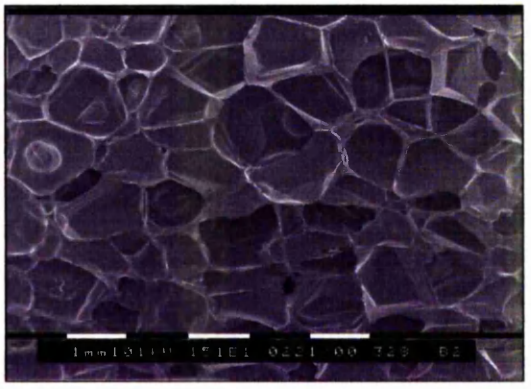

EVA 218 microwave 210 °C

Figure 9.3: EVA 328 foams produced using conventional (left) and microwave techniques (right) at different expansion temperatures (continued overleaf)

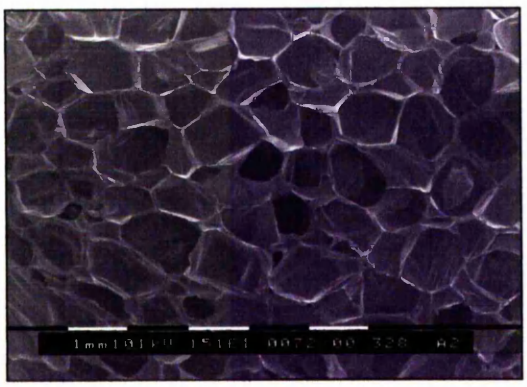

EVA 218 conventional 220 °C

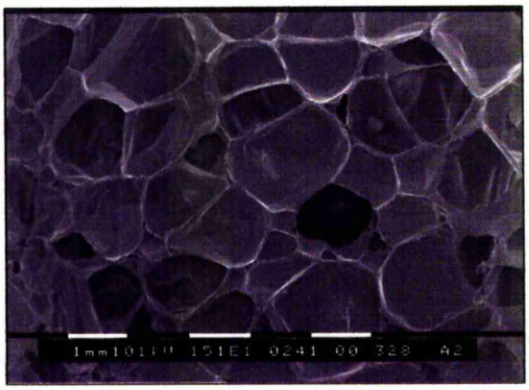

EVA 218 microwave 220 °C

Figure 9.3: EVA 328 foams produced using conventional (left) and microwave techniques (right) at different expansion temperatures (continued)

The micrographs displayed in figures 9.2 and 9.3 show typical cellular structures for the foams based on EVA 218 and EVA 328 heated both conventionally and using microwaves and hot air assistance (170 °C). Observation of figures 9.2 and 9.3 would appear to suggest that the cell sizes of the microwave foamed material are slightly larger than the conventionally produced foam, particularly at the higher expansion temperatures. Determination of cell sizes in this way is, however, highly subjective as the limited number of images shown only represent small fractions of the foamed material. Thus, a more accurate estimation of cell size was performed according to the technique described in section 2.5.2. The mean average cell size results for EVA 218 and 328 foams produced using conventional and microwave heating (with 170 °C hot air assistance) techniques and at a range of expansion temperatures are presented in tables 9.1 and 9.2.

Table 9.1: Mean average cell sizes for conventional and microwave heated EVA 218 foam

Expansion Temperature / °C	**Mean Average Cell Size / mm**	
	Conventional	***Microwave***
180	0.82 ± 0.05	0.85 ± 0.07
190	0.78 ± 0.03	0.75 ± 0.03
200	0.81 ± 0.05	0.93 ± 0.06
210	0.86 ± 0.04	0.99 ± 0.09
220	0.85 ± 0.05	1.06 ± 0.09

Table 9.2: Mean average cell sizes for conventional and microwave heated EVA 328 foam

Expansion Temperature / °C	**Mean Average Cell Size / mm**	
	Conventional	***Microwave***
180	0.88 ± 0.08	0.82 ± 0.09
190	0.85 ± 0.09	0.91 ± 0.07
200	0.89 ± 0.06	0.91 ± 0.06
210	0.82 ± 0.05	0.89 ± 0.07
220	0.87 ± 0.02	0.91 ± 0.06

The data in table 9.1 and 9.2 shows that the mean average cell sizes of the foams produced by both techniques were comparable and were in the range of approximately 0.8 – 1 mm in diameter. The data does suggest that the average cell sizes of the microwave heated foam were slightly higher than the conventionally heated material and support the initial observations made on the micrograph images. However, consideration of the overall error values throws some doubt upon the validity of this conclusion. Areas of increased cell size may be the result of a degree of microwave field non uniformity. This may have resulted in localised areas where the temperature exceeded the set point temperature and sample overheating occurred. Higher melt temperature would result in a lower melt viscosity in these regions (Mahapatro *et al.*, 1998). Consequently, a reduction in melt strength would decrease the resistance of the polymer matrix to the expansive forces of the blowing agent gas and may have allowed larger cells to develop. This argument is supported by the generally larger error values observed for the microwave heated foams which indicate that cell size is more variable and that discrete areas comprising mainly small and mainly large cells existed. However if greater temperatures lowered melt viscosity and created larger cells, a trend of increasing conventional foam cell size with expansion temperature would be expected. This was not observed for the conventionally produced foams and indicated that crosslinking and network restriction may have been the limiting factor in terms of cell size.

Cell size variation in the microwave samples may also be attributed to variable ADCE decomposition gas yields. Figure 3.5 shows that ADCE weight loss was increased and more efficient use of the blowing agent was made at higher temperatures. It has also been shown that as decomposition temperature is increased, the ADCE gas yield

increases significantly (O'Connor, 1999). If, during the microwave foaming process certain areas of the sample exceed the set point temperature whilst some remain below it, the efficiency of ADCE decomposition and subsequent gas yield will vary between these regions. Consequently, different blowing gas volumes may be generated in these areas which could lead to the observed variations in mean average cell sizes.

Conventional cell sizes were, within the limits of experimental error, approximately the same for EVA 218 and EVA 328. The results suggest that the mean average EVA 218 microwave cell size was slightly higher than microwave EVA 328. If it is assumed that maximum cell size is ultimately limited by the network restriction which results from crosslinking, then the difference in gel fraction (at the same crosslinking agent concentration) may cause a difference in the observed cell sizes. The lower gel fraction in 218 (as shown in figure 7.2), is a result of the lower percentage of energetically favourable tertiary hydrogen crosslinking sites. Lower gel fraction would result in lower melt modulus and a correspondingly lower resistance of the molten matrix to the blowing agent gas pressure. This in turn may allow the formation of larger cells.

9.2: Effect of Expansion Temperature on Foam Skin Thickness

The results in tables 7.6 and 7.7 show that the density of the foams produced using both heating methods was significantly affected by the presence of the foam skin. This was particularly noticeable for the low expansion temperature microwave foams where the presence of a significant unfoamed skin increased the overall density of the foam samples. Figure 9.4 shows example cross section images of the skin formed on conventionally foamed samples.

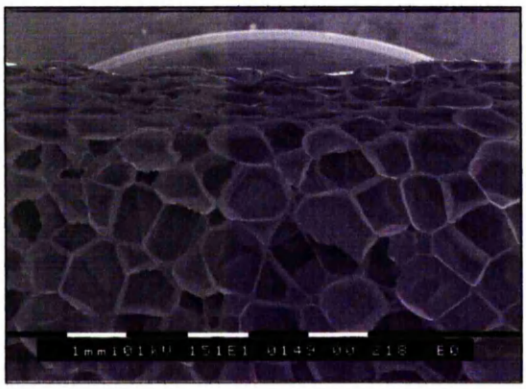

EVA 218 foam edge conventional 220 °C

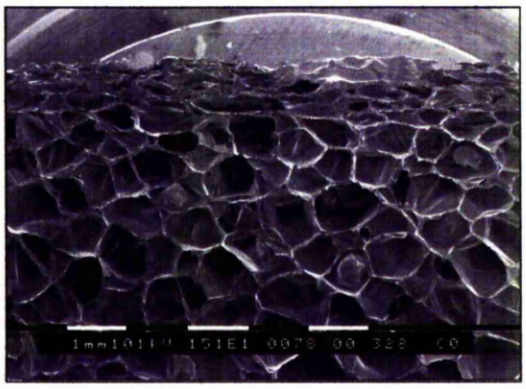

EVA 328 foam edge conventional 220 °C

Figure 9.4: Examples of conventionally heated EVA 218 and EVA 328 foam skin

It was found that the thickness of the conventionally foamed sample skin was independent of expansion temperature and was approximately the same depth for all conventional samples. This was not surprising as conventionally foamed material relied upon conduction of heat through the sample surface to heat and foam the interior. Naturally therefore, foaming occurred at the sample surface first resulting in consistent skin thickness between samples.

The density results in table 7.6 where foam skin was included and visual observations of the samples suggested that a region of unfoamed material was present and surrounded each of the foam samples. Thus, SEM was used to evaluate the extent of the unfoamed skin region and determine the effect of expansion temperature upon it. Figure 9.5 shows cross section images of the skin formed on foam samples of EVA 218 and EVA 328 produced using microwave heating with 170 °C hot air assistance. The samples were taken from same locations on each foam (half way between the sample edge and the centre).

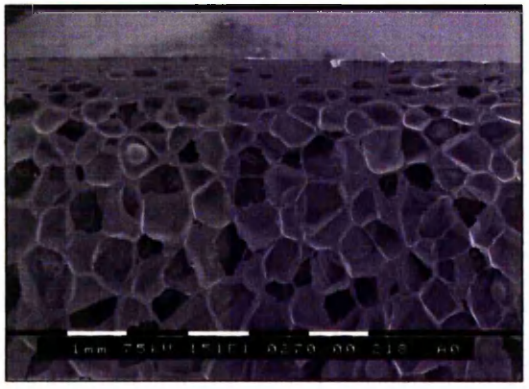

EVA 218 microwave foam edge 180 °C

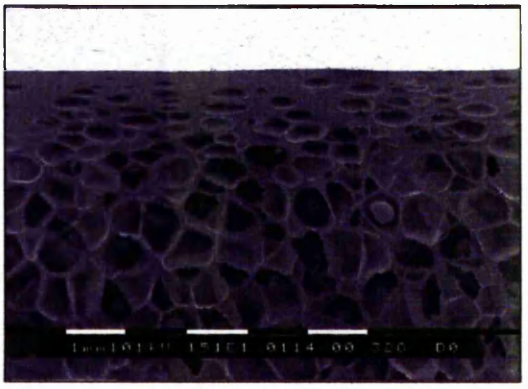

EVA 328 microwave foam edge 180 °C

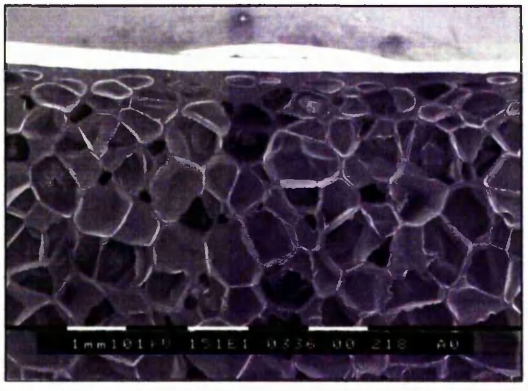

EVA 218 microwave foam edge 190 °C

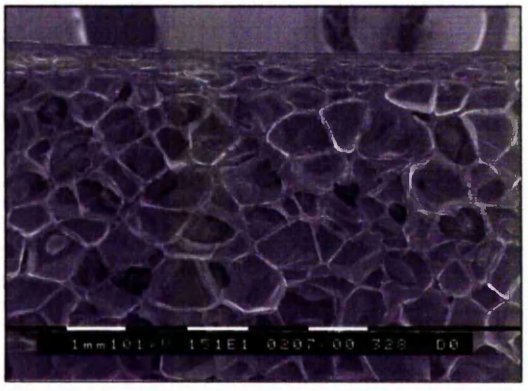

EVA 328 microwave foam edge 190 °C

Figure 9.5: Examples of microwave heated EVA 218 and EVA 328 foam skin cross sections (continued overleaf)

EVA 218 microwave foam edge 200 °C

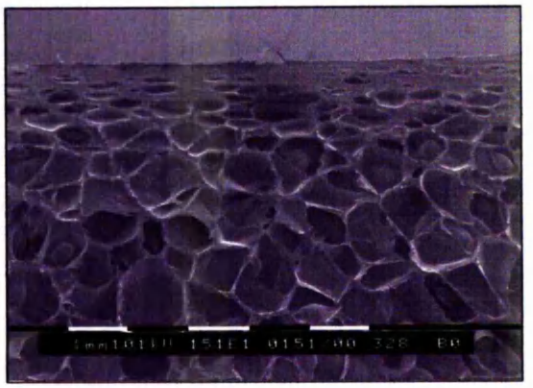

EVA 328 microwave foam edge 200 °C

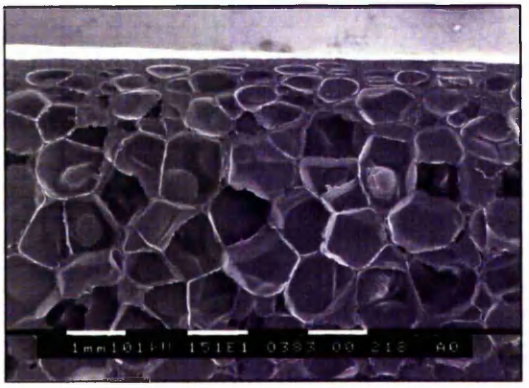

EVA 218 microwave foam edge 210 °C

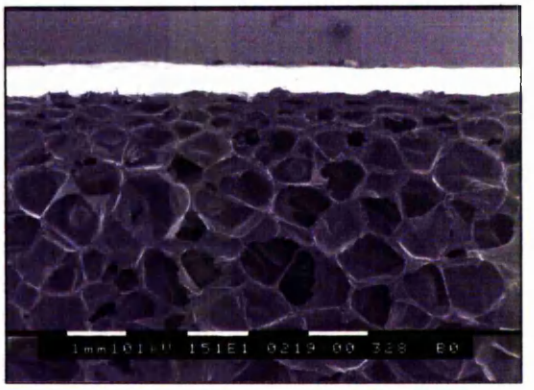

EVA 328 microwave foam edge 210 °C

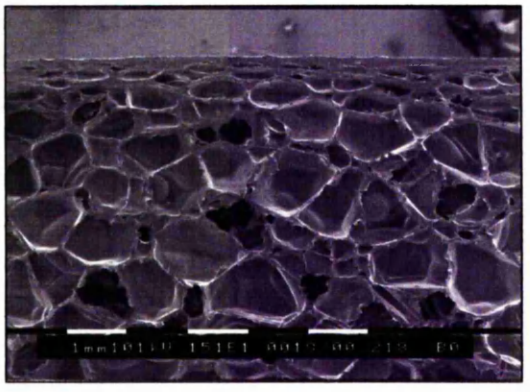

EVA 218 microwave foam edge 220 °C

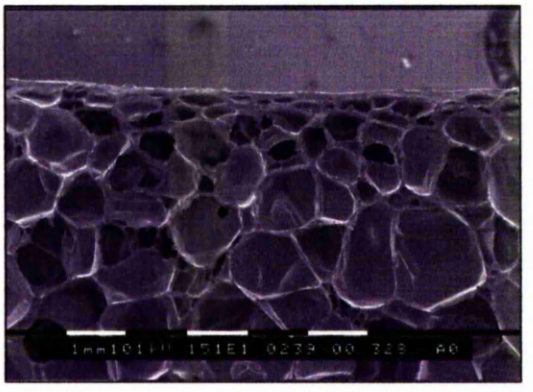

EVA 328 microwave foam edge 220 °C

Figure 9.5: Examples of microwave heated EVA 218 and EVA 328 foam skin cross sections (continued)

An estimation was made of the average skin thicknesses of the foams made using conventional heating and hot air assisted (170 °C) microwave heating methods. Five separate micrograph images were analysed for each polymer, expansion temperature and heating method. The skin thickness was measured using a ruler and then

converted to an actual thickness using the magnification scale bar provided on each micrograph. The results are presented in table 9.3.

Table 9.3: Estimated average foam skin thickness for EVA foams produced using conventional and microwave techniques and a range of expansion temperatures

Expansion Temperature / °C	Foam Skin Thickness / mm			
	EVA 218		EVA 328	
	Conventional	*Microwave*	*Conventional*	*Microwave*
180	0.08 ± 0.05	0.48 ± 0.25	0.03 ± 0.01	0.55 ± 0.37
190	0.06 ± 0.02	0.34 ± 0.07	0.03 ± 0.01	0.32 ± 0.10
200	0.05 ± 0.04	0.22 ± 0.10	0.04 ± 0.01	0.29 ± 0.11
210	0.03 ± 0.01	0.21 ± 0.04	0.03 ± 0.01	0.17 ± 0.07
220	0.04 ± 0.01	0.23 ± 0.06	0.02 ± 0.02	0.14 ± 0.07

The results in table 9.3 show that the conventionally produced foam skin thickness was approximately the same (within the error margins) for EVA 218 and EVA 328. This was expected as the differing vinyl acetate content of the two polymers was unlikely to affect the conventional heating process. It is also noticeable that increasing expansion temperature did not appear to affect the conventional foam skin thickness. Conventional foaming occurred at the sample surface first regardless of expansion temperature and was therefore unlikely to be affected by it unless extreme expansion temperatures were used, in which case polymer degradation, foam collapse and skin thickening may have occurred

On comparison of the two processing methods, it is evident that the skin formed on the microwave heated samples was significantly thicker than on those produced using conventional means. This trend was observed for foams based on both EVA 218 and EVA 328 indicating that it was due to the heating process rather than the base polymer. The increased skin thickness suggests that heat loss from the sample surface was still having an effect on the expansion process at the sample extremities despite the inclusion of supplementary hot air assistance of 170 °C. However, increasing the expansion temperature appeared to reduce the effect of heat loss as a trend of decreasing foam skin thickness with increasing expansion temperature was observed. The microwave skin thickness for the two different polymers was approximately the

same, given the error margins, at each expansion temperature which supports the proposal that the skin thickness was due to the process rather than the polymer.

9.3: Summary

The results in this chapter indicate that the mean average cell sizes of the foams produced using microwave energy were marginally larger than those observed in the conventionally heated and foamed material (although the error margins limit the degree of validity of these findings). This was attributed to a certain degree of microwave field non uniformity resulting in sample temperature gradients and some uneven foaming.

The increased microwave foam thickness (when compared to conventional foams) was attributed to heat losses through the sample surface. Increasing the microwave expansion temperature appeared to reduce overall microwave foam skin thickness.

CHAPTER 10: CONCLUSIONS AND FURTHER WORK

10.1: Conclusions

- The loss factor of EVA increased with increasing vinyl acetate content due to increased polymer polarity. Thus, as the vinyl acetate content was increased, the polymers contained more polar sites which were able to interact with the microwave field and convert the electrical energy to heat.

- The dielectric loss of EVA increased with increasing temperature due to an increase in molecular and dipole freedom. The increased molecular freedom arose from the polymer viscosity reduction as the temperature was increased. It was also concluded that melting of the polymer crystalline regions also increased molecular freedom and dielectric loss. This was supported by observed increases in heating rate (at constant microwave power) at the respective polymer melting regions. Furthermore as the polymer vinyl acetate content was increased (and crystallinity was, therefore, decreased) the increase in heating rate became less pronounced indicating that melting of the crystalline regions was responsible.

- Dicumyl peroxide (DCP) is not polar, however, heating using microwave energy was possible. It was concluded that interaction between the clay support material and the microwave field facilitated microwave heating. Increases in DCP loss were observed in the DCP melting, and the dissociation temperature ranges due to increased molecular freedom and the formation of polar dissociation products respectively.

- The dielectric loss of ADCE showed little change whilst heating to its decomposition temperature. Upon reaching its decomposition temperature ADCE sublimed and evolved gas (mainly nitrogen), it was reasoned, therefore, that no thermal transitions took place before this point such as melting which would increase molecular freedom and hence affect dielectric loss.

- Heating pure LDPE in the waveguide was not possible. A vinyl acetate content of at least 6 % by weight was necessary to increase the loss factor of polyethylene to a level where microwave heating became feasible.

- The initial foam samples made using the waveguide were well foamed in the sample interior but this was surrounded by a thick unfoamed skin. This demonstrated that there was a need for supplemental hot air heating in addition to the microwave energy. It was suggested that heat loss from the sample surface to the surrounding air (at ambient temperature) was the cause of the unfoamed areas.

- The inclusion of cells in the polymer matrix (foaming) reduced the loss factor of the overall system because the cells essentially contained air which is loss free. Therefore, foaming using microwave radiation and maintaining isotherm foaming temperatures became progressively harder as blowing agent decomposition, cell formation and foam expansion took place.

- Microwave field distribution simulations of the combination microwave / hot air oven at frequency ranges of 2.3-2.5 GHz and 6-8 GHz showed that the field was more uniform at the higher frequency range. The lower frequency range was used for processing due to serious reliability problems with the high frequency TWT amplifier.

- Microwave crosslinking of the EVA base polymers was shown to be less effective than conventional crosslinking. It was thought that heat losses from the sample surfaces may have resulted in temperature gradients throughout the samples.

- A reaction rate study on dicumyl peroxide using conventional DSC and microwave calorimetry showed that the reaction rate was slightly slower when using microwave heating.

- Foams based on EVA 218 and 328 were produced using microwave heating alone. The samples were poorly expanded with large portions of the sample remaining unfoamed. Furthermore it was discovered that the majority of foaming in these samples occurred in the centre of the samples which indicated that, despite the field simulations, the majority of the microwave energy was localised in the centre

of the cavity. However, the sample centres showed clear signs of foaming and indicated that if more microwave heating power had been available the temperature of the sample extremities could have been increased and foaming may have been more uniform.

- Batch foam production using variable frequency microwave heating (2.3-2.5 GHz) and 170 °C hot air assistance was achieved. The foams were based on EVA 218 and EVA 328. It was not possible to produce foams based on EVA 206 as its dielectric loss made it unsuitable for heating in this way given the available power.

- The addition of hot air assistance heating (low enough temperature as to cause negligible blowing agent decomposition) to the microwave heating process reduced the effect of heat loss from the sample surface and vastly improved the degree of expansion and foam quality. It was concluded that the hot air raised the loss factor of the sample extremities to a level where the efficiency of the microwave material interaction was increased allowing dielectric heating of the samples to the expansion temperatures.

- The density results for the microwave foams were generally higher and showed a greater degree of variation that the conventional foam specimens. This was attributed to a degree of microwave field non uniformity which resulted in localised areas of the sample where the temperature was either above or below the area measured. The TGA decomposition results for ADCE showed that blowing agent efficiency decreased with decreasing temperature. It was concluded that non uniform sample temperature resulted in variable blowing agent gas yield throughout the sample and the observed variation in foam density. However, at higher expansion temperatures, EVA 328 foam density fell below that of the conventionally heated samples. It was surmised that the lower air temperatures associated with the microwave process helped reduce thermal degradation and subsequent foam densification.

- Microwave and conventionally foamed EVA 218 and 328 samples were compression tested. The modulus results for the microwave heated EVA 218 samples were generally higher than the conventional foam values. It was

concluded that the higher density of the microwave EVA 218 samples resulted in increased polymer fraction and therefore higher stiffness. The modulus values for the microwave foamed EVA 328 samples were closer to the conventional foam results. This was attributed to the greater microwave heating efficiency of EVA 328 resulting in lower density values which were more comparable with those of the conventionally heated samples.

- Detailed cellular structure analysis of the foams using scanning electron microscopy revealed that the microwave heated foams had marginally greater mean average cell size and a greater degree of cell size variation which was attributed to sample temperature gradients. SEM analysis also showed that although the skin thickness of the microwave foamed samples was still greater than the conventionally foamed samples, it was greatly reduced by the hot air assistance and reduced further at higher expansion temperatures.

10.2: Further Work

- The dielectric property data suggested using higher frequency would be more efficient as the loss factor of the formulation components was higher although penetration depth may be affected for thick components at higher frequency.

- Study the variation of crosslinking in different areas of samples crosslinked in the VF oven. The results could be compared with the simulated field distribution.

- Polyethylene can be blended with EVA to form a polymer blend with a higher loss factor than polyethylene alone but may have properties closer to polyethylene than EVA copolymer with equivalent vinyl acetate content. It may, therefore, be possible to produce foams using microwave heating that are more comparable to polyethylene foams.

- Gel contents analysis of larger samples produced using the existing combination oven could be performed to determine the gel content variation throughout a larger sample. It is suggested that increasing the number of heating frequencies may reduce sample temperature gradients and more uniformly crosslink the polymer matrix.

- This work attempted to completely separate the effects of conventional and microwave heating on blowing agent decomposition and foam expansion. For this reason, air assistance temperatures were deliberately limited to 170 °C to prevent blowing agent decomposition occurring directly through hot air heating during microwave processing. However, future work may benefit from the use of slightly higher air assistance temperatures and a degree of overlap between the two heating methods. This may help to complete the foaming of the sample skin and bring foam density values closer together.

- Better temperature control may be required to more accurately monitor sample temperature. Temperature measurements at several sample locations may help to reveal the presence of thermal gradients during processing. This information may then be used to modify the process to ensure more even heating and reduce density, mechanical property and cell size variation.

- A polar crosslinking agent could be used in place of DCP that would interact directly with the microwave field and may improve microwave crosslinking efficiency

- Two of the main problems encountered during the foaming process occurred during the crosslinking and expansion phases of the foaming process. Before the sample reached temperatures where crosslinking could take place and thus increase the melt strength, the polymer would melt and begin to flow. This resulted in a tendency of the foaming sample to stick to the oven support and restrict expansion unless liberal quantities of mould release agent were applied to the support. Secondarily, during the expansion phase, the foam often rose to the point where it came into contact with and adhered to the antenna. These would clearly represent serious issues in a commercial production process. Conventional industrial processes avoid this problem by using stainless steel woven mesh belts and floating the blended polymer sheet on a cushion of hot air during expansion.

  It is proposed, therefore, that foaming equipment that more accurately represents a continuous production oven but with the added facility of microwave heating could be designed and constructed. The oven should include a PTFE or stainless steel woven mesh (if arcing can be avoided) belt to avoid adhesion during

crosslinking. The oven should also have the capability to float the sample on an air cushion to allow biaxial expansion during blowing agent decomposition and foaming. This may be achieved using increased airflow underneath the foaming sheet to lift it off the mesh belt. High power magnetrons could also be used as well as a larger oven. A larger oven would have more modes and would therefore compensate for only having a fixed frequency microwave source. Furthermore, the dielectric results presented in chapter 4 strongly suggested that frequencies higher than 2.45 GHz would be more efficient due to increased material loss factor. Mass produced magnetrons operating at 5.8 GHz and at power levels in excess of 800 W have recently become available (Suhm *et al.*, 2003; Kubel, 2005). Using higher frequencies would also have the benefit of supporting increased modes within the oven, further aiding microwave field distribution. It is proposed that the continuous oven should be divided into two or more heating zones to allow separation of the crosslinking and expansion phases of the foaming process. An oven design is outlined schematically in figure 10.1.

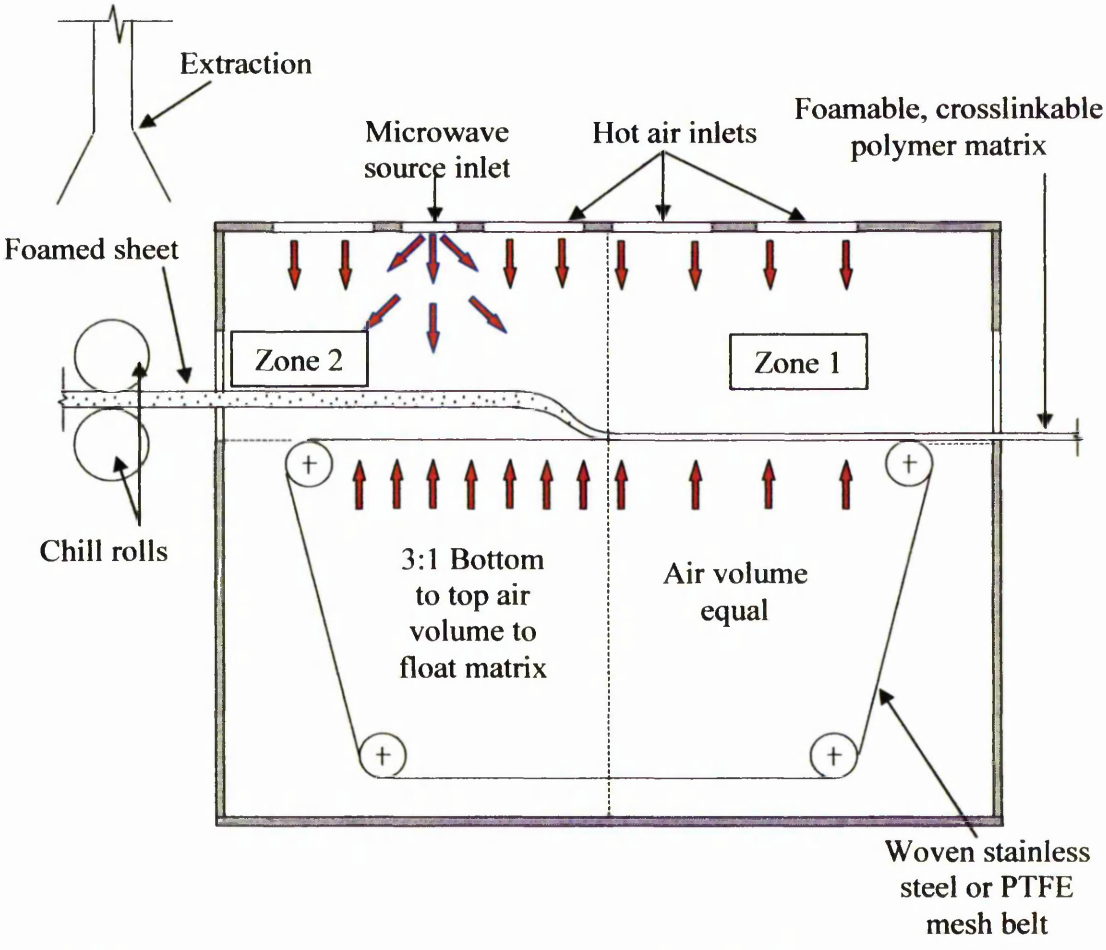

Figure 10.1: Proposed continuous microwave / hot air combination foaming oven

It would be necessary to measure air temperatures using probes that do not interact with microwave energy such as those used in this work. It may not be possible to measure the moving polymer temperature directly using temperature probes. The matrix surface temperature could, however, be measured using infrared pyrometers. Adequate steps must also be taken to avoid leakage of microwave energy from the entrance and exit of the oven.

REFERENCES

Akzo Nobel Chemicals Ltd., *Polymer Chemicals Product Information Trade Literature / Personal Communication,* 2001.

O. Almanza, M.A. Rodriguez-Perez, J.A. de Saja, *The Microstructure of Polyethylene Foams Produced by a Nitrogen Solution Process,* Polymer, Vol. 42, p 7117-7126, 2001.

A. Arefmanesh and S.G. Advani, *Nonisothermal Bubble Growth in Polymeric Foams,* Polymer Engineering and Science, Vol. 35, p 252-260, 1995.

M. Asaaka, K. Torii, E. Yamanaka, Japan. Kokai Tokkyo Koho (To Hitachi Chemical Company Ltd), *43-22 674*, 1968.

ASTM D 3575-00, *Standard Test Methods for Flexible Cellular Materials Made from Olefin Polymers*, ASTM, Philadelphia, Pa. 2000.

M.E. Baird and E. Houston, *Dielectric Behaviour of Ethylene-Vinyl Acetate Copolymers,* Polymer, Vol. 16, p 308-310, 1975.

U. Bandara, *A Systematic Solution to the Problem of Sample Background Correction in DSC Curves,* Journal of Thermal Analysis, Vol. 31, p 1063 – 1071, 1986.

C.J. Benning, *Polyethylene Foam II - Orientation in Thermoplastic Foams,* Journal of Cellular Plastics, Vol. 3, p 174-184, 1967.

C.J. Benning, *Plastic Foams,* Vol. 1, John Wiley and Sons, New York, 1969.

J.J. Bikerman, *Foams,* Springer – Verlag, New York, 1973.

F.W. Billmeyer Jr., *Textbook of Polymer Science, 2nd Ed.*, John Wiley and Sons Inc., New York, 1971.

F.A. Blair, *Cell Structure: Physical Property Relationships in Elastomeric Foams*, Conference, Cellular Plastics, Nattick, USA, p 143 - 152, 1968.

J. Brandrup, E.H. Immergut and E.A. Grulke, *Polymer Handbook, 4th Edition*, Wiley-Interscience, New York, 1999.

D.W. Brazier and N.V. Schwartz, *The Cure of Elastomers by Dicumyl Peroxide as Observed in Differential Scanning Calorimetry,* Thermochimica Acta, Vol. 39, p 7 – 20, 1980.

S. Bringhurst, M.F. Iskander and M.J. White, *Thin-Sample Measurements and Error Analysis of High-Temperature Coaxial Dielectric Probes,* IEEE Transactions on Microwave Theory and Techniques, Vol. 45, p 2073-2083, 1997.

Yu. V. Bykov, K.I. Rybakov, V.E. Semenov, *High-Temperature Microwave Processing of Materials,* Journal of Physics D: Applied Physics, Vol. 34, p55-75, 2001.

D. Campbell and J.R. White, *Polymer Characterization Physical Techniques,* Chapman and Hall, London and New York, 1989.

E.C.L. Cardoso, A.B. Lugao, E. Andrade, L.G. Silva, *Crosslinked Polyethylene Foams, Via EB Radiation,* Radiation Physics Chemistry, Vol. 52, p 197-200, 1998.

P. Cassagnau and A. Michel, *Continuous Crosslinking of Ethylene Vinyl Acetate and Ethylene Methyl Acrylate Copolymer Blends by On-Line Microwave Heating,* Polymer Science and Engineering, Vol. 34, p 1011-1015, 1994.

A. Chatterjee, T. Basak, and K. G. Ayappa, *Analysis of Microwave Sintering of Ceramics,* AIChE Journal, Vol. 44, p 2302-2311, 1998.

ChemFinder, http://chemfinder.cambridgesoft.com/result.asp, 2005.

M. Chen, E.J. Siochi, T.C. Ward and J.E. McGrath, *Basic Ideas of Microwave Processing of Polymers,* Polymer Engineering and Science, Vol. 33, p 1092-1109, 1993.

M. Chen, J.W. Hellgeth, T.C. Ward and J.E. McGrath, *Microwave Processing of Two-Phase Systems: Composites and Polymer Blends,* Polymer Engineering and Science, Vol. 35, p 144-150, 1995.

L. Chen, C.K. Ong, and B.T.G. Tan, *A Resonant Cavity for High-Accuracy Measurements of Microwave Dielectric Properties,* Measurement Science and Technology, Vol. 7, p 1255-1259, 1996.

P. Choquet, M. Quirion and F. Juneau, *Advances in Fabry-Perot Fiber Optic Sensors and Instruments for Geotechnical Monitoring,* Geotechnical News, March 2000.

A.E.S. Clarke, *Cellular Cross – Linked Polyolefins and Initial Studies in Foaming Poly (Vinyl Alcohol),* M.Sc. Dissertation, UMIST, 2000.

J.S Colton and N. P. Suh, *The Nucleation of Microcellular Thermoplastic Foam with Additives: Part I: Theoretical Considerations*, Polymer Engineering and Science, Vol. 27, p 485-492, 1987 **(a)**.

J.S Colton and N. P. Suh, *The Nucleation of Microcellular Thermoplastic Foam with Additives: Part II: Experimental Results and Discussion*, Polymer Engineering and Science, Vol. 27, p 493-499, 1987 **(b)**.

J.S Colton and N. P. Suh, *The Nucleation of Microcellular Thermoplastic Foam with Additives: Theory and Practice*, Polymer Engineering and Science, Vol. 27, p 500-503, 1987**(c)**.

S. Curran, *Evaluation of the Feasibility of Microwave Processing of Polymer Foams,* M.Sc. Dissertation, Manchester Materials Science Centre, UMIST, 1998.

T. De Meuse, C.L. Ryan, E. Occhiello, R. Po and F. Garbassi, *The Chemistry and Processing of Polymeric Materials at Microwave Frequencies,* Polymer News, Vol. 16, p 262-265, 1991.

R.D. Deanin, *Foamed Plastics*, ACS Symposium, Vol. 285, p 469-494, 1985.

S.K. Dutta, A.K. Bhowmick and T.K. Chaki, *Structure Property Relationship of Ethylene Vinyl Acetate Copolymer Grafter with Triallyl Cyanurate by Electron Beam Radiation,* Radiation Physics Chemistry, Vol. 47, p 913-926, 1996.

D.E. Eaves, *New Foams from the Nitrogen Autoclave Process,* Cellular Polymers, Paper 3, 2nd International Conference, Edinburgh, 1993.

D.E. Eaves, *Ethylene Homo and Copolymer Foams,* Journal of Cellular Polymers, Vol. 7, p 297-308, 1988.

D.E. Eaves and N. Witten, *Product and Process Developments in the Nitrogen Autoclave Process for Polyolefin Foam Manufacture,* SPE Antec, Vol. 2 p 1842-1849, Atlanta, 1998.

ERP (Expanded Rubber and Plastics Ltd) (A. Cooper), *U.K Pat 899389,* 1961.

ERP (Expanded Rubber and Plastics Ltd) (A. Cooper), *U.S. Pat 3640915,* 1972.

Exxon, *EVA Product Data Sheet,* 2004.

Fiso, *Fiber Optic Sensors Product Datasheet FOT-L/FOT-H Temperature Sensors,* http://www.fiso.com/themes/roctest/pdf/mc-00028r7_pds-FOT-L_FOT-H.pdf, 2005.

K.C. Frisch and J.H. Saunders, *Plastic Foams,* Part 1, Marcel Dekker Inc. New York, 1972.

I. Garcia-Ruiz and C. D. Aviles-Castro, *Measuring Complex Permittivity of Materials for Frequencies Under 18 GHz,* Applied Microwave and Wireless, Vol. 13 p 56-66, 2001.

Z. Ghazali, A.F. Johnson, K.Z. Dahlan, *Radiation Crosslinked Thermoplastics Natural Rubber (TPNR) Foams,* Radiation Physics and Chemistry, Vol. 55, p 73-79, 1999.

A.N. Gent and A.G. Thomas, *The Deformation of Foamed Elastic Materials,* Journal of Applied Polymer Science, Vol. 1, p 107-113, 1959.

D.L. Gershon, J.P. Calame, T.M. Antonsen and R.M. Hutcheon, *Open-Ended Coaxial Probe for High-Temperature and Broad-Band Dielectric Measurements,* IEEE Transactions on Microwave Theory and Techniques, Vol. 47, p 1640-1648, 1999.

D. Gheysari and A. Behjat, *Radiation Cross-linking of LDPE and HDPE With 5 and 10 MeV Electron Beams,* European Polymer Journal, Vol. 37, p2011-2016, 2001.

L.T. Gibson and M.F. Ashby, *The Mechanics of Cellular Solids,* Proceeding of the Royal Society, A382, 43. 1982.

L.T. Gibson and M.F. Ashby, *Cellular Solids Structure and Properties – Second Edition,* Cambridge University Press, Cambridge, 1997.

P.J. Haines, *Thermal Methods of Analysis, Principles, Applications and Problems,* Blackie Academic and Professional, Glasgow, 1995.

R.H. Harding, *Relationships Between Cell Structures and Rigid Foam Properties,* Journal of Cellular Plastics, Vol. 1, p385 – 394, 1965.

R.H. Harding, *Morphologies of Cellular Material. Resinography of Cellular Plastics,* American Society of Testing Materials, ASTM-STP 414, 1967.

N.C. Hilyard, *Mechanics of Cellular Plastics,* Applied Science Publishers Ltd., London, 1982.

C.N. Hilyard and A. Cunningham, *Low Density Cellular Plastics: Physical Basis of Behaviour,* Chapman and Hall, London, 1994.

Y. Hoshi, I. Sakamoto, K. Mizusawa and M. Kashiwagi, *Recent Developments in EB Processing Equipment,* Radiation Physics and Chemistry, Vol. 46, p 477-480, 1995.

K. Hosoda, N. Shina, (To Furukawa Electric Company Ltd), *U.S. Pat 3651183,* 1972.

M. Huskic and A. Sebenic, *Characterisation of Crosslinked Ethylene-Vinyl acetate Copolymers,* Polymer International, Vol. 31, p 41-44, 1993.

F. Iannace, S. Iannace, G. Caprino and L. Nicolais, *Prediction of Impact Properties of Polyolefin Foams,* Polymer Testing, Vol. 20, p 643-647, 2001.

H.A.S. Jaafar and G.L.A. Sims, *The Thermal Decomposition of Azodicarbonamide (ADC),* Cellular Polymers, Vol. 12, p 303-315, 1993.

J. Jacob, L.H.L. Chia, F.Y.C. Boey, *Thermal and Non-Thermal Interaction of Microwave Radiation with Materials,* Journal of Materials Science, Vol. 30, p 5321-5327, 1995.

H-Jer Tai, *Molecular Structure Development in Peroxide-Initiated Cross-linking of an Ethylene Vinyl Acetate Copolymer and a Metallocene Polyolefin Elastomer,* Polymer Engineering and Science, Vol. 39, p 1577-1583, 1999.

J. Jow, M.C. Hawley, M. Finzel, J. Asmussen Jr, H-H, Lin and B. Manring, *Microwave Processing and Diagnosis of Chemically Reacting Materials in a Single-Mode Cavity Applicator,* IEEE Transactions on Microwave Theory and Techniques, Vol. MTT-35, p 1435-1442, 1987.

J. Jow, M.C. Hawley, M. Finzel and T. Kern, *Dielectric Analysis of Epoxy / Amine Resins Using Microwave Cavity Technique,* Polymer Engineering and Science, Vol. 28, p 1451-1454, 1988.

G. Kamp, *Polymer Characterisation,* Hansar Publishers, Munich, 1980.

P.I. Karkanas and I.K. Partridge, *Cure Modeling and Monitoring of Epoxy / Amine Resin Systems. 1. Cure Kinetics Modeling,* Journal of Applied Polymer Science, Vol. 77, p 1419 – 1431, 2000.

M. Katsuya, K. Nobuyoshi, I. Naruyuki and M. Yoshio, Sanwa Kako Company Limited, *Method of producing Open-cell Foams of Cross-linked Polyolefins,* European Patent Application 0526872 A1, 1993.

C. Khunniteekool, G.L.A. Sims and E.F.T. White, *Structure / Property Relationships of Cross-Linked Polyethylene (PE) and Ethylene Vinyl Acetate Copolymer (EVA) Foams*, ASME Cellular and Microcellular Materials, MD-Vol. 53, p 53-61, 1994.

C. Khunniteekool, G.L.A. Sims, *Structure/Property Relationships of Crosslinked Polyethylene (PE) and Ethylene-Vinyl Acetate Copolymer (EVA) Foams*, Cellular and Microcellular Materials, Vol. 53, p 53-61, 1994.

K. Kircher, *Chemical Reactions in Plastics Processing,* Hanser Publishers, Munich, Vienna, New York, 1987.

H.E. Kissinger, *Reaction Kinetics in Differential Thermal Analysis,* Analytical Chemistry, Vol. 29, p 1702 – 1706, 1957.

D. Klempner and K.C. Frisch, *Handbook of Polymeric Foams and Foam Technology,* Hanser Publishers, Munich, Vienna, New York, Barcelona, 1991.

C.J. Kmiec and V.R. Kamath, *Organic Peroxides for Rubber Cross-linking Including New Peroxide Curing Systems,* Lucidol Pennwalt Technical Publication Reprinted in Part From Rubber and Plastics News, Sept 29th 1980.

H.S. Ku, E. Siores, A. Taube, J.A.R. Ball, *Productivity Improvement Through the use of Industrial Microwave Technologies,* Computers and Industrial Engineering, Vol. 42, p 281-290, 2002.

E. Kubel, *Advancements in Microwave Heating Technology,* Special Focus: Microwave Heating, www.industrialheating.com, January 2005.

T.S. Laverghetta, *Modern Microwave Measurements and Techniques,* Artech House, Norwood MA, 1988.

J. Lee, *Microcellular Cross-linked EVA Foams Produced by Injection Moulding Process,* SPE, ANTEC, New York, p 2060-2064, 1997.

Luxtron, *Fluroptic Thermometers 700 Series Technical Brochure,* http://www.luxtron.com/pdf/m790.pdf, 2005.

C. Y. Ma and C. D. Han, *Foam Extrusion Characteristics of Thermoplastic Polystyrene Foam Extrusion Resin with Fluorocarbon Blowing Agent. 11.*, Journal of Applied Polymer Science, Vol. 28, p 2983-2998, 1983.

A. Mahapatro, N.J. Mills and G.L.A. Sims, *Experiments and the Modelling of the Expansion of Crosslinked Polyethylene Foams,* Cellular Polymers, Vol. 15, p 252-270, 1998.

E.D. Maloney and G. Faillon, *A High Power Klystron for Industrial Processing Using Microwaves,* Journal of Microwave Power, Vol. 9, 1974.

G. Menges, G. Hahn, H. Reichstein, *UHF-Schäumen von Polyethylen,* Plastverarbeiter, Vol. 34, p 1488-1492, 1983.

G. Menges, K. Kircher and B. Franzkoch, *Cross-linkage of Polyethylene in the UHF Field, Using Tertiary Butyl Perbenzoate as the Energy Absorber and Radical Former,* Kunststoffe, Vol. 70, p 45-48, 1980.

G. Menges, K. Kircher, B. Franzkoch and W. Hoffacker, *Cross-linking of Polyethylene in the UHF field Using UHF-active Auxiliaries,* Kunststoffe, Vol. 69, p 430-434, 1979.

R. Meredith, *Engineers' Handbook of Industrial Microwave Heating,* Institute of Electrical Engineers, London, 1998.

A.C. Metaxas, *Microwave Heating,* Power Engineering Journal, p 237-247, 1991.

J.M. Methven, *Foams and Blowing Agents,* RAPRA Review, Vol. 3, No. 1, Permagon Press, 1990.

J. Mijovic and J. Wijaya, *Review of Cure of Polymers and Composites by Microwave Energy,* Polymer Composites, Vol. 11, p 184-190, 1990.

N.J. Mills and H.X. Zhu, *The High Strain Compression of Closed Cell Polymer Foams,* Journal of the Mechanics and Physics of Solids, Vol.47, p 669-695, 1999.

H.E. Naguib, C. B. Park, N. Reichelt, *Fundamental Foaming Mechanisms Governing the Volume Expansion of Extruded Polypropylene Foams,* Journal of Applied Polymer Science, Vol. 91, p 2661-2668, 2004.

H. E. Naguib and C. B. Park, *Strategies for Achieving Ultra Low-Density Polypropylene Foams,* Polymer Engineering and Science, Vol. 42, p 1481-1492, 2002.

J.D. Nam and J.C. Seferis, *Application of the Kinetic Composite Methodology to Autocatalytic – Type Thermoset Prepreg Cures,* Journal of Applied Polymer Science, Vol. 50, p 1555 – 1564, 1993.

P. Navabpour, A. Nesbitt, B. Degamber, G. Fernando, T. Mann and R. Day, *Comparison of the Curing Kinetics of the RTM6 Epoxy Resin System Using Differential Scanning Calorimetry and a Microwave-Heated Calorimeter,* Journal of Applied Polymer Science, Submitted 2005.

A. Nesbitt, B. Degamber, C. Nightingale, T. Mann, G. Fernando and R. J. Day, *Development of a Microwave Calorimeter for Simultaneous Thermal Analysis,*

Infrared Spectroscopy and Dielectric Measurements, Measurement Science and Technology, Vol. 15, p 2313 – 2324, 2004.

C. O'Connor, *Chemical Blowing Agent Systems for Polymer Foam Manufacture,* PhD Thesis, UMIST, 1999.

T.A Osswald and G. Menges *Materials Science of Polymers for Engineers,* Hanser, Munich, 1996.

J. Pallay, P. Kelemenla, H. Berghmans, D. V. Dommelen, *Expansion of Polystyrene Using Water as the Blowing Agent,* Macromolecular Materials and Engineering, Vol. 275, p 18-25, 2000.

M. Palumbo and E. Tempesti, *On the Nodular Morphology and Mechanical Behaviour of a Syntactic Foam Cured in Thermal and Microwave Fields,* Acta Polymer. Vol. 49, p 482-486, 1998.

C.B. Park and L. K. Cheung, *A Study of Cell Nucleation in the Extrusion of Polypropylene Foams,* Polymer Engineering and Science, Vol. 37, p 1-10, 1997.

C.B. Park, D.F. Baldwin and N.P. Suh, *Effect of Pressure Drop on Cell Nucleation in Continuous Processing of Microcellular Polymers,* Polymer Engineering and Science, Vol. 35, p 432-440, 1995.

W. Pip, (To Rohm GmbH), *Method for Foaming Synthetic Resin Bodies With Microwave or High Frequency Energy,* U.S. Patent 4740530, 1988.

D. Porter, W.S. Campbell, E.W. Duck, Assigned to The International Synthetic Rubber Company Ltd, *Process for Producing Moulded Foams From Rubber Lattices by Using Microwave Heating,* U.S. Patent 3737488, 1973.

A.S. Prakash, W.A. Swann, A.N. Strachan, *The Thermal Decomposition of Azodicarbonamide (1,1-Azobisformamide),* Journal of the Chemical Society, Part 1, p 46-50, 1975.

Y. Prasad, K.D.V, Yarlagadda, T.C. Chai, *An Investigation into Welding of Engineering Thermoplastics Using Focused Microwave Energy,* Journal of Materials Processing Technology, Vol. 74, p 199-212, 1998.

R.R. Puri and K.T. Collington **(a)**, *The Production of Cellular Cross-linked Polyolefins-Part 1,* Cellular Polymers, Vol. 7, p56-84, 1988.

R.R. Puri and K.T. Collington **(b)**, *The Production of Cellular Cross-linked Polyolefins-Part 2-The Injection Moulding and Press Moulding Techniques,* Cellular Polymers, Vol. 7, p219-231, 1988.

S. Quinn, *Chemical Blowing Agents: Providing Production, Economic and Physical Improvements to a Wide Range of Polymers,* Plastics Additives and Compounding, p16-21, May 2001.

J.F. Rabek, *Experimental Methods in Polymer Chemistry*, Wiley Interscience, New York, 1980.

D.A. Reed and H.E. Lunk, *U.S. Pat 4560829,* 1985.

M.A. Rodriguez-Perez, O. Alonso, J. Souto and J.A. de Saja, *Thermal Conductivity of Crosslinked Closed Cell Polyolefin Foams,* Polymer Testing, Vol.16, p 287-298, 1997.

N. Sagane, S. Nakata, H. Ueda, T. Matsumura (To Sekisui Chemical Company Ltd), *U.S. Pat 3711584*, 1973.

M.A. Shafi, J.G. Lee and R.W. Flumerfelt, *Prediction of Cellular Structure in Free Expansion Polymer Foam Processing*, Polymer Engineering and Science, Vol. 36, p 1950-1959, 1996.

M.A. Shafi, K. Joshi and R.W Flumerfelt, *Bubble Size Distributions in Freely Expanded Polymer Foams,* Chemical Engineering Science, Vol. 52, p 635-644, 1997.

Y.A. Shangin, V.G. Baranovand L.V. Makarova, *Crystallization Study of Copolymers of Ethylene with Vinyl Acetate,* Polymer Science U.S.S.R, Vol.31, p 2183-2188, 1989.

I. R. Shankland, *CFC Alternatives for Thermal Insulation Foam,* International Journal of Refrigeration, Vol. 13, p 113-121, 1990.

N. I. Sheen and I. M. Woodhead, *An Open-ended Coaxial Probe for Broad-band Permittivity Measurement of Agricultural Products,* Journal of Agricultural Engineering, Vol. 74, p 193-202, 1999.

N. Shiina, M. Tsuchiya and H. Nakae, *Properties and Application Techniques of Cross-linked Polyolefin Foams,* Japan Plastics Age, Vol. 40, p 37-48, 1972.

T. Shinohara, T. Takahashi, K. Yamagudi (To Toray Industries Chemical Company Ltd), *U.S. Pat 3562367*, 1971.

J. Simonik and J. Svoboda, *Simulation of Chemical Foaming of Polymers,* Cellular Polymers, Vol. 9, p 1- 11, 1990.

G.L.A. Sims and H.A.S. Jaafar, *A Chemical Blowing Agent System (CBAS) Based on Azodicarbonamide,* Journal of Cellular Plastics, Vol. 30, p 175-188, 1994.

G. L. A. Sims and C. Khunniteekool, *Cell Size Measurement of Polymeric Foams*, Cellular Polymers, Vol. 13, p 137-146, 1994.

G. L. A. Sims and C. Khunniteekool, *Cell Structure Development in Compression Moulded Polyethylene and Ethylene-Vinyl Acetate Copolymer Foam*, Cellular Polymers III, RAPRA Technology, Paper 13, Coventry, 1995.

G. L. A. Sims and C. Khunniteekool, *Compression Moulded Ethylene Homo and Copolymer Foam I. Effect of Formulation*, Cellular Polymers, Vol. 15, p 1-13, 1996**(a)**.

G. L. A. Sims and C. Khunniteekool, *Compression Moulded Ethylene Homo and Copolymer Foam II. Effect of Processing Conditions and Crystallinity on Cell Structure Development*, Cellular Polymers, Vol. 15, p 14 -29, 1996 **(b)**.

G.L.A. Sims and C. O' Connor, *Modification of Azodicarbonamide Decomposition Characteristics: Interface with Base Polymer and Process Parameters,* Blowing Agent Systems, RAPRA Technology, Shawbury, Paper 2, February 1998.

R.E. Skochdopole and L.C. Rubens, *Physical Property Modifications of Low Density Polyethylene Foams,* Journal of Cellular Plastics, Vol. 1, p 91-96, 1965.

A. Smith, *Zotefoams to Double Output of Nitrogen Foamed Sheet,* Plastics Additives and Compounding, p 32-37, 2000.

K.W. Suh and D.D. Webb, *Cellular Materials,* Encyclopedia of Polymer Science and Engineering, 2nd Edition, John Wiley and Sons, New York, Vol. 3, 1985.

J. Suhm, M. Moller and H. Linn, *New Development for Industrial Microwave Heating,* International Scientific Colloquium; Modelling for Electromagnetic Processing, Hannover, p 131-135, March 24-26, 2003.

B.A. Sultan and E. Sorvik, *Thermal Degradation of EVA and EBA-A Comparison. 1. Volatile Decomposition Products,* Journal of Applied Polymer Science. Vol. 43, p 1737-1745, 1991.

L. Sun, S.S. Pang, A.M. Sterling, I.I. Negulescu and M.A. Stubblefield, *Dynamic Modeling of Curing Process of Epoxy Prepreg,* Journal of Applied Polymer Science, Vol. 86, p 1911 – 1923, 2002.

T.A Instruments, *TGA 2950 Thermogravimetric Analyser Technical Brochure,* http://www.tainst.com, 2005.

M.Y. Teo, H.Y. Yeong and S.W. Lye, *Microwave Moulding of Expandable Polystyrene Foam with Recycled Material,* Journal of Materials Processing Technology, Vol. 63, p 514-518, 1997.

E.T. Thostenson and T.W. Chou, *Microwave Processing: Fundamentals and Applications,* Composites Part A: Applied Science and Manufacturing, 30, p 1055-1071, 1999.

S. Wang, M. Niu and D. Xu, *A Frequency-Varying Method for Simultaneous Measurement of Complex Permittivity and Permeability with an Open-Ended Coaxial Probe,* IEEE Transactions on Microwave Theory and Techniques, Vol. 46, p 2145-2147, 1998.

J.B. Wei, T. Shidaker and M.C. Hawley, *Recent Progress in Microwave Processing of Polymers and Composites*, Trends in Polymer Science, Vol. 4, p 18-24, 1996.

G.J. Wheeler, *Introduction to Microwaves,* Prentice-Hall, Inc., Englewood Cliffs, N.J., 1963.

F.N. Wilkenloh, P.A. Wilson, S.A. Fox, *U.S. Pat 4107354,* 1978.

W. Wu, *Baseline Studies of the Clay Minerals Society Source Clay: Colloid and Surface Chemistry Phenomena,* Clay and Clay Minerals, Vol. 49, p 446-452, 2001.

Z. Xie, J. Yang, X. Huang and Y. Huang, *Microwave Processing and Properties of Ceramics with Different Dielectric Loss,* Journal of the European Ceramic Society, Vol. 19, p 381-387, 1999.

R.J. Young and P.A. Lovell, *Introduction to Polymers,* Chapman and Hall, London, Weinheim, New York, Tokyo, Melbourne, Madras, 1991.

Y. Zhang, D. Rodrigue and A. Ait-Kadi, *High Density Polyethylene Foams. II. Elastic Modulus,* Journal of Applied Polymer Science, Vol. 90, p 2120 – 2129, 2003.

APPENDIX

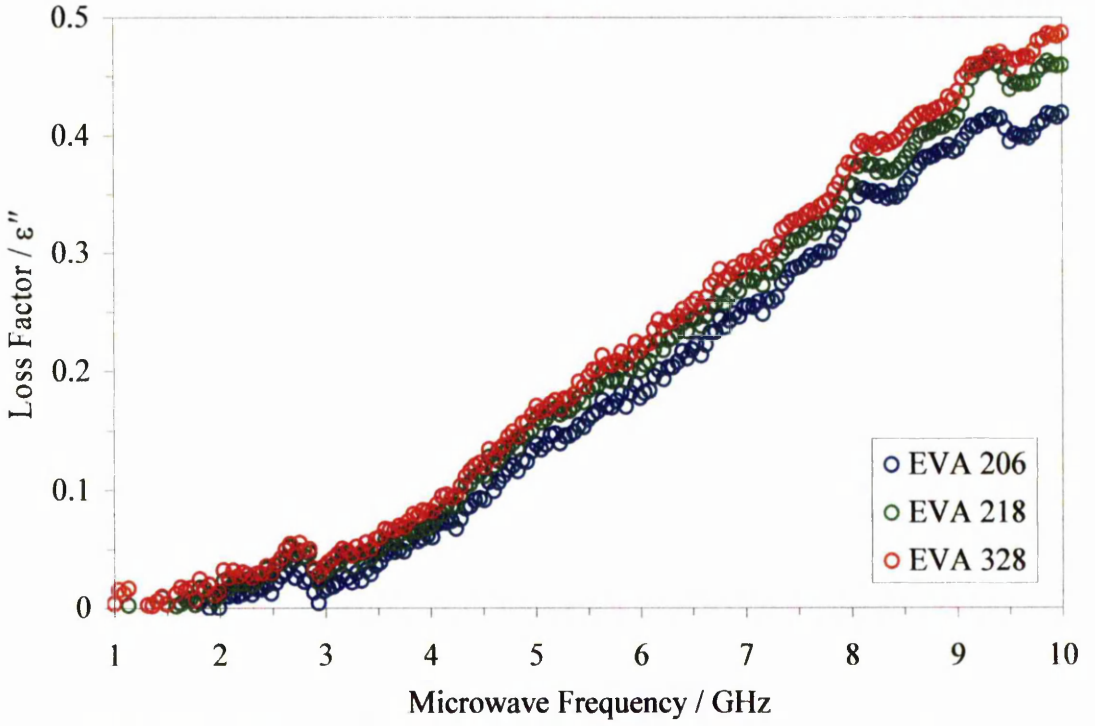

Appendix 1: Variation of loss factor with frequency for three EVA grades blended with 0.5 phr DCP only (non-crosslinked)

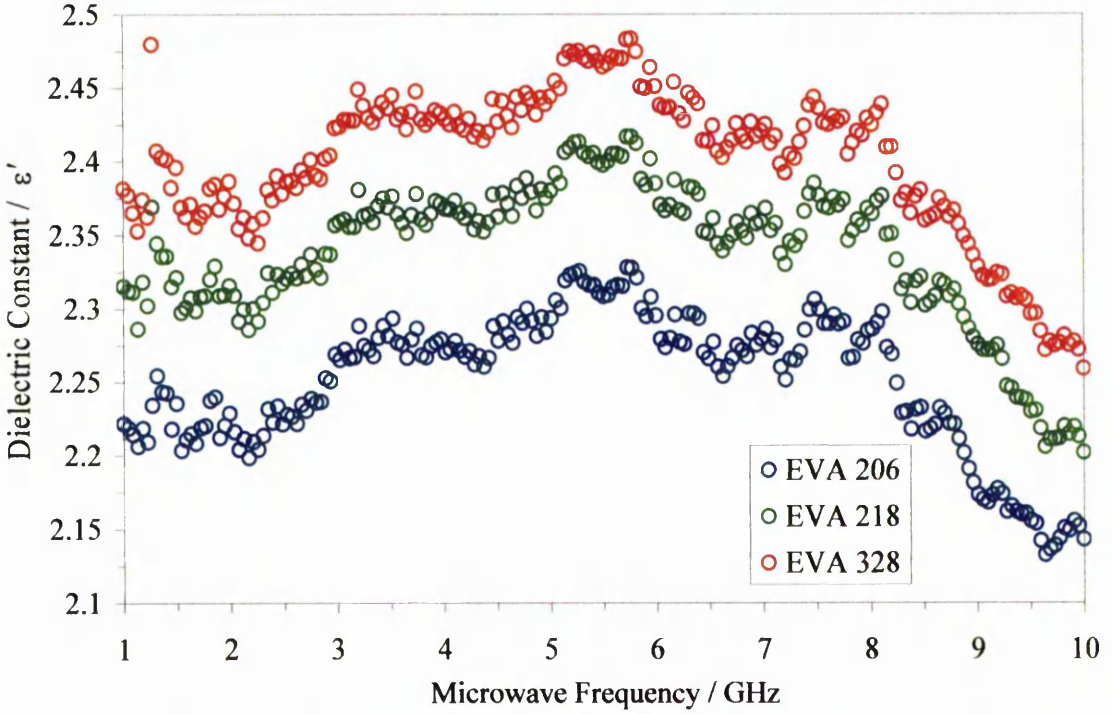

Appendix 2: Variation of dielectric constant with frequency for three EVA grades blended with 0.5 phr DCP only (non-crosslinked)

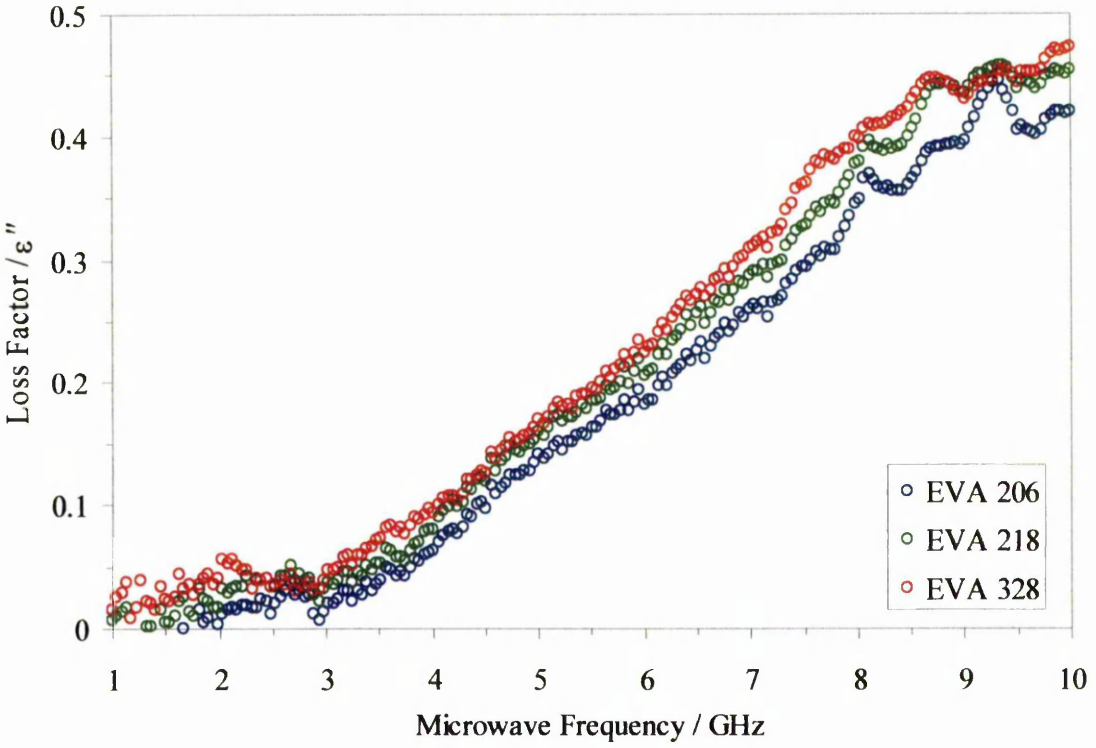

Appendix 3: Variation of loss factor with frequency for three EVA grades blended with 8 phr ADCE only

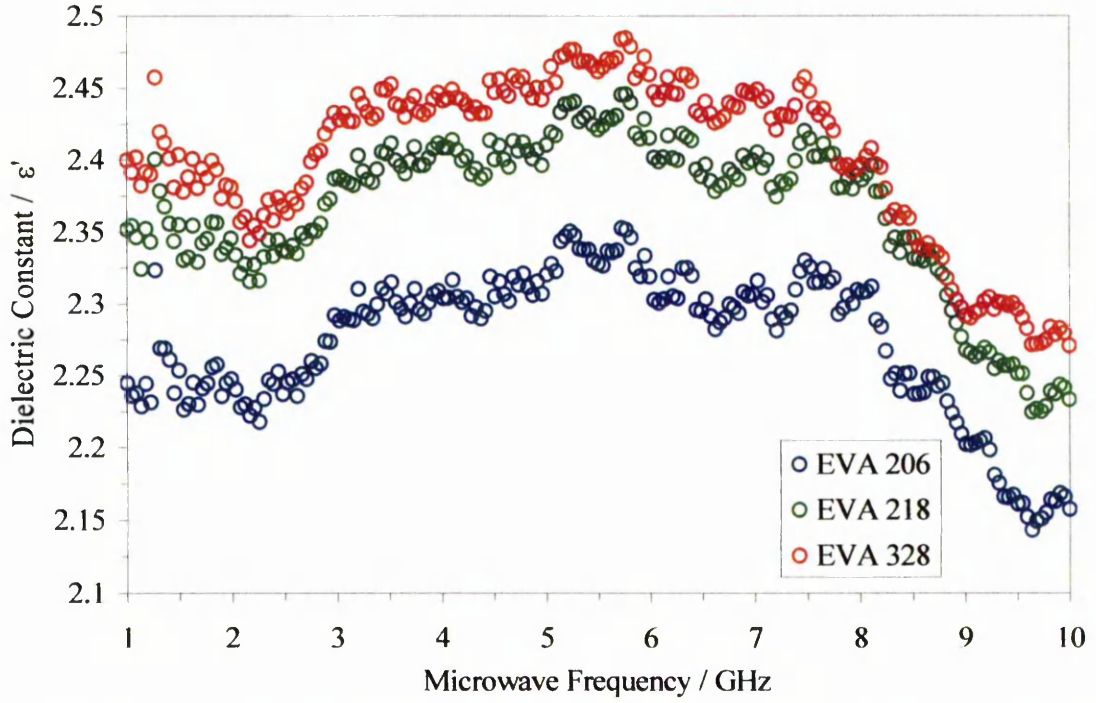

Appendix 4: Variation of dielectric constant with frequency for three EVA grades blended with 8 phr ADCE only

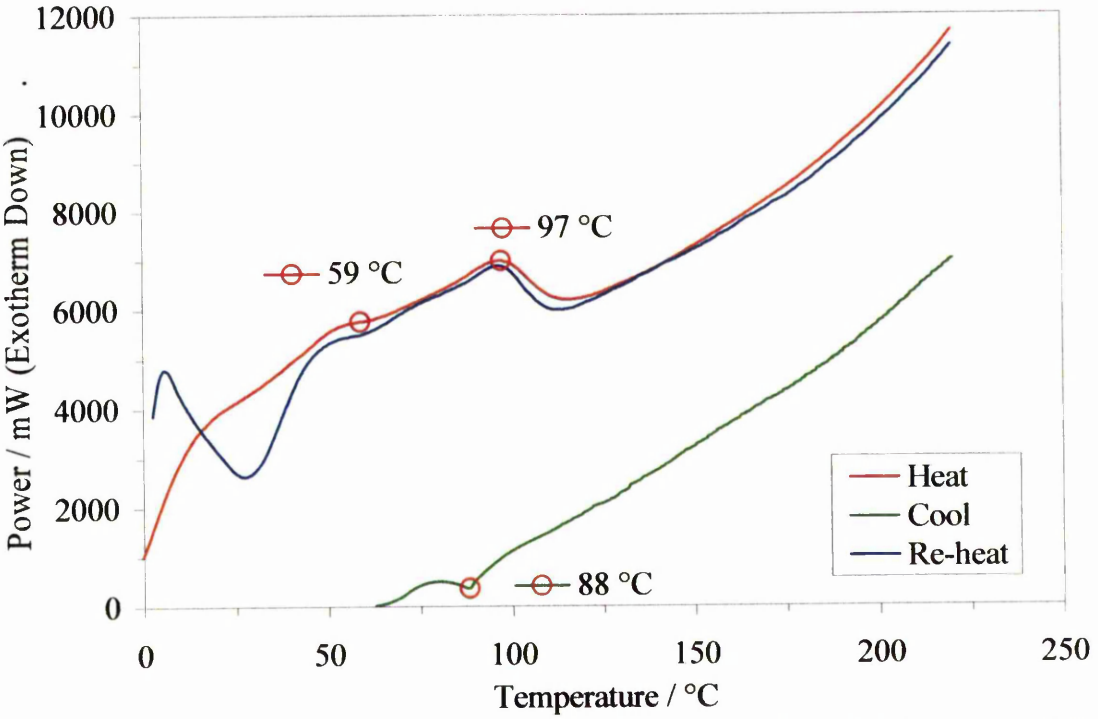

Appendix 5: Microwave calorimeter data for 0.35 g pure EVA 206 heated at 15 K min^{-1}

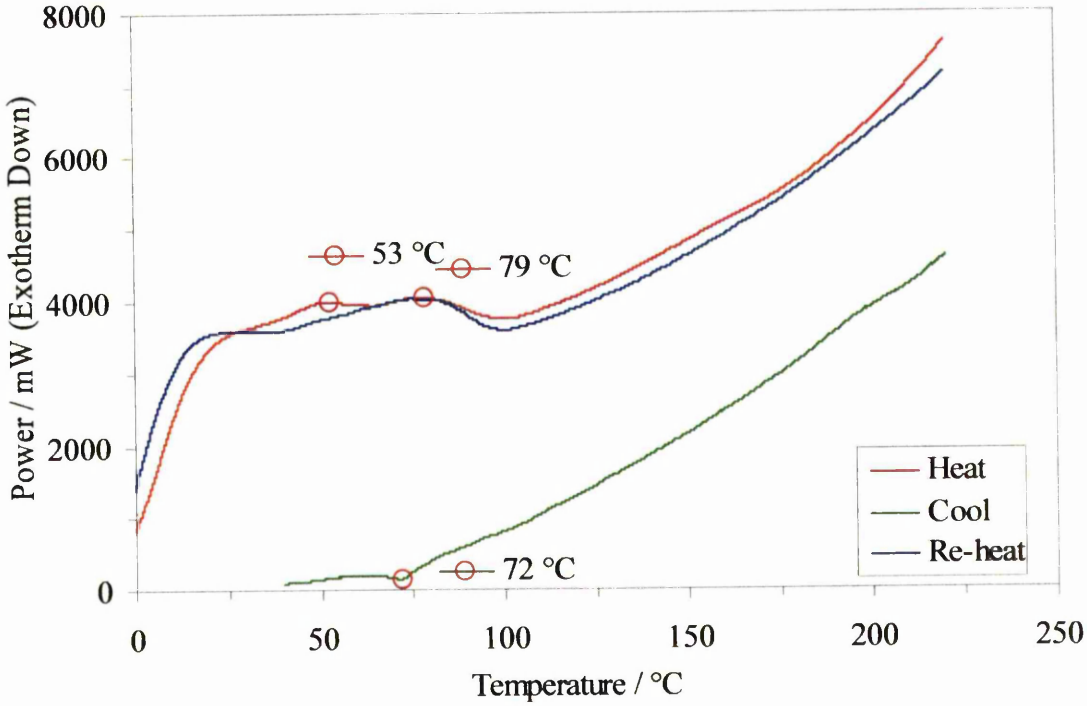

Appendix 6: Microwave calorimeter data for 0.35 g pure EVA 218 heated at 15 K min^{-1}

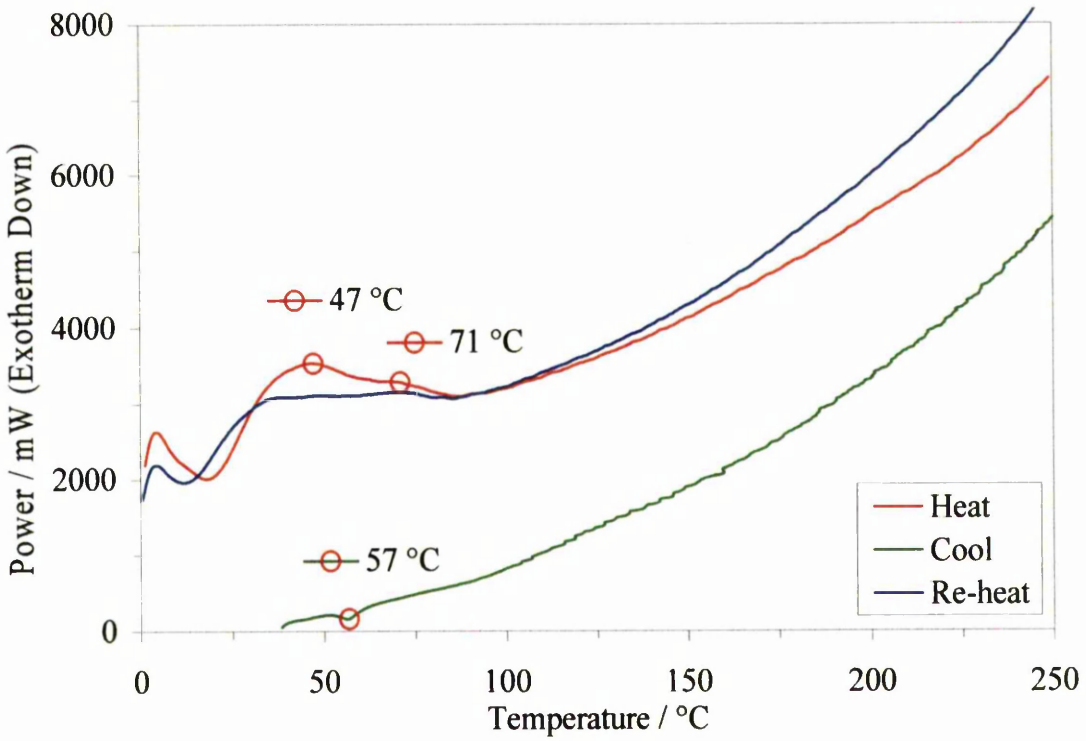

Appendix 7: Microwave calorimeter data for 0.35 g pure EVA 328 heated at 15 K min^{-1}

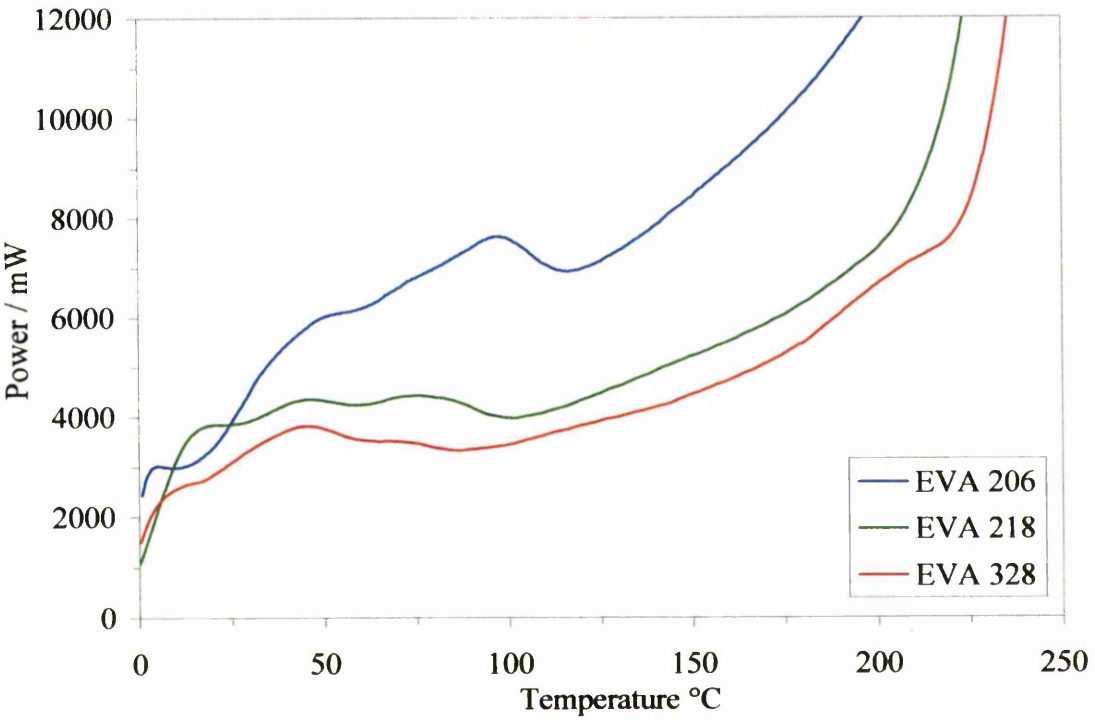

Appendix 8: Microwave calorimeter data for three EVA base polymers blended with 0.5 phr DCP and 8 phr ADCE

Appendix 9: Computer program code for variable frequency microwave foam processing with supplemental hot air heating

```
/*

 control.cpp (OVEN FISO 2xT 1xCAL)

 The program communicates with the 8720ET network analyser (via a GPIB interface) using a
 SICL device session.

 The network analyser and microwave amplifier are used as a power source for heating samples
 in the combination hot air-microwave oven.

 The sample and air temperatures are measured using FOT-H probes (FISO Technologies) connected
 to the FISO BUS system. The temperatures are read as analog outputs via 2x ADC (Pico Technology)
 connected to parallel ports (LPT1 + LPT2).

 The sample temperature is controlled by adjusting the microwave source power. The program uses
 preset control parameters (power and temperature limits) in a parabolic function to calculate the
 required output power of the network analyser.

 The air temperature is controlled by an independent CAL9500 process controller.

 The elapsed time, sample temperature, air temperature, source power and frequency are saved in
 an output file.

*/

#include <fstream.h>  // I/O and file streams
#include <sicl.h>     // HP Standard Instrument Control Library
#include "adc.h"      // ADC drivers
#include <stdlib.h>   // for exit()
#include <time.h>     // for clock()
#include <conio.h>    // for _kbhit()
#include <math.h>     // for log10() and pow()

void main(void)
{
        // declare session identifier, constants and variables
        INST na;

        const double STANDBY_P_dBm = -18.0; // power in dBm for standby
```

```
double f[10],max_P[10],min_P,P1,P2,source_P;
double iso_T,low_T,dT,sample_T,air_T,adcV_1,adcV_2;

int i,num_f;

clock_t zero_t,current_t;
double  elapsed_t;

char filename[16];

ofstream fileOut;

cout << "Please enter a new filename for the data file: ";
cin >> filename;

// open a new file (if file already exists then exit)
fileOut.open(filename,ios::noreplace);

if (fileOut.fail())
{
        cout << "The file already exists!" << endl;
        cout << "Press any key to exit" << endl;
        while (!_kbhit()) {}
        exit(1);
}

// open device session and set I/O timeout (10000 ms)
na = iopen("hpib7,15");
itimeout(na,10000);

// Enter user data
cout << "Enter the cure temperature: ";
cin >> iso_T;
cout << "Enter the low temperature limit: ";
cin >> low_T;

dT = iso_T - low_T;

cout << "Enter number of frequencies: ";
cin >> num_f;

for (i=0;i<num_f;i++)
{
        cout << "Enter frequency (GHz): ";
        cin >> f[i];

        cout << "Enter max analyser power for this frequency (dBm): ";
        cin >> max_P[i];
}
```

```
        cout << "Enter min analyser power (dBm): ";
        cin >> min_P;

        // file header
        fileOut << "Cure temperature " << iso_T << " C" << endl;
        fileOut << "Low temp limit   " << low_T << " C" << endl << endl;

        fileOut << "t(s)\tf(GHz)\tP(dBm)\tsample T\tair T" << endl;

        cout << endl << "Press any key to stop!" << endl;

        // set initial mode
        i = 0;

        // set zero time
        zero_t = clock();

        // loop until a key is pressed
        while (!_kbhit())
        {
                // calculate elapsed time
                current_t = clock();
                elapsed_t = (double)(current_t - zero_t)/CLOCKS_PER_SEC;

                // read sample temperature from Fiso BUS System (ADC on parallel
port LPT1)
                adc10_open_unit(1,12);
                adcV_1  = adc10_get_value();
                sample_T = adcV_1 * 5000/15/4095;

                // read air temperature from Fiso BUS System (ADC on parallel port
LPT2)
                adc10_open_unit(2,12);
                adcV_2 = adc10_get_value();
                air_T  = adcV_2 * 5000/15/4095;

                // set network analyser to CW mode at f[i]
                iprintf(na,"CENT %lf GHZ;SPAN 0 HZ;REST;\n",f[i]);

                // set power for heating from measured sample temperature using
parabolic function
                if (sample_T >= iso_T)
                        source_P = min_P;
                else if (sample_T < low_T)
                        source_P = max_P[i];
                else
                {
                        P2 = pow(10,max_P[i]/10); // conversion from dBm to mW
                        P1 = pow(10,min_P/10);    // conversion from dBm to mW
```

```
                source_P = P1 + ((P2 - P1) * ((iso_T - sample_T)/dT)*((iso_T -
sample_T)/dT));

                source_P = 10*log10(source_P); // conversion from mW to
dBm
            }

            iprintf(na,"POWE %lf;\n",source_P); // set network analyser power

            // output to file
            fileOut << elapsed_t <<"\t"<< f[i] <<"\t"<< source_P <<"\t"<<
sample_T <<"\t"<< air_T << endl;
            cout << elapsed_t <<"\t"<< f[i] <<"\t"<< source_P <<"\t"<< sample_T
<<"\t"<< air_T << endl;

            if (i < num_f - 1) i++; // increment mode
            else i = 0;          // reset to initial mode
        }

        iprintf(na,"POWE %lf;\n",STANDBY_P_dBm);

        // close device session
        iclose(na);
}
```